INFORMATION TO USERS

This manuscript has been reproduced from the microfilm master. UMI films the text directly from the original or copy submitted. Thus, some thesis and dissertation copies are in typewriter face, while others may be from any type of computer printer.

The quality of this reproduction is dependent upon the quality of the copy submitted. Broken or indistinct print, colored or poor quality illustrations and photographs, print bleedthrough, substandard margins, and improper alignment can adversely affect reproduction.

In the unlikely event that the author did not send UMI a complete manuscript and there are missing pages, these will be noted. Also, if unauthorized copyright material had to be removed, a note will indicate the deletion.

Oversize materials (e.g., maps, drawings, charts) are reproduced by sectioning the original, beginning at the upper left-hand corner and continuing from left to right in equal sections with small overlaps.

Photographs included in the original manuscript have been reproduced xerographically in this copy. Higher quality 6" x 9" black and white photographic prints are available for any photographs or illustrations appearing in this copy for an additional charge. Contact UMI directly to order.

Bell & Howell Information and Learning
300 North Zeeb Road, Ann Arbor, MI 48106-1346 USA
800-521-0600

UMI®

THE EFFECT OF TUBE CORRUGATION ON THE STABILITY OF A CORE-ANNULAR FLOW

by

Hsien-Hung Wei

A dissertation submitted to the Graduate Faculty in Engineering in partial fulfillment of the requirements for the degree of Doctor of Philosophy, *The City University of New York*

2000

Bell & Howell Information and Learning Company
300 North Zeeb Road
P.O. Box 1346
Ann Arbor, MI 48106-1346

The manuscript has been read and accepted for the Graduate Faculty in Engineering in satisfaction of the dissertation requirement for the degree of Doctor of Philosophy.

20 September 2000
Date

Professor David Rumschitzki,
Professor David Rumschitzki,
Chair of Examining Committee

September 20, 2000
Date

Professor Mumtaz K. Kassir
Executive Officer

Professor Morton Denn

Professor Peter Ganatos

Professor Charles Maldarelli

Professor David Rumschitzki

Professor Michael Siegel
(New Jersey Institute of Technology,
Department of Mathematical Sciences)

Supervisory Committee

The City University of New York

Abstract

THE EFFECT OF TUBE CORRUGATION ON THE STABILITY OF A CORE-ANNULAR FLOW

By

Hsien-Hung Wei

Advisor: **Professor David S. Rumschitzki**

We focus on the problem of a core-annular flow in a corrugated tube. The motivation for this study derives from liquid-liquid displacement flows in small pores, as occur in secondary oil recovery and core-annular flow in the bronchi. We focus on the effect of tube, pore, or airway corrugation on the stability of such a flow arrangement and investigate whether and how the corrugation encourages or discourages instability compared with the situation of a straight, cylindrical tube. Both viscous (Chapter II & III) and inertial (Chapter IV) dominant theories have been asymptotically developed in the limit of thin annular films ($\varepsilon \to 0$) and small corrugation ($\sigma \to 0$).

Chapter II examines the linear stability of a viscous core-annular flow. The wall corrugation leads to a spatially periodic base flow to leading order. This base flow contributes spatially periodic coefficients to the partial differential equations governing the system's stability. We employ Floquet-Bloch analysis to obtain the eigenvalue spectra of these linear stability equations. We compare the results with the direct numerical solution of the initial value problem of the interfacial dynamics for a given initial condition and a range of parameters. The eigenvalue spectra show multiple-branch structures. In contrast to the straight cylinder theory, an initial disturbance with wave length shorter than the circumference of the undisturbed fluid-fluid interface can be modified due to this interaction

with higher wall corrugation harmonics to excite unstable longer waves and thus lead to a linear instability.

In Chapter III, we extend the linear analysis to the weakly non-linear regime. Linearly unstable long waves saturate in the weakly nonlinear regime due to the non-linearity's wave steepening. The weakly non-linear analysis in a corrugated tube leads to the competition between unstable long waves being shortened and stabilized on the one hand, and these shorter waves exciting new unstable longer waves on the other. We derive and numerically solve the weakly non-linear amplitude equations for this situation and explore the results of this competition for various parameter regimes. For moderate or less strong interfacial tensions, the long wave linear instability excited by the corrugation, as discussed in Chapter II, still can be suppressed by the stabilization from the nonlinear steepening.

In Chapter IV, we study the effect of corrugation on the linear stability of an *inviscid* core-annular flow, which is a complementary problem to the viscous system analyzed in Chapter II. Many qualitative features of the stability are similar to those in Chapter II. However, for a particular combination of the parameters, there is a regime where resonant corrections to the eigenvalue can be so large that a "bridge" of positive growth rates connecting the primary and secondary unstable eigenvalue branches can be present. In this case, the primary wave competes with its first harmonic wave and neither dominates at long (linear) times. The long-term interfacial evolution (in the linear regime) grows in an oscillatory manner.

Acknowledgments

I first would like to express my sincere appreciation to my mentor, Professor David Rumschitzki, for his guidance throughout this research work. I have gained so much inspiration from his great physical insight and his suggestions. I especially thank him for his continuous support, patience and encouragement during my studies.

I also would like to thank my parents and my sister Chia-Lee for always loving me, sharing in both my joys and unhappiness. Their endless love and unconditional support are always my driving force to do whatever I dedicate myself to. I especially thank my wife, Annie Yixin Shou, who is also my best colleague, for always being concerned about me and for listening to me without complaints.

I have to thank Andy Eng in the Department of Chemical Engineering for always providing help whenever I was in need of it. I also would like to thank Ting-Ying Wei, Ravichandra Palaparthi, Nitin Kumar and my fellow graduate students and colleagues in the Department of Chemical Engineering at CUNY for their kind friendships.

To my family

Table of Contents

List of Figures

I. Introduction

A two-fluid core-annular flow (CAF) consists of two immiscible fluids flowing cocurrently in a tube or pore, where one (the annular) fluid wets the tube wall and surrounds the other (core) fluid. CAFs are widely studied and serve as a useful model to analyze a number of technologies and problems of scientific interest such as oil recovery (Slattery 1974), liquid-liquid displacements in porous media (Park & Homsy 1984), lubricated piping (Perziosi *et al.* 1989), and the lung surfactant problem (Otis *et al.* 1993, Halpern & Grotberg 1993).

In secondary oil recovery processes, oil saturates capillary pores in rocks. One tries to displace the oil by using a second, immiscible liquid, usually an aqueous solution with low interfacial tension with the oil (Slattery 1974). If the displacing fluid is less viscous, it will finger into the extant fluid, which sticks to the wall due to its non-slip condition there (Saffman & Taylor 1958). This creates a CAF away from the ends of the finger. The interfacial stability, however, can significantly affect the efficiency of the recovery process. Growing interfacial disturbances can cause the wetting layer to snap and bring the non-wetting phase in contact with the capillary pore wall. Contact line forces attaching the slug to the wall can retard train mobility, thereby make recovery more difficult. In addition, the pore structure may significantly contribute to instability, since uneven boundaries may potentially change flow pattern dramatically and excite an instability. In lubricated pipeling, one introduces a small amount of a more wetting fluid, much less viscous to absorb the velocity gradient such as water and thereby drastically reduce the pumping-transport costs of very viscous crude oil in steel pipes. However, any instability leading to film rupture will bring the much more viscous fluid in contact with the wall. The shearing of this fluid will drastically increase the cost of pumping. In the lung, air travels through a hierarchy of branching tubes, called bronchioles whose inner surfaces are coated by a thin layer of fluid. This cylindrical liquid layer typically maintains its integrity during respiration due to a

surfactant produced in the lungs called DPPC which retards the time scale of the capillary instability to times long compared with the breathing cycle. In premature infants and adults with adult respiration distress syndrome (ARDS), this surfactant is not present or does not function properly, and the air core may become blocked, destroying the CAF and inhibiting respiration. Obviously, whether the flow is stable or not is critical to the proper functioning of these systems.

Clearly, it is important to understand the mechanism of the instabilities in CAFs. We would hope to achieve sufficient understanding to be able to control stability by manipulating the system's parameters. It is essential to start with a simple model based on a perfect CAF (PCAF - perfect meaning co-axial and axisymmetric) through the idealized geometry of a cylindrical tube. When the flow is driven by a pressure gradient, the base flow for a PCAF, a Poiseuille flow field and a purely circular interface, satisfies the Navier-Stokes equation and the appropriate boundary conditions exactly. PCAFs allow us to understand fluid mechanical factors affecting the system's stability by decoupling the geometric complications of a real CAF from the fluid factors. In most applications such as oil recovery and the lung problem, the thickness of the annular fluid is typically much smaller than the tube radius. The dominant factors in the linear stability problems of CAFs are surface tension and viscosity stratification effects. Surface tension is usually important for problems with interfaces and can give a rise to capillary instability where the interfaces are circular. In response to an infinitesimal interfacial disturbance, Rayleigh (1879), Tomotika (1935), Goren (1962) and many others found that capillarity acts in two ways: it destabilizes the interfacial circumferential curvature and stabilizes the axial curvature of an interfacial deflection. The competition is such that disturbances with wavelengths shorter than the undisturbed interfacial circumference are stable and those longer are unstable. This feature of capillarity is independent of the base flow, and arises simply from the cylindrical geometry of the unperturbed fluid-fluid interface. In the presence of viscosity stratification, as studied by Preziosi *et al.* (1989), and Georgiou *et al.* (1992), a shear flow

configuration with a more viscous core fluid can stabilize the destabilization of the capillarity for a band of Reynolds number.

The non-linear aspect of the annular-film system can provide a better understanding of the system's instability, particularly when disturbances that are amplified by the capillary instability grow to finite magnitudes. Gauglitz & Radke (1988)'s study of the no flow case suggested that the core can snap off when the unperturbed annular thickness is above a critical value; otherwise the film can rupture and the system forms stable lobes along the tube as in Hammond (1983). However, the presence of base flow can significantly change the behavior in the non-linear regime. In the weakly nonlinear regime, where disturbances remain finite but much smaller than the annular film thickness, Frenkel *et al.* (1987) and Papageorgiou *et al.* (1990) showed that for strong surface tensions, a Kuramoto-Sivashinky-like equation governs the system's weakly nonlinear evolutions. Papageorgiou *et al.*'s equation included a direct coupling from the core's dynamics through the viscosity stratification. The non-linear term that derives from the shear flow in the base state steepens interfacial deflections. This gives rise to shorter length scales, which become stabilized by the longitudinal curvature of the interfacial tension. This mechanism saturates the capillary instability and can lead to either chaotic interfacial motions or, more typically, to nonlinear traveling curves having more than one length scales depending on the parameter values. As such, the interfacial stability of a PCAF in a circular tube is fairly well understood.

However, in real core-annular flow systems such as occur in oil recovery, two fluids flow through uneven channels in a porous rock, and thus do not possess an ideal geometry like flows in a perfectly cylindrical tube. Similarly, the extensive branching of the bronchiole system represents a system with a frequently changing cross-section. It is thus conceivable that pore corrugation may play a role in determining the real system's stability that is at least as important as the effects already considered. But there are good reasons why one might neglect it in a first analysis. Let's consider briefly how pore corrugations can complicate the problem. First, such a non-ideality will cause the base state to be

significantly changed. Even if the corrugated tube remains axisymmetric, the base flow pattern in a tube of varying cross section will be two-dimensional rather than being a purely axial velocity as a function of the radial position. This deviation from parallel flow can interact strongly with the disturbance introduced in the stability analysis. For instance, consider the flow of a single fluid in a sinusoidal tube. Even for a small Reynolds number Re, inertia can be significant when the axial variation of the tube radius is as rapid as $O(1/Re)$. Moreover, it is unlikely that one would be able to solve for the base state exactly in closed form in such a geometry. Cylindrical tube theory clearly does not include these effects. To access them, it is necessary to extend the scope of this theory to include geometric factors.

Our goal in this study is to develop a systematic approach to investigate the effect of pore corrugation on the instability of a core annular film flow and to see how a non-trivial base flow interacts with a disturbance to determine the system's stability. As expected, the existing works based on PCAF theory can be regarded as a limiting case of our analysis.

Clearly one would like to examine the effect of wall corrugation in general. However, due to its complexity, we make a number of simplifications to idealize the geometry and thus make the problem tractable. First, rather than a corrugation of arbitrary structure, we idealize the geometry and consider a sinusoidal corrugation with amplitude $\sigma\varepsilon$. Here, similar to the PCAF treatments, we define the parameter ε as the ratio of the mean annulus thickness to the mean core radius. Small ε corresponds to the thin film limit. The corrugation parameter σ is measured with respect to the film thickness and can be $O(1)$ in general. Of course, $\sigma = 0$ should reduce to the straight tube case. Thus, $\sigma\varepsilon$ is small relative to the macroscopic geometry of the tube. However, when $\varepsilon << 1$ and $\sigma \sim O(1)$, even though $\sigma\varepsilon$ is small with respect to the core radius, it is still comparable to the film thickness; in that case the film equations become difficult to handle due to quadratic terms arising when applying the boundary conditions at the corrugated wall. If, on the other hand, the corrugation is also small compared with the film thickness(i.e., $\sigma << 1$), then we

can, at the cost of introducing an additional small parameter, linearize the corrugation and simplify our formulation without abandoning our objective. Therefore, by means of perturbation techniques, the steady base flow can be expected to be a superposition of a parallel flow in the cylindrical tube and a correction for the nonparallel fluid motion arising from the corrugation to leading order in the small corrugation parameter. One can then perform a stability analysis order-by-order in the perturbation parameter, of the corresponding base flow.

This work examines three problems concerning the effect of corrugation on the stability of a CAF. We investigate a viscous system in Chapter II in which we derive the leading order base flow and perform the corresponding linear stability. In Chapter III, we extend the analysis to the weakly non-linear regime to see how the corrugation competes with the effect of non-linearity. To access the inertial effect, we also examine the linear stability of an inviscid CAF in Chapter IV. The study of an inviscid system serves as a complementary problem to the viscous dominant theory in Chapter II and III.

II The Effect of Tube Corrugation on the Linear Stability of a Core-Annular Flow

1. Introduction

A two-fluid core-annular flow (CAF) consists of two immiscible fluids flowing cocurrently in a tube or pore, where one (the annular) fluid wets the tube wall and surrounds the other (core) fluid. Core annular flows are widely studied and employed as a useful model to analyze a number of technologies and problems of scientific interest such as secondary oil recovery (Slattery 1974), liquid-liquid displacements in porous media (Park & Homsy 1984), lubricated piping (Perziosi, Chen & Joseph 1989), and the lung surfactant problem (Otis *et al.* 1993, Halpern & Grotberg 1993). To recover oil which is saturating capillary pores in rocks, one can try to displace the oil with a second, immiscible liquid, usually an aqueous solution with low interfacial tension with the oil (Slattery 1974). If the displacing fluid is less viscous, it will finger into the extant fluid, which sticks to the wall due to its non-slip condition there (Saffman & Taylor 1958). This creates a CAF away from the ends of the finger. Any interfacial stability, however, can significantly affect the efficiency of the recovery process. Growing interfacial disturbances can cause the wetting layer to snap and bring the non-wetting phase in contact with the capillary pore wall. Contact line forces attaching the slug to the wall can retard train mobility, thereby make recovery more difficult. In addition, the pore's structure may significantly destabilize the system since the uneven boundaries may potentially change flow pattern dramatically and excite instability. In the lung, air travels through a hierarchy of branching tubes, called bronchioles whose inner surfaces are coated by a thin layer of fluid. This cylindrical liquid layer typically maintains its integrity during respiration due to a surfactant produced in the lungs called DPPC which retards the time scale of the capillary instability to times long compared with the breathing cycle. In premature infants and adults with adult respiration distress syndrome (ARDS), this surfactant is not present or does not function properly, and

the core can become blocked, destroying the CAF and inhibiting respiration. Obviously, whether the flow is stable or not is relevant to the proper functioning of these systems.

Clearly, it is important to understand the mechanism of instability in CAFs because it is often critical to either encourage or discourage the instability's growth. It is not surprising that there are numerous investigations based on a perfect CAF (PCAF - perfect meaning co-axial and axisymmetric) through the idealized geometry of a straight, cylindrical tube. In these studies, the base flow for a PCAF is a Poiseuille flow field with a purely circular interface, which satisfies the Navier-Stokes equation and the appropriate boundary conditions exactly. The dominant effects that influence the linear stability of a CAF are capillarity and viscosity stratification. Capillarity acts in two ways: it destabilizes the interfacial circumferential curvature and stabilizes the axial curvature of an interfacial deflection. The competition is such that disturbances with wavelengths shorter than the undisturbed interfacial circumference are stable and those longer are unstable. This feature of capillarity is independent of the base flow, and arises simply from the cylindrical geometry of the unperturbed fluid-fluid interface.

In the presence of a base flow, Hickox (1971) used Yih's long wavelength technique to examine the linear stability of a CAF with a more viscous film fluid ($m \equiv \mu_2/\mu_1 > 1$, μ_1 and μ_2 being the viscosities of the core and annular fluids, respectively) in the presence of capillarity, viscosity and density stratification and gravity in a vertical tube. In his analysis, for both axisymmetric and non-axisymmetric disturbances, both capillarity and viscosity stratification were destabilizing for long waves (to the leading order in wave number α) and axisymmetric modes were the most unstable. Joseph and coworkers, in a series of papers (Joseph, Renardy & Renardy 1984; Preziosi, Chen & Joseph 1989; Hu & Joseph 1989; Chen, Bai & Joseph 1990; Hu, Lundgren & Joseph 1990, Chen & Joseph 1991), extensively investigated the combination of capillarity and viscosity stratification, for m <1, for which the latter effect is stabilizing. They numerically solved the full Orr-Sommerfeld equation and employed perturbation techniques, e.g. for small m <<1 in their

analyses. In lubricated pipelining m <1 and viscosity stratification can stabilize the destabilization of capillarity for a band of Reynolds number. As such, they showed that there exists a window of stability in Reynolds numbers space in which a CAF is linearly stable. Such window disappears when the film become too thick or when enhancing the film's viscosity relatively to that of the core. In most applications, the thickness of the annular fluid is typically much smaller than the tube radius. In such cases, Georgiou, Maldarelli, Papageorgiou & Rumschitzki (1992) developed thin film asymptotic techniques to analytically examine the linear stability of a PCAF in a vertical arrangement with gravity. They focused on axisymmetric, i.e., the most unstable, disturbances and extended Hickox's $\alpha \rightarrow 0$ analysis to the range of intermediate waves, i.e., waves comparable to the tube circumference. For large surface tensions and for $m < 1$, viscosity stratification can stabilize the capillary instability to the leading order in the ratio ε of the undisturbed annular thickness to the core radius, while viscosity stratification is destabilizing for $m > 1$. A density difference is purely dispersive to the leading order in ε and its stability contribution is a second order effect. In particular, the linear stability is primarily dominated by the fluid-fluid interfacial tension, i.e., capillarity, and viscosity stratification.

The non-linear aspects of a thin-film CAF is important to better understand the system's stability in response to disturbances of finite magnitude and to follow the evolution of linearly unstable waves, since the linear instability governs the dynamics of only infinitesimal disturbances. Hammond (1983) studied the two-fluid CAF in a tube with a thin annular film in absence of a base flow for parameter values where the core's dynamics become irrelevant. His nonlinear analysis showed that long wave disturbances can grow non-linearly and could potentially lead to film bridging the core and forming lenses when sufficient liquid was present. However, the extent of validity of his equation was limited by the thin film approximation which particularly impacts the allowed mean curvature of the interface. This $O(\varepsilon)$ approximation admits a collar volume that never goes through a maximum so that the collar is always stable and need not form a lens. Gauglitz

through a maximum so that the collar is always stable and need not form a lens. Gauglitz & Radke (1988) extended Hammond's analysis in an *ad hoc* manner by keeping the full non-linear circumferential capillary but linearizing everything else in the normal stress balance at the interface. Interestingly, their analysis predicts the transition from collars to lenses, while Hammond's thin film analysis might be able to predict this transition only at a higher order (in ε) approximation.

In presence of a base flow and in the regime of a very strong surface tension, Frenkel *et. al* (1987) found that the Kuramoto-Sivashinky (KS) equation governs the weakly nonlinear evolution of fluids with matched viscosities and densities. In their case, only capillarity destabilizes and the core's dynamics slave those of the film. The non-linear coupling of the base flow through the kinematic condition can saturate the instability and lead to chaotic interfacial motions, as numerically demonstrated (Sivashinky & Michelson 1980). Papageorgiou, Maldarelli & Rumschitzki (1990) developed a weakly non-linear analysis of a CAF for generally different fluid-fluid viscosities and densities and for surface tensions where the core dynamics are integrally coupled to the interfacial evolution. They derived amplitude equations to describe the weakly nonlinear interfacial dynamics which turn out to be the Kuramoto-Sivashinky-like equations modified by the inclusion of non-local integral kernels involving core quantities. In the case of slow and moderate flow, this kernel includes non-local terms reflecting the coupling of the core's dynamics by viscosity stratification to the interface's evolution. The linear analysis yields unstable long waves for $m > 1$, and for some values of the Reynolds number Re when $m < 1$. The non-linear term that derives from the base state shear flow steepens interfacial deflections, giving rise to shorter length scales. These scales then become stabilized by the longitudinal curvature (k^4) of the interfacial tension. This mechanism of saturating the instability can lead to either chaotic interfacial motions or, more typically, to nonlinear traveling waves having more than one length scales. More recently, Kerchman (1995) has developed a strongly nonlinear theory which includes large amplitude deflections. Whereas the above mechanism

is dominant when $\varepsilon^2 J/Re_1$ ($J = \rho_1 \gamma R_1/\mu_1^2$, where ρ_1, μ_1, R_1 are the core fluid's density, viscosity and undisturbed radius and γ is the fluid-fluid tension) is small compared with one, for large $\varepsilon^2 J/Re_1$, this steepening due to the base flow is weaker. The core annular arrangement may thus collapse due to the stronger capillary forces in this limit that are at work in the neighborhood of the interface's trough which can cause the interface to strongly bulge into the core. As a result of all of these linear and non-linear studies, the interfacial stability of a PCAF in a circular tube is fairly well understood.

However, in a real core-annular flow systems such as occurs in secondary oil recovery, two fluids flow through uneven channels in the porous rock and thus do not possess an ideal geometry as in a perfectly cylindrical tube. Similarly, the extensive branching of the bronchiole system represents a system with a frequently changing cross-section. It is thus conceivable that pore corrugation may play a role in determining the system's stability that is at least as important as the effects that have already been considered. But there are good reasons why one might neglect it in a first analysis. Let's consider briefly how pore corrugations complicate the CAF stability problem. First, such geometric non-idealities will change the base state significantly. Even in an axisymmetric tube of varying cross section, the base flow will be two-dimensional, rather than simply an axial velocity as a function of the radial position. This deviation from parallel flow can interact strongly with the disturbance introduced in the stability analysis. For instance, consider the flow of a single fluid in a sinusoidal tube. Even for small Re, inertia can become significant when the axial variation of the tube radius $\frac{dR}{dz}$ is as rapid as $O(1/Re)$. Moreover, it is unlikely that one would be able to solve for the base state, the starting point for a stability analysis, exactly in closed form. Cylindrical tube theory clearly does not include these effects. To access them, it is necessary to extend the scope of this theory to include these varying geometry factors.

channel with varying cross-section (Chow & Soda 1972) have been studied. These works employ perturbation techniques, by using either small corrugation or slow axial variation parameters, for flows at intermediate or high Reynolds numbers. Similar techniques have been applied in interfacial problems. Wang (1981) considered a film flowing slowly down a wavy inclined plate where the striations are parallel to the overall flow. He applied a perturbation method with respect to the small amplitude of the corrugation and found that, for a fixed mean depth of the film, the flow transverse to the striations is decreased relative to that on a smooth plate, while the flow along the striations is increased. Dassori, Deiber & Cassano (1984) analyzed a two-fluid system in a symmetrically sinusoidal, two-dimensional channel. They only focused on the case of a wetting fluid layer with very low density and viscosity relative to the core. Both of the above studies found that the fluid interface exhibited a wavy shape characterized by an amplitude and a phase shift relative to the wall, which are functions of the surface tension, the density ratio, viscosity stratification, the flow rate and the wave number of the wall. Recently, Kang & Chen (1994) extended Wang's analysis to cases with two fluid-fluid interfaces in the planar system and a similar picture resulted. In cases of large corrugations, perturbation techniques as mentioned above are no longer applicable. Pozrikidis (1988) extended Wang's problem to large corrugations by solving the two dimensional creeping flow problem numerically on a periodic domain using a boundary integral method.

Despite the work cited on base flows, linear or non-linear stability issues associated with flows in a corrugated configuration, especially interfacial problems, have only been explored in a preliminary manner. In the case of no flow, Gauglitz & Radke (1990) employed their previous analysis (1988) to examine how constrictions affect the foam formation in gas-liquid displacements for the case where the tube radius varies slowly in the axial direction. They showed that the time needed to snap a collar off strongly depends on the neck radius of the constriction and that the length of the constriction is not crucial to the instability. A similar conclusion was also drawn by Ransokoff, Radke & Gauglitz

on the neck radius of the constriction and that the length of the constriction is not crucial to the instability. A similar conclusion was also drawn by Ransokoff, Radke & Gauglitz (1987) and Ratulowski & Chang (1989) who analyzed the case when constrictions have varied cross-sections.

In the presence of a base flow, Kelly (1967) first studied the inviscid linear stability of a stationary wave without surface tension which is periodic in space and time in the base state. He derived a resonance condition in which the disturbances can excite an instability. Tougou (1978) investigated the stability of a viscous film flowing down an inclined, uneven wall in the presence of surface tension. To leading order in a shallow thickness parameter ε defined as the ratio of the mean film thickness to the wall's wavelength, the linear stability of the base flow is identical to that for the plane wall case. The long-time interfacial evolution as governed by the KS equation, however, is no longer spatially periodic due to the non-parallel base flow.

Our goal in this study is to develop a systematic approach to investigate the effect of pore corrugation on the instability of a core annular film flow and to see how a non-trivial base flow interacts with a disturbance to determine the system's stability. As expected, the existing works based on PCAF theory can be regarded as a limiting case of our analysis.

Clearly one would like to examine the effect of wall corrugation in general. However, due to its complexity, we make a number of simplifications to idealize the geometry and thus make the problem tractable. First, rather than a corrugation of arbitrary structure, we carry out our detailed calculations for a sinusoidal corrugation with amplitude $\sigma\varepsilon$. Here as before, the parameter ε is the ratio of the mean annulus thickness to the mean core radius. Small ε corresponds to the thin film limit. The corrugation parameter σ is measured with respect to the film thickness and can be $O(1)$ in general. Of course, $\sigma = 0$ should reduce to the straight tube case. Thus, $\sigma\varepsilon$ is small relative to the macroscopic geometry of the tube. However, when $\varepsilon \ll 1$ and $\sigma \sim O(1)$, even though $\sigma\varepsilon$ is small with respect to the core radius, it is still comparable to the film thickness; in that case the film equations are thus

difficult to handle due to the quadratic terms arising when applying the boundary conditions at the corrugated wall. If, on the other hand, the corrugation is also small compared with the film thickness (i.e., $\sigma << 1$), then we can, at the cost of introducing an additional small parameter, linearize the corrugation and simplify our formulation without abandoning our objective. Therefore, by means of perturbation techniques, the steady base flow can be expected to be a superposition of a parallel flow in the cylindrical tube and a correction for nonparallel fluid motion arising from the corrugation, to leading order in the small parameter. One can then perform a stability analysis, order-by-order in the perturbation parameter with the corresponding base flow.

2. Governing Equations and Boundary Conditions

Two immiscible, viscous, incompressible fluids are flowing axisymmertically without gravity in a core-annular arrangement in a tube of radius $R_2(z)$ that varies in the axial direction with slight corrugation. See Figure 1. The interface is given by $r = S(z,t)$. The core region, defined by $0 \le r \le S(z,t)$, is occupied by fluid 1 and the annulus, $S(z,t) \le r \le R_2(z)$, is filled by fluid 2. Since the flow fields are assumed to be axisymmetric, they only have velocity components $(u, 0, w)$ in terms of the cylindrical polar coordinates (r,θ,z). We non-dimensionalize the velocity, pressure, length scales, and time with the characteristic quantities W_0, ρW_0^2, R_0, and R_0/W_0, respectively, where W_0 is the axial velocity at the central line $r=0$ in the uncorrugated base flow, ρ is density of the fluids taken for now to be equal, and R_0 is the mean radius of the core. Then the governing equations are given by

$$w_t + uw_r + ww_z = -p_z + \frac{1}{Re_i}\nabla^2 w, \tag{2.1a}$$

$$u_t + uu_r + wu_z = -p_r + \frac{1}{Re_i}\left(\nabla^2 u - \frac{u}{r^2}\right), \tag{2.1b}$$

$$\frac{1}{r}(ru)_r + w_z = 0. \tag{2.1c}$$

where $\nabla^2 = \frac{\partial^2}{\partial r^2} + \frac{1}{r}\frac{\partial}{\partial r} + \frac{\partial^2}{\partial z^2}$, $i = 1, 2$ denotes the core and the annulus, respectively and the Reynolds number is given by $Re_i = \frac{\rho W_0 R_0}{\mu_i}$, μ_i being the viscosity of fluid i, i=1, 2. We use the capital letters U, W and P to denote the core's radial and axial velocities and pressure and the smaller letter u, w, and p for the corresponding film quantities. We use Re_1 for the core as the reference Reynolds number. The annulus Reynolds number is $Re_2 = \frac{Re_1}{m}$, in which $m = \frac{\mu_2}{\mu_1}$ is the viscosity ratio of the annulus to the core.

The following boundary conditions should be used: The velocities vanish at the wall,

$$w = 0,\ u = 0 \ \text{ at } r = R_2(z). \tag{2.2a}$$

Define the jump notation $[\bullet] = (\bullet)_1 - (\bullet)_2$. The velocities are continuous across the interface,

$$[w] = 0\ ,\ [u] = 0 \quad \text{at } r = S(z,t). \tag{2.2b}$$

The tangential stress and normal stress balances at the interface are

$$\left[\frac{1}{Re}(u_z + w_r)(1 - S_z^2) + \frac{2}{Re}u_r S_z - \frac{2}{Re}w_z S_z\right] = 0 \quad \text{at } r = S(z,t), \tag{2.2c}$$

$$-\left[p - \frac{2}{Re}u_r - \left(-p + \frac{2}{Re}w_z\right)S_z + \frac{2}{Re}(u_z + w_r)S_z\right]$$

$$= \frac{J}{Re_1^2}\left(S_{zz} - \frac{1}{S}\left(1 + S_z^2\right)\right)\left(1 + S_z^2\right)^{-3/2} \qquad \text{at } r = S(z,t), \tag{2.2d}$$

where $J = \frac{\sigma_s R_0}{\rho v_1^2}$ is the surface tension parameter used by Chandrasekhar (1968). The kinematic condition, which determines the shapes of the interface, is

$$u = S_t + wS_z \quad \text{at } r = S(z,t). \tag{2.2e}$$

Finally, the core flow field must be bounded at the central line, i.e.,

$$w,\ u \text{ bounded as } r \to 0. \tag{2.2f}$$

3. Base flow

3.1 Scalings

Consider the above arrangement, in the presence of surface tension and viscosity stratification, but neglecting density differences and gravity. To zeroth order in the corrugation parameter σ (i.e., no corrugation), the flow patterns in both fluids are parallel,

i.e., $$\overline{\overline{w}} = \frac{a^2 - r^2}{a^2 + m - 1} \text{ and } \overline{\overline{W}} = 1 - \frac{mr^2}{a^2 + m - 1}, \tag{3.1a ,b}$$

where $a = 1 + \varepsilon$ is the nondimensional (mean) radius of the tube and ε is the ratio of the (mean, when $\sigma \neq 0$) undisturbed film thickness to the (mean) core radius. The thin-film limit requires $\varepsilon << 1$. Since the film variables vary over a radial distance ε, we introduce a stretched film variable $y := 1 - \frac{r-1}{\varepsilon}$. Here $y = 0,\ 1$ correspond to $r = 1 + \varepsilon,\ 1$, i.e., the (average) position of the wall and the fluid-fluid interface, respectively. Then, since $m = O(1) >> \varepsilon$, the σ =0 velocity profile of the annular layer is a linear shear flow to order ε: $\overline{\overline{w}} = \frac{2\varepsilon}{m} y + O(\varepsilon^2)$. The core flow is still parabolic, i.e., $\overline{\overline{W}} = 1 - r^2 + \frac{2\varepsilon}{m} r^2 + O(\varepsilon^2)$. The interface is the perfectly cylindrical surface r=1. The imposition of a corrugation alters the flow fields. The thin film, unlike the core, can only support an axial correction to the driving pressure gradient in response to the corrugation and it transmits this variation to the core via an interfacial deflection. Let us begin by examining the scalings that govern the perturbed base flow.

The corrugated wall is given by $R_2(z) = 1 + \varepsilon(1 + \sigma\phi(z))$, where $\phi(z)$ is a prescribed order one function of z, the corrugation factor σ is assumed to be small compared with 1, and σ=0 gives the uncorrugated system. In terms of y, the wall's shape function is $y = -\sigma\phi(z)$. Let the perturbed (due to $\sigma \neq 0$) quantities $(\overline{w}', \overline{u}', \overline{p}')$ and $(\overline{W}', \overline{U}', \overline{P}')$

correspond to the film and core, respectively. We represent the steady interface, perturbed by the wall's corrugation, by $S_b(z) = 1 + \bar{\delta}\eta(z)$, where $\eta(z)$ is an unknown order one function. We shall seek scalings for the above dynamic quantities and for the perturbed interface ($\bar{\delta}$) in terms of ε and σ.

The introduction of the thin film variable y makes the thin film limit ($\varepsilon \to 0$) explicit. It also separates the film's radial scale from its axial and from both scales in the core. As such, radial derivatives in the film are large, i.e., $\frac{\partial}{\partial r} = -\frac{1}{\varepsilon}\frac{\partial}{\partial y}$. To find the appropriate scalings, we follow the procedures used by Hammond (1983) or Papageorgiou *et al.* (1990). The scalings basically follow from the fact that the thin annulus can support only a lubrication flow. Let us begin by considering the no slip condition for the axial velocity at the wall ($y = -\sigma\phi(z)$) and Taylor expanding about y=0. This gives $\bar{w}' \sim \sigma\varepsilon/m$. Continuity gives $\bar{u}' \sim \varepsilon\bar{w}' \sim \sigma\varepsilon^2/m$. Meanwhile, the steady state kinematic condition gives $\bar{\delta} \sim \bar{u}'/\bar{\bar{w}} \sim \sigma\varepsilon$. This deflection causes a perturbed pressure across the interface. In general, thin film shear flows develop dominant pressures that drive lubrication layer flows. Therefore, the film perturbed pressure dominates the normal stresses and balances the surface tension terms. One can estimate it as $\bar{p}' \sim J\bar{\delta}/Re_1^2 \sim J\varepsilon\sigma/Re_1^2$. It follows from (2.1a) that the perturbed axial velocity in the film scaled as $\bar{w}' \sim J\bar{\delta}\varepsilon^2/mRe_1$ from the film's lubrication equations. Equating these orderings with those derived from the no-slip condition gives $J/Re_1 \sim 1/\varepsilon^2$. This is the scaling relation necessary in order to obtain the non-trivial base state and the corresponding stability analysis. Let us turn to the core scalings. So as to over-determine neither to film nor the core problem, there needs to be a balance between core and film quantities in either the tangential stress condition or the continuity of axial velocity at the interface. The former case leads to a trivial solution to leading order in the core. Thus, the continuity of the axial velocities at the interface gives the $\bar{W}'$ scale. The lack of r-z scale separation in the core then determines that $\bar{W}'$ and $\bar{U}'$

are both of order $\sigma\varepsilon/m$ and $\overline{P}' \sim \sigma\varepsilon/m\,Re_1$. Based on such scalings, the leading order tangential stress balance is dominated by the film flow. As we shall see, the corrugated base state is film-determined as in Hammond's analysis, and the core flow just slaves that of the film.

There are two different consistent situations of interest here. First, we consider slow fluid motions and large surface tension, i.e., $Re_1 \sim \varepsilon$ and $J \sim 1/\varepsilon$, and then order one flows and very large surface tensions $Re_1 = O(1)$ and $J \sim 1/\varepsilon^2$ corresponding to moderate fluid motions. In the former case, the core's inertia is negligible and the core flow is governed by the Stokes equation. In the latter, the core's inertia enters in a perturbative manner and its flow pattern is expected to be expressible in terms of Kummer's hypergeometric function. However, as previously mentioned, due to the core-slaving of the film, these cases differ in their core flow patterns but have identical film flows. Accordingly, the surface tension number J and Reynolds number always appear in the film solution as J/Re_1, i.e., together and not individually. In the present work, we concentrate on the creeping flows corresponding to the former case.

For $Re_1 \sim \varepsilon$, $J \sim 1/\varepsilon$, we posit regular perturbation expansions and substitute these quantities into the governing equations and boundary conditions to formulate the leading order steady corrugated flow problem.

3.2 The Leading Order Base Flow

Following the scales outlined, the film flow has the following asymptotic expansions:

$$w = \overline{\overline{w}} + \sigma\varepsilon\overline{w} + O(\sigma^2\varepsilon,\ \sigma\varepsilon^2), \tag{3.2a}$$

$$u = \sigma\varepsilon^2\overline{u} + O(\varepsilon^2\sigma^2, \varepsilon^3\sigma), \tag{3.2b}$$

$$p = \overline{\overline{p}} + \frac{\sigma}{\varepsilon^2}\overline{p} + O(\frac{\sigma^2}{\varepsilon^2}, \frac{\sigma}{\varepsilon}). \tag{3.2c}$$

For the core,

$$W = \overline{\overline{W}} + \sigma\varepsilon\overline{W} + O(\varepsilon\sigma^2, \varepsilon^2\sigma), \tag{3.2d}$$

$$U = \sigma\varepsilon\overline{U} + O(\varepsilon\sigma^2, \varepsilon^2\sigma), \tag{3.2e}$$

$$P = \overline{\overline{P}} + \sigma\overline{P} + O(\sigma^2, \varepsilon\sigma), \tag{3.2f}$$

where $\overline{\overline{\ }}$ denotes the uncorrugated base state which is a two-fluid Poiseuille flows and has a uniform gradient in each region and $\overline{\ }$ denotes the corrugated base state correction. Substituting (3.1a), (3.1b) and (3.2a)-(3.2f) into the governing equations (2.1a)-(2.1c) and boundary conditions (2.2a)-(2.2f) expanded around the uncorrugated state (σ=0), eliminating the zeroth order of corrugation and letting $Re_1 = \varepsilon\lambda$ and $J = J_0/\varepsilon$, where λ and J_0 are $O(1)$, gives the leading order equations in σ and ε:

For the film,

$$0 = -\overline{p}_z + \frac{m}{\lambda}\frac{\partial^2\overline{w}}{\partial y^2}, \tag{3.3a}$$

$$0 = \overline{p}_y, \tag{3.3b}$$

$$-\frac{\partial\overline{u}}{\partial y} + \frac{\partial\overline{w}}{\partial z} = 0. \tag{3.3c}$$

For the core,

$$0 = -\overline{P}_z + \frac{1}{\lambda}\nabla^2\overline{W}, \tag{3.3d}$$

$$0 = -\overline{P}_r + \frac{1}{\lambda}\nabla^2\left(\overline{U} - \frac{\overline{U}}{r^2}\right), \tag{3.3e}$$

$$\frac{1}{r}\frac{\partial}{\partial r}(r\overline{U}) + \frac{\partial}{\partial z}\overline{W} = 0. \tag{3.3f}$$

The boundary conditions become the following:

At $y = 0$ (the $\sigma = 0$ wall),

$$\overline{w} = \frac{2\phi}{m}, \ \overline{u} = 0. \tag{3.4a}$$

At $r = 1$ or $y = 1$ (the $\sigma = 0$ interface), the velocities are continuous :

$$\overline{W} - 2\eta = \overline{w} - \frac{2}{m}\eta, \overline{U} = 0. \tag{3.4b}$$

Tangential stress : $$m\frac{\partial \overline{w}}{\partial y} = 0, \tag{3.4c}$$

Normal stress : $$\overline{p} = \frac{J_0}{\lambda^2}(\eta_{zz} + \eta), \tag{3.4d}$$

Kinematic condition: $$\overline{u} = \frac{2}{m}\eta_z \ , \tag{3.4e}$$

At the center line,

$$\text{as } r \to 0, \ \overline{W} \text{ and } \overline{U} \text{ are bounded.} \tag{3.4f}$$

The solution of (3.3), subject to (3.4a) and (3.4c), is the film's velocity profile in terms of the prescribed wall function ϕ and the unknown interface function η :

$$\overline{w}(y,z) = \frac{\lambda}{m}\overline{p}_z\left(\frac{1}{2}y^2 - y\right) + \frac{2}{m}\phi(z) \ , \tag{3.5a}$$

$$\overline{u}(y,z) = \frac{\lambda}{m}\overline{p}_{zz}\left(\frac{1}{6}y^3 - \frac{1}{2}y^2\right) + \frac{2}{m}\phi_z(z)y \ . \tag{3.5b}$$

By substituting the film's velocity and pressure into the static kinematic condition (3.4e) and integrating once dz, one gets an equation for the leading order static interfacial deflection

$$\frac{J_0}{3m\lambda}(\eta_{zzz} + \eta_z) + \frac{2}{m}\eta = \frac{2}{m}\phi. \tag{3.6}$$

We retain the common factor m for our discussion of the physical meanings of the terms in (3.6) later in the stability analysis. Note that, when deriving (3.6), an additional constant of integration appears. To see that one can, without loss of generality, choose it to be zero, note that the film's flow rate Q is

$$Q/2\pi = \int_{S_b}^{R_2} w(r,z)rdr = \int_{-\sigma\phi}^{1-\sigma\eta}\left[\overline{w}(y) + \overline{w}(y,z)\right]dy$$

$$= \frac{\varepsilon^2}{m} + \sigma\varepsilon^2\left(-\frac{J_0}{3m\lambda}(\eta_{zzz} + \eta_z) + \frac{2}{m}(\phi - \eta)\right) + O(\varepsilon^3,\ \varepsilon^2\sigma^2,\ \varepsilon^3\sigma). \qquad (3.7)$$

The leading order in (3.7) comes from the shear flow at $\sigma = 0$, and the leading order deviation due to corrugation is just the constant of integration from (3.6). Choosing it to be zero retains the $\sigma = 0$ flow rate. Alternatively, we can leave the $\sigma \neq 0$ flow rate on prescribed and absorb the arbitrary constant C by redefining η as $\eta' = \eta + \frac{m}{2}C$.

The perturbation pressure gradient drives a perturbed base flow through the interfacial deflection. Since the fluids are viscous, a shear stress in the core fluid balances this pressure gradient, thereby retarding the core's motion. One expects the deflection η of the interface to be independent of the viscosity ratio m, since both the normal and the tangential components of the stress conditions are film-dominated, i.e., contain only film variables to leading order. Observe also from (3.6) that the interface will be out of phase with the wall: shear tends to align the interface and the wall, whereas the interfacial tension (in J_0) introduces a phase-shift motion. As expected, the higher the interfacial tension, the higher the interface-wall phase shift.

From the solution of (3.6) for the shape function η of the interface, one can obtain the complete solution for the film by plugging into (3.5a) and (3.5b). The solution to (3.6) should be a linear combination of a homogeneous and a particular solution. However, since the wave number of the homogeneous solution is complex, we set its coefficients to zero because otherwise the homogeneous solution would lead to an unbounded interface as $|z| \to \infty$. We therefore only retain the particular solution. If the wall function ϕ is periodic to the leading order in the corrugated base flow, the interface should also be periodic and have the same periodicity as the wall. Thus, we consider a trial solution of the form $\eta = c_1 cos(kz) + c_2 sin(kz)$, or $(\phi,\ \eta) = \left(\hat{\phi},\ \hat{\eta}\right)exp(ikz) + \left(\hat{\phi}^*,\ \hat{\eta}^*\right)exp(-ikz)$. Thus,

$$\hat{\eta} = \frac{1}{1 + \frac{J_0}{6\lambda} ik\left(1 - k^2\right)} \hat{\phi}. \tag{3.8}$$

For the core flow at the leading order of the corrugation, define a stream function $\overline{\Psi}$ such that

$$\overline{W} = \frac{1}{r}\frac{\partial \overline{\Psi}}{\partial r} \quad , \quad \overline{U} = -\frac{1}{r}\frac{\partial \overline{\Psi}}{\partial z}. \tag{3.9}$$

$\overline{\Psi}$ satisfies the creeping flow equations

$$E^2 E^2 \overline{\Psi} = 0, \tag{3.10}$$

where $E^2 = \frac{\partial^2}{\partial r^2} - \frac{1}{r}\frac{\partial}{\partial r} + \frac{\partial^2}{\partial z^2}$, and is subject to (3.4b) and (3.4f).

Since η is already known in terms of ϕ, one can solve the core flow for $\overline{\Psi} = \hat{\Psi}(r)\exp(ikz)$ to get

$$\hat{\Psi}(r) = ArI_1(kr) + Br^2 I_0(kr), \tag{3.11}$$

where

$$A = \frac{1}{(2-k)I_0(k) + kI_1(k)}\left(-\frac{I_0(k)}{I_1(k)}\left((2+1/m)\hat{\eta} - \frac{1}{m}\hat{\phi}\right)\right), \tag{3.12a}$$

$$B = \frac{1}{(2-k)I_0(k) + kI_1(k)}\left((2+1/m)\hat{\eta} - \frac{1}{m}\hat{\phi}\right), \tag{3.12b}$$

and $I_1(kr)$ and $I_0(kr)$ are the modified Bessel functions of orders 0 and 1.

The core velocities follow from (3.9). We can summarize the corrugated base flow patterns for each fluid for an arbitrary $O(1)$ wall function $\phi(z)$ in the case $Re_1 \sim \varepsilon$, $J \sim 1/\varepsilon$ as follows:

For the film,

$$w_b = \overline{\overline{w}} + \overline{w} = \frac{2\varepsilon}{m} y + O(\varepsilon^2) + \varepsilon\sigma\left(\frac{J_0}{m\lambda}(\eta_{zz} + \eta_z)\left(\frac{1}{2}y^2 - y\right) + \frac{2}{m}\phi\right) + O(\varepsilon^2\sigma, \sigma^2\varepsilon), \tag{3.13a}$$

$$u_b = \bar{u} = \varepsilon^2\sigma\left(\frac{J_0}{m\lambda}(\eta_{zzz}+\eta_z)(\frac{1}{6}y^3-\frac{1}{2}y^2)+\frac{2}{m}\phi_z y\right)+O(\varepsilon^3\sigma,\sigma^2\varepsilon^2), \tag{3.13b}$$

$$p_b = \bar{\bar{p}}+\bar{p} = \bar{\bar{p}}+\frac{\sigma}{\varepsilon^2}(\eta+\eta_{zz})+O(\frac{\sigma}{\varepsilon},\frac{\sigma^2}{\varepsilon}); \tag{3.13c}$$

for the core,

$$\begin{aligned} W_b &= \bar{\bar{W}}+\bar{W} \\ &= 1-r^2+\frac{2\varepsilon}{m}r^2 \\ &+\varepsilon\sigma\frac{1}{F(k)}\left((2+\frac{1}{m})\eta-\frac{1}{m}\phi\right)\left(-\frac{I_0(k)}{I_1(k)}kI_0(kr)+2I_0(kr)+krI_1(kr)\right)+O(\varepsilon^2\sigma,\varepsilon\sigma^2), \end{aligned} \tag{3.13d}$$

$$U_b = \bar{U} = -\varepsilon\sigma\frac{1}{F(k)}\left(-\frac{I_0(k)}{I_1(k)}I_1(kr)+rI_0(kr)\right)\left((2+\frac{1}{m})\eta_z-\frac{1}{m}\phi_z\right)+O(\varepsilon^2\sigma,\varepsilon\sigma^2), \tag{3.13e}$$

$$P_b = \bar{\bar{P}}+\bar{P} = \bar{\bar{P}}+\sigma\frac{1}{F(k)}\left((2+\frac{1}{m})\eta-\frac{1}{m}\phi\right)\left(-\frac{I_0(k)}{I_1(k)}C(k)+D(k)\right)+O(\varepsilon\sigma,\sigma^2), \tag{3.13f}$$

where

$$C(k) = \frac{k^2}{2}(I_2(kr)-I_0(kr))+\frac{I_1(kr)}{r},$$

$$D(k) = (2-2k)I_0(kr)+(\frac{2}{r}-k^2r)I_1(kr)+I_2(kr),$$

$$F(k) = (2-k)I_0(k)+kI_1(k).$$

In the above solution, the base flow is film-determined and the core slaves the film. For a moderate flow $Re_1 \sim O(1)$, $J \sim 1/\varepsilon^2$, the perturbed pressures $\bar{p}' \sim \sigma/\varepsilon$ rather than $\sim\sigma/\varepsilon^2$ and $\bar{P}' \sim \sigma\varepsilon$ rather than $\sim\sigma$ in the film and core, respectively, and the perturbed velocities retain the same orderings as earlier. As a result, the formulation of the film problem remains unchanged, whereas that of the core flow will be altered. Let $J = J_0/\varepsilon^2$ and $Re_1 = \lambda$. We give only the corresponding core flow equations, which are

$$-2r\overline{U}+\left(1-r^2\right)\overline{W}_z=-\overline{P}_z+\frac{1}{\lambda}\nabla^2\overline{W}, \tag{3.14a}$$

$$\left(1-r^2\right)\overline{U}_z=-\overline{P}_r+\frac{1}{\lambda}\left(\nabla^2\overline{U}-\frac{\overline{U}}{r^2}\right), \tag{3.14b}$$

and the continuity equation is (3.3f).

We can again introduce the streamfunction used earlier to eliminate $\overline{P}$ to obtain

$$\left(1-r^2\right)\frac{\partial}{\partial z}\left(E^2\overline{\Psi}\right)=E^2E^2\overline{\Psi}. \tag{3.15a}$$

Following Papageorgiou *et al.* (1990) one can solve the core in terms of Kummer's confluent hypergeometric function $M\left(b,2,2ar^2\right)$(Abramowitz & Stegun 1972), where

$$a=\frac{1}{2}(k\lambda)^{1/2}e^{-i\pi/4} \text{ and } b=1+k^2/8a-a/2.$$

The solution for the Fourier Transform of the streamfunction in the core is

$$\hat{\Psi}(r)=A_1(k)rI_1(kr)+B_1(k)rN_1(kr), \tag{3.15b}$$

$$A_1(k)=\frac{\left((2+1/m)\hat{\eta}-\hat{\phi}/m\right)N_1(k)}{k\left[N_1(k)I_0(k)-N_2(k)I_1(k)\right]},$$

$$B_1(k)=-\frac{\left((2+1/m)\hat{\eta}-\hat{\phi}/m\right)I_1(k)}{k\left[N_1(k)I_0(k)-N_2(k)I_1(k)\right]},$$

$$N_1(kr)=\int_0^r\left[I_1(k)K_1(kt)-I_1(kt)K_1(kt)\right]t^2e^{-at^2}M\left(b,2,2at^2\right)dt,$$

$$N_2(kr)=\int_0^r\left[I_0(k)K_1(kt)+I_0(kt)K_1(kt)\right]t^2e^{-at^2}M\left(b,2,2at^2\right)dt.$$

3.3 Results Pertaining to the Leading Order Base Flow

Since we only consider the particular solution, the base flow in the corrugated configuration exhibits the same periodicity as the wall. Because the film is very thin, its inertia is negligible (this is a consequence of its lubrication flow) and the corrugation of the wall propagates into the flow via the viscous shear and the perturbation pressure. Typical

streamlines in the film are shown in Figure 2. The streamlines are almost in phase with the wall (no-slip) near the wall and become increasingly out phase with increasing y. In addition, the magnitude of the spatial oscillation of streamlines decreases with increasing distance from the wall in the film due to the interface's resistance to being corrugated. To understand the key features of the base flow, consider the amplitude of η and the interface -wall phase shift θ

$$Amp = \frac{1}{\sqrt{1+\left[\frac{J_0}{6\lambda}\, k\left(1-k^2\right)\right]^2}}, \tag{3.16}$$

$$\theta = tan^{-1}\left(-\frac{J_0}{6\lambda}\, k\left(1-k^2\right)\right). \tag{3.17}$$

Figures 3(a) and (b) show how Amp and θ depend on the wave number k of the wall, respectively. We also compare these results with Wang's analysis of a film of a single viscous fluid flowing down a wavy inclined plate in the thin film limit. For zero interfacial tension, $\hat{\eta} = \hat{\phi}$ and the interface and the wall remain in phase and of equal amplitude for all k. For infinite interfacial tension, $\hat{\eta} = 0$, and the interface remains $r = 1$ for all k. For fixed, finite interfacial tension, the interfacial deflection or deformation becomes smaller as k increases, i.e., capillarity resists short wave corrugations.

The phase shift reflects the relative effect of capillarity and shear. Recall that if (3.6) contained only a shear flow contribution, the interface would be in phase with the wall. However, derivatives from the capillary terms induce a phase shift, and thus the shorter waves (large k), the larger the phase shift. Also, short axial waves do not see the circumferential curvature and thus reduce our case to the planar result.

In the absence of capillarity, $\eta = \phi$. An in-phase and equal-amplitude wall-interface configuration means that the film flow is locally parallel. Capillarity resists short waves interfacial corrugations as seen by the first term in (3.6) partially balancing the wall corrugation's effect on the interface. Let us now examine physically why capillarity induces

a phase shift. Consider the film's flow rate calculated via (3.7) and evaluated at a node of $\phi(z)$ where the wall's corrugation does not directly cause a net flow across this z-cut. That is, we require the corrugation to leave the flow rate unchanged to leading order. This yields an equation of the form $f(\eta, \eta_z, \eta_{zzz}) = 0$. If ϕ and η are periodic and in phase, this latter equation has no unknowns for a fixed k and cannot, in general, be satisfied. On the other hand, if η and ϕ are periodic and of the same form but with a phase angle α between them, then $f(\eta, \eta_z, \eta_{zzz};\alpha) = 0$ allows solution for the phase angle α. Consider a simple $sin(kz)$ shape. Then, for short waves, the longitudinal contribution, which goes as $k^3 cos(kz)$, dominates the circumferential contribution of $-k cos(kz)$ to give the planar result. However, for long waves, the latter dominates and lead to a negative phase shift. The magnitude of this phase shift increases as the interfacial tension increases.

The special case $k = 1$ results in the circumferential and longitudinal curvature contributions balancing and thus in $\eta = \phi$. Thus the interface shape again exactly follows the wall and the flow pattern is locally parallel. As we shall see, the corresponding linear stability for this particular case is the same as that for the uncorrugated case to leading order in ε.

Since this discussion focuses exclusively on the film, it applies equally well to the case of $O(1)$Reynolds number and very high interfacial tension $O(1/\varepsilon^2)$, where the capillary force again appears as $J/Re_1 \sim O(1/\varepsilon^2)$. As we shall see below, the corresponding linear stability analysis will also not rely on details of the core's dynamics and both cases will be governed by the same interfacial evolution equation. Thus the cases differ only in the core's dynamics.

The above analysis is based on the scaling $J/Re_1 = 1/Ca \sim 1/\varepsilon^2$, where the Capillary number $Ca = \mu_1 \overline{\overline{W}}(r = 0)/\gamma = Ca_0 \varepsilon^2$. As we shall see, the linear stability equation corresponding to small Ca_0 is similar (to the leading order in ε) to a linearized version of

Hammond's (1983) problem with no base flow. If $\varepsilon^2 J/Re_1 >> 1$, then the surface tension will dominate (p_z will dominate w_{rr} in the equation of motion), and to leading order in σ, the base flow interface will simply be cylindrical and the wave number of a disturbance $\alpha = 1$ will be a neutral mode. If $\varepsilon << \varepsilon^2 J/Re_1 << 1$, capillarity will not affect the interface's shape ($\eta = \phi$) to leading order (w_{rr} will dominate the equation of motion). These results agree with simply taking the corresponding limit of (3.6).

4. Linear Stability

4.1 Scalings

With the asymptotic, steady base flows derived above, we now begin the corresponding asymptotic linear stability analysis. Let us introduce an infinitesimal, axisymmetric disturbance of size δ ($\delta << \sigma, \varepsilon$) at the steady interface in such a way that $S(z,t) = S_b(z) + \delta\xi(z,t)$, where $S_b(z)$ is the interface of the corrugated base state and $\xi(z,t)$ is an unknown order-one function responsible for the disturbance. In analogy to the procedure used in treating the base flows, we first estimate the scalings of the disturbed quantities before formulating the perturbation scheme. If (w',u',p') and (W',U',P') represent the disturbed quantities for the film and the core, respectively, then following Georgiou *et al.* (1992), one can estimate the scalings of these quantities in the case of $Re_1 \sim \varepsilon$ and $J \sim 1/\varepsilon$ from the scaling relations used in the base flows and from the governing equations and boundary conditions. From the normal stress condition, $p' \sim \delta/\varepsilon^3$. Balancing w' with p' in the lubrication equations in the film gives $w' \sim \delta$, and $u' \sim \varepsilon\delta$ follows by continuity. By reasoning similar to that in the base flow for the core, both W' and U' are order δ, and P' is order δ/ε. As we shall see below, by plugging the appropriate asymptotic expansions into the governing equations and boundary conditions

and extracting the corrugated base flow's contribution from these equations, one can derive a set of equations that govern the system's stability to leading order in δ .

4.2 Formulation of the Linear Stability

Recall that the base flow at leading order in σ and ε satisfies the leading order (also in σ and ε) dynamic equations and boundary conditions exactly. Thus, at zeroth order in δ, one should recover the base flow. The linear stability of the system appears at first order in δ, after one extracts the base state relations.

Following the above scalings, and noting that the primed quantities all depend on in principle σ and ε, we define the following asymptotic expansion for the disturbed flow quantities:

For the film,

$$w = \bar{w} + \delta w', \; u = \bar{u} + \varepsilon\delta u', \; p = \bar{p} + \frac{\delta}{\varepsilon^3} p', \qquad \text{(4.1a, b, c)}$$

and for the core,

$$W = \bar{W} + \delta W', \; U = \bar{U} + \delta U', \; P = \bar{P} + \frac{\delta}{\varepsilon} P, \qquad \text{(4.1d, e, f)}$$

where the bar quantities denote the base flow quantities, which have nontrivial σ and ε expansions. If the asymptotic series converge, full knowledge of this base state to all orders in σ and ε provides an exact solution of the nonlinear, steady state Navier-Stokes equation subject to the corrugated boundary's conditions. We have only solved the base flow asymptotically and have thus far only determined its leading order contributions explicitly. However, when substituting (4.1) into (2.1) and (2.2), we will use the fact that the full steady state solution satisfies the steady state equations and boundary conditions exactly and its truncated solutions satisfy these equations/conditions exactly up to the order of truncation; this will allow us to retain only terms of $O(\delta)$ and lower. The coefficients will only contain explicit contributions from the leading order corrugated base flow. As

such, this step can be achieved without knowing any details of the higher order solutions of the base state.

The film's governing equations become

$$0 = -p'_z + \frac{m}{\lambda} w'_{yy}, \tag{4.2a}$$

$$0 = p'_y, \tag{4.2b}$$

$$-u'_y + w'_z = 0, \tag{4.2c}$$

For the core,

$$0 = -P'_z + \frac{1}{\lambda}\nabla^2 W', \tag{4.2d}$$

$$0 = -P'_r + \frac{1}{\lambda}\left(\nabla^2 U' - \frac{U'}{r^2}\right), \tag{4.2e}$$

$$\frac{1}{r}(rU')_r + W'_z = 0, \tag{4.2f}$$

subject to the boundary conditions below.

On the wall:

$$y = -\sigma\phi, \quad w' = 0, \quad u' = 0. \tag{4.3a}$$

At the interface, one expands around the base state interface $S_b(z)$. The leading terms in ε and δ for each boundary condition, after one eliminates the contributions from the base flows, are the following:

The continuity of the velocity components at the interface contributes the following $O(\delta)$ terms:

$$-\xi\left(\frac{2}{m} + \sigma\bar{w}_y^{(1)}\right)_{y=1} + w'(y = 1 - \sigma\eta) = -2\xi + W'(r = 1) + O(\sigma\varepsilon),$$

$$U'(r = 1) = O(\varepsilon). \tag{4.3b}$$

The tangential stress leads with $O(\delta/\varepsilon)$ and is dominated by the film :

$$-w'_y(y = 1 - \sigma\eta) + \sigma\xi\bar{w}_{yy}^{(1)}(y = 1) = O(\varepsilon), \tag{4.3c}$$

Note that the base film flow causes an $O(\delta\,\sigma/\varepsilon)$ perturbation in the tangential stress at the interface due to the corrugation. In order to bring this effect of corrugation into the leading order and at the same time to avoid any coupling with the core (i.e., $O(\delta\,\sigma/\varepsilon)>>O(\delta)$), we also assume $\sigma >> \varepsilon$.

Here again, the leading $O(\delta)$ normal stress balance condition has a contribution only from the film:

$$\text{at } y = 1-\sigma\eta,\ p' = \frac{J_0}{\lambda^2}\left(\xi_{zz}+\xi\right)+O(\sigma\varepsilon). \tag{4.3d}$$

Note that unlike (4.3b) and (4.3c), the normal stress condition for the disturbed interface does not contain the base flow (neither its interface nor its pressure) at leading order. From the normal stress (2.2d), the curvature κ can be split up as:

$$\kappa = \kappa_b + \kappa',$$

where

$\kappa_b = \left[S_{bzz} - \frac{1}{S_b}\left(1+S_{bz}^2\right)\right]\left(1+S_{bz}^2\right)^{-3/2}$ represents the curvature arising from the base state's interface S_b, and the disturbed curvature is

$$\kappa' = \delta\left\{\xi_{zz}+\frac{\xi}{S_b^2}\left(1+S_{bz}^2\right)-\frac{2}{S_b}S_{bz}\xi_z-\xi_z S_{bz}\left[\frac{S_{bzz}}{\left(1+S_{bz}^2\right)}-\frac{1}{S_b}\right]\right\}\left(1+S_{bz}^2\right)^{-3/2}+O(\delta^2).$$

The corrections to (4.3d) deriving from κ' are of order $\sigma\varepsilon$ or higher and are thus not retained.

Finally, the leading order $O(\delta)$ of the kinematic condition gives

$$\begin{aligned}&-\sigma\varepsilon\,\bar{u}_y^{(1)}(y=1)\cdot\xi+\varepsilon u'(y=1-\sigma\eta)\\&=\xi_t+\left(\frac{2\varepsilon}{m}(1-\sigma\eta)+\sigma\varepsilon\bar{w}^{(1)}(y=1)\right)\xi_z+\left(-\frac{2}{m}\xi+w'(y=1)\right)\sigma\varepsilon\eta_z+O(\varepsilon^2).\end{aligned} \tag{4.3e}$$

This suggests introducing a long time scale $\tau = \varepsilon t$ to eliminate ε from the leading order kinematic condition.

At the central line,

$$\text{as } r \to 0,\ W' \text{ and } U' \text{ remain bounded} \tag{4.3f}$$

Solving for w' and u' from (4.2a)-(4.2c) gives

$$w' = \frac{\lambda}{2m} p'_z y^2 + Cy + D, \tag{4.4a}$$

$$u' = \frac{\lambda}{6m} p'_{zz} y^3 + \frac{1}{2} C_z y^2 + D_z y + E, \tag{4.4b}$$

where $C = -\frac{\lambda}{m} p'_z (1 - \sigma\eta) + O(\sigma^2)$, $D = -\frac{\lambda}{m} p'_z \sigma\phi + O(\sigma^2)$ and $E = O(\sigma^2)$. We substitute (4.4) into (4.3e) to derive an asymptotic form of the film's evolution equation inclusive of corrugation. With the knowledge of the steady corrugated base flow (3.5) and the corresponding interfacial shape determined by equation (3.6), the kinematic condition (4.3e) yields the following leading order interfacial evolution equation involving corrugation that describes the linear stability of the system:

$$\xi_\tau + \frac{2}{m}\xi_z + \frac{J_0}{3m\lambda}(\xi_{zz} + \xi)_{zz} + \sigma\left[(\eta - \phi)\cdot\left(\frac{4}{m}\xi - \frac{J_0}{m\lambda}(\xi_{zz} + \xi)_z\right)\right]_z + O(\varepsilon, \sigma^2) = 0. \tag{4.5}$$

This equation consists of an $O(1)$ straight tube contribution and of a new $O(\sigma)$ term in square brackets arising from the (small) corrugation. Recall that we have assumed $\sigma >> \varepsilon$ to bring the corrugation into the leading orders. The dependence on the corrugation is reflected by the variation of the base film's thickness $(\eta - \phi)$, which is given by the solution to (2.8).

4.3 Analysis of the Linear Stability

To order $\sigma\varepsilon\delta$, the interfacial evolution equation (4.5) derived for $J \sim 1/\varepsilon$, $Re_1 \sim \varepsilon$ does not contain core quantities, just the wall and base flow interface functions $\phi(z)$ and $\eta(z)$. The equations for the film velocities u' and w' are explicit in ϕ and η and are

immediately determined by the solution $\xi(z,\tau)$. Calculation of U' and W' require knowledge of u' and w'. The core's dynamics slave those of the film.

For σ=0, i.e., the uncorrugated limit, (4.5) gives,

$$\xi_\tau + \frac{2}{m}\xi_z + \frac{J_0}{3m\lambda}(\xi_{zzz} + \xi_{zz}) = 0. \tag{4.6}$$

This agrees with Georgiou *et al.* (1992) in the case of $F = -1$ and $l = 1$ (their notation, i.e., in absence of gravity and density stratification). For $\sigma \neq 0$, equation (4.5) is a partial differential equation involving the quantity $(\eta - \phi)$, the film thickness deviation in the steady corrugated base flow. In the special case of k=1, the film thickness is uniform (i.e., $\eta = \phi$, and thus there is no corrugation correction) and flow pattern is locally parallel; thus the linear stability is the same as the case of σ=0 at the leading order in ε.

Before considering the detailed response of the system to a general disturbance, we examine the limiting cases of very long waves and very short waves. Since the wavelength of the disturbance may be modified by its interaction with the corrugation, the dominant wavelength(s) may vary during the system's evolution from a monochromatic disturbance. Whether the wavelength of the system's response lies in one of these extreme regimes depends on the corrugation size σ, initial wavelength $2\pi/\alpha$ of the disturbance, the wavelength $2\pi/k$ of the wall, and the time scale of interest. For instance, as we shall see, a disturbance with a very short wavelength can interact with a comparably short wavelength wall; the resulting wavelength remains very short for short times, but at long times, as we shall see below, may result in a long wavelength response.

(i) *Long wave limit*

To examine the long wave regime ($\alpha << 1$), we introduce the long length scale $z \sim O(1/\alpha) >> 1$ by the new $O(1)$ variable $x = \alpha z$. It follows that $\frac{\partial}{\partial z} = \alpha \frac{\partial}{\partial x} \sim O(\alpha) << 1$.

Using this new space variable and expanding (or using Yih's 1967 technique on) (4.5) in powers of α up to $O(\alpha^2)$ gives:

$$\xi_\tau + \sigma(\eta-\phi)_z \frac{4}{m}\xi + \alpha\left[\frac{2}{m}\xi_x + \sigma(\eta-\phi)\frac{4}{m}\xi_x - \sigma(\eta-\phi)_z \frac{J_0}{m\lambda}\xi_x\right] + \alpha^2\left[\frac{J_0}{3m\lambda}\xi_{xx} - \sigma(\eta-\phi)\frac{J_0}{m\lambda}\xi_{xx}\right] + O(\sigma\alpha^3, \alpha^4) = 0 \quad (4.7a)$$

Note that the corrugation term $(\eta-\phi)_z$ still varies over the length scale $2\pi/k$ of the corrugated wall. If $\alpha >> \sigma$, the disturbance will not grow until times of $O(\sigma^{-1})$. This agrees with the normal long wave behavior discussed (Hickox 1971, Smith 1989, and Chen & Joseph 1991) extensively in the corrugation-free case σ=0. A non-zero interfacial disturbance induces a temporal variation. For $\alpha \to 0$, (4.7a) becomes

$$\xi_\tau + A(z)\xi = 0, \quad (4.7b)$$

where $A(z) = \sigma(\eta-\phi)_z \frac{4}{m}$. The solution to (4.7b) is

$$\xi(z,\tau) = \xi_0(z)exp(-A(z)\tau), \quad (4.7c)$$

for a step change disturbance $\xi_0(z)$ at $\tau = 0$. Since the base flow's film thickness $\sigma(\eta-\phi)_z$ varies periodically in z, a local negative value can lead to growth. This contrasts with the straight-tube theory where, as $\alpha \to 0$, the Poiseuille base state has no growth. As we shall see in the eigenvalue spectrum, corrugation can excite (unstable) modes other than the σ=0 mode as well.

(ii) *Short wave limit*

This short wave discussion holds only for $\alpha \sim O(1)$ compared with ε, since it is derived from equation (4.5). Equation (4.5) is based on lubrication in the film, which requires length scales $O(z) >> O(r)$. Therefore, the film lubrication breaks down when the disturbance's wavelength is comparable to the film thickness.

For very short waves ($1/\varepsilon >> \alpha >> 1$), we use a stretched variable $x = \alpha z$. Thus $\frac{\partial}{\partial z} = \alpha \frac{\partial}{\partial x} \sim O(\alpha) >> 1$ which, instead of the regular perturbation expansions in Yih's method, leads to a boundary layer type perturbation due to the dramatic variation deriving from the highest (4th) derivative. Then (4.5), in descending orders of α, becomes

$$\xi_\tau + \alpha^4 \left[\frac{J_0}{3m\lambda} \xi_{xxxx} - \sigma(\eta - \phi) \frac{J_0}{m\lambda} \xi_{xxxx} \right] + O(\alpha^3, \sigma\alpha^3) = 0. \qquad (4.8)$$

Since $\alpha >> k$, the corrugation is locally flat with respect to the disturbance. Therefore, the dominant effect in this limit is $O(\alpha^4)$ from the longitudinal capillarity. Its contribution is stabilizing, and the disturbance decays with the time. This argument is valid for a time scale $\tau \le O(\sigma^{-1}\alpha^{-4})$. Otherwise, for longer times as we shall see, higher harmonics from an interaction with the corrugation can cause long wavelengths to develop and thus cause the system to evolve beyond the short wave range.

Note that viscosity stratification contributes a common factor $1/m$ to the spatial operator of the interfacial evolution equation (4.5). This means that the magnitude of the growth rate (including the corrugation correction) decreases as the film fluid becomes more viscous. This is because a more viscous outer fluid retards fluid motion and makes the system more dissipative.

4.4 Methods to Solve for the Film's Evolution

As noted, the inclusion of corrugation leads to a base flow that is no longer parallel (except for $k = 1$) and is non-uniform in the axial direction. This will also lead to a partial differential equation for its linear stability which has non-constant coefficients that vary in the axial direction. For such an equation, the usual Fourier transform methods become much less useful. If we idealize the wall's variation as a sinusoidal profile, one should expect that the resulting base flow will lead to stability equations that will also be spatially

periodic. We shall apply Floquet-Bloch theory to solve this partial differential equation. The basis of this method is a theorem by Floquet which asserts that the solution of a linear ordinary differential equation whose (non-constant) coefficients are periodic with a common period is the product of an exponential and a periodic function, the latter having the same period as the coefficients. In practice, if one introduces, say, a monochromatic Fourier mode $\exp(i\alpha z)$ (α arbitrary) disturbance, one can expect that such a disturbance interacts with the periodic corrugation via the base flow. This interaction causes the disturbance to be modulated as $\exp(i(\alpha \pm k)z)$. The modulated disturbance continues interacting with the periodic base flow and generates further modulated waves as $\exp(i(\alpha \pm nk)z)$ (n =1,2,...). Since each individual wave pattern is clearly not a solution of the interfacial evolution equation, it is reasonable that the overall behavior of numerous modulated disturbances can act as an envelope of a primary $2\pi/\alpha$ – wavelength wave superimposed upon a secondary $2\pi/k$ (and all of its higher harmonics) – wavelength wave. Bloch functions are therefore the appropriate trial functions to describe the above phenomena and are employed instead of Fourier modes for the temporal linear instability analysis.

Below we invoke two procedures using Bloch-type functions. First, we solve an eigenvalue problem deriving from (4.5) and construct a solution to (4.5) using this theorem. Alternatively, we directly solve (4.5) numerically for various fixed initial wavelengths of the interfacial perturbations and see how the interface evolves in the presence of a corrugation. We then compare the results of the two procedures.

4.4.1 Eigenvalue Problem

Define the trial Bloch function expression for $\xi(z,\tau)$ as

$$\xi(z,\tau) = exp(i\alpha z)\sum_{n=-\infty}^{\infty}\hat{\xi}_n\, exp(inkz + \omega\tau). \tag{4.9}$$

Note that, as mentioned, the expression (4.9) is to be an eigenfunction of (4.5). ω is the eigenvalue or the complex growth rate arising in the temporal analysis (i.e., ω is the Laplace transform variable) and, for a monochromatic initial disturbance, α is the primary disturbance's wave number. The prefactor to the sum acts as a modulating factor for the interaction between the disturbed and base flows. Use of (4.9) guarantees a bounded solution in the z (the axial coordinate) domain if (4.9) converges as $n \to \infty$ for each fixed instant τ, and translates (4.5) into an infinite hierarchy of algebraic equations for the coefficients $\hat{\xi}_n$ and ω. If the wall function is a pure mode of wave number k, then from (3.8), $\eta - \phi = \left(\hat{\eta} - \hat{\phi}\right)e^{ikz} + \left(\hat{\eta} - \hat{\phi}\right)^{*} e^{-ikz}$ and this hierarchy becomes

$$\sigma Q^{-}(n)\,\hat{\xi}_{n-1} + (\omega + P(n))\,\hat{\xi}_n + \sigma Q^{+}(n)\,\hat{\xi}_{n+1} = 0, \tag{4.10}$$

where, by defining $\beta(n) = \alpha + nk$,

$$P(n) = \frac{4i}{m}\beta(n) - \frac{J_0}{3m\lambda}\beta^2(n)\left(1-\beta^2(n)\right), \tag{4.11a}$$

$$Q^{+}(n) = i\beta(n)\left(\hat{\eta} - \hat{\phi}\right)^{*}\left[\frac{4}{m} - \frac{J_0}{m\lambda}i\beta(n+1)\left(1-\beta^2(n+1)\right)\right], \tag{4.11b}$$

$$Q^{-}(n) = i\beta(n)\left(\hat{\eta} - \hat{\phi}\right)\left[\frac{4}{m} - \frac{J_0}{m\lambda}i\beta(n-1)\left(1-\beta^2(n-1)\right)\right]. \tag{4.11c}$$

Note that one can express (4.10) in terms of a tridiagonal matrix whose the principal and off-diagonal elements are $P(n)$ and $\sigma Q^{\pm}(n)$, respectively. Note also $\sigma << 1$ means that this matrix is in fact a diagonal matrix perturbed along its principal super and sub-diagonals only. If the wall function is an arbitrary function with period $2\pi/k$, the matrix may, in general, have all non-zero elements. It is worth mentioning that the infinite hierarchy (4.10) has, in general, an infinite number of solutions ω. We seek only the (dominant) eigenvalue – the one with the maximum real part.

(i) *Numerical Solution of the Eigenvalue Problem*

The eigenvalue ω is determined by setting the determinant of (4.10) to zero, and will be a function of J_0, λ, m, k, σ, and α. The determinant gives,

$$D = \begin{vmatrix} \bullet & \bullet & & [0] & \\ \sigma Q^-(n-1) & \omega + P(n-1) & \sigma Q^+(n-1) & & \\ & \sigma Q^-(n) & \omega + P(n) & \sigma Q^+(n) & \\ & & \sigma Q^-(n+1) & \omega + P(n+1) & \sigma Q^+(n+1) \\ & [0] & & \bullet & \bullet \end{vmatrix} = 0. \qquad (4.12)$$

For a truncation at some value of n, one can calculate the eigenvalues of this matrix equation (4.10) numerically. One then increases n until the dominant eigenvalues (not only the dominant *one*) no longer change significantly with n. In addition, as a check, we also apply determinant / matrix perturbation theory in σ to determine the correction to the growth rate as the result of $\sigma \neq 0$. Since (4.9) implies that all wave patterns $(\alpha \pm nk)$ should belong to the same growth rate, as we shall see, since replacing α by $\alpha \pm k$ leaves D in (4.12) unchanged, the eigenvalue spectra are k-periodic in α-space. We thus need only calculate one (the "primary ") branch of the spectrum with respect to that at $\sigma = 0$, and we can then extend it periodically in α.

(ii) *Matrix Perturbation Theory*

By expanding (4.12) in σ, we have

$$D_0 + \sigma^2 D_2 + O(\sigma^4) = 0, \qquad (4.13)$$

where

$$D_0 = \prod_j (\omega + P(j)),$$

$$D_2 = -\sum_n \prod_{j \neq n, n+1} (\omega + P(j)) Q^+(n) Q^-(n+1),$$

Hence we expect that the growth rate ω has an expansion in powers of σ :

$$\omega = \omega_0 + \sigma^2\omega_2 + O(\sigma^4). \tag{4.14}$$

Note that the correction to the growth rate appears with coefficient σ^2 and should require observation times roughly of order $1/\sigma^2$ to be distinguished from the straight tube case. In order to bring the effect of the corrugation into the leading order correction, one requires $\sigma >> \varepsilon^{1/2}$ so that the $O(\varepsilon^2)$ terms that arises from the straight tube PCAF analysis in deriving (4.5) are of higher order than the corrugation terms.

In Appendix I, we carry out the matrix perturbation calculation and find for the dominant eigenvalue

$$\begin{aligned}\omega_2 &= \frac{Q^+(0)Q^-(1)}{P(1)-P(0)} + \frac{Q^+(-1)Q^-(0)}{P(-1)-P(0)} \\ &= \left\|\hat{\eta}-\hat{\phi}\right\|^2 F(0)\left(\frac{F(1)}{P(1)-P(0)} + \frac{F(-1)}{P(-1)-P(0)}\right),\end{aligned} \tag{4.15}$$

where $F(n) = \dfrac{4i\beta(n)}{m} + \dfrac{J_0}{m\lambda}\beta(n)^2\left(1-\beta(n)^2\right)$ is a dispersion expression associated with $\alpha \pm nk$, i.e., by substituting (4.9) for ξ into the $O(\sigma)$ part of (4.5) for an uncorrugated wall. Notice that $\omega_0 = -P(0)$ is the growth rate of the uncorrugated $\sigma = 0$ flow. The expressions $P(\pm1)$, $P(0)$, $F(\pm1)$, and $F(0)$ in (4.15) only involve the interactions between the primary disturbance's wave number α and its first harmonics $\alpha \pm k$. In fact, (4.15) follows simply by truncating (4.12) into a 3×3 matrix with respect to the central element $\omega + P(0)$, expanding the matrix and solving when $\sigma << 1$. The corrugated geometry is reflected by $\sigma\left\|\hat{\eta}-\hat{\phi}\right\|$. The numerators in (4.15) represent the off-diagonal interactions from the $O(\sigma)$ terms of (4.10). The large parenthesis, which we shall call f, in (4.15) can be understood as follows. Write the Laplace transform of (4.5) in operator notation as $\omega\xi + L\xi = 0$ and let $\xi = \xi_0 + \sigma\xi_1 + \sigma^2\xi_2 + O(\sigma^3)$ and $L = L_0 + \sigma L_1 + O(\sigma^2)$. In Appendix II, we redo (4.15) by this method and show that the denominators originate from $L_0\xi_1$. In

particular, they are related to the differences between eigenvalues, which encode information as to the time necessary for growth due to one branch to overtake growth due to the other.

(iii) *Growth Rate Correction in the Long Wave Limit*

Turning once again to the long primary wave regime (i.e., $\alpha << 1$), we can examine the correction to the growth rate in this limit. Its α expansion is

$$\omega_2 = \alpha\omega_2^{(1)} + \alpha^2\omega_2^{(2)} + O(\alpha^3). \tag{4.16}$$

As $\alpha << 1$, $\beta(n) \to \pm nk$. Thus F and f depend only on the wall's wave number k. f is real-valued, and with the convective part $\frac{4i\alpha}{m}$ of $F(0)$, yields an $O(\alpha)$ growth correction of

$$\omega_2^{(1)} = \frac{4i}{m}\frac{\left\|\hat{\eta} - \hat{\phi}\right\|^2}{\Delta}\left(-\frac{2}{3}\left(\frac{J_0}{\lambda}\right)^2 C_k^2 + 16k^2\right). \tag{4.17}$$

Here $C_k = k^2\left(1-k^2\right)$ is the contribution from the curvature of the base flow's interface and $\Delta = \frac{1}{9}\left(J_0/\lambda\right)^2 C_k^{\,2} + 4k^2$. Since the $O(\alpha)$ growth correction is purely imaginary, it is purely dispersive and a correction to the stability first occurs at $O(\alpha^2)$.

$$\omega_{2r}^{(2)} = \left\|\hat{\eta} - \hat{\phi}\right\|^2\left[\frac{J_0}{m\lambda\Delta}\left(-\frac{2}{3}\left(J_0/\lambda\right)^2 C_k^2 + 16k^2\right) + \frac{4}{m\Delta}\left(\frac{8J_0}{3\lambda}C_k + \frac{40J_0}{3\lambda}k^2\left(1-2k^2\right) - \frac{40C_k^2 q}{27\Delta}\right)\right]. \tag{4.18}$$

Here $q = 2k^2(1-k^2)$ is the $\alpha \to 0$ limit of the interaction of capillary terms from α and from $\alpha \pm k$.

4.4.2 Initial Value Problem

In order to confirm the stability behavior predicted by the eigenvalue spectrum discussed above and to see the (linear) dynamics of the interface's evolution, including the modulation of the initial wavelength with time, it is useful to solve the initial value problem directly. To discretize the axial coordinate z, we employ a Bloch-type form in the sense of a spectral method, i.e.,

$$\xi(z,\tau) = \sum_{n=-N}^{N} a_n(\tau)\cos((\alpha+nk)z) + b_n(\tau)\sin((\alpha+nk)z), \tag{4.19}$$

where N is the mode number cutoff, subject to the initial condition $\xi(z,\tau=0) = \cos(\alpha z)$. $a_n(\tau)$ and $b_n(\tau)$ are the amplitude functions that depend on τ. In comparison with the eigenvalue problem, ξ should be a linear combination of all eigenmodes rather than the single mode described in (4.9), i.e.,

$$\xi(z,\tau) = \sum_j c_j \xi_j(z,\tau), \tag{4.20}$$

where $\xi_j(z,\tau) = e^{i\alpha z}\sum_{-\infty}^{\infty}\hat{\xi}_{jn}e^{inkz+\omega_j\tau}$ for the "j" th mode. Therefore, in terms of the initial value problem, $a_n(\tau)$ and $b_n(\tau)$ should contain contributions from all possible eigenmodes and their asymptotic behavior as $\tau \to \infty$ should correspond to the mode of the eigenvalue spectrum with dominant growth rate. Notice that we retain only a finite number of modes. Substituting (4.19) into (4.5) leads to a system of ordinary differential equations for the amplitudes $a_n(\tau)$ and $b_n(\tau)$. We use a 12th order Adam-Moulton algorithm from the IMSL library to solve these ODEs. For a fixed number $2N+1$ of modes, we determine the solutions $a_n(\tau)$ and $b_n(\tau)$ within a 0.1% absolute error tolerance. We keep increasing the number of modes until the spatial evolution at a fixed time no longer changes significantly.

5. Results and Discussion

5.1 Eigenvalue Spectrum

Using the methods outlined above for equation (4.5), we find features of the eigenvalue spectrum that are rather different from those of the straight tube. Since (4.5) is linear, an arbitrary disturbance can be decomposed into a linear combination of functions that spans $L^2(\Re)$, and the solution is the same linear combination of the responses to the functions in this set. If the basis is an eigenfunction basis, then the response to an eigenfunction is just the product of that eigenfunction with its corresponding eigenvalue. In principle, every eigenstate corresponding to each eigenvalue should be taken into account in the response to a disturbance. As we shall see in Figure 4, the character of the eigenvalue spectrum shows the existence of a banded structure in which each band represents a continuous spectrum of the corresponding eigenvalue as a function of the initial disturbance's wave number α. Such structures illustrate k -periodicity in α -space. This is obvious from the k -periodicity of the coefficients in (4.5) or from (4.10).

The eigenvalue spectra (the real parts of eigenvalues here) are shown in Figure 4 for different wall wave numbers with dotted curves (the primary branch) and dashed (the secondary branch) curves. Note that since we introduce a long time scale $\tau = \varepsilon t$, the true eigenvalues should be $\varepsilon\omega$. For comparison, the solid lines in Figures 4 represent the uncorrugated case for $\sigma = 0$. In contrast to the uncorrugated case $\sigma = 0$, most of short wave disturbances give rise to growth. For k >2, there are narrow gaps of stable wave number between the unstable branches in the short wave spectrum. This eigenvalue spectrum represents the direct effects of capillarity and its interaction with the wall's harmonics $(\alpha + nk)$ (i.e., $\omega_r \sim \frac{J_0}{3m\lambda}(\alpha+nk)^2\left(1-(\alpha+nk)^2\right)+O(\sigma^2)$). The maximum growth rate for a given initial disturbance wave number α depends on the relative position of the unstable branches. As we shall see, if the branch with the highest growth rate for α is not the primary branch, the long-time evolution may lead to the dominance of a

wavelength other than α. The initial value calculation in the next section will confirm this behavior. In addition to this effect of the periodic spectrum due to corrugation, there is also an $O(\sigma^2)$ deviation of the primary branch from the straight tube growth rate. This latter correction can displace the critical wave number of the primary branch in either direction from its straight tube value of one.

5.2 Interfacial Evolution & Growth Rate Correction

Figures 5(a) and (b) show the interfacial evolutions at a particular position (z=0) for different sets of initial and the wall wave numbers $(\alpha,k)$with fixed J_0/λ =1, $m=1$ and $|\alpha - k| = 0.5$, corresponding to spectra in Figures 4(a) and (b). Figure 5(a) is the case of an initial long wavelength (α<1) disturbance and evolutions for both shorter and longer times are shown. The interface grows slowly until $\tau \approx 120$ when it begins a noticeable exponential growth. Notice that the frequency of later development is also quicker. Figure 5(b) shows the case upon imposing a short wavelength initial disturbance that would be stable in an uncorrugated tube and has a negative growth contribution from the primary branch. Consequently, the short wave disturbance decays initially; it then interacts with the corrugation (when $\tau \approx 10 \sim 20$) and leads to growth. The change from decaying to growth implies that the *apparent* dominant eigenmode has changed from short to long times due to corrugation. The long-term linear interfacial behavior corresponds to the mode with the dominant growth rate predicted by the eigenvalue spectrum. Thus, to identify which modes contribute to the long-time evolution, we compare the solution of the initial value problem with functional form,

$$A\cos\left(Im\left(\omega_{dominant}\right)\tau + B\right)\exp\left(Re\left(\omega_{dominant}\right)\tau\right), \qquad (5.1)$$

where $\omega_{dominant}$ is the eigenvalue with the largest real part discernible from the eigenvalue spectrum for the given α in Figures 4. We choose the prefactor A and phase

angle B by matching the profile from the moment at which it develops a clearly oscillatory/ exponential pattern. Afterwards, as Figures 5 indicate, the linear growth oscillates as $Im\left(\omega_{dominant}\right)$ and grows as $Re\left(\omega_{dominant}\right)$, as expected. The excellent agreement in Figures 5 shows that $\omega_{dominant}$ belongs to the secondary eigenbranch.

Figures 6(a) and (b) are the spatial evolutions corresponding to Figures 5(a) and (b), respectively. There are a number of wavelengths that contribute to the observed evolution. For a long wave initial disturbance, Figure 6(a1) shows the short time evolutions. The wavelength (~12) that dominates the later evolution is much shorter than the initial wave (~30 for $\alpha = 0.2$). Its wave number of $0.5=|\alpha - k|$ is just the first wall harmonic of the initial disturbance and characterizes the long time (linear) behavior. The evolution for long times is shown in Figure 6(a2). The resulting capillary growth rate numerically matches $\frac{J_0}{3m\lambda}(\alpha-k)^2\left(1-(\alpha-k)^2\right)$ approximately, which is consistent with Figure 5(a).

Similarly, in the case of a short wave initial disturbance in Figure 6(b), the short wavelength disturbance decays at the earlier stage of the evolution, then gradually grows with a longer wavelength. The first harmonic interaction again leads to a predominant first harmonic's wave number of 0.5, but now this wavelength exceeds the initial value $\alpha = 1.2$. Therefore, in contrast to the straight tube, even an initial short wavelength disturbance can lead to the unstable growth of a long wave due to the coupling to its higher wall harmonics through the corrugation. Figure 5(b) clearly indicates the transition between the decaying (primary) mode and growing first harmonic mode. One can understand this transition by expressing the time-dependent solution in terms of all the eigenstates $f_j(z)$ as

$$\xi = a_p f_p(z) e^{\omega_p \tau} + \sum_{\text{branch } j} a_j f_j(z) e^{\omega_{<j>}\tau}. \qquad (5.2a)$$

The subscript p represents the primary branch, which is related to the uncorrugated $\sigma = 0$ stability. $\{a_j\}$ are coefficients determined by the initial condition. Let us consider only the primary and secondary branches

$$\xi \approx a_p f_p(z) e^{\omega_p \tau} + a_2 f_2(z) e^{\omega_{<2>} \tau} \cdots, \tag{5.2b}$$

where, from our analysis $\omega_p = -\frac{2}{m} i\alpha + \frac{J_0}{3m\lambda}\alpha^2\left(1-\alpha^2\right) + O(\sigma^2)$ and

$$\omega_{<2>} = -\frac{2}{m} i(\alpha - k) + \frac{J_0}{3m\lambda}(\alpha - k)^2\left(1-(\alpha-k)^2\right) + O(\sigma^2).$$

By defining the eigenvectors corresponding to the different eigenvalues, one can show that $a_p \sim O(1)$, $a_2 \sim O(\sigma)$. Therefore, the short time evolution is governed by the primary branch. However, the secondary unstable branch can dominate for long times if real(ω_p) < real($\omega_{<2>}$) (note: real(ω_p) < 0 here) and the system stays in the linear regime. A transition that implies there exists a critical time τ^*, when the amplitude of such a growing mode is about $q \sim 1-10$ times that of the primary, i.e., $\sigma\left|e^{\omega_{<2>}\tau}\right| \sim q\left|e^{\omega_p \tau}\right|$, when the growing mode becomes important. Clearly,

$$\tau^* \approx ln\left(q\sigma^{-1}\right)/\text{real}(\omega_{<2>} - \omega_p) \tag{5.3}$$

Therefore, the smaller the corrugation or real($\omega_{<2>} - \omega_p$), the later the transition, and short wave disturbances remain stable longer. The parameter in Figure 5(b) gives $\tau^* \approx 14$ for $q = 10$, which predicts this onset of instability. Note that the time scale $ln(1/\sigma)$ is slower than $O(\sigma^{-1})$ estimated from the evolution equation (4.5).

For $\tau << \tau^*$, the primary branch dominates, and one may be interested in how its growth rate deviates from the $\sigma = 0$ case due to corrugation. Figures 7(a) and (b) show the growth rate deviation $\delta\omega_r$ for the primary branch. The comparison between the numerical and the analytical matrix perturbation results – (4.16) gives its long wave limit – is very

good and verifies that $\delta\omega_r$ is $O(\sigma^2)$ for small enough σ. However, as Figure 7(b) shows, larger wall wave numbers k show larger discrepancies between the numerical and the matrix perturbation results at large σ. Since the off-diagonal elements in (4.10) may grow relative to the principal diagonal ones with increasing k, retaining the determinant perturbation equation (4.13) to $O(\sigma^2)$ is probably no longer adequate. To understand these curves, they should be viewed in conjunction with Figures 7. For k=1.7, the corrugation is slightly stabilizing for long waves ($\alpha \to 0$) and becomes destabilizing for short waves due to the corrugation's excitation of unstable long wave wall-harmonics of the initial short wave disturbance. Since $\delta\omega_r$ therefore crosses zero, i.e., has a neutral point at about $\alpha = 1.4$ for the chosen parameters, and since $\delta\omega_r$ scales to leading order with σ^2, the three curves in Figure 7(a) all cross at $\alpha \approx 1.4$, $\delta\omega_r$=0. This is not the case in Figure 7(b) since, as Figure 4(d) shows, for k=2.7, corrugation is always destabilizing. The non-montonicity of the derivative of $\delta\omega_r$ for Figure 7(b) and not for Figure 7(a) will be taken up below.

Let us now examine how the growth rate correction due to be corrugation varies with the parameter values k and J_0/λ in Figures 8(a) and (b), respectively. These figures again should be viewed in conjunction with Figures 4. There are a few trends worth noting. First, in Figure 8(a), the effect of corrugation disappears (for α not too large) for small k. This simply states that a long wave wall corrugation appears essentially flat relative to a short α-wave disturbance, and thus does not affect its stability. Second, notice that all of the curves in Figures 8 rise sharply for large α. As noted, this corresponds to the destabilization of short wave disturbances via their ability to excite unstable long waves through coupling to higher corrugation harmonics. Thus short α-waves that would be stable in straight tubes are destabilized at order σ^2, as we see for large α. Third, notice that the curves for $k \geq 2$ no longer have monotonic first derivatives. This derives from the fact that the eigenvalue spectra in Figures 4 have α-gaps where the corrugated tube flow is

not unstable. This is not the case for $k < 2$. Note that since corrugation has two effects on the system's stability, the $O(\sigma^2)$ correction to the primary branch as well as the coupling to other branches, the absolute value of the correction in Figures 8 is not just determined by the width of this gap. Finally, both the capillary instability as well as its corrugation correction grow with $J_0/\lambda = 1/Ca_0$. Thus Figure 8(b) shows the correction growing for different values of J_0/λ. This must be compared with the change in the primary branch J_0/λ before drawing conclusions. Notice that the $\alpha \to 0$ correction can change sign both with k and with J_0/λ. Equation (4.18) shows that $\omega_{2r}^{(2)}$'s sign is a balance between the k^2 originating from the shear flow and the factors involving the capillarity contribution $C_k J_0/\lambda$ from the wall's corrugation. The entire corrugation is multiplied by $\left\|\hat{\eta} - \hat{\phi}\right\|^2$, which is zero if the base state maintains a parallel flow as in the k=1 case.

The analysis thus far has presumed $J/Re_1 \sim 1/\varepsilon^2$. However, either a stronger or a weaker scaling for J/Re_1 can significantly change the stability characteristics. Fortunately, as we shall now see, we can extend the previous analysis to both stronger and weaker capillary cases with only minor changes in the analysis.

5.3 Strong Interfacial Tension Case

As discussed earlier in the content of the base flow, a very strong interfacial tension, i.e., $\varepsilon^2 J/Re_1 >> 1$ (here $J_0/\lambda >> 1$) can smooth the base flow's interface. Let $S = J_0/\lambda = \varepsilon^2 J/Re_1$. Recall from eqn (3.6), a strong interfacial tension $S >> O(1)$ generates a flat interface to leading order with a correction one order of S^{-1} higher, i.e., a deviated base state film thickness of $\eta - \phi = -\phi + O(S^{-1})$, due to the flatter interface. Its stability follows from examining (4.5). The convective term (from the film's base flow) $\frac{2}{m}\xi_z$ becomes small relative to capillarity $\frac{S}{3}(\xi_{zz} + \xi)_{zz}$ at $O(\sigma^0)$, and $\frac{4}{m}\xi << \frac{S}{m}(\xi_{zzz} + \xi_z)$

at $O(\sigma)$. For $\sigma S >> O(S^0)$, the base flow is absent from the leading order. Together with the flatter interface, a rescaling of the time variable brings the time derivative to $O(S)$,

$$S\left[\xi_{\tau'} + \frac{1}{3m}(\xi_{zz} + \xi)_{zz} + \frac{\sigma}{m}\left(\phi(\xi_{zz} + \xi)_z\right)_z\right] + O(S^0) = 0. \tag{5.4}$$

Therefore, the interfacial evolution reduces to that of the static, no-flow case to the leading order in ε, which is the linearized form of Hammond's equation (1983) for a corrugated tube. Capillarity dominates over flow, $P(n)$ reduces to $-C(n)$, where $C(n) = \frac{S}{3m}\beta^2(n)\left(1-\beta^2(n)\right)$ (see 4.11) and $\hat{\eta}$ drops out to yield the growth rate correction (4.15) in this large S limit:

$$\omega_2 = \frac{3S}{m}\left\|\hat{\phi}\right\|^2 C(0)\left(\frac{C(1)}{C(0)-C(1)} + \frac{C(-1)}{C(0)-C(-1)}\right) + O(S^0), \tag{5.5a}$$

whose long wave $\alpha \to 0$ expansion is

$$\omega_2 = -6\left\|\hat{\phi}\right\|^2 \frac{S}{m}\alpha^2 + O(\alpha^3) \text{ for } \alpha \to 0. \tag{5.5b}$$

Large k or high tension enhances the effects of $C(\pm 1)$. Here corrugations ($\left\|\hat{\phi}\right\| \neq 0$) make a $O(\sigma^2)$ stabilizing contribution to the $O(1)$ unstable long waves and this contribution is independent of k, except for the implicit dependence through $\left\|\hat{\phi}\right\|^2$. The reason for this stabilization is that for $k >> \alpha$, the corrugation simply adds a short wavelength component to the disturbance, which capillarity stabilizes.

In the absence of the base flow at leading order, an interesting phenomenon occurs. Since ϕ still appears in (5.4), the spectrum will still be k-periodic and there will be points where different branches cross, and thus where (5.5a) breaks down. Obviously, (5.5a) is not applicable there since its denominator becomes comparable to σ^2. This leads to an $O(\sigma)$ resonant correction to the growth rate. Particularly when $k < 2$ and such resonances occur at α in the long wave regime whose the growth rate is positive, the corrugation can

destabilize more significantly than the usual case where the base flow enters leading order. To illustrate, we restrict our attention to $1 < k < 2$ and consider a resonance that occurs at $\alpha = k/2$ in the long wave regime. Since there may be corrections different of orders for a given range of α, we use an iterated perturbation scheme (see Appendix II for details) to solve the following modified determinant equation and to obtain the maximum growth rate in this range of α:

$$\left(\omega - \frac{S}{3m}C(0)\right)\left(\omega - \frac{S}{3m}C(1)\right)\left(\omega - \frac{S}{3m}C(-1)\right) + \sigma^2 G_2(\omega_0) = 0, \qquad (5.6)$$

where $G_2(\omega_0) = -\left(\frac{S}{m}\right)^2 \|\hat{\phi}\|^2 C(0)\left(C(1)(\omega_0 - \frac{S}{3m}C(1)) + C(-1)(\omega_0 - \frac{S}{3m}C(1))\right)$, and ω_0 is the $O(\sigma^0)$ eigenvalue of either the primary $(= -C(0))$ or the secondary branch $(= -C(-1))$. For $\alpha \approx k/2, C(0) \approx C(-1)$, this gives,

$$\left(\omega - \frac{S}{3m}C(0)\right)^2 \approx -\sigma^2 G_2(\omega_0)\left(\omega_0 - \frac{S}{3m}C(1)\right)^{-1},$$

for the $O(\sigma)$ correction to the primary branch. This correction is one order larger in σ than that the correction that occurs when the base flow enters at leading order. A typical growth rate correction for this very high tension case is shown in Figure 9. The comparison between the direct numerical results of the matrix equation (4.12) and those of the asymptotic equation (5.6) is very good and confirms the enhanced unstable correction excited by this resonance.

5.4 Less Strong Interfacial Tension Case

In the straight-tube case, it is well known (Chen & Joseph 1991 and Georgiou *et al.* 1992) that the presence of a strong base flow can prevent the capillary instability where the core flow enters the leading order interfacial stability problem. Let us examine what happens when we decrease the strength of capillarity relative to shear for the corrugated case.

Consider a less strong interfacial tension, e.g., $S = \varepsilon^2 J/Re_1 << 1$, which magnifies the importance of the shear flow. Recall (eqn. (3.6)) that the base interface thereby follows the wall (i.e., $\eta = \phi$) and the film becomes of uniform thickness with a resulting local parallel flow to the leading order in σ and S. For $\varepsilon << S << 1$, the corrugation impacts the leading order stability only indirectly via the deflection of the base flow's film thickness $\sigma(\eta - \phi) \approx -\frac{\sigma S}{6}(\phi_{zz} + \phi) = O(\sigma S)$. An explicit corrugation correction must then be $O(\sigma\varepsilon S)$. We use the constraint $\varepsilon << S << 1$ and the corresponding leading order base flow contribution. Without significant change from the previous analysis, one can expand (4.5) and its base flow in S to obtain following evolution equation:

$$\xi_t + \frac{2}{m}\xi_z + S\left[\frac{1}{3m}(\xi_{zz} + \xi)_{zz}\right] - \sigma S\left[\frac{2}{3m}(\phi_{zz} + \phi_z)\xi\right]_z + O(\varepsilon S, \sigma S^2) = 0. \qquad (5.7)$$

Since there is no translational symmetry due to the wall's corrugation, shear contributes to leading order. Capillarity comes in at $O(S)$ and corrugation at $O(\sigma S)$. The growth rate correction (4.15) in powers of S is

$$\omega_2 = S^2 k^2(1 - k^2)\|\hat{\phi}\|^2 \frac{4i\alpha}{9m} + O(S^3). \qquad (5.8)$$

Corrugation enters ω at $O(\sigma^2 S^2)$ in a purely dispersive manner and becomes non-dispersive only at the very high order $O(\sigma^2 S^3)$; it has very little impact. Higher order contributions such as $O(\varepsilon S)$ from the straight-tube PCAF will be comparable to such corrugation corrections unless $\sigma^2 S^2 >> \varepsilon$, which would be restricted to extremely thin films.

As Georgiou *et al.* (1992) and Papageorgiou *et al.* (1990) have shown, a surface tension $S = \varepsilon^2 J/Re_1 \sim \varepsilon$ couples the core to the leading order interfacial stability, which for $m < 1$ can lead to a shear / viscosity stratification that can stabilizes long waves. In the presence of corrugation, the evolution equation, inclusive of core-coupling (see in Appendix III for details), becomes

$$\xi_\tau + \frac{2}{m}\xi_z + \frac{\varepsilon J_0}{3m\,Re_1}(\xi_{zz}+\xi)_{zz} + \frac{\varepsilon}{2m}\gamma_z - \sigma\varepsilon\left[\left(\frac{2}{3m}(\phi_{zzz}+\phi_z) - \frac{\bar{\gamma}}{2m}\right)\xi\right]_z + O(\varepsilon^2,\sigma^2\varepsilon) = 0. \tag{5.9}$$

where J_0 and Re_1 are $O(1)$, γ and $\bar{\gamma}$ represent the shear coupling from the disturbed and base core flow, respectively. As in (5.7), the correction to the growth rate due to corrugation is $O(\sigma^2\varepsilon^3)$, which is of even higher order than the $O(\varepsilon^2)$ contribution from PCAF theory here and is probably negligible.

5.5 A Wall with Multiple Length Scale Corrugations

Pore waviness usually includes many wavelengths and its shape can be decomposed in terms of Fourier components in such cases. It may lead to multiple modulations due to an eigenvalue spectrum with multiple periodicities. As an example, we consider a wall that has corrugations with two wave numbers, say, ($k1$,$k2$)=(1.6,2.4) and (2.4,3.2). We have chosen these pairs to have the greatest common divisor k=0.8 so as to yield identical long-time dominant waves. The corrugated base flow is simply (eqn. (3.6)) the superposition of the two individual wall wave patterns for the given J_0/λ, m,σ. The corresponding linear stability reduces to a penta-diagonal matrix eigenvalue problem.

$$\sigma Q_2^-(n)\hat{\xi}_{n-n_2} + \sigma Q_1^-(n)\hat{\xi}_{n-n_1} + (\omega + P(n)) + Q_1^+(n)\hat{\xi}_{n+n_1} + \sigma Q_2^+(n)\hat{\xi}_{n+n_2} = 0, \tag{5.10}$$

where $Q_s^\pm(n) = Q^\pm(n,\ k \to k\cdot n_s)$, n_s an integer, for s=1, 2. The traces of the largest eigenvalues as functions of α for both ($k1$,$k2$)=(1.6,2.4) and (2.4,3.2) are shown in Figure 10. Recall from the single wavelength wall, the growth rate of the secondary branch may be higher than that of the primary branch. For $k > 2$ the growth rates have α-bands that are stable and a judicious choice of excitation wavelength α >1 can lead to a stable system response. Figure 10 reveals that, for the pairs of k's chosen, no such gaps persist, despite their appearance in each (2.4 or 3.2) monochromatic wall's spectrum. Moreover, as

$(k1,k2)$=(2.4,3.2) shows, the peaks need not be symmetric.

In order to confirm the above eigenvalue spectra and understand two-wall wavelength interactions, we again adopt the initial value approach. The initial interface profile is $\xi(z,\tau=0)=0.1cos(\alpha z)$. The initial wave number α for both cases is 0.2 within the range in which the growth rate of the primary branch is quite small and the non-primary branch is expected to dominate. The interfacial evolutions at $z=0$ for both $(k1,k2)$=(1.6,2.4) and (2.4,3.2) are shown in Figures 11(a) and (b), respectively. Comparison between the long time evolution of the initial value approach and the maximum growth predicted by the Bloch function method again shows excellent agreement. For $(k1,k2)$=(1.6,2.4), the interface grows slowly before a transition signaling the dominance of the secondary branch occurs at $\tau \approx 80$. The later development shows faster growth and oscillation than the earlier portion. The case of $(k1,k2)$= (2.4,3.2) is similar but the transition occurs at $\tau \approx 50$. Thus the fastest growing modes have been changed after interaction and, as we shall see below, the corresponding wave patterns change concurrently.

The entire interfacial evolutions in the space for both cases are shown in Figures 12(a) and (b). The interfacial evolution grows with the initial wavelength from the primary branch at the earlier stage of evolution, then interacts with the corrugations, where a shorter wavelength with a faster growth takes over for the long times. The wave number of the fastest growing mode is about 0.6 because the initial wave α has been modified to be $|\alpha+k1-k2|$. This wave's growth rate dominates those of the other harmonic modes. It also explains the meaning of the non-primary branch for small α in Figure 10.

5.6 Application to Oil Recovery

As a typical example of a liquid-liquid displacement, consider an oil film of μ_2 = 10cP surrounding a water slug (μ_1 = 1cP) with an interfacial tension of 10 dyne/cm in a $200\mu m$ diameter pore. A typical velocity of slug is about 1 cm/s. Consider a film thickness of

10 μm or $\varepsilon \sim 0.1$. These numbers give $J/Re_1 \sim 1000$ with $Re_1 \sim 1$ and $J \sim 1000$, which is within the range of our analysis. With these parameters, the straight cylindrical pore theory gives a maximum growth rate of 0.5 min^{-1} i.e., about a 1.4 min doubling time, with wavelength 888 μm and a wave speed of 141 μm/s for $\alpha_{max} = 0.707$ with a critical wavenumber of one. Consider a sinusoidal (one-wavelength) corrugation, of small amplitude, say 1.0 μm (still detectable), giving $\sigma = 0.1$, and a wall's wavelength of 350 μm (k=1.8), shorter than the mean pore circumference of 628 μm. Consider now a short wave disturbance of 500 μm or α=1.26 >1, which would be stable in a straight tube. With the given corrugation, this perturbation excites an unstable wave of $\alpha' = |1.26 - 1.8| = 0.54$ or L =1164 μm with a growth rate of 0.4 min^{-1}. This is the major effect of corrugation. In addition, there is a more minor effects from the perturbation of the primary branch which modifies the maximum growth rate to 0.48 min^{-1} and hardly changes the wave speed. It also shift the critical wavenumber for the primary branch to 0.99(3906) from 1. If the wall's wavelength is equal to the pore diameter of 200 μm ($k = \pi$), then the maximum growth rate is slightly larger at 0.55 min^{-1} and its wave speed is 145 μm/s.

6. Summary and Conclusions

We use asymptotic methods to study the effect of pore corrugation on the base flows and the corresponding linear stability of a core-annular flow for the particular range of parameters $J/Re_1 \sim 1/\varepsilon^2$. The small parameters are the scaled film thickness ε and corrugation strength σ. We show that both the leading order base flow and its leading order stability are film-determined in this limit, and the core's dynamics slaves those of the film. The film dynamics remains unchanged for slow or intermediate fluid motion, even though the core motion may be modified.

Corrugation does not only modify the magnitude (at $O(\sigma^2)$) of the unstable branch of eigenvalues that appears in the straight-tube case and thereby, changes its critical wave

number but, due to the (wall wave number) k-periodicity of the spectrum in (disturbance wave number) α-space, it also introduces other unstable branches to the eigenvalue spectrum. For example, in the straight-tube case, a short wavelength monochromatic simply decays with unchanged wavelength. In contrast, in the corrugated tube case for $k<2$, the short wave initial disturbances are stabilized at short times, but they excite unstable long waves via coupling to the corrugation harmonics for longer times of $O(ln(1/\sigma))$. For $k>2$, however, there are stable short wave gaps between the adjacent branches and certain initial short waves will not excite unstable long waves, although others will. Since real systems contain more than one wall wave length, this stable gap may no longer appear due to an interaction between different wall wave lengths. Therefore, real pore systems are rarely linearly stable.

The theory can be extended to the range of $J/Re_1 >> 1/\varepsilon$. The stability of the very strong surface tension case, i.e., $J/Re_1 >> 1/\varepsilon^2$, reduces to the no flow limit because of the relatively weak strength of the base film flow. The corrugation can contribute a stability $O(\sigma)$ correction to the primary branch growth rate in some ranges of parameters due to a resonance. For less strong tension as $1/\varepsilon << J/Re_1 << 1/\varepsilon^2$, the growth rate correction is $O(\sigma^2 S^3)$ where $S = \varepsilon^2 J/Re_1$; at this order corrugation effects are negligible compared with non-leading order straight-tube corrections. At $J/Re_1 \sim 1/\varepsilon$, however, the dynamics of the core contribute in determining the interfacial shape in the base flow as well as to the system's linear stability, but the corrugation effect on the growth rate is rather negligible.

An alternative way for the core-coupling to become significant is when the core fluid is much more viscous than the film fluid, say $m \sim O(\varepsilon)$. Here, core-coupling should be expected for both the base flow and its stability. However, a very weakly viscous film fluid can destroy lubrication in the film.

Appendix I: Matrix Perturbation Theory

Expanding (4.13) in a Taylor series in σ about $\omega = \omega_0$ yields

$$D_0(\omega = \omega_0) + \sigma^2 \omega_2 \left.\frac{\partial D_0}{\partial \omega}\right|_{\omega=\omega_0} + \sigma^2 D_2(\omega = \omega_0) + O(\sigma^4) = 0. \tag{A2.1}$$

It follows from the fact $D_0(\omega = \omega_0) = 0$ that

$$\omega_2 = -D_2 \Big/ \left(\frac{\partial D_0}{\partial \omega}\right)\Big|_{\omega=\omega_0}, \tag{A2.2}$$

where

$$\begin{aligned} D_2(\omega_0) = &- \sum_{n=0,-1} \prod_{j\neq n,n+1} [\omega_0 + P(j)] Q^+(n) Q^-(n+1) \\ &- \sum_{n=0,-1} \prod_{j\neq n,n+1} [\omega_0 + P(j)] Q^+(n) Q^-(n+1). \end{aligned} \tag{A2.3}$$

Each term in the second sum on the right side of (A2.3) has the common factor $(\omega_0 + P(0))$=0. Similarly,

$$\left(\frac{\partial D_0}{\partial \omega}\right)\Big|_{\omega=\omega_0} = \prod_{j\neq 0} (\omega_0 + P(j)), \tag{A2.4}$$

Substitution of (A2.3) and (A2.4) into (A2.2) results in

$$\omega_2 = \frac{Q^+(0)Q^-(1)}{P(1) - P(0)} + \frac{Q^+(-1)Q^-(0)}{P(-1) - P(0)}. \tag{4.15}$$

An alternative route to (4.15) is to use the solvability condition for the perturbed matrix equation. Equation (4.10) can be expressed as

$$\left(\underline{\underline{L_0}} + \sigma \underline{\underline{L_1}}\right)\underline{\chi} = (-\omega)\underline{\chi}, \tag{A2.5}$$

where

$$\underline{\underline{L_0}} = \begin{bmatrix} \bullet & \bullet & & [0] & \\ 0 & P(n-1) & 0 & & \\ & 0 & P(n) & 0 & \\ & & 0 & P(n+1) & 0 \\ & [0] & & \bullet & \bullet \end{bmatrix}, \tag{A2.6a}$$

$$\underline{\underline{L_1}} = \begin{bmatrix} \bullet & \bullet & & [0] & \\ Q^-(n-1) & 0 & Q^+(n-1) & & \\ & Q^-(n) & 0 & Q^+(n) & \\ & & Q^-(n+1) & 0 & Q^+(n+1) \\ & [0] & & \bullet & \bullet \end{bmatrix}, \tag{A2.6b}$$

and $$\underline{\chi} = \begin{bmatrix} \bullet & \hat{\xi}_{n-1} & \hat{\xi}_n & \hat{\xi}_{n+1} & \bullet \end{bmatrix}^t \neq \underline{0}. \tag{A2.6c}$$

Expand ω and $\underline{\chi}$ in σ as

$$\omega = \omega_0 + \sigma\omega_1 + \sigma^2\omega_2 + \ldots, \tag{A2.7}$$

$$\underline{\chi} = \underline{\chi_0} + \sigma\underline{\chi_1} + \sigma^2\underline{\chi_2} + \ldots. \tag{A2.8}$$

Substitute (A2.7) into (A2.5) to get, to the leading order in σ,

$$O(\sigma^0): \underline{\underline{L_0}}\,\underline{\chi_0} = (-\omega_0)\underline{\chi_0}. \tag{A2.9}$$

The zero-order eigenvalue ω_0 of the primary branch is $-P(0) = -\dfrac{2i\alpha}{m} + \dfrac{J_0}{3m\lambda}\alpha^2(1-\alpha^2)$, and the corresponding eigenvector is $\underline{\chi_0} = [\bullet \;\; 0 \;\; 1 \;\; 0 \;\; \bullet]^t$, with the 1 being the $n = 0$ component.

The next order in σ gives

$$O(\sigma): \left(\underline{\underline{L_0}} + \omega_0\underline{\underline{I}}\right)\underline{\chi_1} = -\left(\underline{\underline{L_1}} + \omega_1\underline{\underline{I}}\right)\underline{\chi_0}. \tag{A2.10}$$

With $(\bullet,\bullet)$ denoting the complex inner product, and $(a\bullet, b\bullet) = a\bar{b}(\bullet,\bullet)$ for complex scalars a and b, the solvability condition requires

$$\left(\left(\underline{\underline{L}}_1 + \omega_1 \underline{\underline{I}}\right)\underline{\chi}_0 , \underline{y}_0\right) = 0, \tag{A2.11}$$

where $\underline{y}_0$ is the right eigenvector of the adjoint $\underline{\underline{L}}_0^+$ of $\underline{\underline{L}}_0$ with eigenvalue $\overline{(-\omega_0)}$ and $\left(\underline{\chi}_0 , \underline{y}_0\right) = 1$.Since $\underline{\underline{L}}_0$ is diagonal, it turns out that $\underline{y}_0 = \underline{\chi}_0$. Therefore,

$$\omega_1 = -\overline{\left(\underline{y}_0 , \underline{\underline{L}}_1 \underline{\chi}_0\right)}. \tag{A2.12}$$

Since $\underline{\underline{L}}_1 \underline{\chi}_0 = \left[\bullet \;\; 0 \;\; Q^+(-1) \;\; 0 \;\; Q^-(1) \;\; 0 \;\; \bullet\right]^t$, whose $Q^+(-1)$ and $Q^-(1)$ are the $n = -1$ and $n = +1$ components, respectively, (A2.12) gives $\omega_1 = 0$. To solve $\underline{\chi}_1$, let the components of $\underline{\chi}_1 = \left[a_j\right], j = -N,..,-1,\ 0,\ 1,..,N$. Then the components of (A2.10) are :

$$\text{for } j = 0,\ \left(P(0) + \omega_0\right)a_0 = 0; \tag{A2.13a}$$

$$\text{for } j = \pm 1,\ \left(P(\pm 1) + \omega_0\right)a_{\pm 1} = -Q^{\mp}(\pm 1); \tag{A2.13b}$$

$$\text{otherwise, } \left(P(j) + \omega_0\right)a_j = 0. \tag{A2.13c}$$

Solving (A2.13) for a_j, one gives

$$\underline{\chi}_1 = \left[\bullet \;\; 0 \;\; \frac{-Q^+(-1)}{\left(P(-1) + \omega_0\right)} \;\; a_0 \;\; \frac{-Q^-(1)}{\left(P(1) + \omega_0\right)} \;\; 0 \;\; \bullet\right]^t, \tag{A2.14}$$

where, since $\omega_0 = -P(0)$, a_0 is arbitrary.

We proceed to the next order in σ as

$$O(\sigma^2): \ \left(\underline{\underline{L}}_0 + \omega_0 \underline{\underline{I}}\right)\underline{\chi}_2 = -\omega_2 \underline{\chi}_0 - \underline{\underline{L}}_1 \underline{\chi}_1, \tag{A2.15}$$

Again, the solvability condition gives

$$\omega_2 = -\overline{\left(\underline{y}_0 , \underline{\underline{L}}_1 \underline{\chi}_1\right)}. \tag{A2.16}$$

Evaluating $\underline{\underline{L}}_1 \underline{\chi}_1 = \left[\bullet \;\; 0 \;\; -\frac{Q^+(-1)Q^-(0)}{P(-1) + \omega_0} - \frac{Q^-(1)Q^+(0)}{P(1) + \omega_0} \;\; 0 \;\; \bullet\right]^t$ in (A2.16) then also leads to (4.15).

Another way to derive (4.15) is to solve the differential equation (4.5) by eliminating its secular term (the Lindstedt-Poincare technique). It is instructive and straight forward. Setting $\xi(z,\ \tau) = \hat{\xi}(z)e^{\omega\tau}$ in (4.5) gives

$$\left(H_0 + \sigma H_1\right)\hat{\xi} = (-\omega)\hat{\xi}, \tag{A2.16}$$

where

$$H_0 = \frac{2}{m}\frac{\partial}{\partial z} + \frac{J_0}{3m\lambda}\left(\frac{\partial^2}{\partial z^2} + \frac{\partial^4}{\partial z^4}\right),$$

$$H_1 = (\eta - \phi)\left[\frac{4}{m}\frac{\partial}{\partial z} - \frac{J_0}{m\lambda}\left(\frac{\partial^2}{\partial z^2} + \frac{\partial^4}{\partial z^4}\right)\right] + (\eta - \phi)_z\left[\frac{4}{m} - \frac{J_0}{m\lambda}\left(\frac{\partial}{\partial z} + \frac{\partial^3}{\partial z^3}\right)\right].$$

Again, we expand ω as in (A2.7) and,

$$\hat{\xi} = \hat{\xi}_0 + \sigma\hat{\xi}_1 + \sigma^2\hat{\xi}_2 + \ldots, \tag{A2.17}$$

Substitution (A2.17) and (A2.7) into (A2.16), the leading order equation in σ becomes

$$O(\sigma^0): H_0\hat{\xi}_0 = -\omega_0\hat{\xi}_0\ , \tag{A2.18}$$

Taking the normal mode $\hat{\xi}_0 = e^{i\alpha z}$ results in $\omega_0 = -\frac{2i\alpha}{m} + \frac{J_0}{3m\lambda}\alpha^2\left(1-\alpha^2\right)$. The next order in σ gives

$$O(\sigma): \left(H_0 + \omega_0\right)\hat{\xi}_1 = -\left(H_1 + \omega_1\right)e^{i\alpha z}\ . \tag{A2.19}$$

Since the inhomogeneous part of (A2.19) contains a secular or resonant term $\omega_1 e^{i\alpha z}$ which would yields an unbounded solution for $\hat{\xi}_1$, it must vanish, or $\omega_1 = 0$. As such, the solution of $\hat{\xi}_1$ is

$$\hat{\xi}_1 = -\left[\frac{\left(\hat{\eta} - \hat{\phi}\right)i(\alpha + k)e^{i(\alpha+k)z}}{\omega_0 + P(1)} + \frac{\left(\hat{\eta} - \hat{\phi}\right)^* i(\alpha - k)e^{i(\alpha-k)z}}{\omega_0 + P(-1)}\right]G(\alpha). \tag{A2.20}$$

where $G(\alpha)=\frac{4}{m}-\frac{J_0}{m\lambda}i\alpha\left(1-\alpha^2\right)$ and $P(\pm1)$ are given in (4.11a).

For $O(\sigma^2)$,

$$\left(H_0+\omega_0\right)\hat{\xi}_2=-\omega_2 e^{i\alpha z}-H_1\hat{\xi}_1 \ . \tag{A2.21}$$

However,

$$\begin{aligned} H_1\hat{\xi}_1=\left\|\hat{\eta}-\hat{\phi}\right\|^2\left[\frac{-\alpha(\alpha+k)}{\omega_0+P(1)}G(\alpha+k)+\frac{-\alpha(\alpha-k)}{\omega_0+P(-1)}G(\alpha-k)\right]G(\alpha)e^{i\alpha z} \\ +Ae^{i(\alpha+2k)z}+Be^{i(\alpha-2k)z}. \end{aligned} \tag{A2.22}$$

whose coefficient of $e^{i\alpha z}$ contributes secular terms. ω_2 is thus obtained by combining these with $\omega_2 e^{i\alpha z}$ to eliminate the whole secular contribution in the inhomogeneous part of (A2.22), which also gives (4.15).

Appendix II

For $S >> 1$, the Bloch matrix / determinant is obtained by just slightly changing the definitions of $P(n)$ and $Q^{\pm}(n)$. For (5.4), (4.11) is modified to

$$P(n) = -\frac{S}{3m}\beta^2(n)\left(1-\beta^2(n)\right), \tag{A3.1a}$$

$$Q^{+}(n) = -\hat{\phi}^{*}\frac{S}{m}\beta(n)\beta(n+1)\left(1-\beta^2(n+1)\right), \tag{A3.1b}$$

$$Q^{-}(n) = -\hat{\phi}\frac{S}{m}\beta(n)\beta(n-1)\left(1-\beta^2(n-1)\right). \tag{A3.1c}$$

The resulting determinant D of (4.10) is also modified by just following the above definitions for the elements. For $0 \le \alpha < k$ with $k > 1$, $\omega + P(0)$ (the primary α-branch) and $\omega + P(-1)$ (the secondary $(\alpha - k)$ branch) at the $O(\sigma^0)$ determinant D_0 give the same ω_0 at $\alpha = k/2$. Also, $\omega + P(1)$ (the secondary $(\alpha + k)$ branch) and $\omega + P(-1)$ have the same ω_0 at $\alpha = 0$. These multiplicities contribute at $O(\sigma)$ to the growth rate correction rather than at $O(\sigma^2)$.

In order to solve for ω by taking the interaction between these three branches into account regardless of the range of α, we rearrange the determinant D in the following way. We first extract $\omega + P(0)$, $\omega + P(-1)$, and $\omega + P(1)$ from D_0 as the $O(\sigma^0)$ determinant, and then combine the other terms of D_0 together with D_2 into the $O(\sigma^2)$ contribution. This modification yields

$$G_0(\omega) + \sigma^2 G_2(\omega) = 0, \tag{A3.2}$$

$$G_0 = (\omega + P(-1))(\omega + P(0))(\omega + P(1)), \tag{A3.3a}$$

which contains the primary and two secondary branches.

$$G_2 = D_2 \Big/ \prod_{j \neq 0,\pm 1}(\omega + P(j)). \tag{A3.3b}$$

We solve (A3.2) for ω by an iteration scheme by evaluating the right hand side of (A3.2) at $\omega = \omega_0$:

$$G_0(\omega) + \sigma^2 G_2(\omega_0) = 0. \qquad \text{(A3.4)}$$

For the case in Figure 9, to use (A3.4) for obtaining the maximum growth rate, we choose ω_0 as $-P(0)$ for $0 \le \alpha \le k/2$, and as $-P(-1)$ for $k/2 \le \alpha < 3k/2$.

Appendix III

Let $J = J_0/\varepsilon$ where J_0 is $O(1)$ and $Re_1 = O(1)$, We first develop the base flow in a perturbation expansion in this limit for small wall non-uniformity. Expansions in σ and ε for $\sigma << \varepsilon$ for the base flows of both regions and the interface are the follows.

$$S_b = 1 + \sigma\varepsilon\eta_1 + \sigma\varepsilon^2\eta_2 + \ldots \ . \tag{A4.1}$$

For the film,

$$w_b = \overline{\overline{w}} + \sigma\varepsilon\overline{w}_1 + \sigma\varepsilon^2\overline{w}_2 + \ldots., \tag{A4.2a}$$

$$u_b = \sigma\varepsilon^2\overline{u}_1 + \sigma\varepsilon^3\overline{u}_2 + \ldots., \tag{A4.2b}$$

$$p_b = \overline{\overline{p}} + \sigma\overline{p}_1 + \sigma\varepsilon\overline{p}_2 + \ldots \ . \tag{A4.2c}$$

For the core,

$$W_b = \overline{\overline{W}} + \sigma\varepsilon\overline{W}_1 + \ldots \ , \tag{A4.3a}$$

$$U_b = \overline{\overline{U}} + \sigma\varepsilon\overline{U}_1 + \ldots \ , \tag{A4.3b}$$

$$P_b = \overline{\overline{P}} + \sigma\varepsilon\overline{P}_1 + \ldots \ . \tag{A4.3c}$$

Substitution of the expansions (A4.1)-(A4.3) into the governing equations and boundary conditions which are also expanded in σ and ε, give at the leading order,

$$\overline{w}_{1yy} = 0, \tag{A4.4b}$$

$$\overline{p}_{1y} = 0, \tag{A4.4b}$$

$$\overline{u}_{1y} = \overline{w}_{1z} \ , \tag{A4.4c}$$

$$-2r\overline{U}_1 + \left(1 - r^2\right)\overline{W}_{1r} = -\overline{P}_{1z} + \frac{1}{Re_1}\nabla^2\overline{W}_1, \tag{A4.5a}$$

$$\left(1 - r^2\right)\overline{U}_{1z} = -\overline{P}_{1r} + \frac{1}{Re_1}\left(\nabla^2\overline{U}_1 - \frac{\overline{U}_1}{r^2}\right), \tag{A4.5b}$$

$$\frac{1}{r}\left(r\overline{U}_1\right)_r + \overline{W}_{1z} = 0, \tag{A4.5c}$$

$$\text{at } y = 0,\ \overline{w}_1 = \frac{2}{m}\phi\ ,\ \overline{u}_1 = 0, \tag{A4.6}$$

$$\text{at } y = r = 1,\ \overline{W}_1 = \left(2 - \frac{2}{m}\right)\eta_1 + \frac{2}{m}\phi,\ \overline{U}_1 = 0, \tag{A4.7}$$

$$\text{at } y = r = 1,\ \overline{w}_{1y} = 0, \tag{A4.8}$$

$$\overline{p}_1 = \frac{J_0}{Re_1^2}\left(\eta_{1zz} + \eta_1\right), \tag{A4.9}$$

$$\text{at } y = 1,\ \ \overline{u}_1 = \frac{2}{m}\eta_{1z}\ . \tag{A4.10}$$

The film solutions are,

$$\eta_1 = \phi\ ,\overline{w}_1 = \frac{2}{m}\phi,\ \overline{u}_1 = \frac{2}{m}y\phi_z. \tag{A4.11)-(A4.13}$$

As discussed earlier for $\varepsilon^2 J/Re_1 << 1$, this is consistent with the film flow being a local parallel shear flow.

As in (3.15), introduction of the streamfunction (3.9) in the core leads to a solution in terms of Kummer functions as

$$\hat{\Psi}_1(r) = A(k)rI_1(kr) + B(k)rN_1(kr), \tag{A4.14a}$$

where, let $a = \frac{1}{2}\left(k\,Re_1\right)^{1/2}e^{-i\pi/4}$ and $b = 1 + k^2/8a - a/2$,

$$A(k) = \frac{2\hat{\phi}N_1(k)}{k\left[N_1(k)I_0(k) - N_2(k)I_1(k)\right]}\ , \tag{A4.14b}$$

$$B(k) = -\frac{2\hat{\phi}I_1(k)}{k\left[N_1(k)I_0(k) - N_2(k)I_1(k)\right]}, \tag{A4.14b}$$

$$N_1(kr) = \int_0^r \left[I_1(k)K_1(kt) - I_1(kt)K_1(kt)\right]t^2 e^{-at^2} M\left(b,2,2at^2\right)dt, \tag{A4.14c}$$

$$N_2(kr) = \int_0^r \left[I_0(k)K_1(kt) + I_0(kt)K_1(kt)\right]t^2 e^{-at^2} M\left(b,2,2at^2\right)dt. \tag{A4.14d}$$

The leading order interface will generate the next order in ε of the base flow as well. Note that (A4.12) and (A4.13) result in $\overline{w}_{1y} = 0$ and $\overline{u}_{1yy} = 0$, respectively. For the film, the governing equations and boundary conditions at the next order in ε are

$$0 = -\overline{p}_{1z} + \frac{m}{Re_1}\left(\overline{w}_{2yy} - \overline{w}_{1y}\right) = -\overline{p}_{1z} + \frac{m}{Re_1}\overline{w}_{2yy}, \tag{A4.15a}$$

$$0 = \overline{p}_{2y} + \frac{m}{Re_1}\overline{u}_{1yy} = \overline{p}_{2y}, \tag{A4.15b}$$

$$-\overline{u}_{2y} + \overline{u}_1 + \overline{w}_{2z} = 0, \tag{A4.15c}$$

$$\text{at } y = 0,\ \overline{w}_2 = \frac{2}{m}\left(1 - \frac{2}{m}\right)\phi, \tag{A4.16}$$

$$\text{at } y = r = 1,\ -m\overline{w}_{2y} = \overline{\gamma}, \tag{A4.17}$$

$$\text{at } y = r = 1,\ \overline{p}_2 + \frac{2m}{Re_1}\overline{u}_{1y} - \overline{P}_1 + \frac{2}{Re_1}\overline{U}_{1r} = \frac{J_0}{Re_1^2}\left(\eta_{2zz} + \eta_2\right), \tag{A4.18}$$

$$\text{at } y = 1,\ \overline{u}_2 = \frac{1}{m}\left(1 - \frac{4}{m}\right)\eta_{1z} + \frac{2}{m}\eta_{2z}\ , \tag{A4.19}$$

In (A4.17a):

$$\overline{\gamma} = \left(\overline{W}_{1r} + \overline{U}_{1z}\right)_{r=1}, \tag{A4.20}$$

represents the perturbed core's shear stress at the unperturbed interface and can be evaluated from (A4.14). By using $\overline{\gamma} = \hat{\overline{\gamma}}\, exp(ikz)$, this becomes

$$\hat{\overline{\gamma}} = -\frac{\hat{\phi} I_1(k) e^{-b} M(a,\ 2,\ 2b)}{\left(N_1(k) I_0(k) - N_2(k) I_1(k)\right)}.$$

Thus, $\overline{w}_2$ and $\overline{u}_2$ follow from (A4.15a), (A4.15c) and (A4.16) as

$$\overline{w}_2 = \frac{Re_1}{m}\overline{p}_{1z}\left(\frac{1}{2}y^2 - y\right) - \frac{\overline{\gamma}}{m}y + \frac{2}{m}\left(1 - \frac{2}{m}\right)\phi, \tag{A4.21a}$$

$$\bar{u}_2 = \frac{Re_1}{m}\bar{p}_{1zz}\left(\frac{1}{6}y^3 - \frac{1}{2}y^2\right) + \left(\frac{1}{m}\phi_z - \frac{\bar{\gamma}_z}{2m}\right)y^2 + \frac{2}{m}\left(1 - \frac{2}{m}\right)\phi_z y. \quad \text{(A4.21b)}$$

Substitution of (A4.21) into (A4.19) along with (A4.9) gives the following equation for η_2

$$\frac{2}{m}(\eta_2 - \phi) = -\frac{J_0}{3m\,Re_1}(\eta_{1zzz} + \eta_{1z}) - \frac{\bar{\gamma}}{2m}. \quad \text{(A4.22)}$$

Therefore, η_2 can be determined because η_1 and $\bar{\gamma}$ are known from the leading order solutions. Note that $\eta_1 = \phi$ from (A4.11) here. Thus the capillary terms of (A4.22) can be recast in terms of the wall's function ϕ. $\bar{p}_2$ can be solved from (A4.15b) and (A4.18). Here we give only the film solutions. As we shall see, $\bar{p}_2$ and the core quantities ($\overline{W}_2$, $\overline{U}_2$, $\overline{P}_2$) do not contribute to the linear stability at the leading order in σ.

We now proceed to the leading order stability analysis. Following Papageorgiou *et al.* (1990), we introduce an infinitesimal interfacial disturbance to the interface such that $S = S_b(z) + \delta\xi(z, t)$. A scaling analysis similar to the one above results in the following expansion for the disturbed flows:

For the film,

$$w = w_b + \varepsilon\delta w' + \ldots,\ u = u_b + \varepsilon^2\delta u' + \ldots,\ p = p_b + \frac{\delta}{\varepsilon}p' + \ldots, \quad \text{(A4.23)}$$

and for the core,

$$W = W_b + \delta W' + \ldots,\ U = U_b + \delta U' + \ldots,\ P = P_b + \delta P' + \ldots, \quad \text{(A4.24)}$$

After substitution of (A4.23) and (A4.24) into the governing equations and boundary conditions, we extract the corrugated base flow contribution and find the following equations and boundary conditions:

For the film,

$$0 = -p'_z + \frac{m}{Re_1}w'_{yy}, \quad \text{(A4.25a)}$$

$$0 = p'_y, \quad \text{(A4.25b)}$$

$$-u'_y + w'_z = 0, \tag{A4.25c}$$

and for the core

$$\left(1-r^2\right)W' - 2rU' + O(\varepsilon,\ \sigma\varepsilon) = -P'_z + \frac{1}{Re_1}\nabla^2 W', \tag{A4.26a}$$

$$\left(1-r^2\right)U'_z + O(\varepsilon,\ \sigma\varepsilon) = -P'_z + \frac{1}{Re_1}\left(\nabla^2 U' - \frac{U'}{r^2}\right). \tag{A4.26b}$$

$$\frac{1}{r}(rU')_r + W'_z = 0. \tag{A4.26c}$$

The $O(\varepsilon)$ correction above arises from the introduction of the long time scale $\tau = \varepsilon t$ in the kinematic condition. $O(\sigma\varepsilon)$ connections come from the corrugated base flow. As we shall see below, the disturbed quantities W', U', P' in the core contain $O(\sigma^0)$ and $O(\sigma)$ contribution as do those of the film at the leading orders in σ. $O(\sigma\varepsilon)$ terms are of higher order.

$$\text{At } y = -\sigma\phi,\ \ w' = 0\ ,\ \ u' = 0\,. \tag{A4.27}$$

At the base interface S_b,

$$W'(r=1) = 2\left(1-\frac{1}{m}\right)\xi + O(\sigma\varepsilon),\ U' = O(\varepsilon), \tag{A4.28}$$

$$m\left(-w'_y(y = 1-\sigma\eta_1) + \sigma\xi\overline{w}_{2yy}(y=1)\right) = \gamma + O(\sigma\varepsilon), \tag{A4.29}$$

$$p' = \frac{J_0}{Re_1^2}\left(\xi_{zz} + \xi\right), \tag{A4.30}$$

$$\begin{aligned} &-\left(\sigma\varepsilon\,\bar{u}_y^{(1)} + \sigma\varepsilon^2\,\bar{u}_{2y}\right)_{y=1}\cdot\xi + \varepsilon^2 u'(y = 1-\sigma\eta_1) \\ &= \varepsilon\xi_\tau + \sigma\varepsilon\left(\frac{2}{m}(\phi-\eta_1)\xi_z - \frac{2}{m}\eta_{1z}\cdot\xi\right) \\ &+\sigma\varepsilon^2\left(\left(-\frac{2}{m}\eta_2 + \frac{4}{m^2}\eta_1 + \overline{w}_2(y=1)\right)\xi_z + \left(\frac{4}{m^2}\xi + w'(y=1)\right)\eta_{1z} - \frac{2}{m}\eta_{2z}\cdot\xi\right). \end{aligned} \tag{A4.31}$$

In (A4.29) again,

$$\gamma = \left(W'_r + U'_z\right)_{r=1} \tag{A4.32}$$

represents the disturbed core's interfacial shear stress. (A4.28a) implies that (W', U', P') should have contributions at $O(\sigma^0)$ and $O(\sigma)$.

In (A4.31), the long time scale $\tau = \varepsilon t$ is the scale of the interfacial motion. The film flow can be solved by (A4.25), (A4.27) and (A4.29) in terms of the core quantity γ as

$$\begin{aligned} w' = & \frac{Re_1}{2m} p'_z y^2 - \left(\frac{\gamma}{m} + \frac{Re_1}{m} p'_z\right) y \\ & + \sigma\left[\left(\frac{Re_1}{m}\bar{p}_{1z}\cdot\xi + \frac{Re_1}{2m} p'_z \cdot \eta_1\right) y - \left(\frac{\gamma}{m} + \frac{Re_1}{m} p'_z\right)\phi\right] + O(\sigma^2), \end{aligned} \tag{A4.33a}$$

$$\begin{aligned} u' = & \frac{Re_1}{6m} p'_{zz} y^3 - \left(\frac{\gamma_z}{m} + \frac{Re_1}{m} p'_{zz}\right)\frac{y^2}{2} \\ & + \sigma\left[\left(\frac{Re_1}{m}\bar{p}_{1z}\cdot\xi + \frac{Re_1}{2m} p'_z \cdot \eta_1\right)_z \frac{y^2}{2} - \left(\frac{\gamma}{m}\phi + \frac{Re_1}{m} p'_z \phi\right)_z y\right] + O(\sigma^2). \end{aligned} \tag{A4.33b}$$

Substitution of (A4.32) and (A4.33) into (A4.31) along with the information from the base flow given in (A4.22) results in (5.9)

$$\xi_\tau + \frac{2}{m}\xi_z + \frac{\varepsilon J_0}{3m\,Re_1}\left(\xi_{zz} + \xi\right)_{zz} + \frac{\varepsilon}{2m}\gamma_z - \sigma\varepsilon\left[\left(\frac{2}{3m}\left(\phi_{zzz} + \phi_z\right) - \frac{\bar{\gamma}}{2m}\right)\xi\right]_z + O(\varepsilon^2, \sigma^2\varepsilon) = 0$$

The core's interfacial shear γ is an implicit function of ξ and σ, and its value requires the solution of (A4.26), (A4.28), and (A4.28) in terms of ξ from the film solutions.

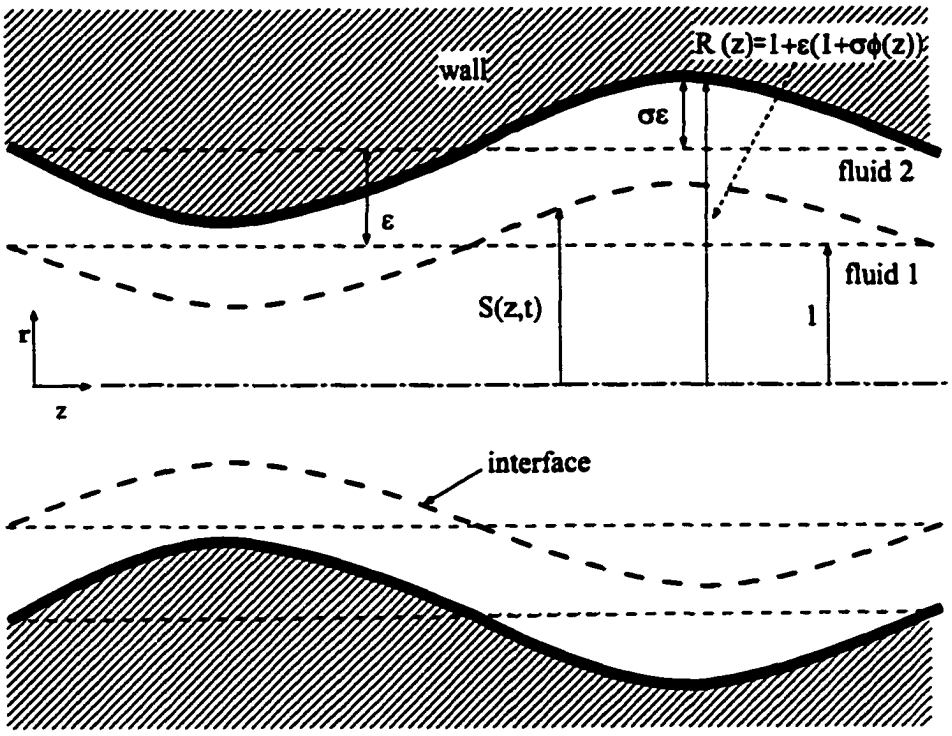

Figure 1. The flow geometry of a core annular flow in a corrugated tube.

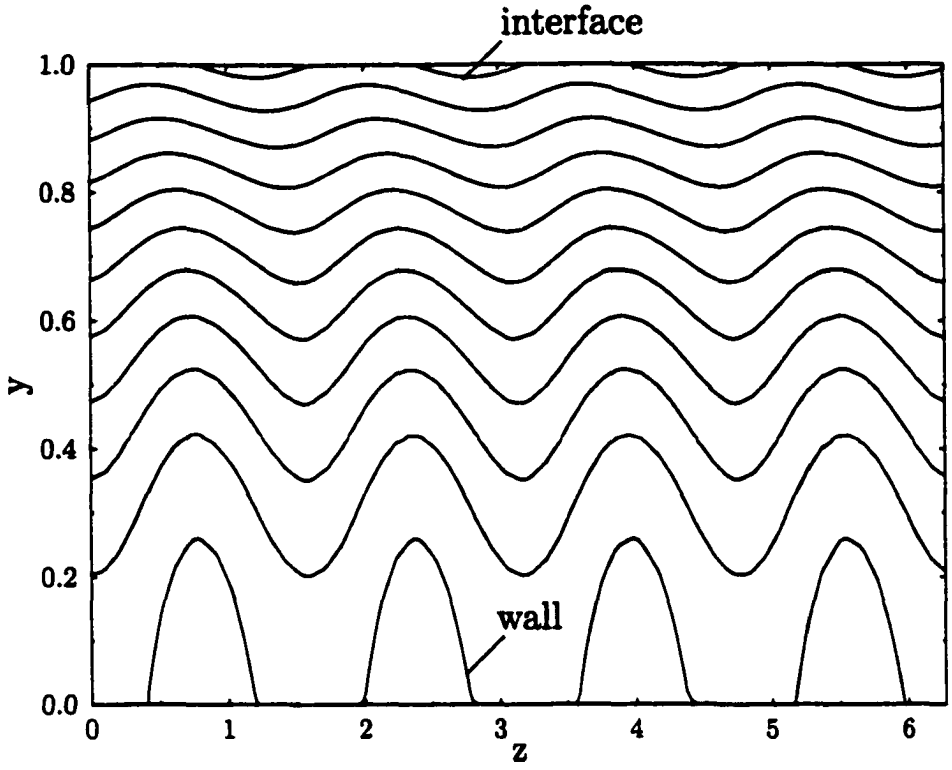

$J_0/\lambda=1.0$, m=1.0, k=4.0, $\sigma=0.2$

Figure 2. A typical streamline of the base film flow. Flow is to the right.

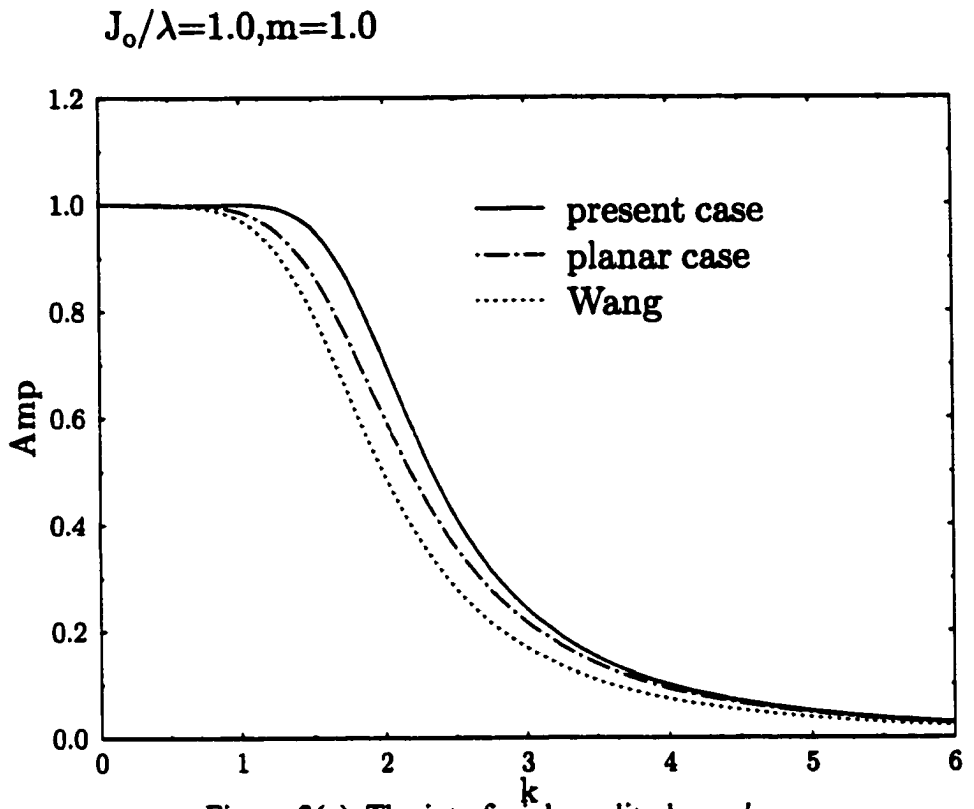

Figure 3(a). The interfacial amplitude vs. k

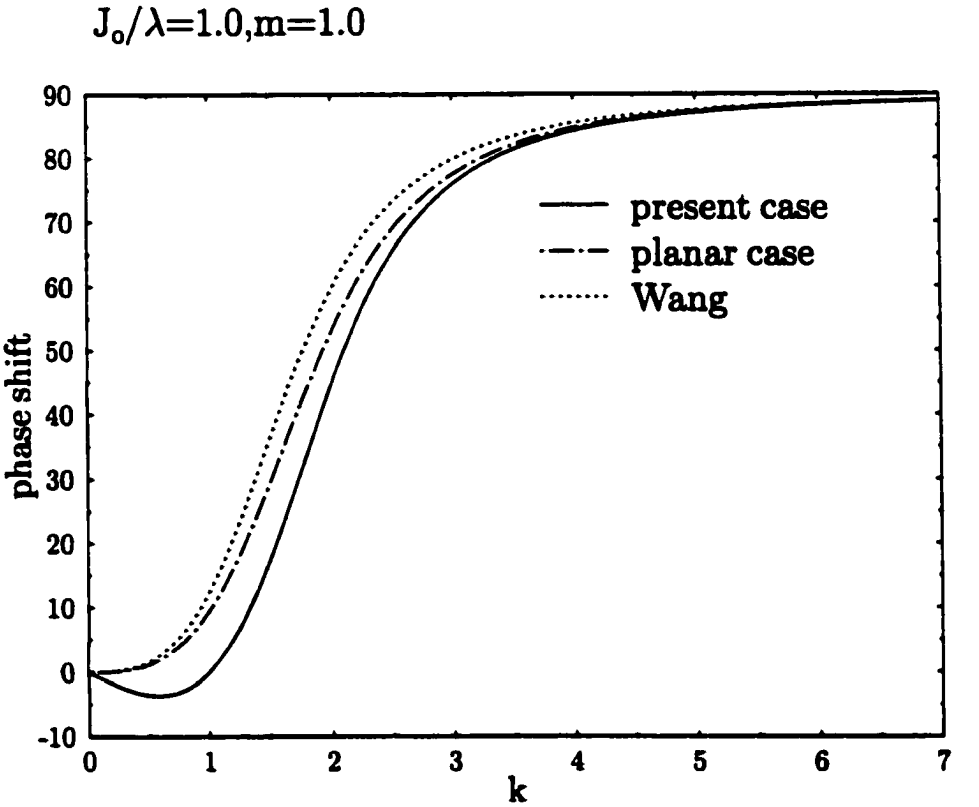

Figure 3(b). The phase shift between the interface and the wall vs. k

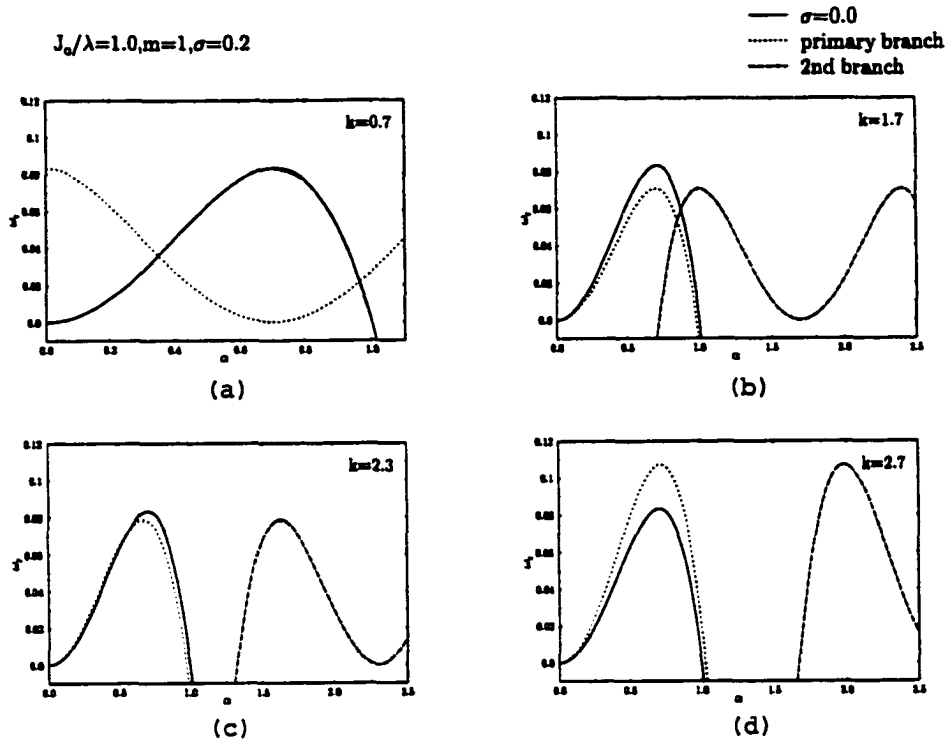

Figure 4. The eigenvalue spectrum (growth rate curves) for various k.

α=0.2, k=0.7, σ=0.2

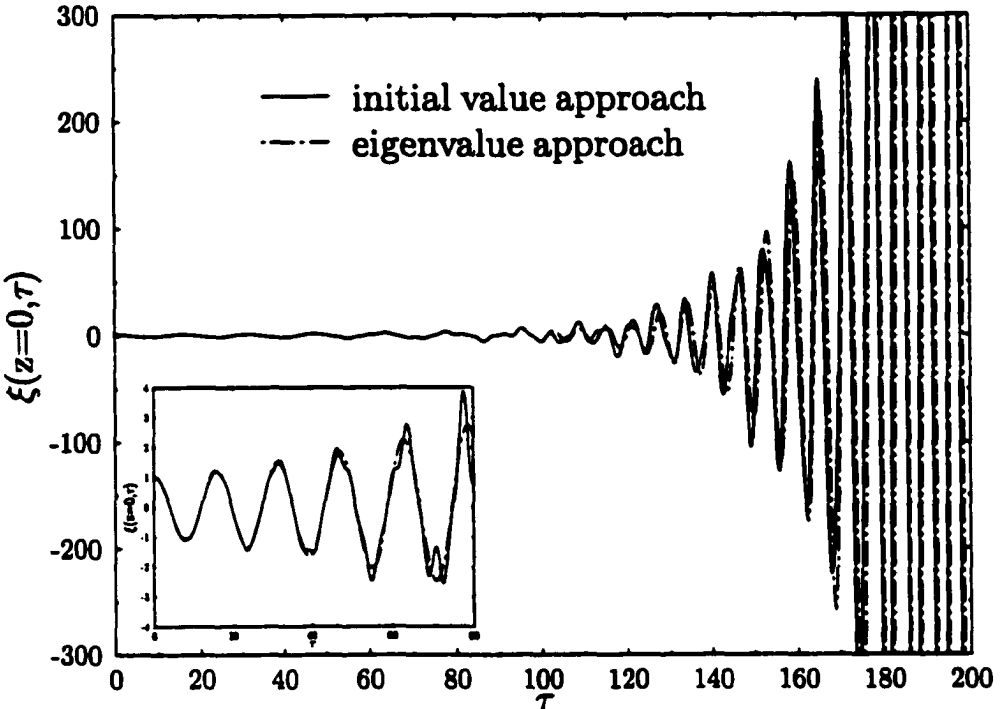

Figure 5(a). The temporal behavior of the interfacial amplitude at z =0 for α = 0.2, k = 0.7, σ = 0.2

α=1.2,k=1.7,σ=0.2

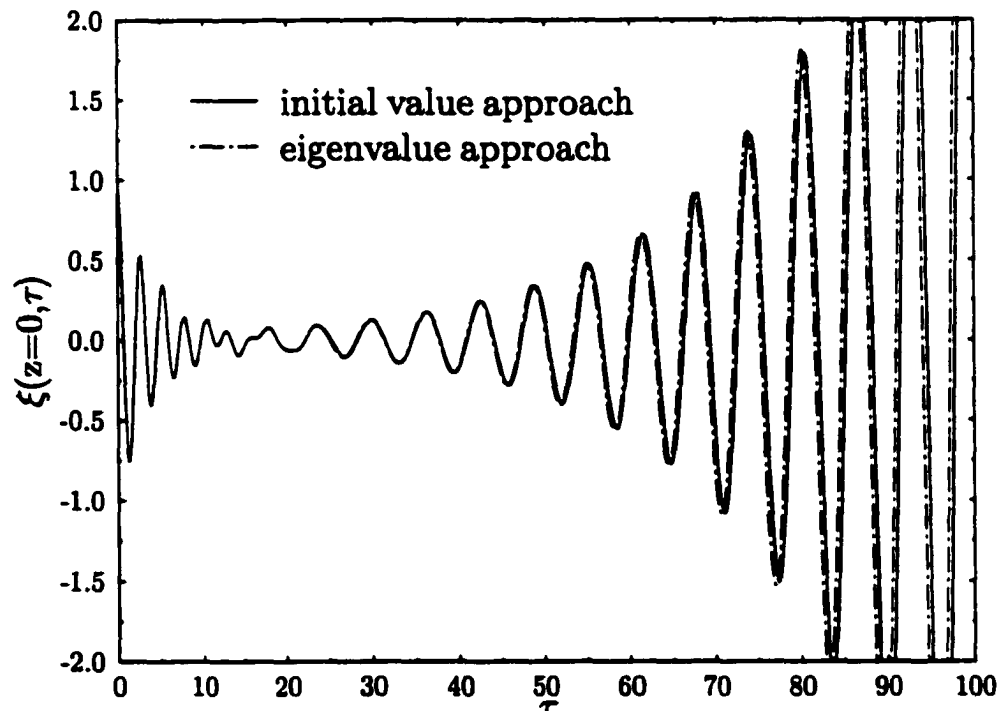

Figure 5(b). The temporal behavior of the interfacial amplitude at z =0 for α = 1.2, k = 1.7, σ = 0.2

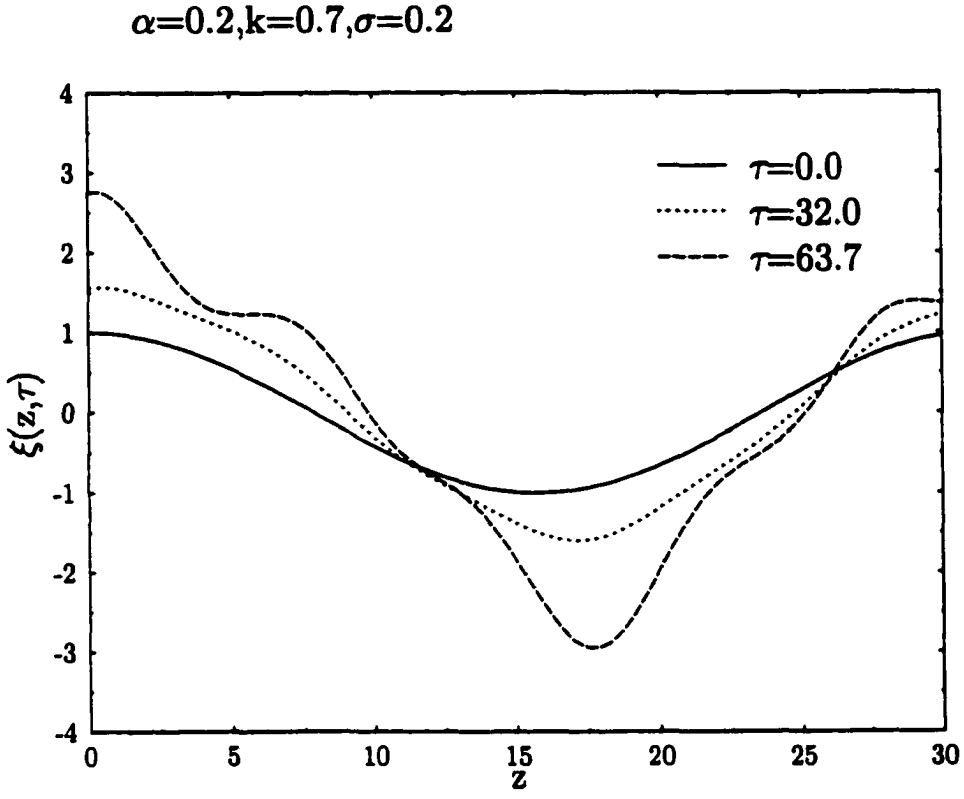

Figure 6(a1). The corresponding spatial evolutions for shorter times for Figure 5(a)

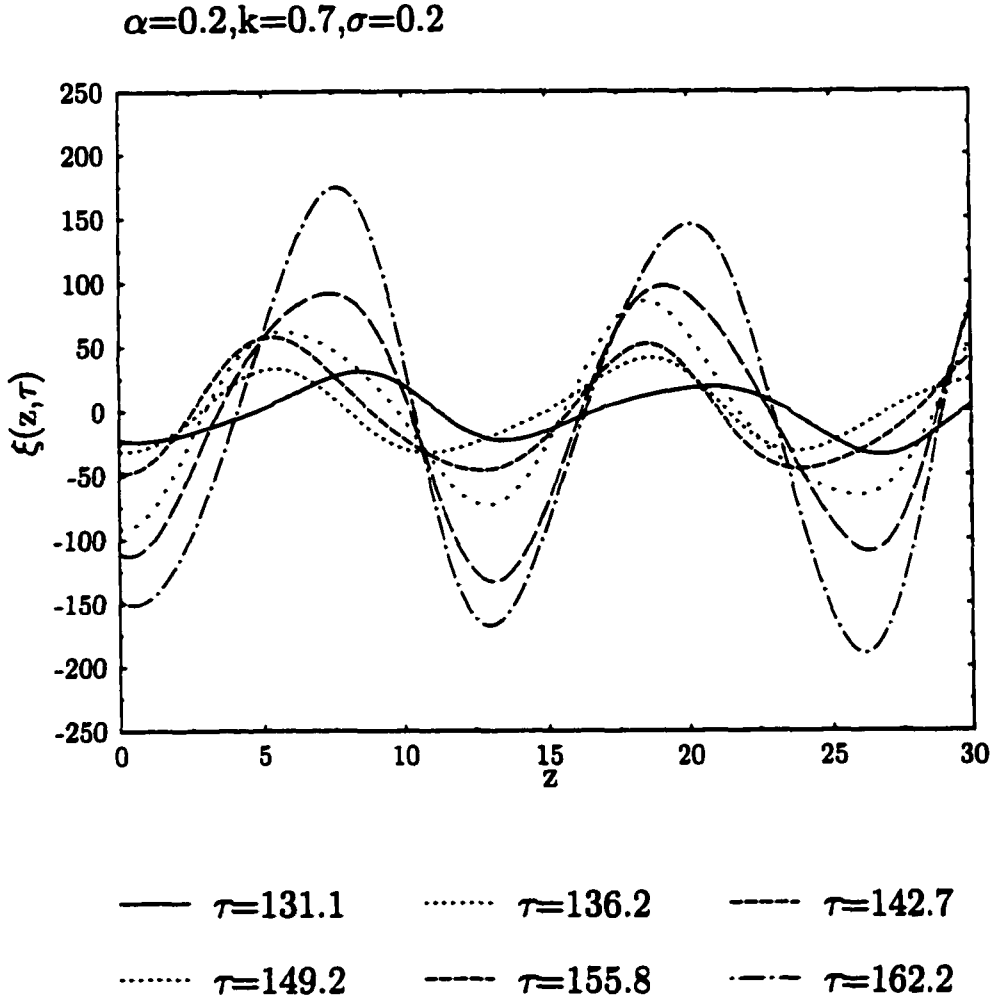

Figure 6(a2). The corresponding spatial evolutions for various long times for Figure 5(a)

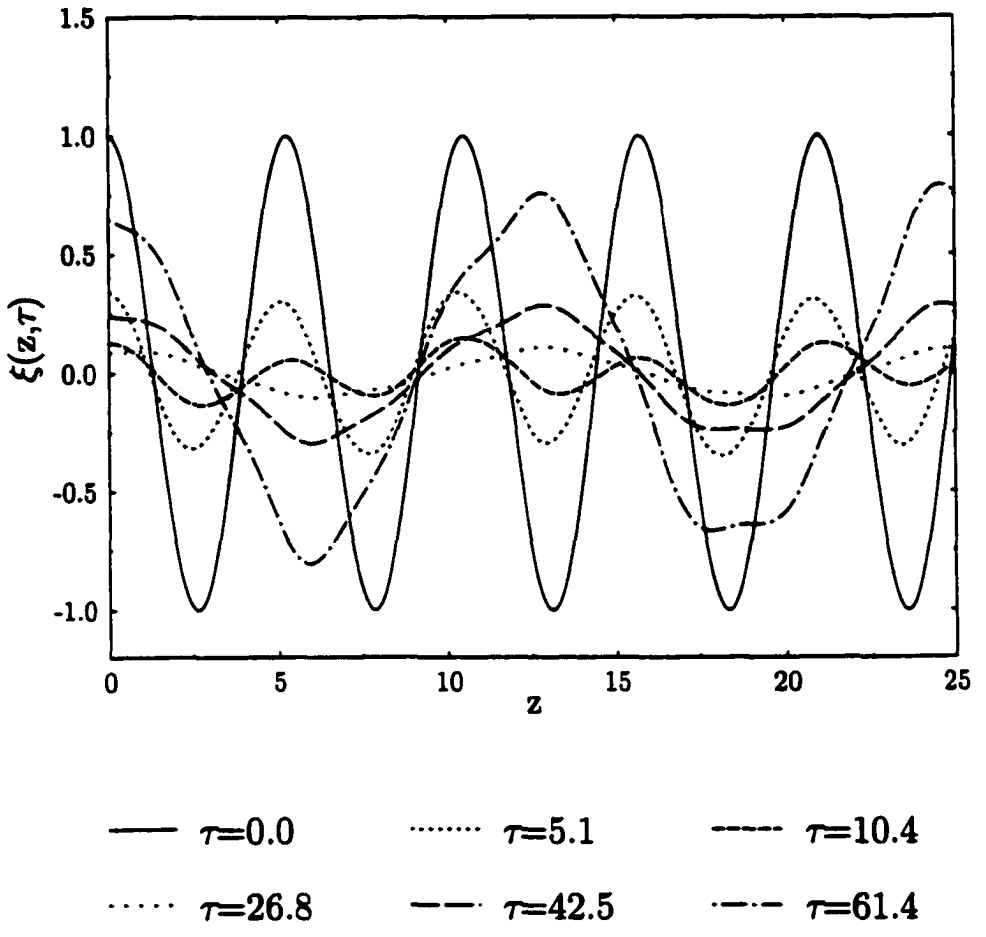

Figure 6(b). The corresponding spatial evolutions for various times for Figure 5(b)

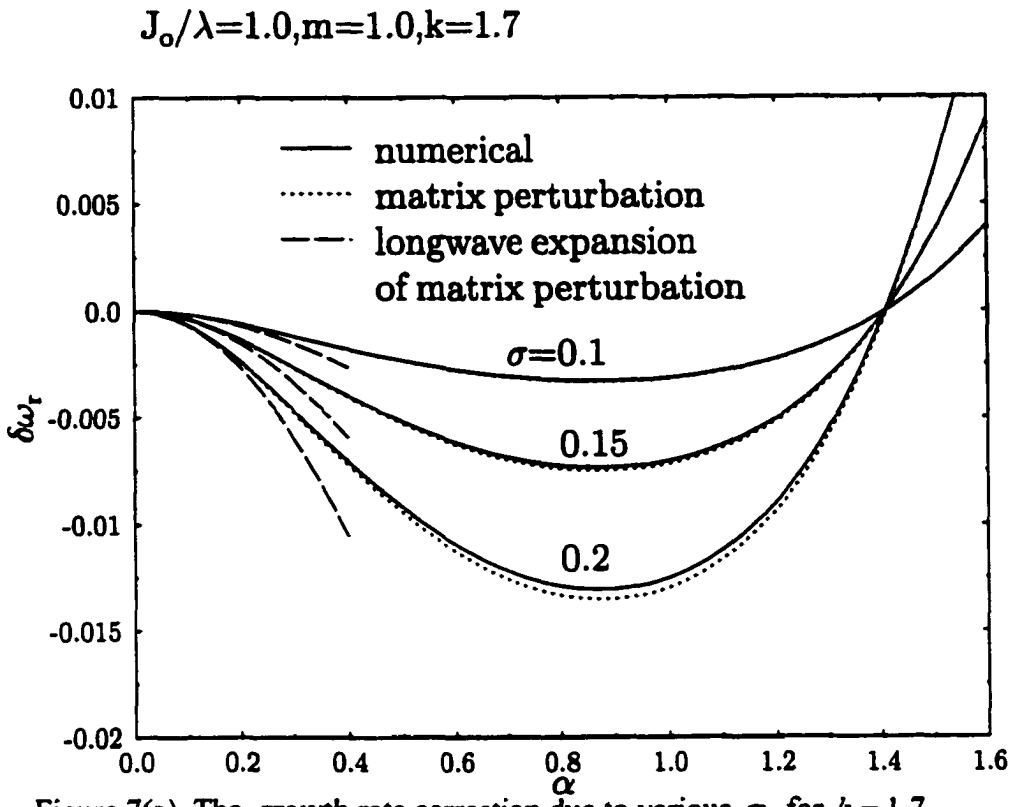

Figure 7(a). The growth rate correction due to various σ for $k = 1.7$.

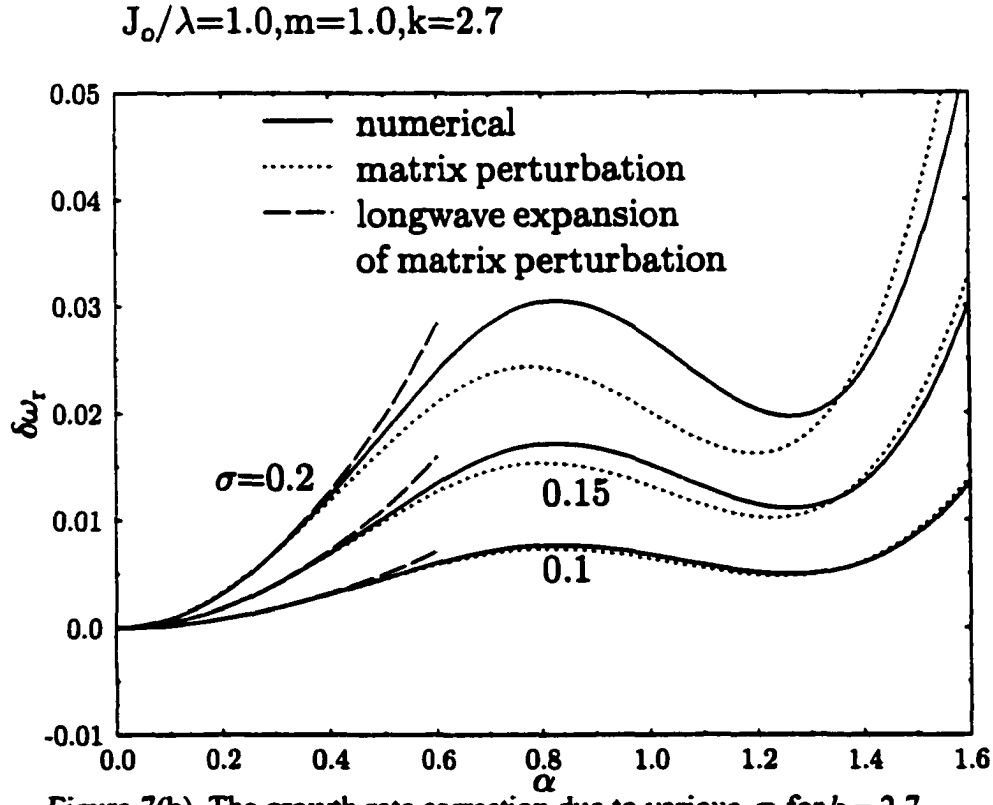

Figure 7(b). The growth rate correction due to various σ for $k = 2.7$.

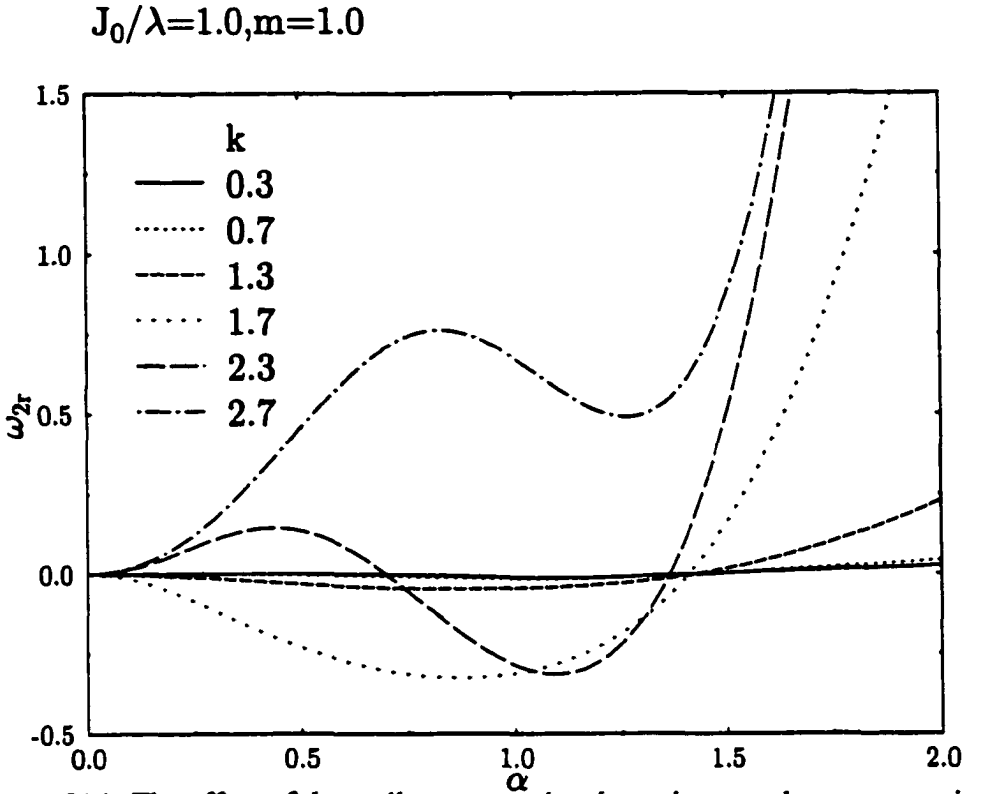

Figure 8(a). The effect of the wall wave number k on the growth rate correction.

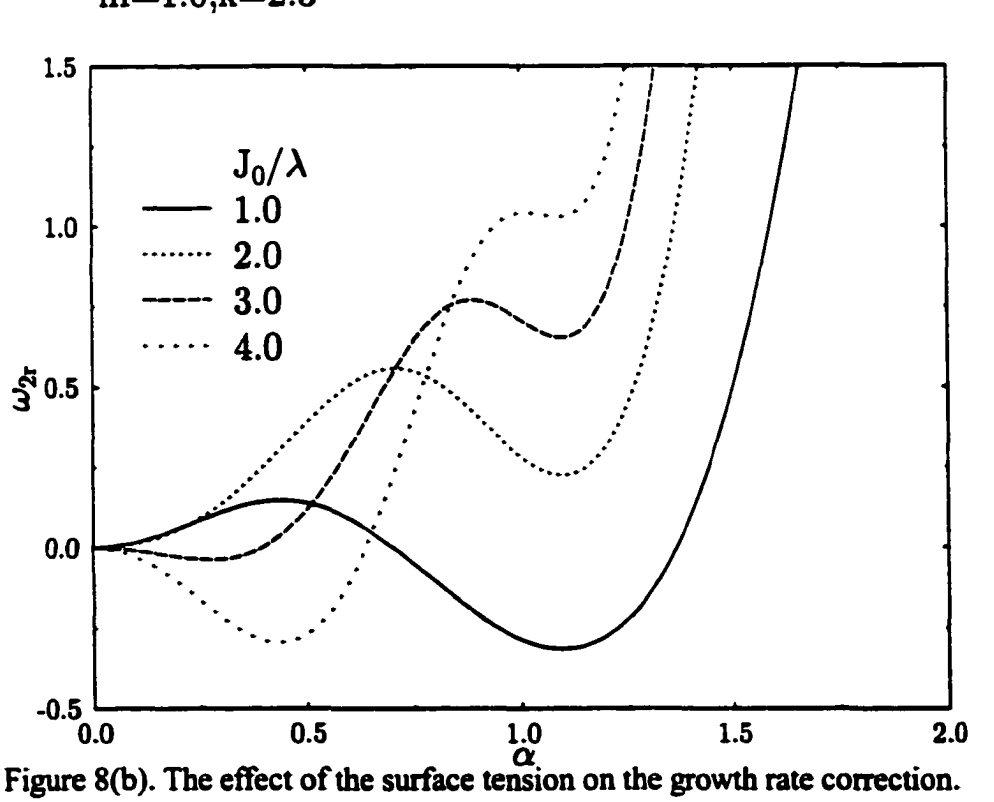

Figure 8(b). The effect of the surface tension on the growth rate correction.

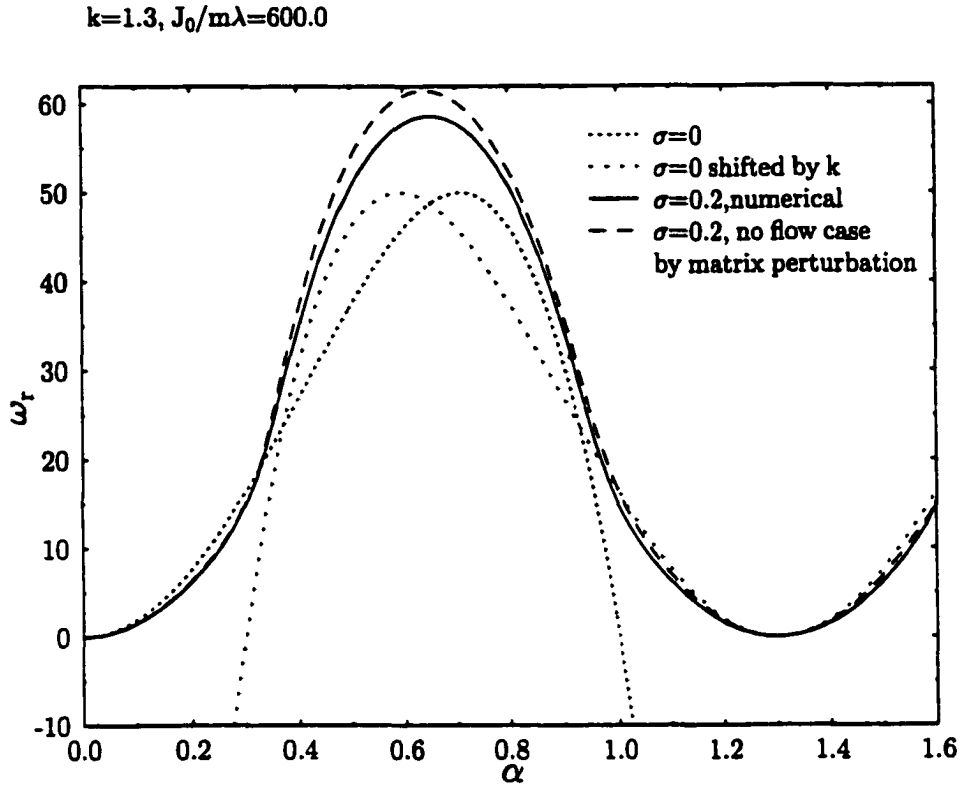

Figure 9. The growth rate as $J_0/\lambda = 600$, $m = 1$, $k = 1.3$, $\sigma = 0.2$

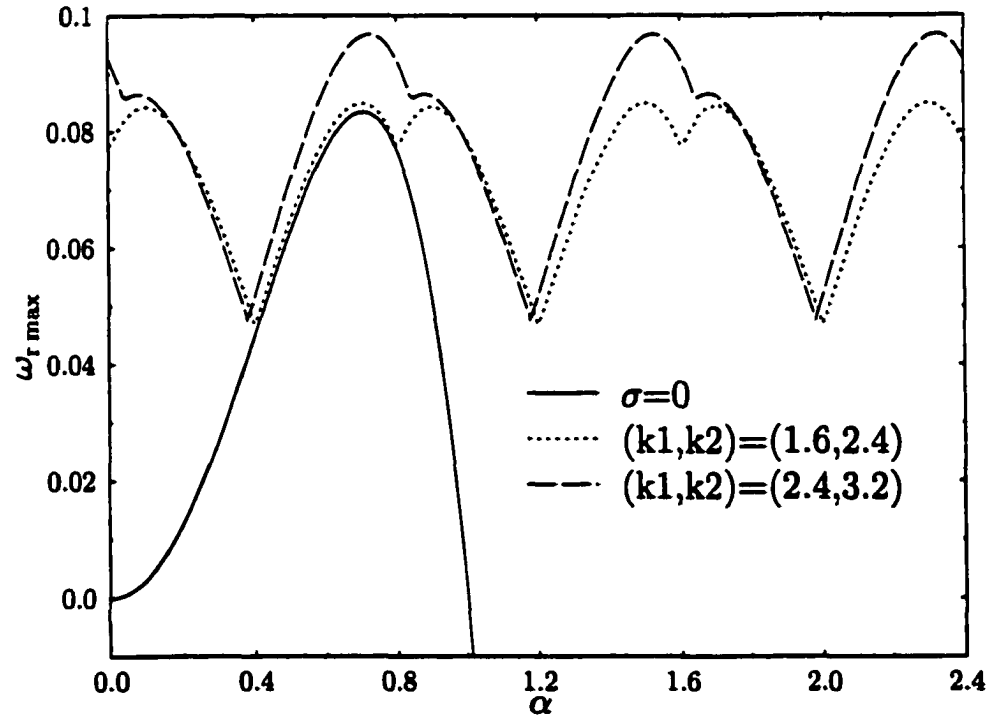

Figure 10. The growth rate in the presence of two wall wavelengths.

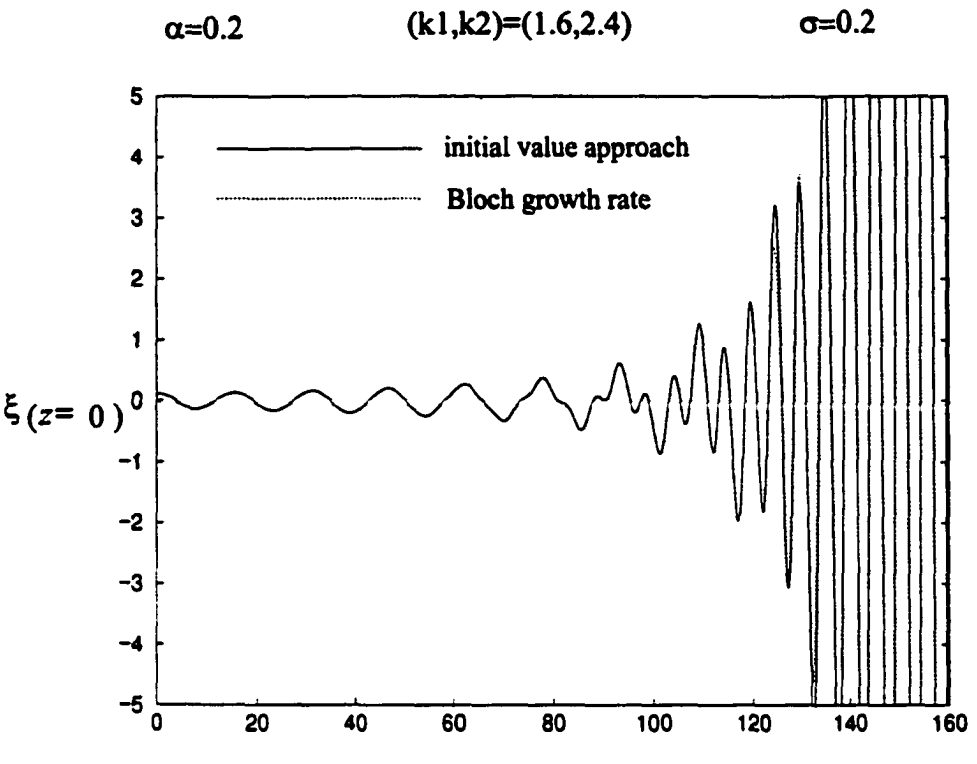

Figure 11(a). The interfacial evolutions at z =0 for ($k1$,$k2$) = (1.6,2.4).

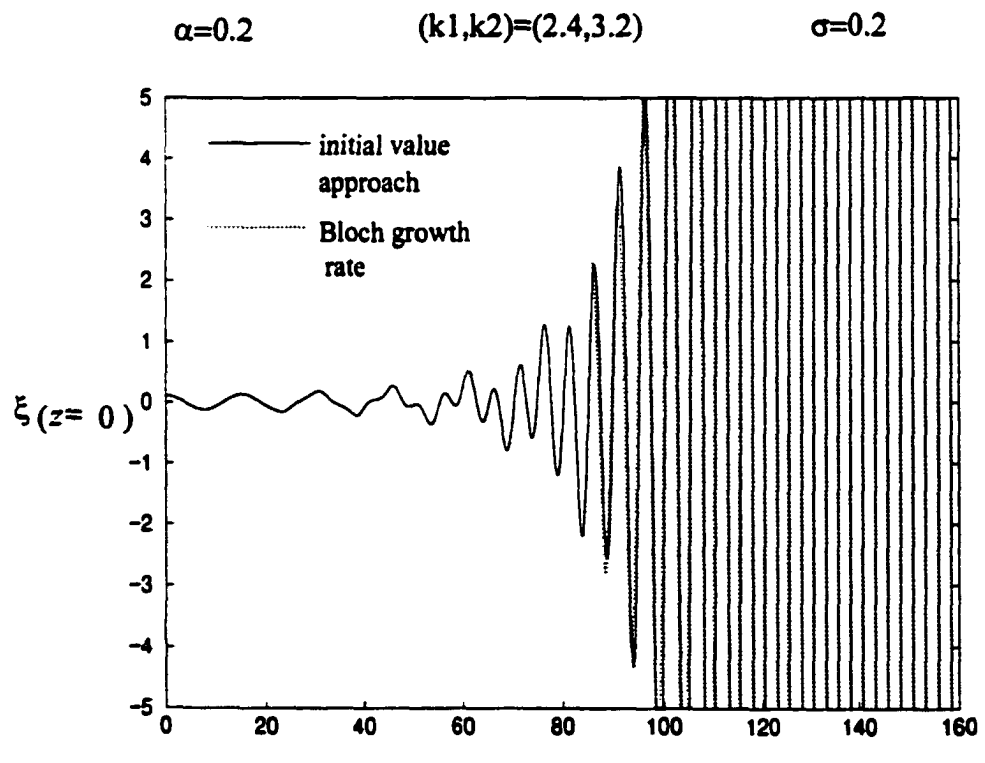

Figure 11(b). The interfacial evolutions at z =0 for ($k1$,$k2$) = (2.4, 3.2).

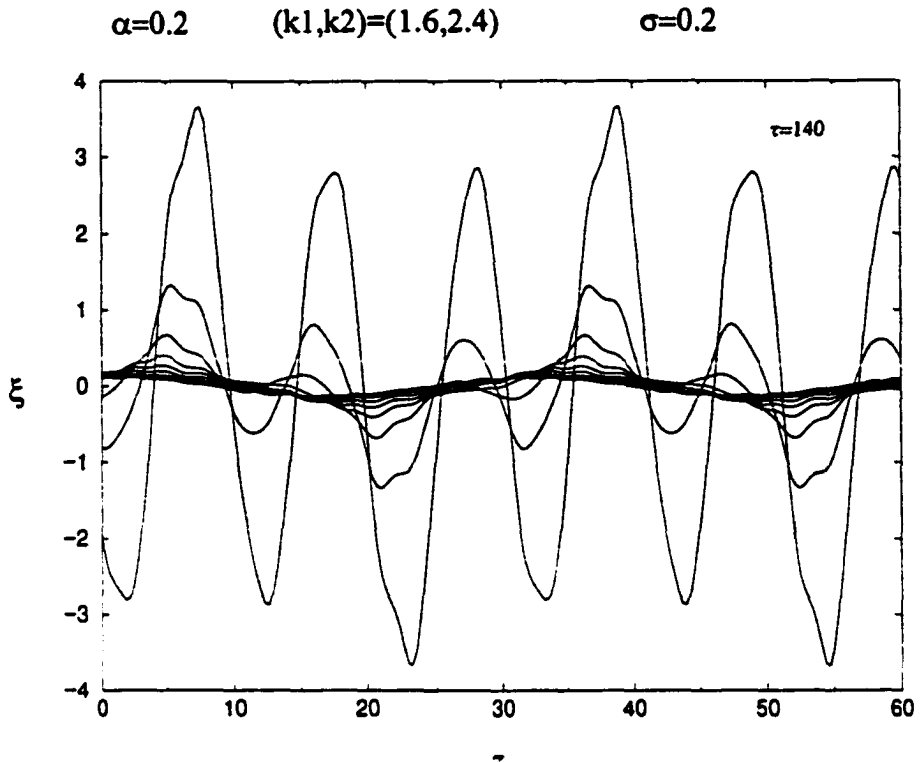

Figure 12(a). The corresponding spatial evolutions for the case in Figure 11(a).

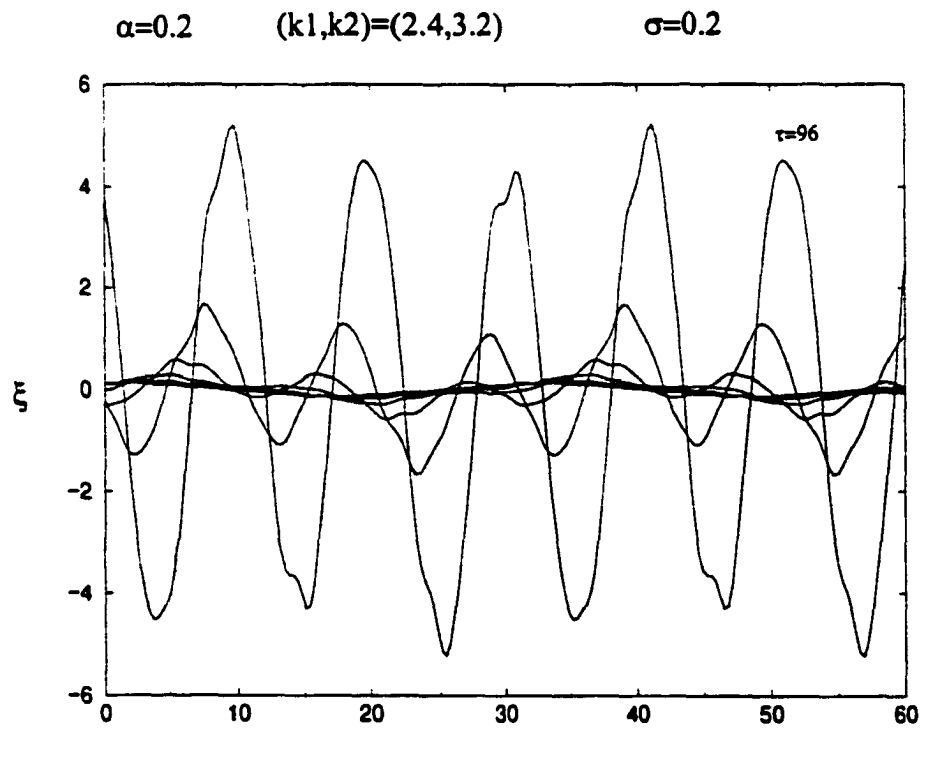

Figure 12(b). The corresponding spatial evolutions for the case in Figure 11(b).

III The Weakly Non-Linear Interfacial Stability of a Core Annular Flow in a Corrugated Tube

1. Introduction

Core annular flows (CAFs) have recently been used as model systems for improving many technologies such as oil recovery (Slattery 1974) and understanding respiratory distress in the lung, including surfactant transport (Halpern & Grotberg 1993). A perfect core annular flow (PCAF) in a straight, circular tube of uniform cross section is often adopted as an ideal model on which most studies are based. Understanding the mechanism of instability in this system is important because one may want to encourage or discourage instability depending on the application. The linear stability, for both the case with and without a base flow, is characterized by capillary, viscosity stratification and density stratification. Infinitesimal disturbances arise at the fluid-fluid interface and they may grow or be damped. Capillarity generally plays the most decisive role in determining the interfacial stability in the cylindrical geometry and in particular in the CAF. Capillarity acts in two ways: it destabilizes the interfacial circumferential curvature and stabilizes the longitudinal curvature of an interfacial deflection. The result of this competition is that disturbances with wavelengths shorter than the undisturbed interfacial circumference are linearly stable and those longer are linearly unstable due to capillarity. For a combination of capillarity and viscosity stratification, Joseph and coworkers (Preziosi, Chen & Joseph 1989, Hu & Joseph 1989 and Chen, Bai & Joseph 1990) have performed extensive investigations of CAFs by numerically solving the Orr-Sommerfeld equation. They have found for the parameter regime characteristic of lubricated pipelining (Preziosi *et al.* 1989) that viscosity stratification can stabilize the long wave destabilization of the capillarity at large enough, but not too large, Reynolds numbers. There exists a window of stability in Reynolds number space in which the CAF is linear stable. For most applications of

interest, the annular fluid's thickness is much smaller than the tube radius. Georgiou *et al.* (1992) has developed thin film asymptotics to analytically examine the linear stability of a PCAF in a vertical arrangement. With axisymmetric disturbances whose wavelengths are comparable to the tube circumference, they have shown analytically that viscosity stratification can stabilize the capillary instability for m <1 while it is destabilizing for m >1.

Study of the non-linear stability regime of these thin-film systems is important to better understand the system's response to disturbances of finite magnitude as well as to investigate the fate of linearly unstable waves. Hammond (1983) studied the two-fluid CAF in a tube with a thin annular film in absence of a base flow, for which the core's dynamics become irrelevant at leading order in the ratio ε of the film thickness to the undisturbed core radius. His nonlinear analysis showed that long wave disturbances can grow non-linearly and this suggests that they could potentially lead to film break up into lenses when sufficient liquid is present. However, the extent of validity of his equation was limited by the thin film approximation, which particularly impacts the mean curvature of the interface. This $O(\varepsilon)$ approximation admits a collar volume that never goes through a maximum so that the collar is always stable and need not form a lens. Gauglitz & Radke (1988) extended Hammond's analysis in an *ad hoc* manner equivalent to a Pade, rather than a Taylor, approximate by keeping the full non-linear circumferential curvature in the capillary but linearizing everything else in the normal stress balance at the fluid-fluid interface. Their analysis can predict the transition from collars to lenses, while Hammond's thin film analysis might be able to predict this transition only at a higher order in ε approximation.

In presence of a base flow and a very strong surface tension, Frenkel *et al.* (1987) found that the Kuramoto-Sivashinky (KS) equation governs the weakly nonlinear evolution of fluids with matched viscosities and densities. In their case, only capillarity destabilizes and the core's dynamics slave those of the film. The non-linear coupling to the base flow

through the kinematic condition can steepen unstable interfacial long waves. This gives rise to shorter length scales which become stabilized by the longitudinal component (the fourth derivative of the interfacial deflection) of the interfacial tension force. The Kuramoto-Sivashinky equation has arisen in a variety of applications and exhibits complex dynamic behaviors depending on the period length. Numerical solutions on a periodic domain have exhibited nontrivial steady states (Chang 1987), traveling waves (Hooper & Grimshaw 1989), and spatial and temporal chaotic motions (Sivashinky & Michelson 1980, Hyman *et al.* 1986, Hyman & Nicolaenko 1986). The most important feature of these investigations is that KS seems to yield smooth and *bounded* solutions.

Frenkel (1988) suggested extending his approach to incorporate viscosity stratification and inertia of the core flow, and anticipated that the small amplitude equation would include an additional term which may contribute dispersive and dissipative effects. Papageorgiou, Maldarelli & Rumschitzki (1990) (referred to herein as PMR) systematically developed a weakly non-linear analysis of CAF film flows for generally different viscosities and densities and for surface tensions where the core dynamics are integrally coupled to the interfacial evolution. They derived an amplitude equation to describe the interfacial dynamics which turns out to be a Kuramoto-Sivashinky equation modified via the inclusion of additional terms containing integral kernels involving core quantities. In the case of slow and moderate flows, this equation has non-local terms that reflect the coupling due to viscosity stratification of the core's dynamics to the interfacial evolution. These core-coupling terms also give rise to additional dispersive and dissipative effects. They can lead to either chaotic interfacial motions for weak dispersion, or more typically to nonlinear traveling waves having more than one length scales for strong dispersion. PMR's additional terms demonstrate the regularizing effect of dispersion. This complements and is consistent with the model results obtained by Kawahara (1983) and Kawahara & Toh (1988) who added a simple third derivative dispersion term to the KS equation and found regularization.

The point here is that, apparently, the Kuramoto-Sivashinky-like systems can saturate the linearly unstable waves in the weakly non-linear regime. Kerchman (1995) has extended these results to a more general investigation of the strongly nonlinear interfacial dynamics of a CAF, including large amplitude disturbances. His analysis includes the weakly nonlinear analysis as special case. KS-type saturation of the instability occurs for sufficiently small $\varepsilon^2 J/Re_1$ (where $Re_1/J = \mu_1 W_0/\gamma$, μ_1 being the core viscosity, W_0 the centerline base flow velocity and γ the interfacial tension, can be regarded as the capillary number based on the core fluid). When $\varepsilon^2 J/Re_1$ is sufficiently large, though, the core-annular arrangement may collapse because the interface can strongly bulge into the core as a result of strong capillary forces acting in the neighborhood of an interfacial trough. As such, the interfacial stability of a PCAF in a circular tube is fairly well understood.

However, in real core-annular flow systems such as occur in secondary oil recovery, two fluids flow through uneven channels in the porous rock, and thus do not possess an ideal geometry like flows in a perfectly cylindrical tube. Similarly, the extensive branching of the bronchiole system represents a system with a frequently changing cross-section. It is thus conceivable that pore corrugations may play a role in determining the system's stability that is at least as important as the effects already considered. But there are good reasons why one might neglect them in the first analysis. Let us consider briefly how pore corrugations complicate the problem. First, such non-ideality will cause the base state to be significantly changed. Even the axisymmetric base flow pattern in a tube of varying cross section will be two-dimensional, rather than just a purely axial velocity as a function of only the radial position. This deviation from parallel flow can interact strongly with the disturbance introduced in the stability analysis. For instance, consider the flow of a single fluid in a sinusoidally varying tube, even for small Reynolds number Re. Inertial effects can be significant when the axial variation of the tube radius $\frac{dR}{dz}$ is as rapid as $O(1/Re)$. Moreover, it is unlikely that one would be able to solve for the base state exactly in closed

form. Cylindrical tube theory clearly does not include these effects. To access them, it is necessary to extend the scope of this theory to include the varying geometry.

There have been several studies of base flows without an accompanying stability analysis. Wang (1981) consider a film flowing slowly down a wavy inclined plate, where the striations are parallel to the overall flow. He applied a perturbation method with respect to the small amplitude of the corrugation. He found that for a fixed mean film depth, the flow transverse to the striations is decreased relative to that of a smooth plate while the flow along the striations is increased. Dassori, Deiber & Cassano (1984) analyzed a two-fluid system in a symmetric sinusoidally varying two dimensional channel. They only focused on the case of an outer fluid (e.g., a gas) with very low density and viscosity ratios relative to the core fluid. They found that the fluid interface exhibited a wavy shape, characterized by an amplitude and a phase shift relative to channel, which are functions of surface tension, density, viscosity ratios, flow rate, and the wave number of the wall. Recently, Kang & Chen (1994) extended Wang's analysis to the case with two fluid-fluid interfaces in a planar system and a similar picture resulted. In cases of large variation due to corrugation, perturbation techniques as above are no longer applied. Pozrikidis (1988) extends Wang's problem to large corrugations and solves the two dimensional creeping flow numerically on a periodic domain by using the boundary integral method. He shows that Wang's asymptotic analysis overestimates the effect of the wall's waviness on the deflection of the interface, particularly at high flow rates.

However, linear or non-linear stability issues associated with flows in the corrugated configuration, especially interfacial problems, have only been explored in a preliminary manner. In the case of no flow, Gauglitz & Radke (1990) employed their previous analysis (1988) to examine how constrictions affect foam formation in gas-liquid displacements for the case where the radius varies slowly in the axial direction. They showed that the time needed to snap a collar off strongly depends on the neck radius of the constriction and that the length of the constriction is not crucial to the instability. A similar

conclusion was also drawn by Ransokoff, Radke & Gauglitz (1987) and Ratulowski & Chang (1989), who analyzed the case where constrictions have various cross-sections.

Tougou (1978) investigated the linear and weakly nonlinear stability of a viscous film flowing down an inclined, uneven wall in the presence of surface tension. In the leading order of a shallow thickness parameter ε, defined here as the ratio of the mean film thickness to the wall's wave length, the linear stability of the base flow is identical to that for the plane wall case. His weakly nonlinear analysis derived a KS-type equation incorporating the wall's non-uniformity and showed that the long-time interfacial evolution for an asymptotically long wave wall and is no longer spatially periodic due to the non-parallel base flow.

We have developed an analysis (Wei & Rumschitzki, 2000-Chapter II) that uses asymptotic methods and Floquet-Bloch theory to analytically examine the linear stability of a CAF in a corrugated tube. We develop steady base flows in an asymptotic sense in powers of ε and σ, the latter characterizing the strength of the corrugation relative to the mean annulus thickness. We then derive the corresponding linear stability to the leading order in both small parameters. This procedure leads to a linear interfacial evolution equation with non-constant coefficients. Floquet-Bloch theory leads to the eigenvalue spectra as a function of the wall's wave number k and these spectra exhibit periodicity in α-space, where α is the wave number of the initial disturbance. Direct numerical solutions of the interfacial evolution partial differential equation for a variety of initial conditions are performed and compare very well with the eigenvalue spectra. The results reveal that the wave length of the initial interfacial disturbance is modified due to interactions with the wall's corrugation. As a result, in contrast to the case of a CAF in straight tube, an initial disturbances whose wave length is shorter than the circumference of the undisturbed fluid-fluid interface can also lead to an instability due to the unstable higher wall corrugation harmonics excited by the initial disturbance.

The above discussion suggests two opposing trends in the weakly nonlinear regime of a core-annular flow in a tube of varying cross section. On the one hand, coupling of an initially short wave length disturbance to the wall's corrugation excites unstable long wave length wall harmonics of the initial disturbance. On the other hand, the nonlinearity in KS and related equations steepen growing long waves, thereby shortening their effective wave length and stabilizing them via the fourth derivative capillary term. Our aim in this chapter is to systematically extend our previous analysis into the weakly non-linear regime in order to examine which of these trends dominates. In particular, can the nonlinearity saturate all of the unstable harmonics generated by the corrugation and will the resulting dynamics be chaotic or regular?

2. Mathematical Formulation

2.1 Governing Equations and Boundary Conditions

Two immiscible, viscous, incompressible fluids are flowing axisymmertically in a core-annular arrangement in a horizontal tube of radius $R_2(z)$ that varies in the axial direction with slight corrugation. The interface is given by $r = S(z,t)$. The core region, defined by $0 \le r \le S(z,t)$, is occupied by fluid 1 and the annulus, $S(z,t) \le r \le R_2(z)$, is filled by fluid 2. Since the flow fields are assumed to be axisymmetric, they only have velocity components $(u,0,w)$ in terms of the cylindrical polar coordinates (r,θ,z). We non-dimensionalize the velocity, pressure, length scales and time with the characteristic quantities W_0, ρW_0^2, R_0, and R_0/W_0, respectively, where W_0 is the axial velocity at the central line $r=0$ (NB: application to the respiratory problem requires a rescaling with γ/μ where γ is the surface tension, rather than the center line velocity) in the uncorrugated base flow, ρ is density of the fluids taken for now to be equal, and R_0 is the mean radius of the core.

The non-dimensional governing equations in each phase are given by

$$w_t + uw_r + ww_z = -p_z + \frac{1}{Re_i}\nabla^2 w, \tag{2.1a}$$

$$u_t + uu_r + wu_z = -p_r + \frac{1}{Re_i}\left(\nabla^2 u - \frac{u}{r^2}\right), \tag{2.1b}$$

$$\frac{1}{r}(ru)_r + w_z = 0, \tag{2.1c}$$

where $\nabla^2 = \frac{\partial^2}{\partial r^2} + \frac{1}{r}\frac{\partial}{\partial r} + \frac{\partial^2}{\partial z^2}$, $i = 1, 2$ denotes the core and the annulus, respectively and the Reynolds number is given by $Re_i = \frac{\rho W_0 R_0}{\mu_i}$. We use Re_1 for the core as the reference Reynolds number. The annulus Reynolds number is $Re_2 = \frac{Re_1}{m}$, in which $m = \frac{\mu_2}{\mu_1}$ is the viscosity ratio of the annulus to the core.

Define the jump notation $[\bullet] = (\bullet)_1 - (\bullet)_2$. The following boundary conditions are used: The velocities vanish on the wall

$$w = 0,\ u = 0, \quad \text{at } r = R_2(z). \tag{2.2a}$$

The velocities are continuous across the interface,

$$[w] = 0,\ [u] = 0, \quad \text{at } r = S(z,t). \tag{2.2b}$$

The tangential stress and normal stress balances apply at the fluid-fluid interface:

$$\left[\frac{1}{Re}(u_z + w_r)(1 - S_z^2) + \frac{2}{Re}u_r S_z - \frac{2}{Re}w_z S_z\right] = 0, \quad \text{at } r = S(z,t), \tag{2.2c}$$

$$-\left[p - \frac{2}{Re}u_r - \left(-p + \frac{2}{Re}w_z\right)S_z + \frac{2}{Re}(u_z + w_r)S_z\right]$$

$$= \frac{J}{Re_1^2}\left(S_{zz} - \frac{1}{S}\left(1 + S_z^2\right)\right)\left(1 + S_z^2\right)^{-3/2}, \quad \text{at } r = S(z,t), \tag{2.2d}$$

where $J = \frac{\gamma R_0}{\rho v_1^2}$ is the surface tension parameter used by Chandrasekhar (1968) and where γ is the interfacial tension. The kinematic condition, which determines the shapes of the interface, is

$$u = S_t + wS_z, \quad \text{at } r = S(z,t), \tag{2.2e}$$

Finally, the core's flow field must be bounded at the central line, i.e.,

$$w \text{ bounded and } u = 0 \text{ as } r \to 0. \tag{2.2f}$$

2.2 Scalings and Asymptotic Formulation

In the previous study on the linear stability, we found that the scaling relation $J/Re_1 \sim 1/\varepsilon^2$ yields a non-trivial corrugated base flow in the CAF configuration and we have determined the base flows at the leading order in ε and σ. The solution for the flow pattern is determined by the interfacial deflection η ($S_b = 1 + \sigma\varepsilon\eta + ...$), which the following equation for the interfacial shape governs:

$$\frac{J_0}{3\lambda}(\eta_{zzz} + \eta_z) + 2\eta = 2\phi, \tag{2.3}$$

where $J = J_0/\varepsilon$ and $Re_1 = \lambda\varepsilon$, λ and J_0 both order one constants. Note that the solution to η is independent of the viscosity stratification m since the core does not contribute to leading order at these scales and $J_0/6\lambda$ is just the ratio of the capillary to the shear forces ($Re_1/J = Ca$). Then the film solution is

$$w_b = \bar{\bar{w}} + \bar{w} = \frac{2\varepsilon}{m}y + \varepsilon\sigma\left(\frac{J_0}{m\lambda}(\eta_{zzz} + \eta_z)(\frac{1}{2}y^2 - y) + \frac{2}{m}\phi\right) + O(\varepsilon^2,\ \varepsilon^2\sigma,\ \sigma^2\varepsilon), \tag{2.4a}$$

$$u_b = \bar{u} = \varepsilon^2\sigma\left(\frac{J_0}{m\lambda}(\eta_{zzz} + \eta_z)(\frac{1}{6}y^3 - \frac{1}{2}y^2) + \frac{2}{m}\phi_z y\right) + O(\varepsilon^3\sigma, \sigma^2\varepsilon^2), \tag{2.4b}$$

$$p_b = \bar{\bar{p}} + \bar{p} = \bar{\bar{p}} + \frac{\sigma}{\varepsilon^2}(\eta + \eta_{zz}) + O(\frac{\sigma}{\varepsilon}, \frac{\sigma^2}{\varepsilon}). \tag{2.4c}$$

We briefly summarized the film base flow here and neglect the core since it merely slaves the film (up to $O(1)$ Re_1) and does not contribute to the system's stability. Also, as noted in Chapter II, the previous analysis can also be extended to both $\varepsilon^2 J/Re_1 >> 1$ and $\varepsilon << \varepsilon^2 J/Re_1 << 1$ regimes without significant change to the formulation.

With the asymptotic, steady base flows derived from the previous study, we now begin the corresponding asymptotic weakly nonlinear stability analysis. Instead of an infinitesimal disturbance for the linear analysis, we introduce a finite, axisymmetric disturbance of size δ at the steady interface in such a way that $S(z,t) = S_b(z) + \delta\xi(z,t)$, where $S_b(z)$ is the interface of the corrugated base state, $\xi(z,t)$ is an unknown order one function responsible for the disturbance, and δ is small compared with the undisturbed core radius and film thickness, i.e., $\delta << |S_b|, \varepsilon$. Clearly, $\delta \to 0$ recovers the base flows, and $O(\delta)$ leads to the linear stability problem. In general, the fully non-linear analysis allows $\delta \sim \varepsilon$, which means that the size of the disturbance is comparable to the film thickness. However, we would like to scale $\delta = \delta(\sigma,\varepsilon) << \varepsilon$ to constraint disturbances within the weakly nonlinear regime.

We first determine the scalings of the disturbed quantities before formulating the perturbation scheme. We follow the scaling procedure used in the linear analysis, which is similar to Hammond (1983), Papageorgiou *et al.* (1990) and Georgiou *et al.* (1992). We use ε, the ratio of the undisturbed film thickness to the mean core radius as the small parameter. By introduction of a stretched film variable $y = 1 - \frac{r-1}{\varepsilon}$, we can make the thin film explicit and separate the film's radial scale from its axial scale and from both scales in the core. As such, radial derivatives in the film are large, i.e., $\frac{\partial}{\partial r} = -\frac{1}{\varepsilon}\frac{\partial}{\partial y}$. Let (w', u', p') and (W', U', P') represent the disturbed quantities for the film and the core, respectively. One can estimate the scalings of these quantities in the case

of $Re_i \sim \varepsilon$ and $J \sim 1/\varepsilon$ by using the scaling relation for the base flows together with the governing equations and boundary conditions. From the normal stress condition, $p' \sim \delta/\varepsilon^3$. Relating w' with p' by the use of the lubrication equations in the film brings out $w' \sim \delta$, and $u' \sim \varepsilon\delta$ follows by continuity. For the core, which lacks separable length scales, both W' and U' are of order δ, which is a consequence of the continuity of velocity, and P' is of order δ/ε from the equations of motion.

We now need to know the order of δ. Since the annular region is thin, the lubrication equations govern the flow there. The film's non-linear inertia is of higher order, and thus the non-linear terms in the stability analysis derive from the kinematic condition. This condition couples the derivative of the disturbed interface position either to the base flow velocity at the disturbed interfacial position, or directly to the disturbed flows. Thus, the kinematic condition should provide the scaling of δ in this weakly non-linear analysis. We begin with the expansions for the film,

$$w = w_b + \delta w', \quad u = u_b + \varepsilon\delta u', \quad p = p_b + \frac{\delta}{\varepsilon^3} p' \qquad \text{(2.5a)-(2.5c)}$$

and for the core,

$$W = W_b + \delta W', \quad U = U_b + \delta U', \quad P = P_b + \frac{\delta}{\varepsilon} P', \qquad \text{(2.5d)-(2.5f)}$$

where the quantities with subscript 'b' denote the base flow quantities, which have nontrivial σ and ε expansions. Let $(w_b, u_b) = (\varepsilon\bar{w} + ..., \sigma\varepsilon\bar{u} + ...)$ for the film base flow. Then the kinematic condition, evaluated at the base interface S_b expanded with respect to δ, gives

$$\delta\left(-\sigma\varepsilon\bar{u}_y\xi + \varepsilon u'\right) - \delta^2 u'_y \xi + O(\sigma\delta^2)$$

$$= \delta\xi_t + \varepsilon\delta\bar{w}\xi_z + \delta S_{bz}\left(-\bar{w}_y\xi + w'\right) + \delta^2\xi_z\left(-\bar{w}_y\xi + w'\right) + O(\delta^3). \qquad (2.6)$$

Note that $S_{bz} \sim \sigma\varepsilon$ here. We introduce the long time scale $\tau = \varepsilon t$ to capture the dynamics of the leading order of (2.6) at $O(\varepsilon\delta)$. Since the weakly non-linear analysis requires

$\delta/\varepsilon << 1$, δ/ε should be scaled using the system's small parameters ε and σ. Different scaling choices for the parameters may lead to different dynamic characters. We shall discuss this in the next section.

As we shall see below, after plugging the appropriate asymptotic expansions into the governing equations and the boundary conditions and extracting the corrugated base flow contribution from these equations, one can derive an equation that governs the system's stability up to δ^2 within the weakly nonlinear regime. At zeroth order in δ, one should recover the base flow. After using the base state relations, the linear stability of the system appears at the first order in δ, and δ^2 should give any additional weakly nonlinear effect. In order to allow a larger scope to this scaling analysis and to provide the context for a general discussion later on, it is more convenient to keep δ unscaled in eqn. (2.5) during the formulation.

A full knowledge of the base state to all orders in σ and ε provides an exact solution of the nonlinear, steady state Navier-Stokes equation subjected to the corrugated boundary's conditions. We have only solved the base flow asymptotically and have thus far only determined its leading order contributions explicitly. However, when substituting (2.5) into (2.1) and (2.2), we shall use the fact that the full steady state solution satisfies the steady state equations and boundary conditions exactly and its truncated solutions satisfy these equations / conditions exactly up to the order of truncation. This will allow us to retain only terms of $O(\delta)$ and higher. The coefficients will only contain explicit contributions from the leading order of the corrugated base flow. As such, this step can be achieved without knowing any details about the higher order solutions of the base states.

Let $Re_1 = \varepsilon\lambda$ and $J = J_0/\varepsilon$, where λ and J_0 are $O(1)$. In order for the corrugation terms to be of lower order than the first ε-order correction to leading order (see the tangential stress condition below), we assume $\sigma >> \varepsilon$, which for these scales, also

decouples the core. From this point, we drop the primes for the disturbed quantities. The leading order of the film's governing equations become

$$0 = -p_z + \frac{m}{\lambda} w_{yy}, \tag{2.7a}$$

$$0 = p_y, \tag{2.7b}$$

$$-u_y + w_z = 0. \tag{2.7c}$$

For the core, we have

$$0 = -P_z + \frac{1}{\lambda}\nabla^2 W, \tag{2.7d}$$

$$0 = -P_r + \frac{1}{\lambda}\left(\nabla^2 U - \frac{U}{r^2}\right), \tag{2.7e}$$

$$\frac{1}{r}(rU)_r + W_z = 0, \tag{2.7f}$$

subject to the boundary conditions below:

On the wall:

$$y = -\sigma\phi, \;\; w = 0, \;\; u = 0. \tag{2.8a}$$

At the interface $r = S(z, t)$, we expand around the base state interface $S_b(z)$. After eliminating the base flow contributions, the leading terms in ε and δ for each boundary condition (other than the kinematic condition eqn. (2.6)) are:

Continuity of velocity to $O(\delta)$

$$-\xi\left(\frac{2}{m} + \sigma\overline{w}_y^{(1)}\right)_{y=1} + w(y = 1 - \sigma\eta) = -2\xi + W(r = 1) + O(\sigma\varepsilon);\; U(r = 1) = O(\varepsilon). \tag{2.8b}$$

The tangential and normal stress balances to leading order $O(\delta/\varepsilon)$ are dominated by film variables:

$$-w_y(y = 1 - \sigma\eta) + \sigma\xi\overline{w}_{yy}^{(1)}(y = 1) = O(\varepsilon), \tag{2.8c}$$

$$\text{at } y = 1 - \sigma\eta, \;\; p = \frac{J_0}{\lambda^2}(\xi_{zz} + \xi). \tag{2.8d}$$

In (2.8c), $\overline{w}^{(1)}$ is the coefficient of the $O(\sigma\varepsilon)$ axial velocity in (2.3a) for the film's base flow. Note that the normal stress does not contain the base flow's interface to leading order. From (2.2d), one can separate the curvature κ into the base flow interface S_b's contribution $\kappa_b = \left[S_{bzz} - \frac{1}{S_b}\left(1+S_{bz}^2\right)\right]\left(1+S_{bz}^2\right)^{-3/2}$ plus a the disturbed curvature

$$\kappa' = \delta\left\{\xi_{zz} + \frac{\xi}{S_b^2}\left(1+S_{bz}^2\right) - \frac{2}{S}S_{bz}\xi_z - \xi_z S_{bz}\left[S_{bzz} - \frac{1}{S_b}\left(1+S_{bz}^2\right)\right]\left(1+S_{bz}^2\right)^{-1}\right\}\left(1+S_{bz}^2\right)^{-3/2},$$

The base flow's curvature κ_b balances the base flow's normal stress. In κ', the interaction terms, such as $\delta S_{bz}\xi \sim \delta\sigma\varepsilon$ that derive from S_z^2 are of higher order than $\delta\left(\xi_{zz}+\xi\right)$.

Solving for w and u from (2.7a)-(2.7c) gives

$$w = \frac{\lambda}{2m}p_z y^2 + Cy + D, \tag{2.9a}$$

$$u = \frac{\lambda}{6m}p_{zz}y^3 + \frac{1}{2}C_z y^2 + D_z y + E, \tag{2.9b}$$

where $C = -\frac{\lambda}{m}p_z(1-\sigma\eta) + O(\sigma^2)$, $D = -\frac{\lambda}{m}p_z\sigma\phi + O(\sigma^2)$ and $E = O(\sigma^2)$. We then substitute (2.9) into (2.6) and use (2.8d) to derive (2.10), the weakly nonlinear interface evolution inclusive of corrugation.

$$\begin{aligned}&\xi_t + \frac{2}{m}\xi_z + \frac{J_0}{3m\lambda}\left(\xi_{zz}+\xi\right)_{zz} + \sigma\left[(\eta-\phi)\cdot\left(\frac{4}{m}\xi - \frac{J_0}{m\lambda}\left(\xi_{zz}+\xi\right)_z\right)\right]_z + \\ &\left(\frac{\delta}{\varepsilon}\right)\left(-\frac{2}{m}\xi\xi_z - \frac{J_0}{m\lambda}\left(\xi\left(\xi_{zzz}+\xi_z\right)\right)_z\right) + O\left(\varepsilon,\sigma^2,\delta\sigma\varepsilon^{-1}\right) = 0.\end{aligned} \tag{2.10}$$

At the leading order in δ, this equation recovers the linear analysis, which consists of the straight tube contribution and of the $O(\sigma)$ term in square bracket due to the corrugation. The dependence on the corrugation is reflected by the variation of the base flow film thickness $(\eta-\phi)$ with z. The next order in δ (here $O(\delta/\varepsilon)$) gives the leading non-linear terms. The first nonlinear term comes from the shear flow and is the usual (e.g.,

Papageorgiou *et al.* 1990) Kuramoto-Sivashinsky term. The second nonlinear term arises from the capillarity. Note that we still remain in the laboratory frame (that is, we retain the convective term $\frac{2}{m}\xi_z$) instead of switching to a moving frame because of the presence of the corrugation. As we shall see in the next section, special forms of (2.10) apply to different scalings of J_0/λ, and thus of δ.

2.3 Numerical Method

To examine the impact of corrugation on the system's stability, it is necessary to compare the numerical simulations for $\sigma = 0$ with those for $\sigma \neq 0$. Since the numerical solution must be calculated on a periodic domain, it is useful to employ spectral methods. Consider a periodic domain with period $2\pi/\beta$. We construct the solution to ξ as

$$\xi(z,\tau) = a_0(\tau) + \sum_{n=1}^{N}\left(a_n(\tau)cos(\beta nz) + b_n sin(\beta nz)\right), \qquad (2.11)$$

subject to a cosine wave initial condition $\xi(z,\tau = 0) = A cos(\alpha z)$ of initial wave number α. We choose the amplitude A of the initial interfacial profile is relatively small (e.g., $A = 0.1$) so that its development starts within the linear regime. For $\sigma = 0$, the linear dispersion equation for mode n has a growth rate $\frac{J_0}{3m\lambda}(\beta n)^2\left(1-(\beta n)^2\right)$, which suggests that the modes with $\beta n > 1$ should decay with time and those with $\beta n < 1$ should grow as linearly unstable waves. For $\sigma \neq 0$, however, the wavelength $2\pi/k$ of the wall enters. Although k can be an arbitrary real positive number independent of the choice of the initial wave number α, we choose it to have a rational ratio with α so as to guarantee that there is a period over which both the initial disturbance and the wall are periodic. We can choose β to be the greatest common divisor of k and α, and let $(k, \alpha) = (n_k, n_\alpha)\beta$ where n_k are n_α are fixed integers. We also choose α and k such that α belongs to the linear

unstable branch according to our linear theory (see Chapter II, Wei and Rumschitzki, 2000). With this choice, inserting (2.11) into (2.10) results in a system of ordinary differential equations for amplitudes $a_n(\tau)$ and $b_n(\tau)$. We employ a 4th order Runge-Kutta method to solve these temporal equations and use time steps from 2×10^{-4} to 10^{-3}, depending on the parameters. We choose the number N of modes retained large enough to resolve the spatial variation so that high harmonic modes decay. Typically N = 16 is chosen for the most simulations. We determine $a_n(\tau)$ and $b_n(\tau)$ within 1% absolute error tolerance. We check the spatial convergence by doubling the number of modes to verify that the spatial evolution does not change significantly.

3. Results and Discussion

We now examine the numerical solutions for the weakly non-linear interfacial evolution as given by (2.10). We examine the case when $\varepsilon^2 J/Re_1$ is $O(1)$ and between $O(1)$ and $O(\varepsilon)$.

3.1 Strong Interfacial Tension Case $\varepsilon^2 J/Re_1 \sim O(1)$

Let us first consider the strong interfacial tension case $\varepsilon^2 J/Re_1 \sim O(1)$. In the absence of corrugation at $\sigma = 0$, (2.10) becomes

$$\xi_\tau + \frac{2}{m}\xi_z + \frac{J_0}{3m\lambda}\left(\xi_{zz}+\xi\right)_{zz} - \left(\frac{\delta}{\varepsilon}\right)\left(\frac{2}{m}\xi\xi_z + \frac{J_0}{m\lambda}\left(\xi\left(\xi_{zzz}+\xi_z\right)\right)_z\right) = 0. \qquad (3.1)$$

This equation is equivalent to those given by Aul (1989), Kerchman & Frenkel (1994), Kalliadasis & Chang (1994) and Kerchman (1995) in the small amplitude disturbance limit. Note that there are weakly non-linear terms deriving from both shear and capillarity. Unlike the Kuramoto-Sivashinsky (KS) equation which only has a non-linearity due to shear that can saturate linearly unstable waves, the presence of the capillary non-linearity can,

depending on the relative strength of the shear and capillarity, even amplify the linear instability. It can thus in principle cause growth beyond the weakly nonlinear regime. That is, even though the solutions to this equation may predict a long-term evolution whose interfacial disturbances may remain bounded, they may become comparable to the mean film thickness, and so equation (3.1) may not be uniform valid in time (see Kalliadasis & Chang 1994 and Kerchman 1995). In the analysis of Kerchman (1995), for relatively small order one values of J_0/λ, the solutions show quasi-periodic or chaotic features similar to KS and thus the instability saturates in the weakly non-linear regime. For intermediate ranges of J_0/λ (about 0.7 in our notation), more film fluid can drain into the core. The film generally becomes more flattened but has larger bulges into the core. However, for even larger J_0/λ (about 0.9), strong core-bulging processes cause large interfacial amplitudes. Even though this solution remains numerically bounded, it is no longer weakly nonlinear and suggests that the core may snap off and break the CAF topology. These results qualitatively agree with Aul & Olbricht 's (1990) experiments.

Even though Kerchman's work is based on a strongly nonlinear analysis, the weakly nonlinear equation (3.1) shall show most of its qualitative features. When $\sigma \neq 0$, whether the corrugation or the non-linearity dominates or whether both are comparable, depends on J_0/λ and the size of perturbation δ. To bring the corrugation into the leading orders in the weakly non-linear regime, we choose $\delta \sim \sigma\varepsilon$ so that the non-linearity and the corrugation compete at the same order of σ in (2.10). We thus choose $\sigma = 0.2$ and $\delta/\varepsilon = 0.15$ throughout this subsection. Note that even though δ is scaled by the corrugation, we retain its size $\delta = 0.15\varepsilon$ for the limit $\sigma = 0$ for the comparison. We first numerically confirm the features of (3.1) for $\sigma = 0$ and then directly compare them with the case of (2.10) with corrugation. To do so, we remain in the laboratory frame throughout these simulations, even for $\sigma = 0$, rather than going to a moving frame, because it is more convenient for the corrugation case.

For $\sigma = 0$, as suggested by Kerchman (1995), we choose J_0/λ =0.7 and $m = 1$ to ensure that the resulting long-time interfacial evolution is bounded in the weakly nonlinear regime. We impose an initial disturbance α with small amplitude and a single unstable wavelength ($\alpha = 0.6$). Figure 1(a) shows a series of snapshots of the spatial-temporal interfacial evolution. At the early stages of the evolution, the interface grows according to the linear theory. When the interfacial amplitude size becomes sufficiently large (at about $\tau \sim 60$), non-linear effects become important and the interface then undergoes a local curvature change due to nonlinear coupling. As in Kerchman's results, the upper part of the interface flattens and forms two humps and the lower part appears sharper with a high curvature around the trough. But unlike the symmetric humps formed in the no flow case by Hammond (1983), these two humps are asymmetric due to the base state shear flow at the leading order in ε. The long-term development is shown in Figure 1(b). Steady waves are established at about $\tau \approx 100$, and travel with a speed $c \approx 2$ (due to the retention of the linear convective term $\frac{2}{m}\xi_z$) in space. Note that even though the waves appear to be traveling backwards in the z-direction due to the time between traces, they actually travel forwards. During the given time interval $\Delta\tau$ =20, the waves travel over a distance $c\Delta\tau \approx$ 40. The resulting waves move a distance slightly less than four-times the dominant wave length $2\pi/\alpha$ ($4 \cdot 2\pi/0.6 \approx 41.9$). Therefore, the waves look as if they are traveling backwards.

Corrugation has the potential of complicating these pictures for $\sigma = 0$. Recall in the linear theory that the corrugation can respond to a short wave disturbance by exciting the growth of long wave wall harmonics of the initial disturbance at times of order $O(ln(1/\sigma))$. It may be interesting to see whether the nonlinearity accelerates or decelerates this corrugation-modified long wave instability. As such, we select the following cases for a preliminary examination of the impact of corrugation on the solution of eqn. (2.10):

(α,k)=(0.6,1.8), (1.2,1.8), and (1.8, 2.4). According to the linear theory, in the first case, the primary interfacial action is growth (0.6<1) with the initial unstable wavelength later augmented by the higher harmonics of the wall corrugation. The latter two cases, however, will begin with a decaying initial disturbance which only at later times excites unstable harmonics whose resulting linearly unstable wavelengths coincide with those of the previous case. That is, all three of these cases have a dominant unstable wave number 0.6 in the linear regimes. Figures 2 - 4 show the spatial-temporal evolutions of these three cases.

At first glance, these long-term evolutions generally show the same dominant wavelength and give similar interfacial shapes and traveling waves as does the $\sigma = 0$ case. However, there are some different details in the local interfacial behavior. In contrast to $\sigma = 0$, temporally oscillatory motions are present in the quasi-steady traveling waves as they pass the crests and troughs of the wall. In Figure 2 with (α,k)=(0.6,1.8), similar to Figure 1(b), the interface first amplifies the initial long wave mode. However, it then develops quasi-steady traveling waves with temporal oscillations visible every two frames in 20 time units. When imposing a short wavelength disturbance such that $|\alpha - k| < 1$, as in Figures 3 and 4, the interface undergoes a transition from the decaying mode with an initial short wave length disturbance to a growing mode with a long wave length in the linearly unstable regime; thus the time required to significantly enlarge the amplitude into the non-linear regime is prolonged. For (α,k)=(1.2,1.8) as shown in Figure 3, the evolution reaches a quasi-steady state at $\tau \approx 200$, but then shows almost identical local oscillatory behavior to Figure 2. In the case of (α,k)=(1.8,2.4), the transient state (not shown) takes even longer to develop because of the more rapid decay of the initial mode. The long-term interfacial motions are similar to those in Figure 3 (note the similarity in shape between waves at τ=300 in Figures 2 and 3, and τ=400 in Figure 4), but the quasi-steady state behavior in Figure 4 is rather different from those in the previous cases. There are four

frames per cycle of oscillatory motions and they have stronger modulations than do the earlier cases. The different numbers per cycle again appear to coincide with the more frequent occurrence of the wall crests and troughs for the large wall wave number k.

Figures 5 show the case of (α,k)=(0.3,2.4) whose most unstable wave is 0.3, but whose wall's wave number is the same as in Figure 4. Here the waves appear more intricate. As shown in Figure 5(b), they appear to require eight frames for an oscillatory cycle when $\tau = 500 \sim 660$. This intricacy is not surprising since the dominant linearly unstable wave is different from the previous cases. Note that all of these corrugation cases have a similar traveling wave speed $c \approx 2$ with a small corrugation correction for each case. The longer the dominant wave length, the longer the time a wave travels over a distance equal to its wave length. On the other hand, the shorter the wall wave length, the more frequently the interface with a longer wave length encounters the wall's crests and troughs; therefore the time periodicity becomes longer. This time periodicity is roughly proportional to the ratio k/α_d of the wall wave number to the dominant wave number α_d. For the same wall's waviness $k = 2.4$ as in Figures 4 and 5, the dominant wave length in Figure 5 is twice that in Figure 4. The resulting oscillation period in Figure 5 is double that in Figure 4. Similarly, for the same dominant wave as in Figures 3 ($k = 1.8$) and 4 but for a different k, we estimate the period in Figure 4 as 1.5 (or 2) times that in Figure 3.

In summary, for J_0/λ=0.7, the results above show that the nonlinear saturation overcomes the continual excitation of new, unstable long waves by the corrugation and leads to steady or quasi-steady traveling waves.

If we increase the scaled inverse capillary number as $S = \varepsilon^2 J/Re_1 >> 1$, the capillary force overwhelms the effect of the base flow, and we might expect to approach Hammond's limit. Recall that in this limit, the leading order base state is cylindrical, i.e., $\eta = 0 + O(S^{-1})$. By assuming $S >> \sigma^{-1}$ and restricting the time scale of interest to $O(S^{-1})$, one finds that the base flow drops from leading order:

$$\xi_\tau + \frac{S}{3m}(\xi_{zz} + \xi)_{zz} + \sigma\frac{S}{m}\left[\phi\cdot(\xi_{zzz} + \xi_z)\right]_z - \left(\frac{\delta}{\varepsilon}\right)\frac{S}{m}\left[\xi(\xi_{zzz} + \xi_z)\right]_z + O(S^0) = 0. \qquad (3.2a)$$

Recall from, Chapter II, section 5.3, in the linear theory the presence of the corrugation can cause a resonance that amplifies the instability by $O(\sigma)$ for some ranges of wavelengths of both the disturbance and the wall. For convenience, let $\tau \to (m/S)\tau$. The leading order of (3.2a) becomes

$$\xi_\tau + \frac{1}{3}(\xi_{zz} + \xi)_{zz} + \sigma\left[\phi\cdot(\xi_{zzz} + \xi_z)\right]_z - \left(\frac{\delta}{\varepsilon}\right)\left[\xi(\xi_{zzz} + \xi_z)\right]_z = 0. \qquad (3.2b)$$

At $\sigma = 0$, this equation reduces to the weakly non-linear version of Hammond's equation, that is, with a linearized version of the cubic non-linearity. Consider an interface with a single long wavelength that is linearly unstable. For $\sigma = 0$, the capillary term can be rearranged as $\left(1 - 3\frac{\delta}{\varepsilon}\xi\right)(\xi_{zz} + \xi_{zzzz}) - \left(\frac{\delta}{\varepsilon}\right)\xi_z(\xi_z + \xi_{zzz})$. The first of these terms involves $h^3 = \left(1 - \frac{\delta}{\varepsilon}\xi\right)^3 \approx \left(1 - 3\frac{\delta}{\varepsilon}\xi\right) + O\left((\delta/\varepsilon)^2\right)$, the cube of the film thickness. This causes the interface's trough (with $\xi < 0$) to grow faster than its crest (with $\xi > 0$), since in the weakly-nonlinear regime it slightly amplifies growth at the trough and suppresses it at the crest relative to the linearly growing interfacial position. The second term causes the interface to levitate to the wall side. It has its strongest effect at the node $\xi = 0$ but no effect on the trough and crest since $\xi_z = 0$ there. As a result of both of these terms, the interface shape forms two symmetric humps at the upper part as well as a deeper and sharper trough at the lower part.

The numerical solution of (3.2b) (with $\alpha = 0.7$) is shown in Figure 6. The rate of change of the solution slows down markedly at $\tau \approx 90$. The interface shape is similar to the solution with Hammond's retention of the cubic factor, although the evolutions in Hammond's case does not reach a steady state. For the case with corrugation, we choose $k = 1.4$ so that the resonance in the linear theory occurs at the initial wave number $\alpha = 0.7$

of disturbance. Even ($0.1cos(\alpha z)$) and odd ($0.1sin(\alpha z)$) (there is no difference for $\sigma = 0$) parities of the initial condition are also chosen for comparison purposes, and the corresponding results are presented in Figures 7(a) and (b), respectively. Note that the wall profiles drawn in Figures 7 are not in true scale and only indicate a relative position between the interface and the wall. In general, the evolution for $\sigma \neq 0$ is more amplified than that for $\sigma = 0$. For an even initial interfacial profile, the interface appears to reach a steady state at $\tau \approx 220$. The two positive humps appear more pronounced than those for $\sigma = 0$, possibly indicating a local influx into the hump region and less drainage into the trough. On the other hand, the odd initial disturbance leads to a more unstable evolution than the even case. The interfacial amplitude is order 10 at $\tau = 100$, which is about 1.5ε and is clearly beyond the weakly non-linear regime. When the two humps form at the crest for the odd initial condition, they seem to grow faster with time rather than slowing down. Thus, this case shows no sign of approaching a steady state. In a qualitative comparison with Gauglitz & Radke (1990), the upper part of our odd initial interfacial profiles corresponds to their "thick-thin" case, which also showed a similar qualitative feature and a faster growing evolution. We also choose an initial condition $\frac{0.1}{\sqrt{2}}(cos(\alpha z) + sin(\alpha z))$ with both even and odd profiles together. The result is shown in Figure 7(c). The evolution also shows features similar to the odd case in Figure 7(b) and grows faster than the even case in Figure 7(a). It seems that the odd initial condition triggers more instability. Note that we restrict our attention to the above no flow limit (3.2a) for time scales $O(S^{-1})$. For even longer time scales, the weak base flow may continue to drive the film-drainage process even longer and form even larger lobes into the core, as shown in Kalliadasis & Chang (1994) or Kerchman (1995).

3.2 Less Strong Interfacial Tension Case $\varepsilon << \varepsilon^2 J/Re_1 << 1$

As shown by Sivashinsky & Michelson (1980) for the flow of a thin film on a vertical wall and Frenkel *et al.* (1987) for a core-annular flow of fluids of matched densities and viscosities, an intermediately strong interfacial tension $\varepsilon << \varepsilon^2 J/Re_1 << 1$ can lead to the Kuramoto-Sivashinsky (KS) equation. Again, let $S = \varepsilon^2 J/Re_1$. The weakly non-linear interfacial evolution at $\sigma = 0$ is governed by

$$\xi_\tau + \frac{2}{m}\xi_z + \frac{S}{3m}(\xi_{zz} + \xi)_{zz} - \left(\frac{\delta}{\varepsilon}\right)\frac{2}{m}\xi\xi_z = 0, \tag{3.3}$$

which, upon switching to a traveling reference frame, is just KS, whose dynamics are well known (e.g., Papageorgiou & Smyrlis 1991). Without the capillary-derived non-linearity that causes film drainage into large troughs, the shear non-linearity $\xi\xi_z$ shortens the growing linearly unstable long waves and the longitudinal component of capillarity saturates its growth. Extensive numerical investigations on a periodic domain (Sivashinsky & Michelson 1980; Frisch, She, & Thual 1986; Hyman & Nicolaenko 1986 and Papageorgiou & Smyrlis 1991) have shown that depending on the number of linear unstable waves per period, the solution generally exhibits complex chaos (long periods), dynamics such as uni- or multi-modal traveling waves, oscillations, or some combinations of these (Hyman & Nicolaenko 1986). However, as demonstrated by Kawahara (1983), the addition of a linear dispersion term (e.g., a third derivative term) to KS can regularize the chaotic motions and form traveling waves. Similar conclusions for more complicated dispersion forms arise from Papageorgiou *et al.* (1990) and Kerchman (1995).

Recall that, in the presence of wall corrugation, the base interface follows the shape of the wall (i.e., $\eta = \phi$). Thus the film thickness is uniform and the film flow is locally parallel to the leading order in σ and S. As a result, one can write the corrugation's contribution to the interfacial stability (see eqn. (2.3)) in terms of the wall function ϕ alone without η. To do this, we note from the base flow that the leading order film thickness is

$\eta - \phi = -\frac{S}{6}(\phi_{zz} + \phi_z) + O(S^2)$. To derive a weakly nonlinear equation that has a leading order corrugation contribution, we restrict our attention to a scaling $\sigma\varepsilon >> \delta$. Under these conditions, the capillary non-linearity $O(\delta S/\varepsilon)$ is of higher order than the corrugation $O(\sigma S)$, to which only a convective part contributes, while the capillary part of the corrugation is of higher order $O(\sigma S^2)$. Thus, one may choose δ to be either of order εS or $\sigma\varepsilon S$. In the former (latter) case, the non-linear term competes with the capillarity (the corrugation). Let us examine the latter case more closely. For $\delta \sim \sigma\varepsilon S$, capillarity is the only leading order term, and both the non-linear and corrugation terms contribute at the first correction. Such a non-linear term competes with the capillary instability when the time scale $\tau \sim O(1/\sigma S)$. However, by this same time, ξ has grown to be $O(e^{1/\sigma})\xi(\tau = 0)$, and thus causes the overall interfacial amplitude $\delta\xi$ to be $O(\sigma\varepsilon S e^{1/\sigma})$. This is beyond the size of δ presumed in this case. Therefore, we choose $\delta \sim \varepsilon S$ in the presence of the corrugation and arrive at

$$\xi_\tau + \frac{2}{m}\xi_z + \frac{S}{3m}(\xi_{zz} + \xi)_z - \sigma S\frac{2}{3m}\left((\phi_{zz} + \phi_z)\xi\right)_z - S\frac{2}{m}\xi\xi_z + O(\varepsilon S) = 0. \qquad (3.4)$$

For $\delta \sim \varepsilon S$, the corrugation term is of higher order than the nonlinear term. Thus, at leading order in S, the evolution is primarily determined by the KS mechanism, and one should expect the linear instability to saturate. However, the coupling to the wall's corrugation might still alter the character of dynamics. One interesting question is whether the introduction of the corrugation can trigger chaotic states for situations where the uncorrugated KS does not lead to chaos, or whether it might inhibit chaos where KS would yield such dynamics. Earlier numerical work on KS equations (Hyman & Nicolaenko 1986 and Papageorgiou & Smyrlis 1991) suggests that corrugation might cause such effects. First, the presence of corrugation can modify the wave lengths of disturbances and, as a result, changes the number of unstable waves per period. In the analysis of Hyman & Nicolaenko (1986), chaotic solutions obtain a large number of unstable waves per period,

whereas steady or traveling states result if the period contains less than about four unstable waves. Thus the excitation of higher wall harmonics by the initial disturbance might succeed in pushing the system towards chaotic motions. On the other hand, these wave interactions also can reduce the number of unstable waves per period so that chaotic motions that originally occurred at $\sigma = 0$ may change to steady or traveling states. Alternatively, chaotic motions can be regularized to traveling waves by the introduction of a dispersion term. Since (3.4) also contains a dispersive corrugation correction $(\phi_{zzz} + \phi_z)\xi_z$, we should expect such regularization.

A numerical solution is again necessary to examine the above possibilities. Since all of terms in (2.14) (except the $O(1)$ convective term) are $O(S)$, we introduce a long time scale $\tau \sim O(1/S)$ to access their dynamics. Let $x = z\sqrt{\nu}$, $\Theta = 6\xi/\sqrt{\nu}$, and $T = (\nu S/3m)\tau$. These substitutions transform (3.4) into a canonical form that is usually adopted in the computation of KS equations,

$$\Theta_T + \frac{6}{S\nu^{1/2}}\Theta_x - \Theta\Theta_x + (\Theta_{xx} + \nu\Theta_{xxxx}) - 2\sigma\left[\frac{1}{\nu}f_1\Theta + \frac{1}{\sqrt{\nu}}f_2\Theta_x\right] = 0, \qquad (3.5)$$

where both $f_1 = f_1(kx/\sqrt{\nu}) = \phi_{xxx} + \phi_x$ and $f_2 = f_2(kx/\sqrt{\nu}) = \phi_{xx} + \phi$ represent the corrugation wall's contributions. Here ν is a parameter and represents the period $\nu^{-1/2}$ chosen in the z -domain. We can define the length of the periodic domain in x for (3.5) by controlling ν. The wall's wave number k from ϕ in (3.4) transforms to a given number n_k of Fourier modes based on a 2π -periodic domain ($k = n_k\sqrt{\nu}$). Consider now a balance of the terms in (3.5). Balancing the circumferential Θ_{xx} and longitudinal curvatures $\nu\Theta_{xxxx}$ again yields a length scale $\nu^{1/2}$. The amplitude can be estimated as $\nu^{-1/2}$ by balancing the nonlinear and capillary terms. A balance with the unsteady term gives the time scale ν. For chaotic motions, ν is usually small. In our numerical simulations, we choose ν=0.027 in the chaotic regime (Papageorgiou & Smyris, 1991). To solve (3.5) numerically, a typical

number of modes is 36 and we apply Gear's method to solve the temporal evolutions within 0.1% absolute error tolerance.

We first simulate (3.5) at $\sigma = 0$ with an odd-parity initial condition $\Theta(x, T = 0) = -sin(x)$, then compare with the case of $\sigma \neq 0$ to see if the chaos persists. Figure 8 presents the evolution in the straight pore case. For v=0.027 and $S/m = 0.02$, the new time T=1 and the amplitude $\Theta = 1$ in this simulation of (3.5) correspond to the old time $\tau \sim 5000$ and amplitude $\xi \sim 0.03$ in (3.4), respectively. As expected, a typical KS evolution exhibits temporal and spatial chaotic motions with four or five wavelengths in a period of 2π. Upon imposing a small corrugation, the evolutions for different wall wave lengths in terms of n_k are shown in Figures 9-12. These results do not indicate any loss of chaotic motion due to the presence of small corrugations of arbitrary n_k. A comparison with the earliest profile (at $T = 0.4$) for all of the corrugated cases with that of the straight pore shows a great similarity in interfacial shapes and wave lengths. This indicates little effect of corrugation for the non-linearly perturbed interfaces. The higher wall harmonics of the initial disturbance do not seem to develop even for time $T = 10$ in the weakly nonlinear regime. On the other hand, if the initial disturbance has a small amplitude, the excitation of higher harmonics may be effective during the earlier evolution and thus control the long time behavior. This would be consistent with the known initial condition dependence of long time KS solutions (Frish *et al.*, 1986).

For small amplitude waves, the nonlinear terms may be insignificant and thus not cause wave steepening. As a result, the active number of unstable waves may not be sufficient to yield truly chaotic motions (Frisch *et al.*, 1986). To put this in another way, one can modify (3.5) by rescaling Θ with the initial amplitude. As a result, a smaller initial amplitude is equivalent to the effect of a larger v, where the evolution tends to be less chaotic. So, Figure 13 shows the evolution from the initial condition

$\Theta(x, T = 0) = -0.1 sin(x)$ in a straight pore to somewhat chaotic motions, although some time snapshots appear almost periodic, e.g., T =4.8, 7.2 and 8.8.

The evolutions for corrugated pores with various wall wave numbers $k = 0.1643\, n_k$ (n_k=2,3,4, and 5) are shown in Figures 14-17. It is quite interesting to note that for n_k=2 (Figure 14) there is a long period where the interface shape is relatively flat and static before abruptly changing to chaos. Such an almost static period also occurs for n_k=3 (Figure 15), but there it occurs between chaotic periods and for a shorter duration than for n_k=2. However, for larger n_k such as 4 and 5 (see Figures 16 and 17, respectively), the evolutions seem as chaotic as in the straight tube case. An understanding of the detailed mechanism of these transitions and interactions that cause them requires further analyses. However, we have demonstrated here that the size of the initial disturbance seems to plays a more important role in determining the detailed structure of the nonlinear motions than the wave length of the wall's corrugation.

All of above preliminary results suggest that, except for detailed interfacial evolutions, chaotic motions originating from the KS terms seem to overwhelm the influence of the wall's corrugation when that corrugation is weak. If we choose σ =100, for example, to (unrealistically) enhance the importance of the periodic coefficients, we find Figure 18. Even though this case violates our small corrugation assumption, we see that the non-constant coefficients indeed can regularize the wave pattern as long as they are strong enough.

4. Summary and Conclusions

Above we investigate the weakly nonlinear interfacial stability of a core-annular flow in the presence of an asymptotically small corrugation. Previous work on the linear stability of this system showed that the corrugation excited higher wall harmonics of the initial disturbance which for the right choices of α and k would be unstable. It was not clear whether the continuous generation of new unstable long waves by the corrugation could be

saturated by the wave steepening non-linear KS mechanism. We have found that all of the waves induced eventually saturated in the weakly-nonlinear regime for moderate strong interfacial tensions (i.e., $J/Re_1 \sim 1/\varepsilon^2$). As in earlier works, very strong tensions may still lead to solutions that blow-up, as demonstrated by our no-flow limit. Thus, as the interfacial deflections grow large, our interfacial equation is no longer valid for asymptotically long times. For slightly weaker tensions (but still in the strong tension regime, i.e., $1/\varepsilon << J/Re_1 << 1/\varepsilon^2$), the interfacial evolutions are governed by Kuramoto-Sivashinsky equations modified by small corrugation corrections. The introduction of these corrugation correction does not appear strong enough to change the qualitative features of the chaos that arises from the standard Kuramoto-Sivashinsky equations, even though smaller initial perturbations may result in a temporary regularization.

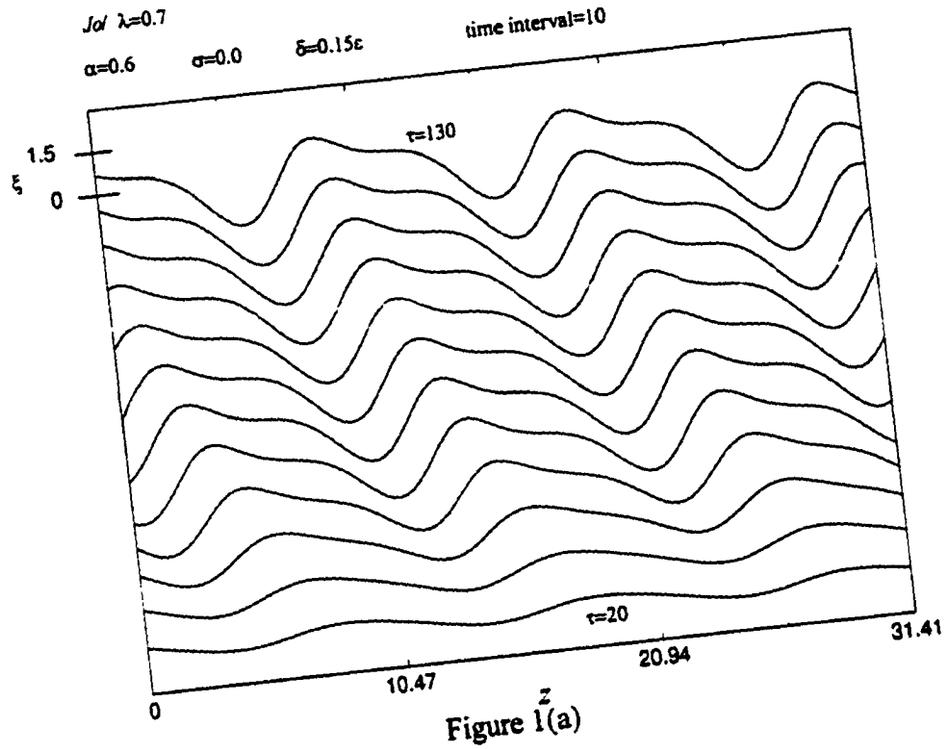

Figure 1(a)

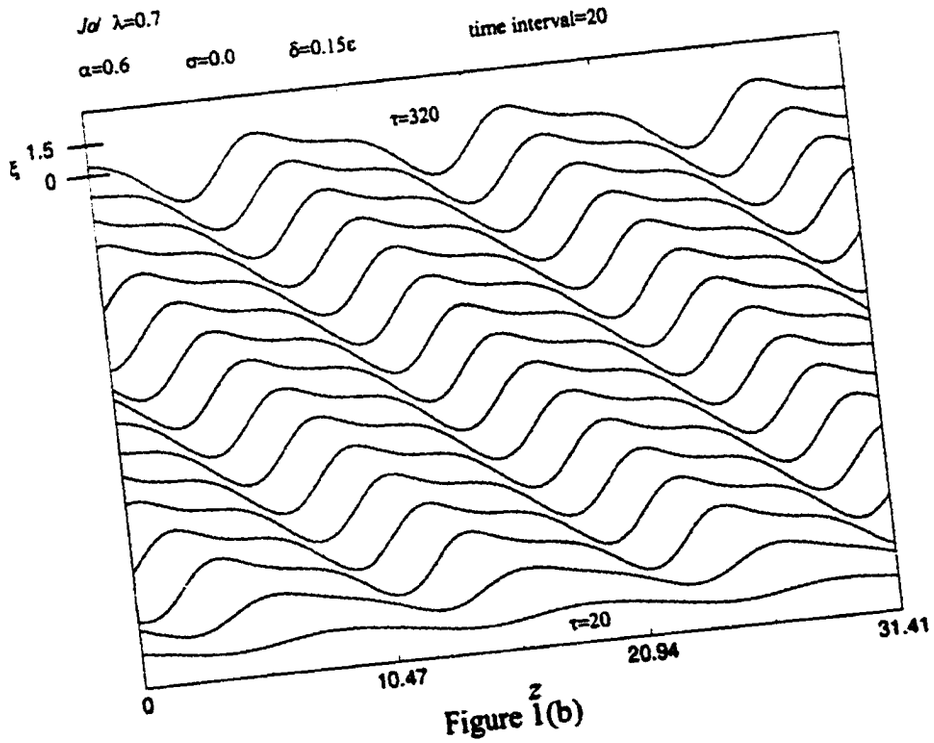

Figure 1(b)

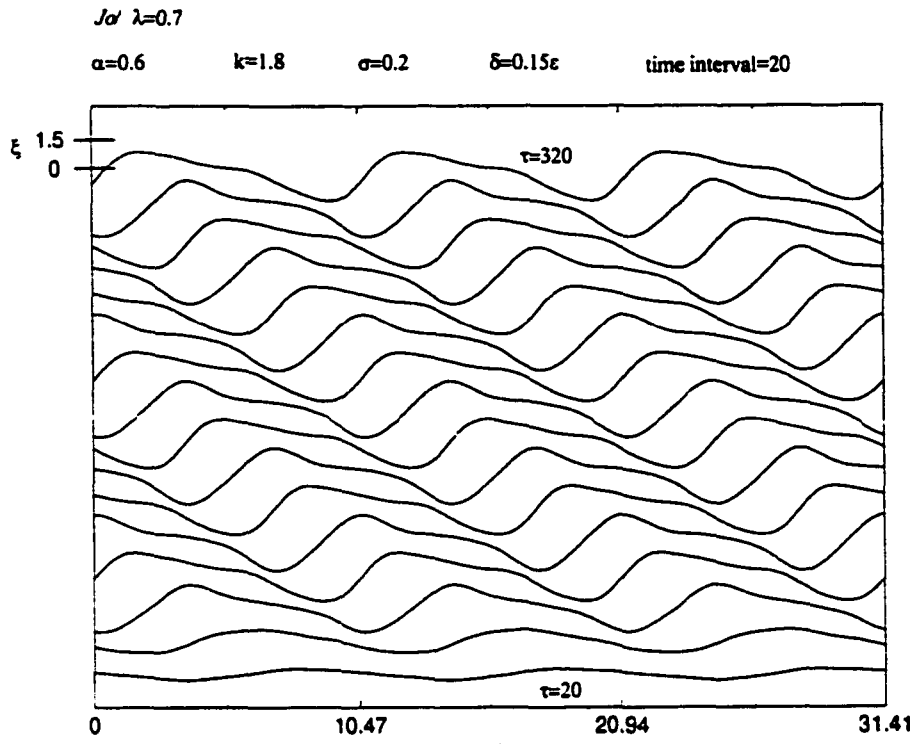

Figure 2

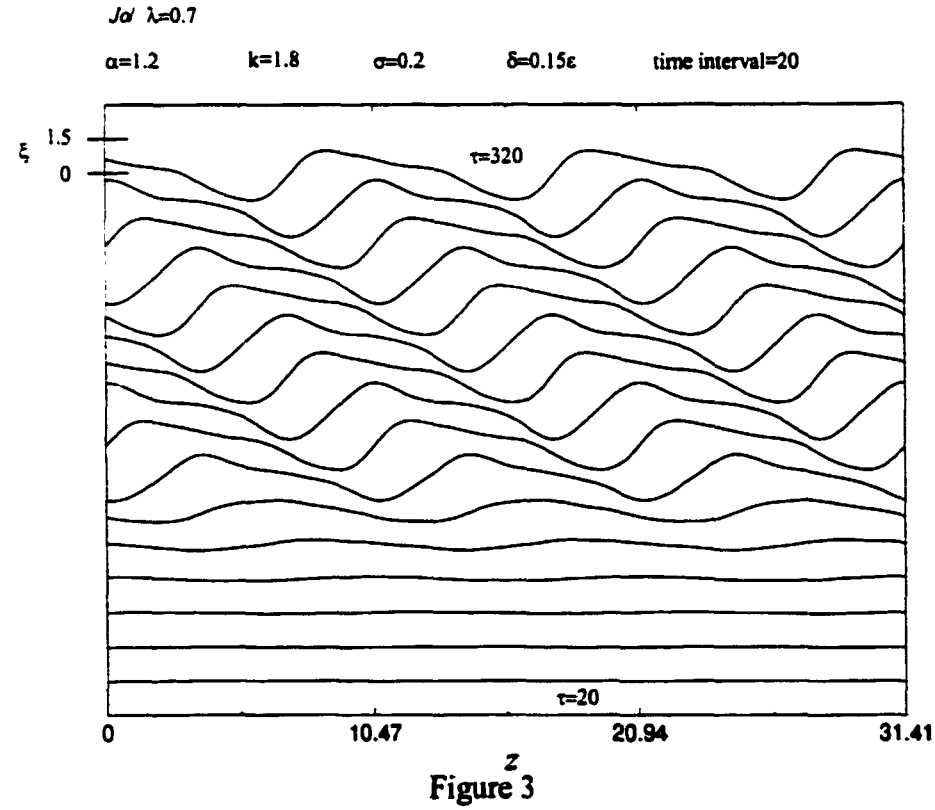

Figure 3

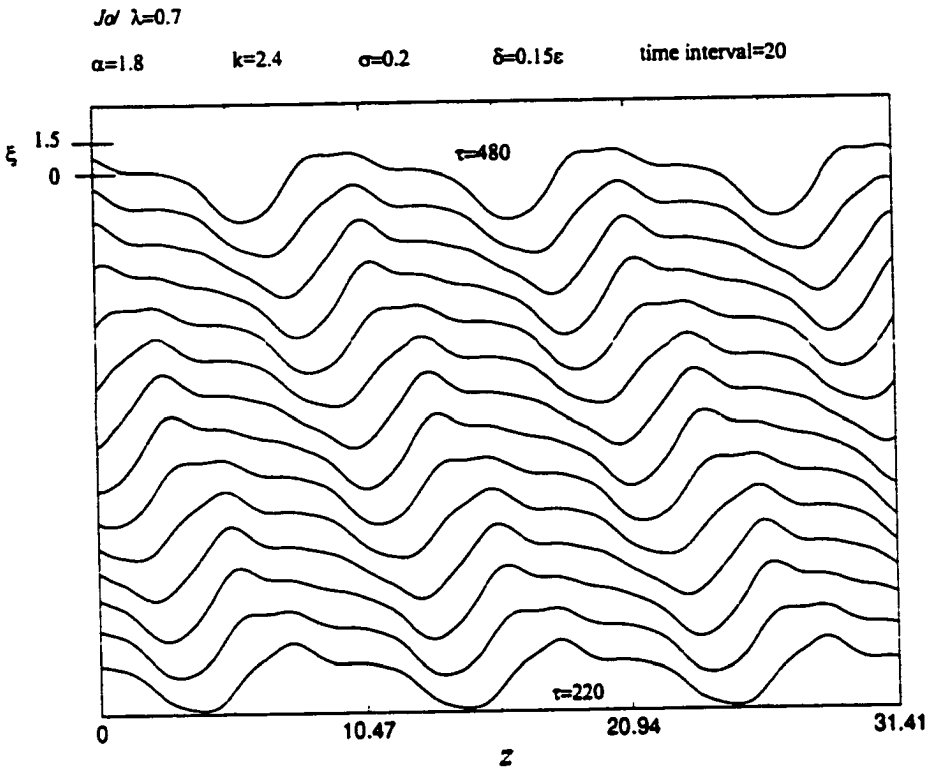

Figure 4

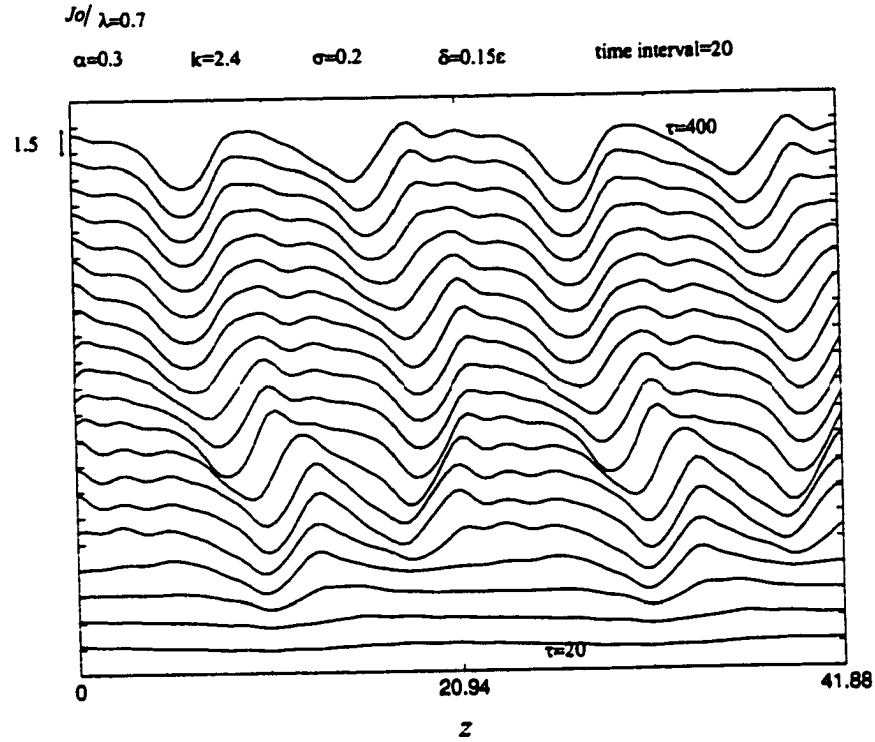

Figure 5(a)

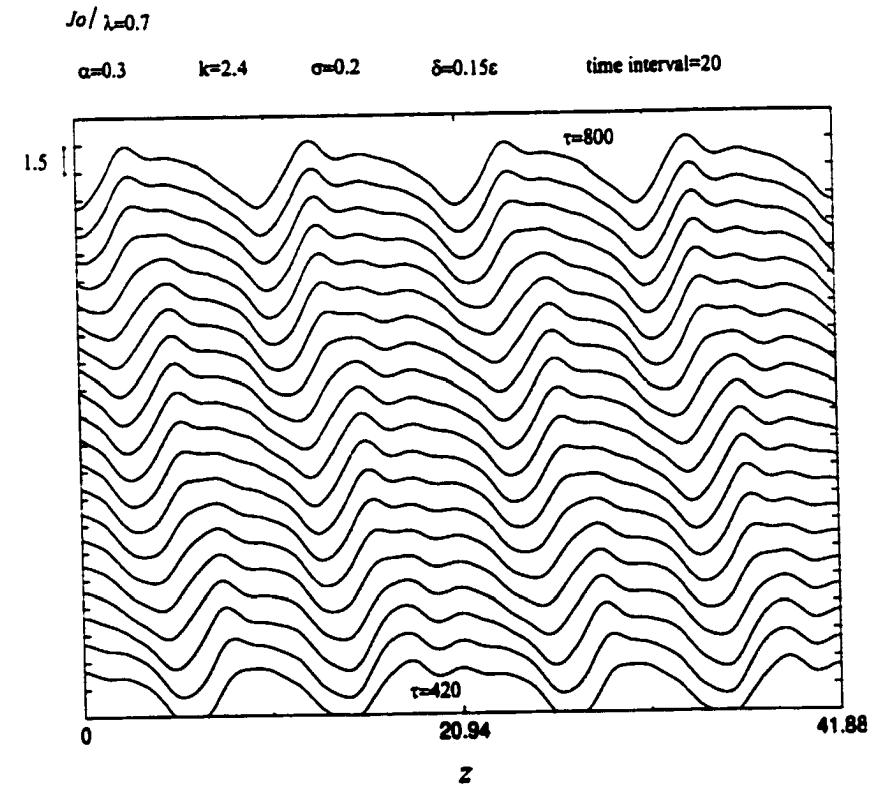

Figure 5(b)

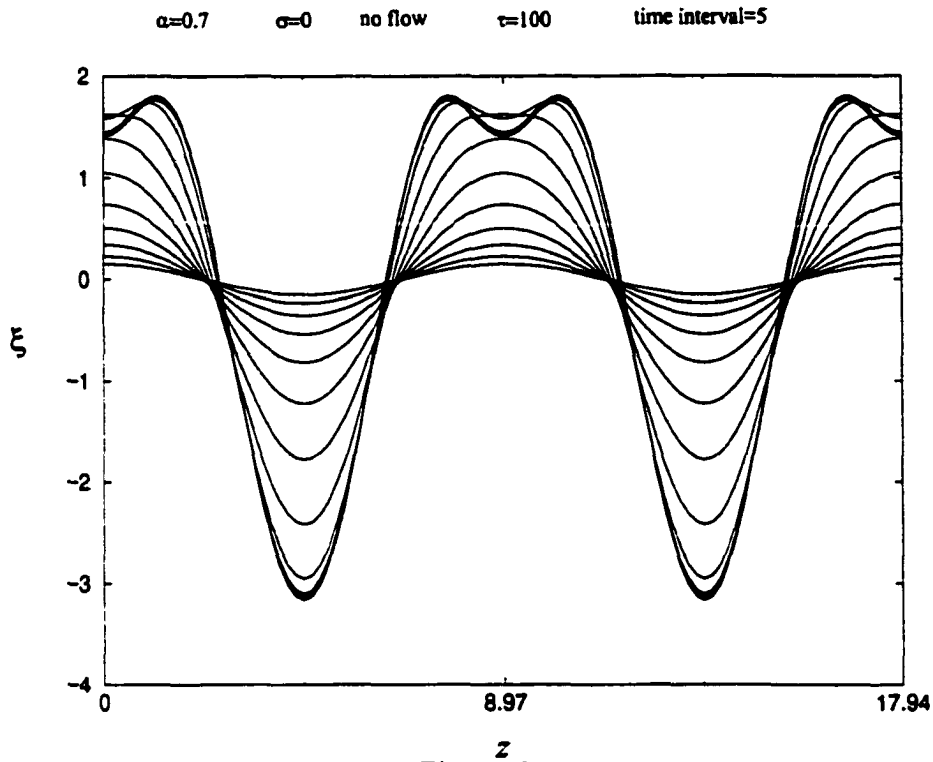

Figure 6

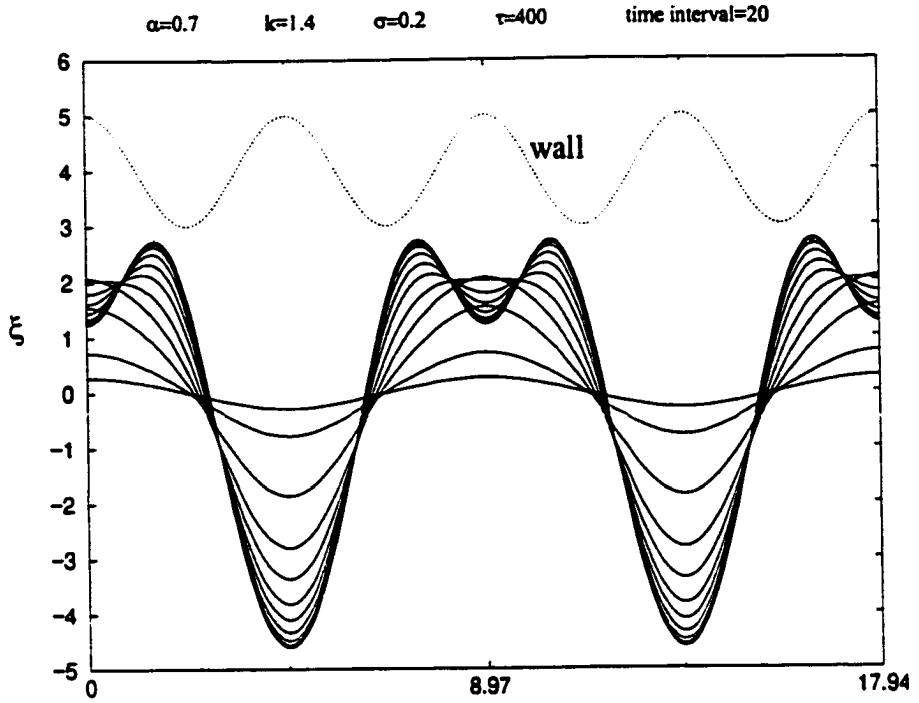

Figure 7(a)

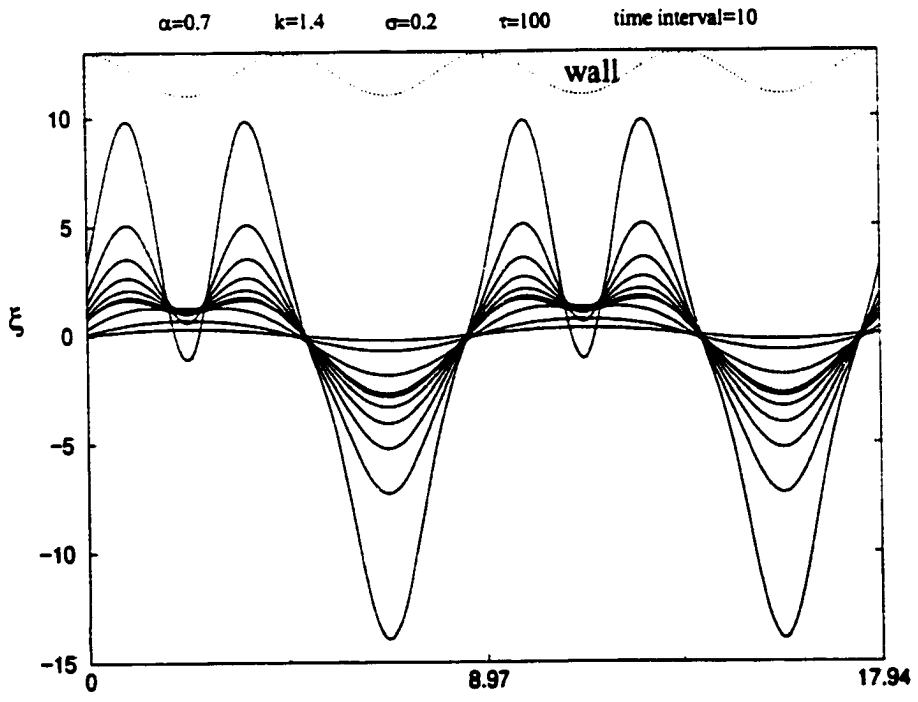

Figure 7(b)

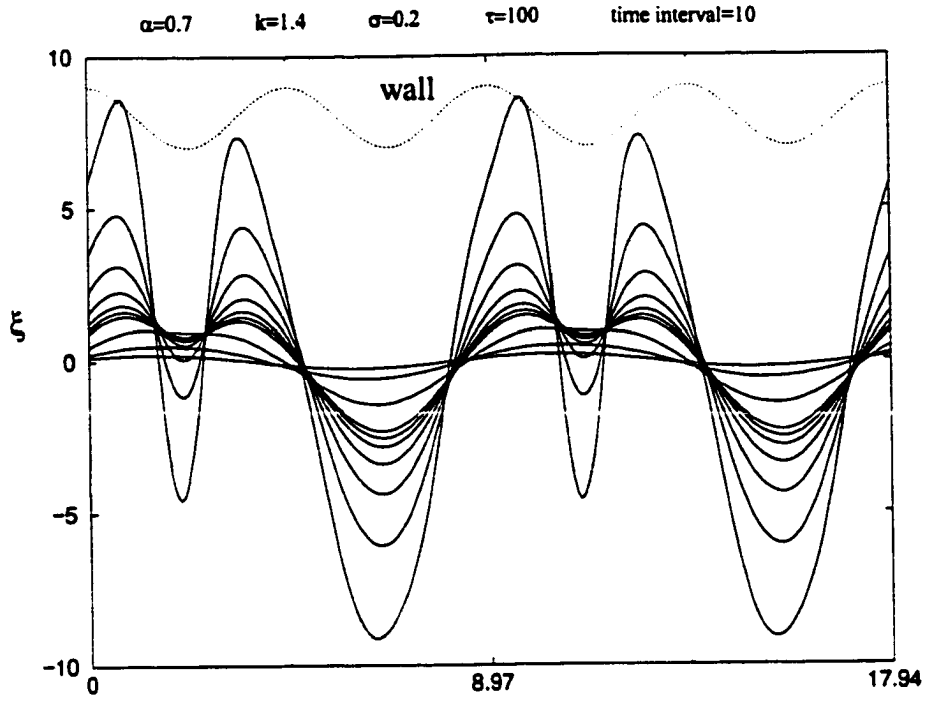

Figure 7(c)

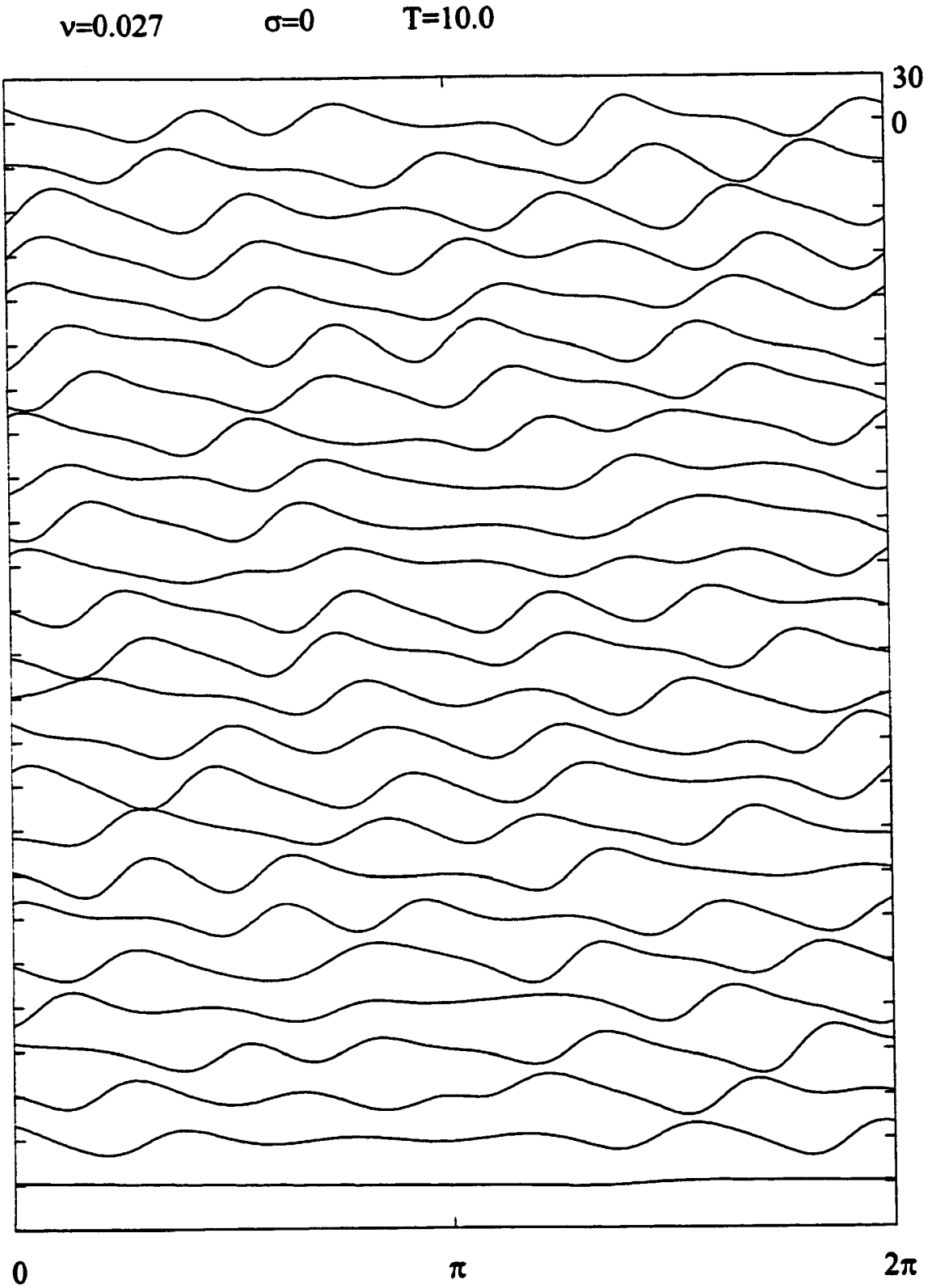

Figure 8

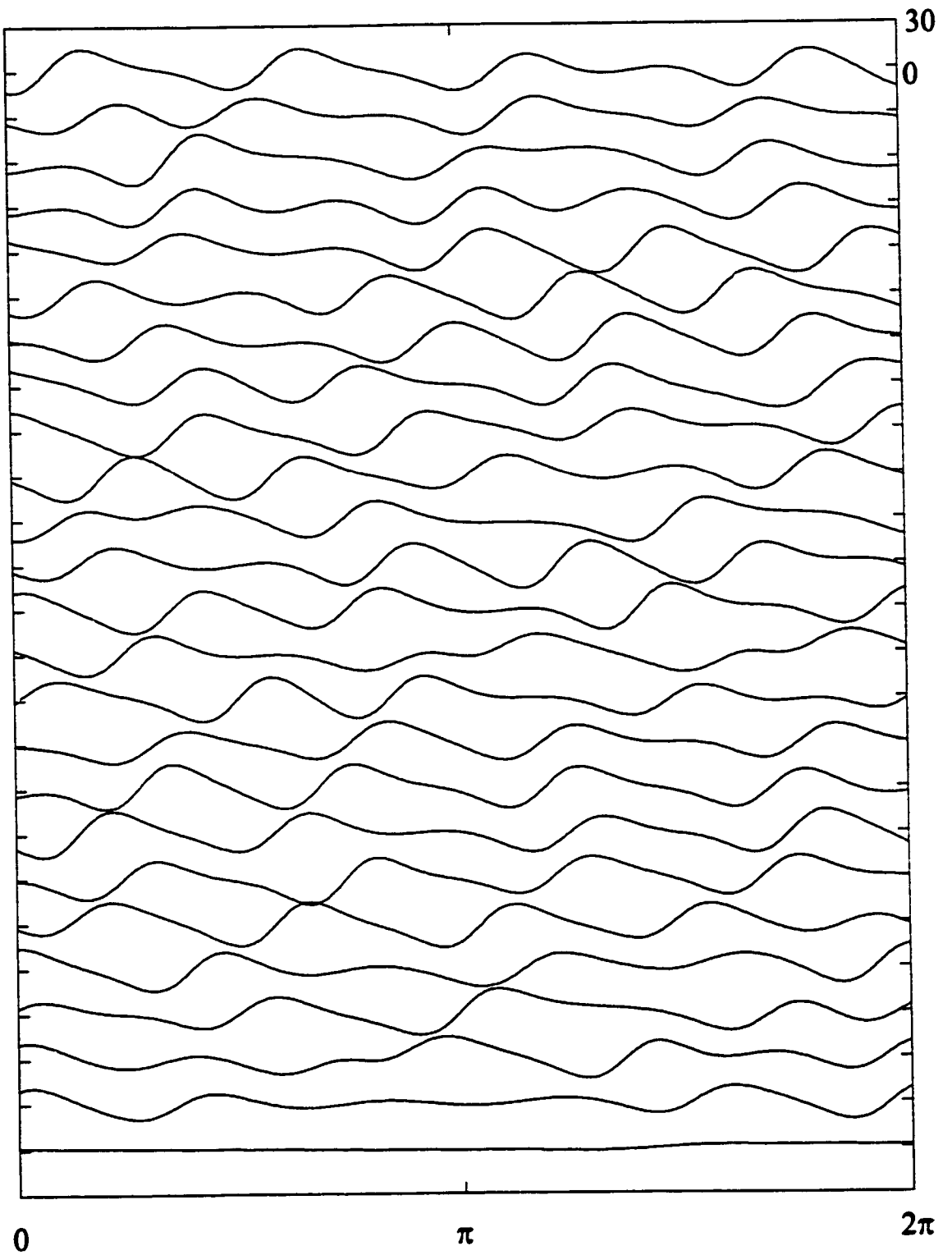

Figure 9

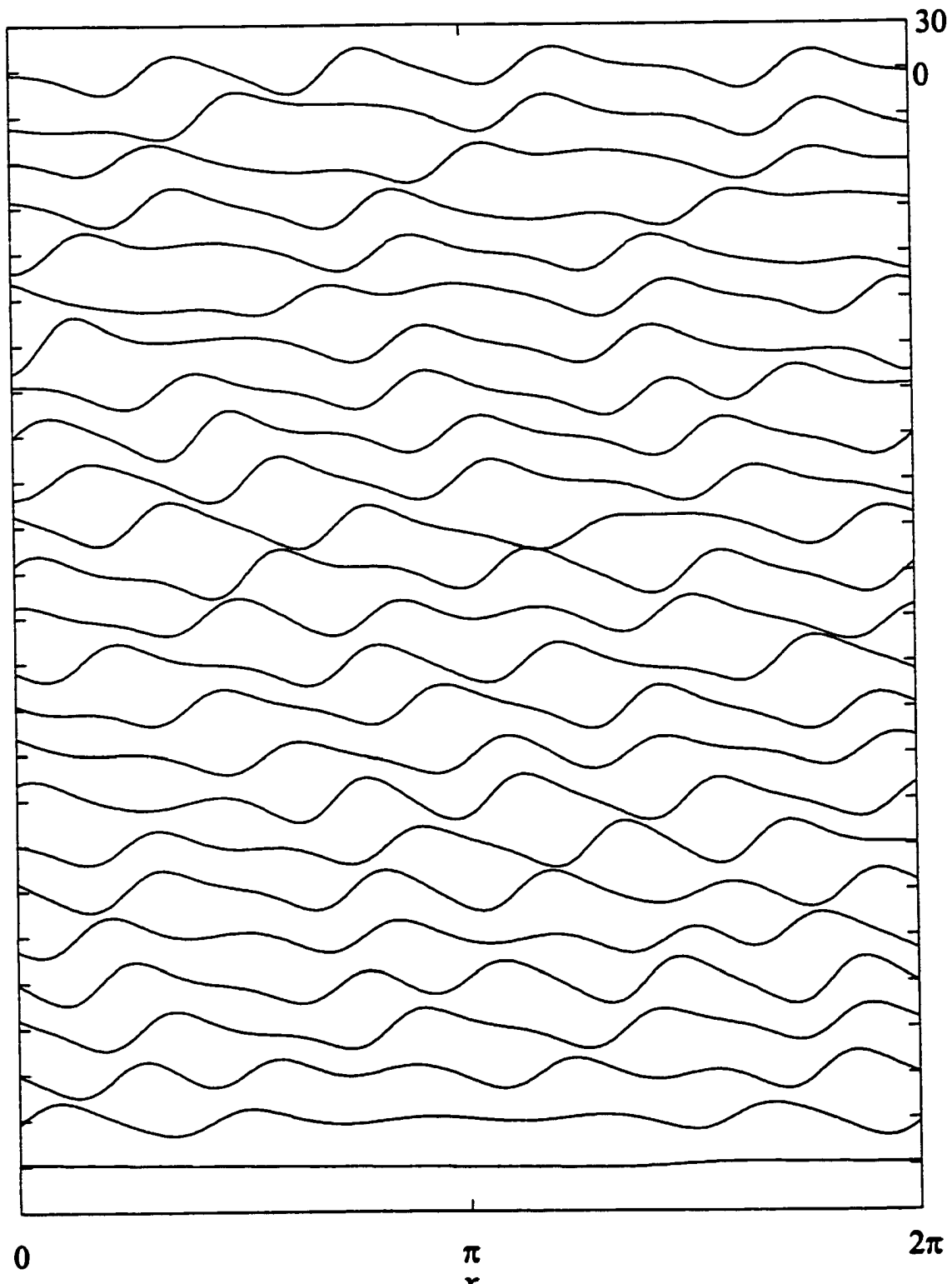

Figure 10

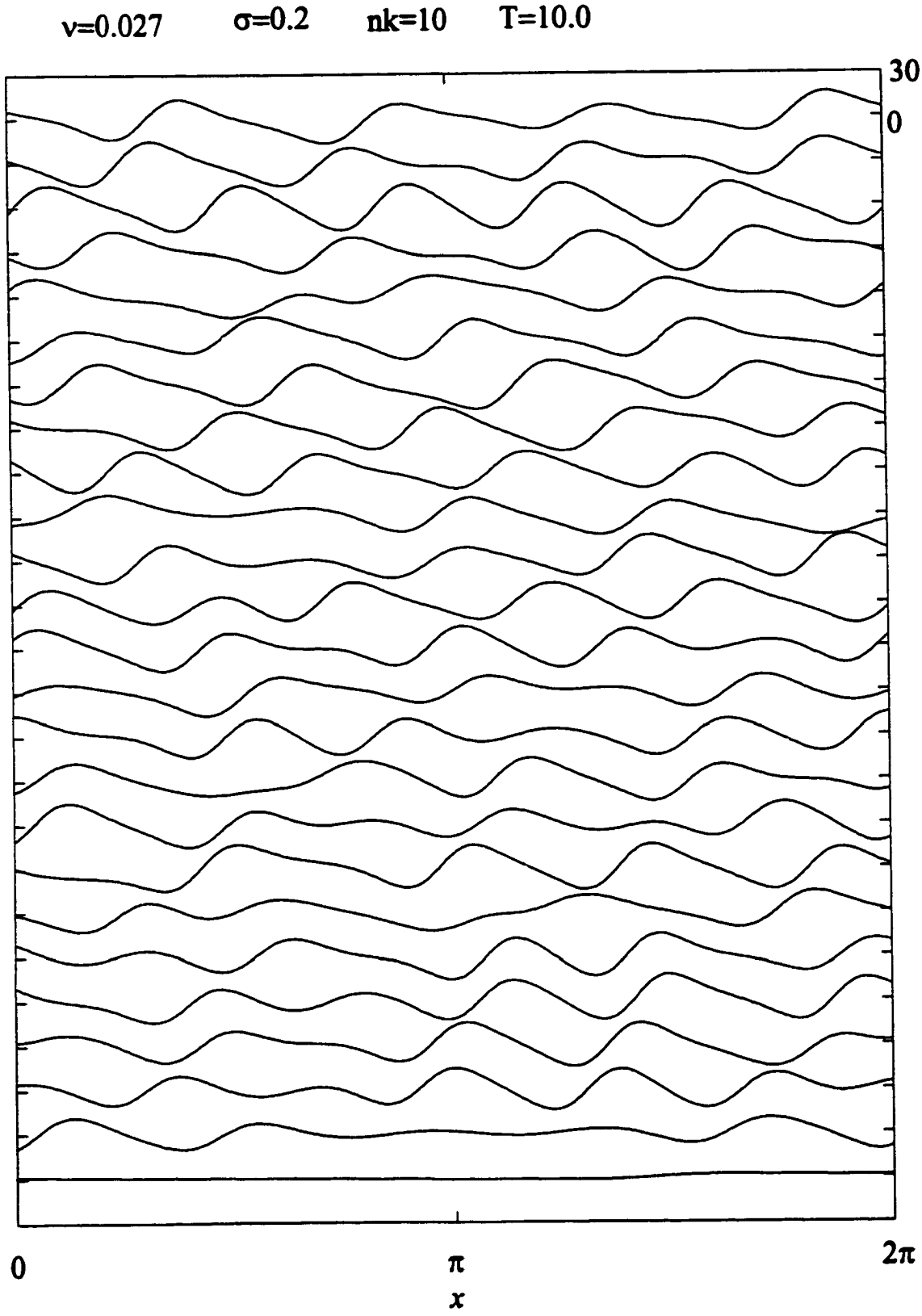

Figure 11

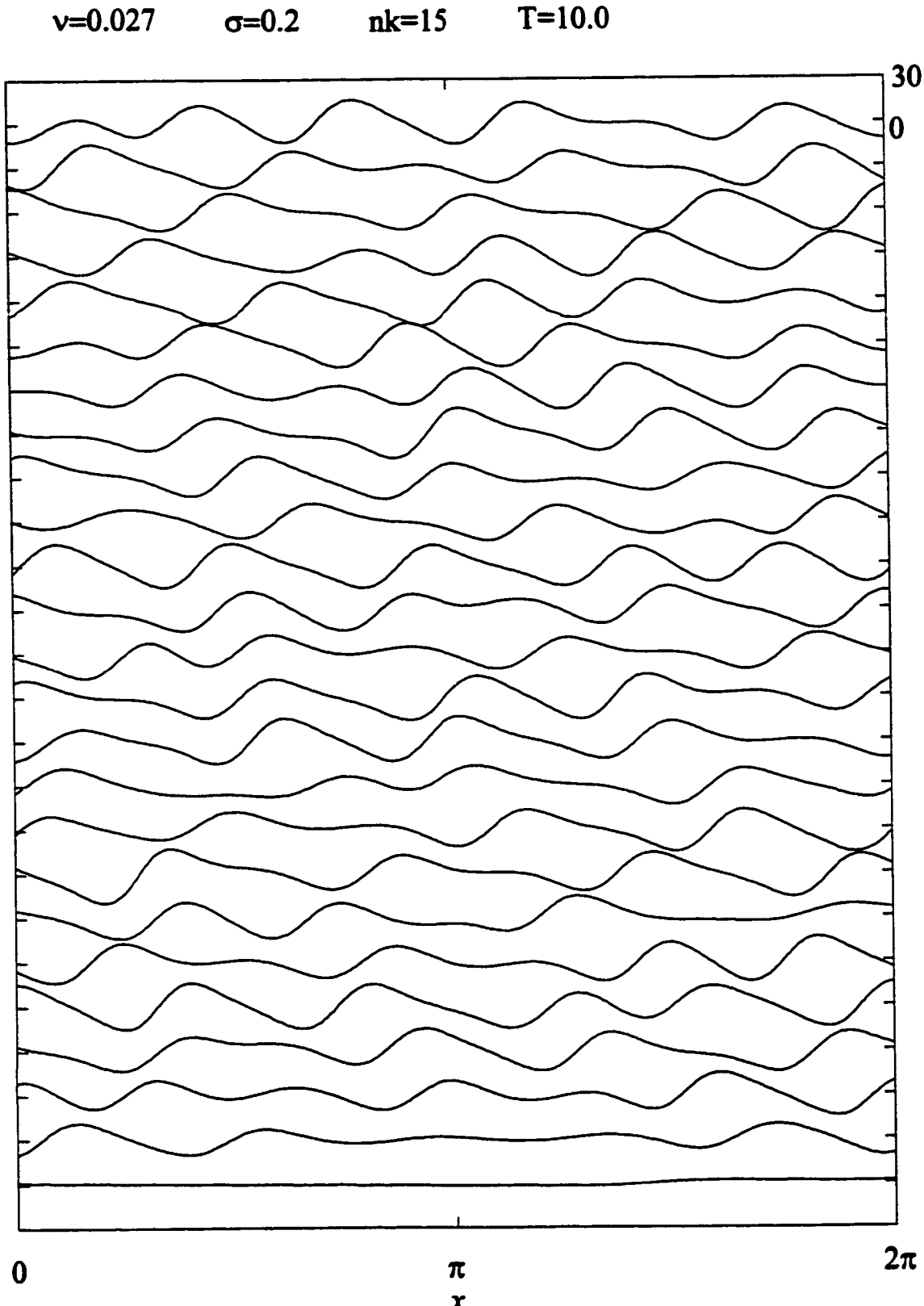

Figure 12

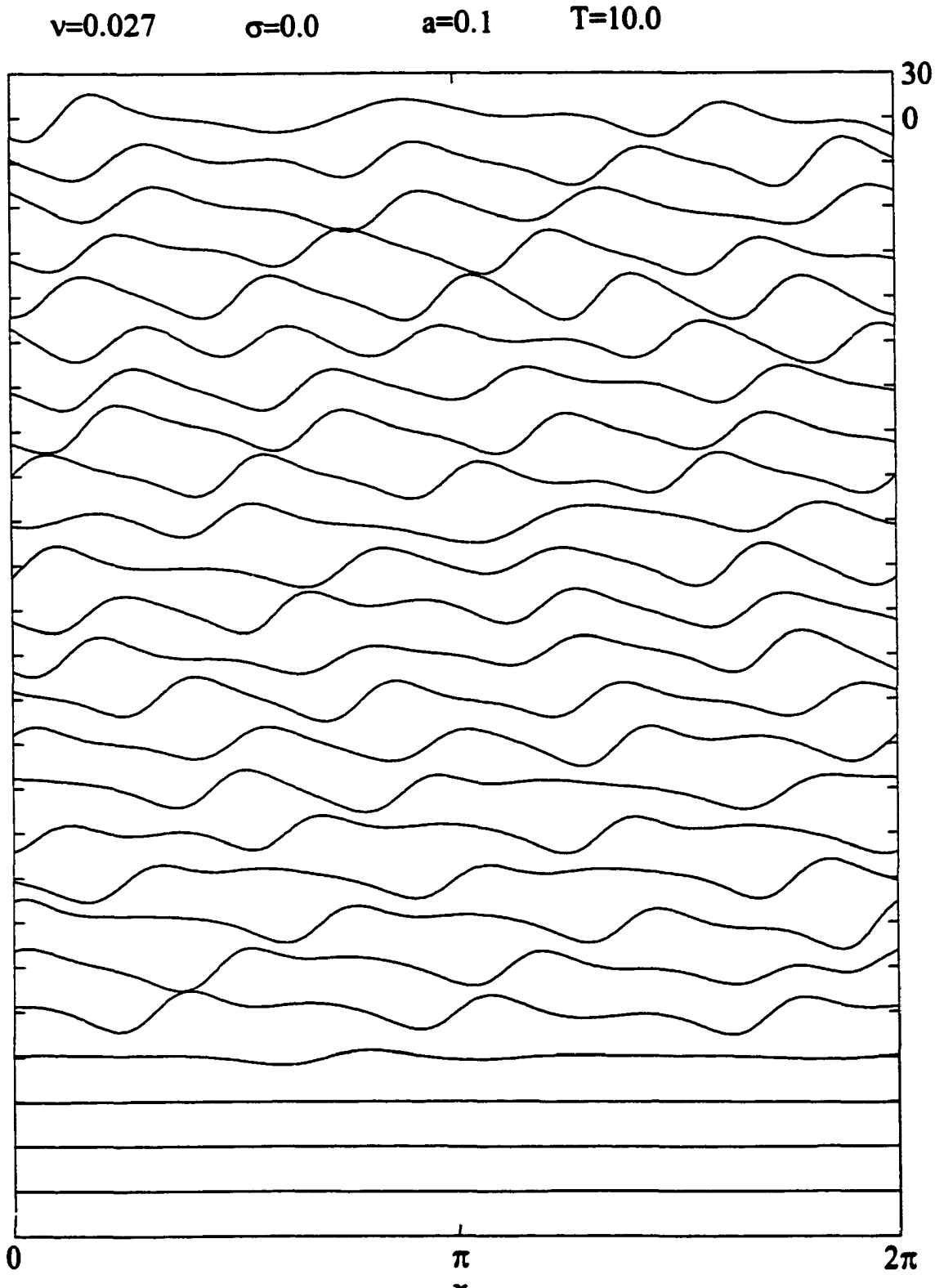

Figure 13

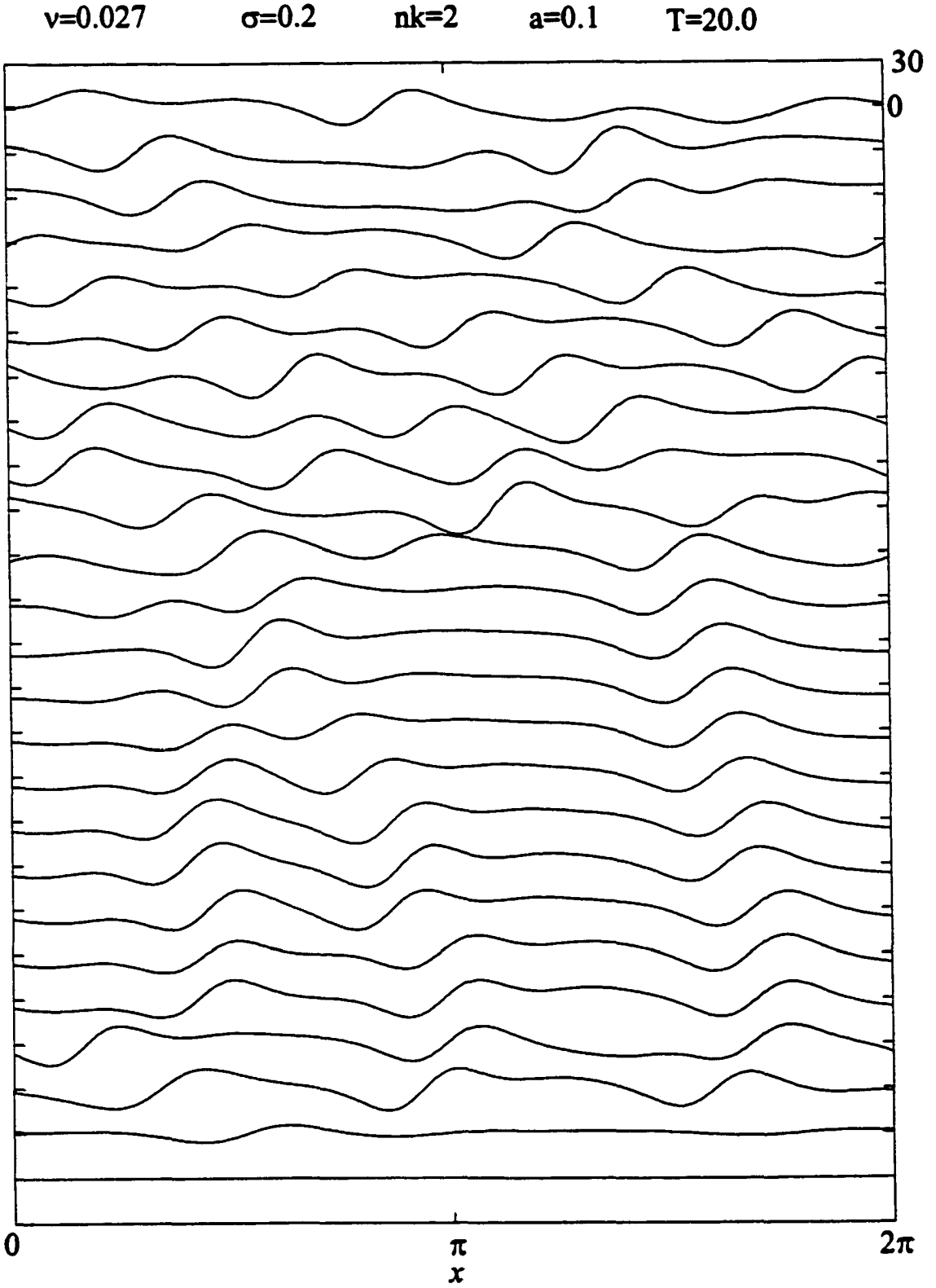

Figure 14

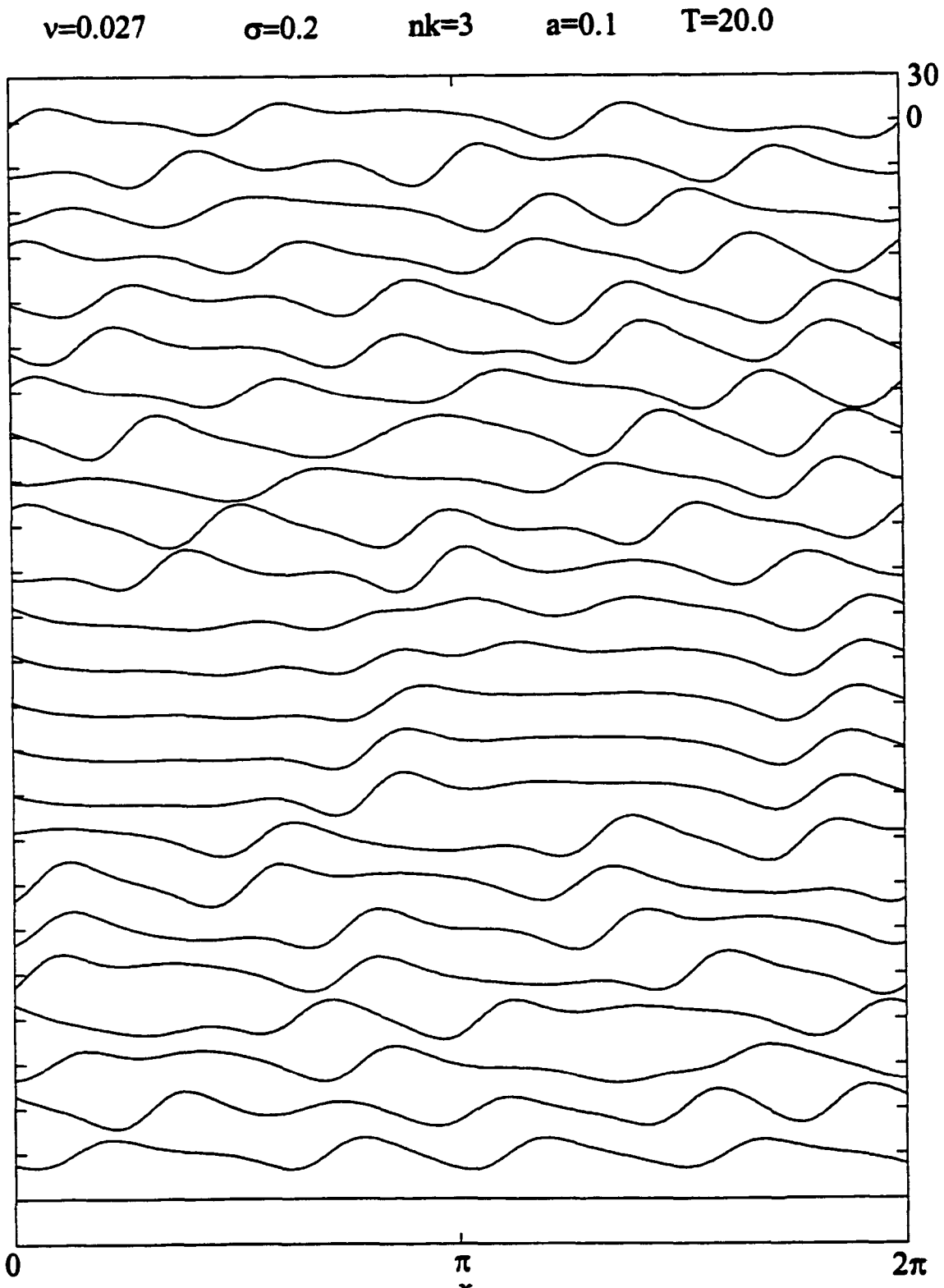

Figure 15

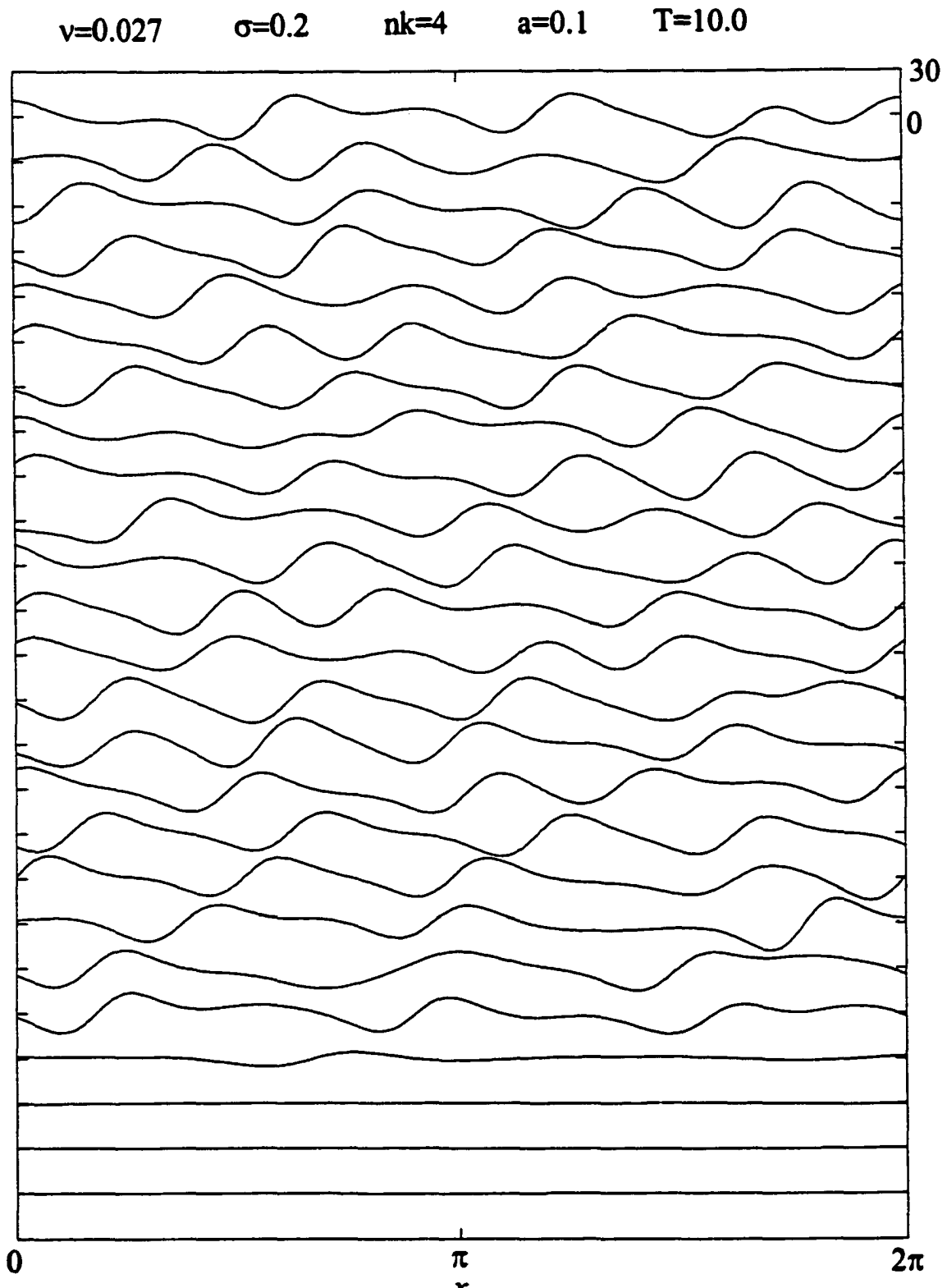

Figure 16

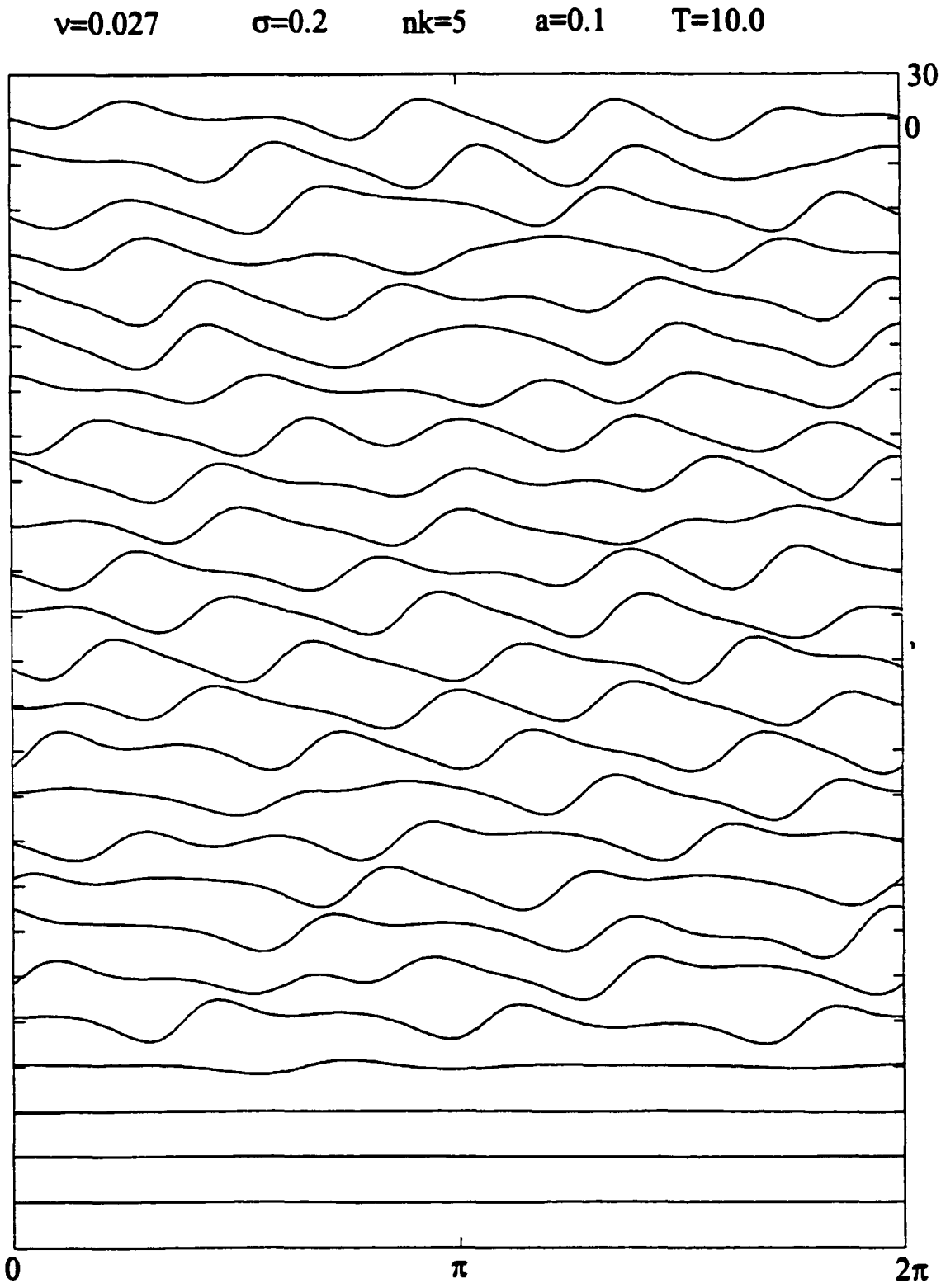

Figure 17

σ=100.0 nk=4 T_{max}=10.0 ΔT=0.4

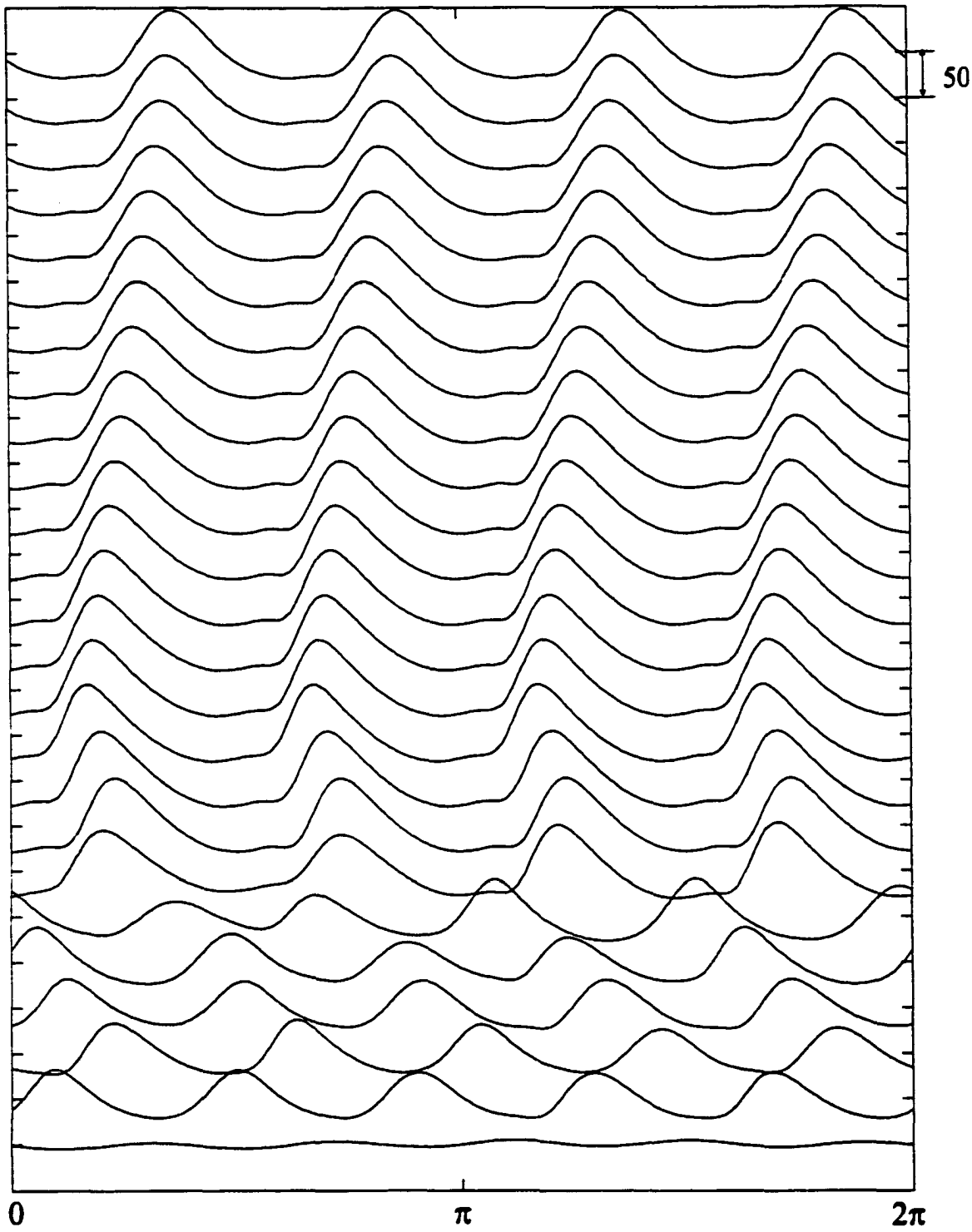

Figure 18

IV The Linear Stability of an Inviscid Core-Annular Flow in a Corrugated Tube

1. Introduction

A two-fluid core-annular flow (CAF) consists of two immiscible fluids flowing cocurrently in a tube or pore, where one (the annular) fluid wets the tube wall and surrounds the other (core) fluid. It is called a perfect core-annular flow (PCAF) if the two fluids are coaxial, and this is the usual assumption (Perziosi *et al.* 1989, Georgiou *et al.* 1992, Papageorgiou *et al.* 1990). Core annular flows are widely studied and employed as a useful model to analyze a number of technologies and problems of scientific interest such as oil recovery (Slattery 1974). The stability of CAFs thus attracts attention since it plays a critical role in the efficiency of such processes. Not surprisingly, there are numerous investigations (e.g., Georgiou *et al.* 1992) of core-annular flows, where the fluids are viscous, but where surface tension dominates viscous effects (small capillary number) and where viscous effects are either comparable or large compared with inertia (order one or lower Reynolds number). Since the source of the primary instability in the cylindrical geometry is surface tension, it may also be of interest for low viscosity fluids or high velocity flows to examine the limiting case where both surface tension and inertia dominate viscosity. Therefore, the inertia-dominated inviscid theory is a complementary problem to the order one or lower Reynolds number problem.

Plateau (1873) and Rayleigh (1879) first examined the capillary instability for a static thread of an inviscid fluid. Surface tension acts in such a way that the longitudinal component of the interfacial curvature is stabilizing and the circumferential component is destabilizing. The competition is such that disturbances with wave lengths shorter than the undisturbed fluid-fluid circumference are stable and those that are longer are unstable. The same basic physics applies to a liquid film on the inside or the outside of a cylindrical tube (Goren, 1962) and in two-phase systems where a cylindrical thread of one fluid is

surrounded by an unbounded second fluid (Tomitika, 1935). Similar features have been found in two-phase systems, whether inviscid or viscous, such as a two fluid core-annular arrangement in a tube without flow (Mikami & Mason 1975) or compound jets (Radev & Tchavdarov 1988, Chauhan *et al.* 1996, Chauhan *et al.* 2000), at least in the case where the two fluids are coaxial. As detailed elsewhere (e.g., Chapter II), the linear and weakly nonlinear stability of the *viscous* PCAF in a straight, uniform tube is well understood (e.g., Hickox 1971, Preziosi *et al.* 1989, Georgiou *et al.* 1992, Papageorgiou *et al.* 1990, Kerchman 1995, etc.). Note that both in the static case (no base flow) as well as in the case of a uniform base flow as in the jet problems, the base flow plays at most a convective role, but does not contribute to the instability.

In practice, though, real systems such as rock pores are not straight, uniform cylinders. It is important to understand whether and how these deviations from an ideal geometry affect the interface's stability and to see whether they, in fact, dominate the stability picture. Obviously, standard PCAF theory cannot describe such non-idealities. The governing equations are the Euler and continuity equations. The corresponding boundary conditions are wall impenetrability, bounded centerline flows, and continuity of normal velocity, the balance of normal stress and the kinematic condition at the fluid-fluid interface. For inviscid flows in straight, cylindrical geometries, one takes the base flow to be unidirectional and uniform (to prevent the Kelvin-Helmholtz instability) with a purely circular interface. The inclusion of a corrugated wall leads to a base flow that is no longer parallel and its non-uniformity in the axial direction may interact strongly with even small interfacial disturbances.

There is an important class of inviscid fluid problems with a free interface and a corrugated geometry that has received a significant amount of attention. A typical example of these problems is the study of wave propagation for a quiescent ocean with a non-uniform depth. These waves are usually generated by interfacial disturbances that interact with gravity and are thus called gravity waves. An inviscid theory can model the large-scale

behaviors of such systems. Rhines (1968) studied inviscid gravity waves over a sinusoidally corrugated bed. By assuming a small corrugation relative to the ocean's depth and shallow water theory (i.e., long wave theory; both the water interface's and the bed's wave lengths are much longer than the mean water depth), he obtained a Mathieu equation governing the linear motions of the free surface. His later (1970) analysis applied Floquet theory to study the properties of this Mathieu equation. The results revealed that when the primary wave number α of the interface is half of the corrugation's wave number k, the solution breaks down (it has a resonance) because the amplitude of the first harmonic wave $(\alpha - k)$ becomes unbounded.

Mitra and Greenberg (1974) investigated the effect of a wavy bottom on the Kelvin-Helmholtz instability. An unbounded upper fluid flows with a uniform velocity over another lower stationary fluid on a wavy bottom, and the base flow's fluid-fluid interface remains flat. They applied a perturbation technique and a strained time variable based on a small parameter σ, the ratio of the bottom's corrugation amplitude to the mean water depth. They showed that for a given wave number and upper flow velocity, if the free surface with a flat bottom and a constant depth is stable (i.e., has a steady traveling wave solution), then the corrugation case is also stable at the same mean depth. They also found the same wave resonance condition as the above. They later (1984) used a similar technique to study gravity water waves for an inviscid fluid over a corrugated sea bed. For the non-resonance case $(\alpha \neq k/2)$, the amplitude of the α wave is $O(1)$ and the corrugation correction to the wave speed is $O(\sigma)$. On the other hand, at the resonance $(\alpha = k/2)$, the resulting $(\alpha - k)$ wave, whose wave number is negative, can travel backward with an $O(1)$ amplitude and an $O(\sigma)$ wave speed correction. This suggested that a reversal of the direction of wave propagation is possible for a time scale of $O(\sigma^{-1})$.

Davies *et al.* (1989) applied linear shallow-water theory to a system of a flat bed with finite-extent patches of ripples with amplitudes much smaller than the mean depth. An

incident wave with a fixed time frequency travels from an upstream, flat bed section. It then enters the wavy section and generates modulated waves. One modulated wave (transmitted) wave continues propagating downstream and another (reflected) wave travels backwards upstream. This is equivalent to a Bragg scattering process. They showed that the ratio of the magnitudes of the incident wave (with wave number α) to that of the reflected wave depends on α/k. When the resonance again occurs at $\alpha = k/2$, this amplitude ratio tends to unity as the periodicity of ripples increases. Liu & Yue (1998) recently investigated the scattering problem of surface waves over a bottom with corrugation small compared to the mean depth. They used a perturbation technique to study the general context of nonlinear wave-wave interactions and justified several resonance classes involving higher order wave interactions. Nachbin & Papanicolaou (1992) used an alternative approach to study a wave scattering problem similar to Davies *et al.*'s problem. In their study, the wave length of the disturbance is much longer than the water's depth but both the amplitude and wave length of the ripples are comparable to the water's depth. Thus shallow water theory is not applicable. They applied conformal mapping and perturbation techniques to develop a theory to analytically calculate the amplitude of the reflected waves. They also numerically solved the full problem by using a boundary-element method, and their theory showed a good agreement with these direct numerical results.

The above-mentioned theories do not include base flows. Another class of free-surface, inviscid fluid problems with corrugated boundaries that includes a base flow is the set of models for sediment transport in river flows (Engelund & Fredsøse 1982). The geometry in such cases does not possess translation invariance and one expects the effect of corrugation to be non-trivial. Kennedy (1963) studied a free-surface inviscid flow with a uniform, ambient velocity over a corrugated and erodible bed. In a frame fixed to the bed, this system can be formulated as a steady flow problem. For a bed with small corrugation amplitude, his linear theory showed there can be a phase shift between the free surface and the undulated bed. This phase shift is either 180° or non-existent, depending on the

magnitude of the mean velocity. Kirby (1988) followed Kennedy's analysis for a non-erodible bed with the same base flow. When the mean base flow velocity matches the wave speed of the gravity waves in stationary water, this resonant solution becomes singular. He also considered a wave scattering problem for a uniform flow over finite ripples on an otherwise flat bottom. When close to the resonance state, the reflection process is enhanced by the presence of a uniform flow. Bontozoglou *et al.* (1991) numerically solved a steady, free-surface, inviscid flow with a uniform mean velocity over a periodic wavy wall. For a certain range of parameters, there is also a series of resonances between the wavy wall and interface, and these resonances cause the interfacial amplitude to become unbounded. They do not, however, perform a stability analysis.

The above-mentioned analyses of wave propagation problems, either with or without mean flows, are linear theories. In the weakly non-linear regime, the evolution of shallow water interfacial waves for stationary water of a constant depth is governed by the well-known Korteweg-de Vries (KdV) equation (Korteweg & de Vries, 1895). This equation admits solitary wave solutions, which have been observed in experiments (Russell 1844, Hammack & Segur 1974) and confirmed by numerical simulations (Zabusky & Kruskal 1965, Fornberg & Whitham 1978). Johnson (1973) studied the related problem that has a slowly varying water depth. Again invoking the shallow water theory and a scaling analysis, he asymptotically derived a KdV equation with non-constant coefficients. He showed that when the depth decreases to a certain level, an initial solitary wave breaks up into a finite number of solitary waves. He later (1994) extended his earlier analysis to waves over a bed with a slowly decreasing depth. Similar KdV equations obtain asymptotically for different scalings. For a length scale of depth variation much longer than the wave length of the disturbance, his numerical results showed that the slowly decreasing depth causes the resulting solitary wave to form a series of wave patterns with slowly-varying amplitudes (i.e., shelves) behind a primary wave.

For the weakly nonlinear analysis in the presence of a mean uniform flow, Zhu (1995) investigated the weakly-nonlinear interfacial evolutions of a uniform inviscid flow over a bottom with an obstacle in the presence of surface tension at the free surface When the ambient velocity is close to the gravity wave speed (again, the resonance condition of the base flow), he used shallow water theory and scaling analysis to asymptotically derive a forced KdV equation with an additional inhomogeneous reflecting the effect of the bottom topography. His numerical solution showed that for a flat initial interface, the Gaussian-shaped obstacle causes the interface to become convex. One convex wave travels upstream while another wave that travels downstream becomes concave. Sammarco *et al.* (1994) studied the weakly nonlinear evolution of a free-surface, uniform ambient flow over a bottom having a small corrugation amplitude compared with the mean depth. At various resonance conditions due to nonlinear wave-wave interactions, they applied a multiple scale technique based on a small wave parameter to derive a nonlinear evolution equation of the complex interfacial amplitude near the resonances. They showed that if the ambient velocity has a slow time-varying harmonic coefficient, then the evolution may exhibit spatial or temporal chaos.

We are interested in the problem of an inviscid, core-annular flow in a circular tube with an axisymmetric cross-section that varies in the axial direction. Because of the presence of both a base flow and corrugation, we expect non-trivial interactions of the two. What differentiates this analysis from those above is the circular geometry and the fluid-fluid interface. Capillarity, as noted is not purely stabilizing in this configuration, and this may interact with the corrugation. Moreover, it provides an additional length scale, the core or tube radius, that does not appear in the Cartesian geometries, and allows for non-trivial scalings appropriate to application that can simplify the problem significantly.

We have developed a theory for the flow of two *viscous* fluids in a CAF (Chapter II, Wei & Rumschitzki 2000) in a tube with asymptotically small corrugations. By means of small parameters characterizing the ratios of the mean film thickness to the mean core radius

and of the mean corrugation amplitude to the mean film thickness, we have asymptotically developed the fluids' base flows and their corresponding linear stability to leading orders. We have employed Floquet-Bloch theory to solve the resulting eigenvalue problem, which exhibits a periodic structure in disturbance wave number α-space. Numerical solutions for interfacial evolutions show that a disturbance with a short wave length, which would be stable in a straight tube PCAF, can excite long wave instabilities due to an interaction with the wall's higher harmonic waves.

In this chapter we analyze the complementary case of an inviscid CAF in a corrugated tube, where inertia is presumed to be dominant (over viscosity) to see whether these features also characterize the inviscid system. We apply techniques similar to those used in the viscous systems above. That is, as in that case, we systematically develop the corrugated base flows and the corresponding linear stability for the inviscid system using the same asymptotically small parameters as we did for the viscous case. The solutions for both the viscous and the inviscid cases will allow us to examine how small corrugations affect the system's base state and its corresponding stability for strong surface tensions when either viscosity or inertia dominates the other.

2. Governing Equations and Boundary Conditions

Two immiscible, inviscid, incompressible fluids with matched densities are axisymmertically flowing in a core-annular arrangement in a horizontal tube of radius $R_2(z)$ that varies in the axial direction with slight corrugation. The interface is given by $r = S(z,t)$. The core region, defined by $0 \le r \le S(z,t)$, is occupied by fluid 1 and the annulus, $S(z,t) \le r \le R_2(z)$, is filled by fluid 2. Since the flow fields are assumed to be axisymmetric with no azimuthal component, they only have velocity components $(u,0,w)$ in terms of cylindrical polar coordinates (r,θ,z). Let W_0 be the sum of the volumetric flow

rates of both fluids divided by the mean cross sectional area of the tube. If one non-dimensionalizes velocities, pressure, lengths, and time with the characteristic quantities W_0, ρW_0^2, R_0, and R_0/W_0, respectively, where ρ is the density of the fluids and R_0 is the mean radius of the core, the non-dimensional Euler and continuity equations for each fluid are

$$w_t + ww_z + uw_r = -p_z, \tag{2.1a}$$

$$u_t + wu_z + uu_r = -p_r, \tag{2.1b}$$

$$\frac{1}{r}(ru)_r + w_z = 0. \tag{2.1c}$$

We have suppressed the subscript i (i=1,2 denoting which fluid) on u ,w , and p in (2.1) for clarity and subscripts r and z represent the corresponding partial derivatives. Introducing the stream function as

$$w = \frac{1}{r}\frac{\partial \psi}{\partial r} \quad , \quad u = -\frac{1}{r}\frac{\partial \psi}{\partial z} \quad , \tag{2.2}$$

for each fluid automatically satisfies the equation of continuity. If the flows are irrotational, then the flows satisfy

$$E^2\psi = 0, \tag{2.3}$$

where $E^2 = \frac{\partial^2}{\partial r^2} - \frac{1}{r}\frac{\partial}{\partial r} + \frac{\partial^2}{\partial z^2}$.

The system is subject to the following boundary conditions. The velocity normal to the wall vanishes and the velocity normal to the interface is continuous there, or

$$\boldsymbol{n}_2 \cdot \boldsymbol{v}_2 = 0 \quad \text{at } r = R_2(z), \tag{2.4a}$$

$$\boldsymbol{v}_1 \cdot \boldsymbol{n} = \boldsymbol{v}_2 \cdot \boldsymbol{n} \quad \text{at } r = S(z,t). \tag{2.4b}$$

Here $\boldsymbol{n}_2(z)$ and $\boldsymbol{n}(z)$ are the unit normals of the wall and the interface, respectively, both pointing outward. Since there is no viscosity to retard fluid motions, there are no tangential stresses. However, the normal stresses balance at the interface, or

$$p_2 - p_1 = We\left(S_{zz} - (1+S_z^2)/S\right)\left(1+S_z^2\right)^{-3/2} \qquad \text{at } r = S(z,t), \tag{2.4c}$$

where $We = \dfrac{\gamma}{R_0 \rho_1 W_0^2}$ is the surface tension parameter, commonly referred to as the Weber number. It is equal to the inverse of the product of the Reynolds and capillary numbers. The kinematic condition in terms of film variables is

$$u_2 = S_t + w_2 S_z \qquad \text{at } r = S(z,t). \tag{2.4d}$$

Finally, the core flow field must be bounded at the central line, which is given by

$$\frac{1}{r}\psi_{1r}\,,\ \frac{1}{r}\psi_{1z} \text{ bounded as } r \to 0. \tag{2.4e}$$

3. Base flow

3.1 Scalings

Consider two immiscible, inviscid fluids with an interfacial tension between them flowing in a core-annular arrangement through a slightly corrugated tube. If there were no tube corrugation, any differentiable axial function $\mathbf{v}_i = (0,0,w_i(r))$, $i = 1, 2$, with uniform pressure would satisfy the steady state base flow equations, although for the flow to be irrotational w_i in each fluid would need to be independent of r. For simplicity and in order to avoid a Kelvin-Helmholtz instability due to interfacial slip of the base flow, it is reasonable to assume the uncorrugated flow profiles of both regions are flat, i.e., uniform, and both equal to W_0. Since the uncorrugated tube is the zeroth order shape in the small corrugation parameter σ, this base flow serves as the zero-order-in-σ base flow, and we thus choose W_0 as the characteristic velocity. Let p and P denote the film and the core pressures, respectively, and let double over bars denote the $O(\sigma^0)$ base flow. Because there is no viscous force to retard the film flow, no pressure force is required to drive the

zero order base flow; thus $\bar{p}_z$ and $\bar{P}_z$ are both zero in σ. We take $\bar{p} \equiv 0$ and, from the normal stress condition for the σ=0 base flow, $\bar{P} = We$.

A small, non-zero corrugation will lead to a steady state base flow that no longer possesses a cylindrical interface and whose velocity field will be perturbed from that of the straight tube. Let $(\bar{u}', \bar{w}', \bar{p}')$ and $(\bar{U}', \bar{W}', \bar{P}')$ represent the perturbed radial velocity, axial velocity and pressure for the film and core, respectively. In addition, let $\bar{\delta}$ be the scale of the deviation of the fluid-fluid interface from the cylindrical shape. Because the applications tend to have annuli that are much thinner than the mean core radius, we focus on the thin annular limit. We introduce the parameter

$$\varepsilon = \frac{\langle R_2 \rangle - \langle R_1 \rangle}{\langle R_1 \rangle},$$

the ratio of the mean annular thickness to the mean core radius, where $\langle \bullet \rangle \equiv \lim_{L \to \infty} \frac{1}{2L} \int_{-L}^{L} \bullet dz$ is the average over z. ε is, by hypothesis, much less than one. Using ε, define a stretched radial film variable $y = 1 - \frac{r-1}{\varepsilon}$, which is order one in the film region. The thin film assumption, via y, separates the radial and axial length scales in the film and leads to large $O(1/\varepsilon)$ radial derivatives there. As we shall now see, the wall corrugation sets up a generally non-zero radial film velocity which translates, by continuity into a perturbation axial velocity that depends on r and z. This results in a velocity and pressure that vary with r and z, forcing the interface to be corrugated and to propagate the axial non-uniformity into the core.

Let the wall's shape be described by

$$r = R_2(z) = 1 + \varepsilon(1 + \sigma\phi(z)), \tag{3.1}$$

or $y = -\sigma\phi(z)$, where ϕ is an order one function and σ is the small corrugation parameter. Let the steady state interface be $r = S(z) = 1 + \bar{\delta}\eta(z)$, where $\bar{\delta}$ is the as yet

unknown magnitude of the interface's deviation from the unit cylinder and $\eta(z)$ is an unknown order one shape function. Taking the Taylor expansion of the impenetrability condition (2.4a) about $y=0$ gives $\bar{u}' \sim \sigma\varepsilon$. Continuity leads to $\bar{w}' \sim \bar{u}'/\varepsilon \sim \sigma$. From the z-component of Euler's equation and a balance of the gradient $\bar{p}'_z$ of the perturbation pressure with ww_z or $\bar{w}'_z$ give $\bar{p}' \sim \sigma$. Finally, the normal stress condition translates this perturbed pressure into a corrugated interface via $p'-P' \sim \bar{\delta} We$. The leading order of the kinematic condition is $u'(1) = \bar{\delta}\eta_z$, which requires $\bar{\delta} \sim \sigma\varepsilon$. The core scalings follow via the continuity of normal velocity at the interface, which gives $\bar{U}' \sim \sigma\varepsilon$. The continuity and Euler equations and the lack of scale separation of the radial and axial direction in the core give $\bar{W}' \sim \sigma\varepsilon$ and $\bar{P}' \sim \sigma\varepsilon$. As a result, the normal stress condition is dominated by the film's pressure. This gives $\bar{p}' \sim \sigma \sim We\sigma\varepsilon$ or $We \sim 1/\varepsilon$. We restrict our attention to this scaling of We.

We assume a regular perturbation expansion for all of the dependent variables and formulate the leading order corrugated base flow by substituting those quantities into the governing equations and boundary conditions. As we shall see, the film flow and the shape of the interface can be determined independently of the core. We can then solve for the core flow in terms of modified Bessel functions and the interface function $\eta(z)$.

3.2 Formulation of the Base Flow

From the above scaling relations, we postulate the following asymptotic expansions in the film,

$$w = 1 + \sigma\bar{w} + O(\sigma\varepsilon, \sigma^2), \tag{3.2a}$$

$$u = \sigma\varepsilon\bar{u} + O(\sigma^2\varepsilon, \sigma\varepsilon^2), \tag{3.2b}$$

$$p = \bar{\bar{p}} + \sigma\bar{p} + O(\sigma\varepsilon, \sigma^2), \tag{3.2c}$$

$$\psi = \bar{\bar{\psi}} + \sigma\varepsilon\bar{\psi} + O(\sigma^2\varepsilon, \sigma\varepsilon^2), \tag{3.2d}$$

and those in the core,

$$W = 1 + \sigma\varepsilon\bar{W} + O(\sigma^2\varepsilon, \sigma\varepsilon^2), \tag{3.3a}$$

$$U = \sigma\varepsilon\bar{U} + O(\sigma^2\varepsilon, \sigma\varepsilon^2), \tag{3.3b}$$

$$P = \bar{\bar{P}} + \sigma\varepsilon\bar{P} + O(\sigma^2\varepsilon, \sigma\varepsilon^2), \tag{3.3c}$$

$$\Psi = \bar{\bar{\Psi}} + \sigma\varepsilon\bar{\Psi} + O(\sigma^2\varepsilon, \sigma\varepsilon^2). \tag{3.3d}$$

Here $\bar{\bar{}}$ stands for the uncorrugated (σ=0) state whose flows are uniform with uniform pressures in each region, and $\bar{}$ denotes the corrugation correction. Substituting these expansions into the governing steady state equations and boundary conditions and expanding about the uncorrugated state, yield the following first-order-in-σ problem:

For the film,

$$\bar{w} = -\bar{\psi}_y\,,\ \bar{u} = -\bar{\psi}_z, \tag{3.4a}$$

$$\bar{\psi}_{yy} = 0, \tag{3.4b}$$

and for the core,

$$\bar{W} = \frac{1}{r}\bar{\Psi}_r,\ \bar{U} = -\frac{1}{r}\bar{\Psi}_z. \tag{3.5a}$$

The core's governing equation is still

$$E^2\bar{\Psi} = 0. \tag{3.5b}$$

The boundary conditions become

$$\text{at } y = 0,\ \bar{u} = \phi_z\,, \tag{3.6a}$$

$$\text{at } y = 1,\ \bar{u} = \eta_z, \tag{3.6b}$$

$$\text{at } y = 1,\ \bar{p} = We_0(\eta_{zz} + \eta), \tag{3.6c}$$

$$\text{at } r = 1,\ \bar{U} = \bar{u}, \tag{3.6d}$$

$$\text{as } r \to 0,\ \frac{1}{r}\overline{\Psi}_r \text{ and } \frac{1}{r}\overline{\Psi}_z \text{ bounded.} \tag{3.6e}$$

In (3.6c), we have defined $We_0 = We\varepsilon$, where We_0 is $O(1)$.

We solve (3.4) for the film's stream function and velocity profile in terms of the given wall function $\phi(z)$ and the unknown interface function $\eta(z)$. We find

$$\overline{\psi} = -(\eta - \phi)\cdot y - \phi, \tag{3.7a}$$

$$\overline{w} = \eta - \phi, \tag{3.7b}$$

$$\overline{u} = (\eta - \phi)_z \cdot y + \phi_z. \tag{3.7c}$$

Note that the corrugated axial velocity in the film is independent of y, which reflects the slip boundary condition at the wall. In order to solve for the interface function $\eta(z)$, we connect the velocity field with the pressure by using the film's Euler equations. Its leading order radial and axial components are

$$\overline{p}_y = 0, \tag{3.8a}$$

$$\overline{w}_z + \overline{p}_z = 0. \tag{3.8b}$$

From (3.8a), $\overline{p}(y) = \overline{p}(y = 1)$. Using this, (3.7b) and (3.6c) in (3.8b), and integrating once yield the equation for the leading order shape of the steady state interface deflection:

$$We_0(\eta_{zz} + \eta) + \eta = \phi + C. \tag{3.9}$$

An integral constant C appears in (3.9). To find C, we first assume that the wall function $\phi(z)$ is periodic with period $2l$ and its mean (over a period) deviation from the straight tube is zero, i.e., $\int_{-l}^{l} \phi\, dz = 0$. The conservation of mass requires the mean of the interface displacement to also be zero, that is $\int_{-l}^{l} \eta\, dz = 0$. Integrating (3.9) over the wall period $2l$ along with the above conditions yields C =0. Alternatively, we may allow the mass displacement due to corrugation be left open and still eliminate the integration constant C by redefining $\eta \to \eta + \dfrac{C}{1 + We_0}$.

We also perform a macroscopic force balance over a period of the wall and assume that there is no net force on the core fluid, i.e.,

$$\int_{A_{out}} P(-\boldsymbol{e}_z)dA + \int_{A_{in}} P\boldsymbol{e}_z dA - \int_{A_s} p\boldsymbol{n}dA = 0, \tag{3.10a}$$

where A_{out} and A_{in} are cross sectional areas normal to z-direction at the both ends of the period, and A_s is the surface area of the interface. Let $n_r = \boldsymbol{n} \bullet \boldsymbol{e}_r$, and S_b be the base flow interfacial position. The r-component of (3.10a) is

$$\int_{A_s} p\boldsymbol{n} \cdot \boldsymbol{e}_r dA = 2\pi \int_{-l}^{l} pS_b\left(1+S_b^2\right)^{1/2} n_r dz = 2\pi \int_{-l}^{l} \left(\bar{\bar{p}} + \sigma\bar{p}\right)(1+\sigma\varepsilon\eta)dz$$

$$= 2\pi\sigma \int_{-l}^{l} \bar{p}dz + O(\sigma^2\varepsilon) = 0, \tag{3.10b}$$

Because the wall is periodic, the inhomogeneous solution η to (3.9) has the same periodicity as the wall. By using (3.6c), (3.8a), (3.9), and (3.10b), the homogeneous part of η should vanish for (3.9) unless $l = l^* \equiv \sqrt{1+We_0^{-1}}/2$, where $2l^*$ is the system's natural wave length. However, $l = l^*$ leads to resonant growth (and decay) of η for $|z| \to \infty$, and thus our asymptotic expansions would be no longer uniform. The z-component of (3.10a) is

$$-\int_{A_{ou}} PdA + \int_{A_{in}} PdA - \int_{A_s} p\boldsymbol{n} \cdot \boldsymbol{e}_z dA$$

$$= -2\pi \int_0^{S_{b,out}} \left(\bar{\bar{P}} + \sigma\varepsilon\bar{P}\right)rdr + 2\pi \int_0^{S_{b,in}} \left(\bar{\bar{P}} + \sigma\varepsilon\bar{P}\right)rdr - 2\pi \int_{-l}^{l} \left(\bar{\bar{p}} + \sigma\bar{p}\right)(1+\sigma\varepsilon\eta)(-\sigma\varepsilon\eta_z)dz. \tag{3.10c}$$

Because, inferred from (3.10b), the interface has the same periodicity as the wall and $\bar{p}$ inherits this periodicity, the first two integrals of (3.10c) cancel, and the last integral scales as $O(\sigma^2\varepsilon)$. This thus satisfies the requirement of no net macroscopic force up to $O(\sigma\varepsilon)$.

With the solution to (3.9) for the interface's shape function $\eta(z)$, one can obtain the complete leading order solution for the film from (3.7). Eqn. (3.9) is a forced harmonic

oscillator. Until now, we have assumed that the wall's function ϕ be periodic with a period $2l = 2\pi/k$, k being the $O(1)$ wall's wave number. We now solve (3.9) for the special case of $\phi(z) = cos(kz)$. Note that we shall assume $k \neq k^* \equiv \sqrt{1 + 1/We_0}$; otherwise the particular solution will grow in z due to a resonance when the wall's wave number equals the system's natural frequency k^*. Since the homogeneous solution for η does not contribute, due to the above macroscopic force balance, η contains only the particular solution which has the same periodicity as the wall. We represent the solution as the real part of the complex solution. For the guess $(\phi, \eta, \Psi) = (\hat{\phi}, \hat{\eta}, \hat{\Psi})exp(ikz)$, and the solution of (3.9) becomes

$$\hat{\eta} = \frac{1}{1 + We_0(1-k^2)}\hat{\phi} \quad \text{or} \quad \eta = \frac{1}{1 + We_0(1-k^2)}cos(kz), \left(k \neq \sqrt{1 + 1/We_0}\right). \tag{3.11}$$

From η and the film's solution, we can solve the core flow from (3.5), (3.6d) and (3.6e). Thus,

$$\hat{\Psi}(r) = -\frac{\hat{\eta}}{I_1(k)} r I_1(kr), \tag{3.12}$$

To summarize, the corrugated base flow patterns for both flow regions are:

For the film,

$$w = 1 + \sigma(\eta - \phi) + O(\sigma\varepsilon, \sigma^2), \tag{3.13a}$$

$$u = \sigma\varepsilon\left((\eta_z - \phi_z)\cdot y + \phi_z\right) + O(\sigma^2\varepsilon, \sigma\varepsilon^2), \tag{3.13b}$$

$$p = \sigma We_0\left(\eta_{zz} + \eta\right) + O(\sigma\varepsilon, \sigma^2). \tag{3.13c}$$

For the core,

$$W = 1 - \sigma\varepsilon\frac{k}{I_1(k)} I_0(kr)\eta(z) + O(\sigma^2\varepsilon, \sigma\varepsilon^2), \tag{3.14a}$$

$$U = \sigma\varepsilon\frac{k}{I_1(k)} I_1(kr)\eta_z(z) + O(\sigma^2\varepsilon, \sigma\varepsilon^2), \tag{3.14b}$$

$$P = We_0\varepsilon^{-1} - \sigma\varepsilon\frac{k}{I_1(k)}I_1(kr)\eta(z) + O(\sigma^2\varepsilon, \sigma\varepsilon^2). \qquad (3.14c)$$

3.3 Results from the Base Flow

Let us begin by analyzing this steady base flow. As we saw above, the interface is wavy and has the same periodicity as the wall (where only the inhomogenous solution contributes). Since the fluids are inviscid, the effect of the wall's corrugation is to set up axial pressure gradients which convectively accelerate and decelerate the fluids as they pass through the narrow and wide parts of the channel. The deflected interface propagates this motion into the core where the radial pressure gradient accounts for the convective acceleration in the radial direction in the core. Recall that (3.9) is in the form of a forced harmonic oscillator. The solution (3.11) for the interface function η contains two frequencies, the forcing k of the wall and the natural frequency $k^* \equiv \sqrt{1 + 1/We_0}$. The latter contains the surface tension. There are two important indices of the wall corrugation's interfacial modulation : the ratio of the interface's amplitude to the wall's

$$Amp = \frac{1}{|1 + We_0(1-k^2)|}, \qquad (3.15a)$$

and the phase shift θ between the interface's and the wall's functions, η and ϕ, respectively :

$$\theta = \begin{cases} 0^0, & 1 + We_0(1-k^2) > 0 \\ 180^0, & 1 + We_0(1-k^2) < 0 \end{cases}. \qquad (3.15b)$$

θ is either 0^0 or 180^0 and it depends on the difference $k^{*2} - k^2 = (1 + We_0(1-k^2))/We_0$ of the squares of the two frequencies. Because of (3.11), a positive (negative) sign of $1 + We_0(1-k^2)$ corresponds to the interface and wall being in-phase (out-of-phase).

Figure 2 shows the dependence of the interfacial amplitude on the wall's wave number for various We_0. Note that all curves cross at $k = 1$, where the wall's wave length is equal

to the undisturbed circumference of the interface. In this case, neither the pressure nor the velocities in the film vary with z. Therefore, the overall flow fields are locally parallel in order to maintain a constant flow rate. The resulting leading order interface shape follows the wall exactly, i.e., $\eta = \phi$ ($Amp = 1$). This conclusion also obtains for the case of zero capillarity in (3.9). In addition, for a given surface tension, there exists the singular point noted above where a resonance occurs at the natural frequency k^*. The monotonically growing ($k < k^*$) and decaying ($k > k^*$)curves are separated by $k = k^*$, and represent interface-wall in-phase and out-of-phase configurations, respectively.

Figures 3 show that the film streamlines appear in-phase (a & b) and out-of-phase (c) for different relations between k and $k^* = \sqrt{2}$. A positive $1 + We_0(1-k^2)$ can result from either a weak longitudinal capillarity ($k < 1$) or when $1 > We_0(k^2 - 1) > 0$. For k <1, the circumferential curvature of the interface's capillarity has a stronger effect than its longitudinal component. This yields (from (3.6c)) higher and lower film pressures at the crests (maxima in $S_b(z)$) and the troughs of the interface, respectively. From Bernoulli's theorem, the speed at the crest becomes slower and remains uniform across the film (due to (3.7b)). Thus, the film flow within the interface's crest requires a larger cross section in order to allow the fluid to obey mass conversation. Similarly, the interface's trough requires a smaller cross section in the film. One should recognize that, in the thin film limit, the film cross sectional area is $\pi\left(R_2^2 - S_b^2\right) = 2\pi\varepsilon\left(1 + \sigma(\phi - \eta)\right) + O(\varepsilon^2, \varepsilon^2\sigma)$. It is the product of the mean interface's circumference 2π and the film thickness $\varepsilon\left(1 + \sigma(\phi - \eta)\right)$ at the leading order in ε. The variation of the interface's circumference due to the corrugation is of higher order $O\left(\varepsilon^2\sigma\right)$. Thus the variation of the film cross sectional area only arises from the variation $\varepsilon\sigma(\phi - \eta)$ of the film thickness. Accordingly, an in-phase arrangement between the interface and the wall is the only option for $k < 1$. Moreover, the interfacial amplitude is expected to be less than the wall's in order to maintain a wider (narrower)

cross section for the interface's crest (trough) for this in-phase arrangement. Figure 3(a) shows this situation. The amplitudes of the wall and the interface is 0.5 and 0.25, respectively, for the parameters in Figure 3(a). Note that a larger k decreases the film's pressure, thereby increasing the speed and shrinking the cross section, and raising the interfacial amplitude. This explains the left branches in Figure 2 for $k < 1$.

For $k > 1$, the film pressure is lower (higher) at the interface's crest (trough). When the wall's wave number k is only slightly larger (a shorter wall wave length) than 1 (e.g., $k = 1.2$ and $We_0 = 1$), it is still possible to have $1 > We_0(k^2 - 1)(>0)$, $Amp > 1$ and the interface has a slightly larger amplitude than the wall. This results in slightly faster (slower) speed and slightly smaller (larger) cross section at the interface's crest (trough). One finds only slight differences in the cross section when the wall and interface are in-phase as in Figure 3(b). From another perspective, because in this case capillarity is not strong enough to push θ to π, $k \to 1^+$ should tend towards the in-phase, no-capillary limit of $k = 1$. Note that for $k < k^*$, the interfacial amplitude increases as k increases.

On the other hand, negative $1 + We_0(1 - k^2)$ represents stronger longitudinal capillarity ($k > 1$). Again, in the film flow, the *interface's* crest has a faster speed with lower pressure, whereas the trough has the slower speed. Therefore, a narrower (wider) cross section is required for the crest (trough). This requires an out-of-phase arrangement. This case is shown in Figure 3(c) for We_0=1.0 and k =2.0. Note that a stronger capillary force tends to decrease the interface's amplitude.

The resonant case of $1 + We_0(1 - k^2)$=0 or $k = k^*$, is the critical state between the in-phase and out-phase configurations. The interface's amplitude grows or shrinks linearly with z. When the film's thickness is no longer small relative to the core, or no longer large relative to the corrugation, our analysis breaks down.

Even though the above discussion assumes a strong surface tension $We \sim 1/\varepsilon$, we can extend the range of the We scale without changing the details of our formulation. If

$We >> 1/\varepsilon$, the capillary pressure dominates the z-component of the Euler equations at the leading order in σ. The leading order interface remains cylindrical in shape, i.e., $\eta = O(We^{-1})$. The resulting axial velocity $w = 1 - \sigma\phi + O(\sigma We_0^{-1})$. It directly reflects a slower (faster) speed for a wider (narrower) tube cross section. However, unlike in the viscous case, a very strong capillarity does not lead to the no-flow limit due to wall slip. Let us briefly turn into a less strong tension $We << 1/\varepsilon$, where we restrict $1 << We << 1/\varepsilon$ here so as to keep the core's dynamics decoupled and to maintain the above formulation. In such a case, inertial effects dominate. The resulting interface follows the shape of the wall ($\eta = \phi$) at leading order in σ. An even weaker capillary force brings the core's contribution to leading order via the normal stress condition, which will change the analysis significantly.

4. Linear Stability

4.1 Scalings

We now to begin the linear stability analysis of the above base flow. Introduce an infinitesimal, axisymmetric disturbance of size δ ($\delta << \varepsilon, \sigma$) at the interface in such a way that $S(z,t) = S_b(z) + \delta\xi(z,t)$ where $S_b(z)$ is the interface of the base state and $\xi(z,t)$ is an unknown order one function that characterizes the interfacial disturbance. In analogy to the procedure for treating the base flows, one determines the scalings for the disturbed quantities before formulating the perturbation problem. Let (w', u', p') and (W', U', P') denote the disturbed quantities for the film and the core, respectively. Based on the assumption $We \sim 1/\varepsilon$, one can estimate the scalings of these disturbed quantities. For the film flow, the normal stress sets up a capillary pressure $p' \sim We\delta \sim \delta/\varepsilon$. Relating w' with p' by the axial component of the Euler equation brings out that $w' \sim p' \sim \delta/\varepsilon$. We thus have $u' \sim \delta$ from continuity. For the core flow, the continuity of the normal velocity at

the interface yields $U' \sim \delta$. Continuity and the Euler equation in the core lead all of the core's disturbed quantities to have the same scale δ. By applying the above scalings of the disturbed flows and extracting the base flow contribution from the governing equations and the boundary conditions at the leading order in δ, we shall derive the linear stability equations below.

4.2 Formulation of the Linear Stability Problem

Define the following asymptotic expansions for the disturbed flow quantities. For the film,

$$(w,\ u,\ p,\psi) = (w_b,\ u_b,\ p_b,\ \psi_b) + (\frac{\delta}{\varepsilon}w',\ \delta u',\ \frac{\delta}{\varepsilon}p',\ \delta\psi'), \tag{4.1}$$

and for the core,

$$(W,\ U,\ P,\ \Psi) = (W_b,\ U_b,\ P_b,\ \Psi_b) + (\delta W',\ \delta U',\ \delta P',\ \delta\Psi'), \tag{4.2}$$

where "b" denotes the base state. One substitutes (4.1) and (4.2) into (2.1)-(2.4), and retains terms up to $O(\delta)$ by eliminating the contribution from the base flow. Recall that velocities have been scaled with W_0. Dropping the primes, then, we have the following: For the film flow, the dynamic Euler equations at $O(\delta/\varepsilon)$ become

$$w_t + w_z + \sigma\left(\bar{w}w_z + \bar{w}_z w - w_y\bar{u} - \bar{w}_y u\right) = -p_z + O(\sigma\varepsilon), \tag{4.3a}$$

$$0 = \frac{1}{\varepsilon}p_y + O(\varepsilon), \tag{4.3b}$$

where $\bar{}$ quantities are the corrugation corrections to the base flow in (3.2), and time has an $O(1)$ scale. Equation (4.3b) suggests that disturbed pressure remains uniform across the film as typically occurs in situations, e.g. lubrication or boundary layer theory, where the transverse scales are much larger than the normal length scale. The stream function equation and the velocity are, to leading order,

$$\psi_{yy} = 0,\ w = -\psi_y,\ u = -\psi_z. \tag{4.3c}$$

Thus, these suggest that $w = w(z,t)$ is independent of y as well to leading order. For the core flow, the equations are

$$E^2\Psi = 0, \tag{4.4a}$$

$$W = \frac{1}{r}\Psi_r, \; U = -\frac{1}{r}\Psi_z. \tag{4.4b}$$

The boundary conditions are prescribed as the follows: The normal component of the velocity along the corrugated wall is zero and gives,

$$\text{at } y = -\sigma\phi, \; u = \sigma\phi_z w. \tag{4.5a}$$

At the interface, the normal stress balance at $O(\delta/\varepsilon)$ is

$$\text{at } y = 1-\sigma\eta, \quad p = We_0(\xi_{zz} + \xi) + O(\varepsilon\sigma). \tag{4.5b}$$

The film's disturbed pressure is primarily supported by the disturbed capillary force and the base interface's contribution is of higher order ($O(\sigma\varepsilon)$). At $O(\delta)$, the continuity of normal velocity at the interface requires

$$-\sigma\bar{u}_y\big|_{y=1}\xi + u(y=1-\sigma\eta) - \sigma\bar{w}(y=1)\xi_z = U(r=1) + O(\sigma\varepsilon). \tag{4.5c}$$

The core perturbation velocities are bounded at the central line $r = 0$. Finally, the kinematic condition from the film side at $O(\delta)$ gives

$$-\sigma\,\bar{u}_y\big|_{y=1}\xi + u(y=1-\sigma\eta) = \xi_t + \left(1+\sigma\bar{w}(y=1)\right)\xi_z + \sigma w(y=1)\eta_z. \tag{4.5d}$$

We solve (4.3) with (4.5a) to yield the disturbed film flow fields

$$w = -A(z,t), \; u = -A_z y - \sigma(A\phi)_z, \tag{4.6}$$

where A is an unknown function of both z and t. Substituting (4.6) into Euler's equation (4.3a) and the kinematic condition (4.5d) and using (4.5b) yield the following set of coupled stability equations for the film:

$$\xi_t + A_z + \xi_z + \sigma\left[(\xi - A)(\eta - \phi)\right]_z = 0, \tag{4.7a}$$

$$A_t + A_z + \sigma\left(A\cdot(\eta-\phi)\right)_z = We_0(\xi_{zzz} + \xi_z). \tag{4.7b}$$

Note that the time scale here is $O(1)$, rather than the longer $O(\varepsilon)$ scale in the viscous case (Georgiou *et al.* 1992 and Wei & Rumschitzki 2000) and thus causes more rapid capillary growth than in the viscous case. This is because the flow accelerates or decelerates in response to the capillary pressure alone. Also note that the corrugation contribution is reflected by the variation of the base film thickness $(\eta - \phi)$ which depends on the wall function ϕ and Weber number We_0 from (3.9).

4.3 Analysis of the Linear Stability

Up to order $\sigma\delta$, the interfacial evolution equations (4.7) do not contain core quantities. That is, the core's dynamics slave those of the film. The σ=0, i.e., the uncorrugated limit recovers the straight tube result.

$$\xi_t + A_z + \xi_z = 0, \tag{4.8a}$$

$$A_t + A_z = We_0(\xi_{zzz} + \xi_z). \tag{4.8b}$$

We can eliminate $A(z, t)$ to obtain a single equation for ξ

$$\xi_{tt} + 2\xi_{tz} + \xi_{zz} + We_0(\xi_{zzzz} + \xi_{zz}) = 0. \tag{4.8c}$$

This gives $\omega = -i\alpha \pm \alpha\sqrt{We_0(1-\alpha^2)}$. It leads to long wave ($\alpha < 1$) destabilization while short wave disturbances lead to standing waves that do not decay. The real part of ω in dimensional form is $\alpha\sqrt{1-\alpha^2}\left(\varepsilon\gamma/\rho R_0^3\right)^{1/2}$ which is independent of velocity. It also agrees with Goren's (1962) eqn. (24) in the thin film limit of his inviscid (with static base state) result. Note that, for the static case, the characteristic velocity and time scale should be $\left(\gamma/\rho R_0\right)^{1/2}$ and $\left(R_0^3\rho/\gamma\right)^{1/2}$, respectively. The imaginary part of ω arises from the uniform flow and does not contribute to the stability. The straight-tube stability is thus identical to that of the static inviscid case, since the two systems are identical up to a change of (non-inertial) reference frame.

For $\sigma \neq 0$, eqns (4.7) have non-constant coefficients arising from the factor $(\eta - \phi)$. For the special case of $k = 1$, where the resulting film thickness is uniform ($\eta = \phi$), the coefficients in (4.7) are constant. Therefore, due to the locally parallel flow fields, the corrugation does not contribute to the instability and the equations reduce to the cylindrical tube theory at the leading order in ε and σ. A similar argument also applies for a less strong capillarity, $1 << We << 1/\varepsilon$ or $\varepsilon << We_0 << 1$; as discussed in the base flow section $\eta = \phi$ at the leading order. For these special cases, one should consider the next order in the small parameters to see the effect of corrugation.

It is also instructive to consider two limiting cases: very long and very short wave disturbances α. Because the initial disturbance's and the wall's wave lengths may be of different length scales, the wall's modulation can result in a wave length that may be either longer or shorter than that of the initial disturbance. This modulated wave length depends on the corrugation size σ, the wavelength $2\pi/\alpha$ of the initial disturbance, the wall's wave length $2\pi/k$ and the time scale. Let us first consider the long wave ($\alpha << 1$) limit with $k = O(1)$. We rescale $\tilde{z} = \alpha z$ and expand equations (4.7) in powers of α. This yields

$$\xi_t + \alpha(A_z + \xi_z) + \sigma\alpha(\eta - \phi)_z(\xi - A) + \sigma\alpha(\eta - \phi)(\xi_z - A_z) = 0, \tag{4.9a}$$

$$A_t + \alpha(A_z - We_0\xi_z) + \sigma\alpha(\eta - \phi)_z A + \sigma\alpha(\eta - \phi)A_z = O(\alpha^3). \tag{4.9b}$$

Because $\eta - \phi = f(k\tilde{z}/\alpha)$ varies with the wall's wave length scale $2\pi/k$ rather than with the disturbance's long wave length scale $2\pi/\alpha$, $\alpha(\eta - \phi)_z = (\eta - \phi)_{\tilde{z}} \sim O(k)$, not $O(\alpha)$.

If $\alpha >> \sigma$, disturbances respond as if the wall were uncorrugated and only had a circumferential curvature for times of $O(\alpha^{-1})$; they grow and convect as $exp((i\alpha \pm \alpha\sqrt{We_0})t)$. For $\sigma >> \alpha$ and $k = O(1)$, equations (4.9) in the limit $\alpha \to 0$ become

$$\xi_t + \sigma(\eta - \phi)_z(\xi - A) = 0, \tag{4.10a}$$

$$A_t + \sigma(\eta - \phi)_z A = 0. \tag{4.10b}$$

with solution

$$A(\tilde{z},t) = A(\tilde{z},\ t = 0)\exp(-\sigma(\eta - \phi)_z t), \tag{4.11a}$$

$$\xi(\tilde{z},t) = \left(\xi(\tilde{z},\ t = 0) + \sigma A(\tilde{z},\ t = 0)(\eta - \phi)_z t\right)\exp(-\sigma(\eta - \phi)_z t). \tag{4.11b}$$

As a result, a local variation of the base film thickness can also cause growth in time.

On the other hand, one can expect a very short wave disturbance ($\varepsilon^{-1} >> \alpha >> k$) not to see the wall's corrugation because the disturbance's wave length is much shorter than the wall's. In such a case, $(\eta - \phi)$ varies slowly in $\tilde{z}$ due to $k/\alpha << 1$. Suppose, as well, that $\alpha >> 1$. Now ξ and A vary over the short $2\pi/\alpha$ scale while $(\eta - \phi)$ varies over the longer $2\pi/k$ scale. Then (4.7) in this limit becomes:

$$\xi_t + \alpha\left(A_z + \xi_{zz} + \sigma(\eta - \phi)(\xi - A)_z\right) = O(\alpha^0), \tag{4.12a}$$

$$A_t - \alpha^3 We_0 \xi_{zzz} = O(\alpha). \tag{4.12b}$$

Eliminating A leads to

$$\xi_{tt} + \alpha^4\left(1 - \sigma(\eta - \phi)\right)We_0 \xi_{zzzz} = O(\alpha^3) \tag{4.12c}$$

Note that for $\alpha >> 1$, $\sigma(\eta - \phi)$ varies slowly in $\tilde{z}$ due to $k/\alpha << 1$. As a result, for times of $O(\alpha^{-2}\sigma^{-1/2})$, the corrugation is unimportant, the system shows no growth and it just reduces to the $\sigma = 0$ case. For even longer times, an interaction with the wall results in much longer $O(\alpha - nk)$ waves which may destabilize the prior stable state or excite other unstable modes.

In general, our theory holds for wave numbers $\alpha << O(\varepsilon^{-1})$. Eqns (4.7) are based on the assumption that the axial length scale is much longer than the radial one in the film. When we would like to consider wavelengths short enough to be comparable to the film thickness, our theory breaks down.

Because the interface's evolution equations (4.7) have non-constant coefficients, the usual Fourier transform methods are not useful. Following our previous approach for the

analogous viscous system (Chapter II, Wei & Rumschitzki 2000), we again employ Floquet-Bloch theory. The basic idea, in brief, is that an initial disturbance with wave number α can interact with the wall's corrugation (with wave number k) via the non-constant coefficients whose periodicity is $2\pi/k$. This interaction generates higher wall harmonics of the initial disturbance ($\alpha \pm nk$), and their superposition yields a Bloch function that is an appropriate eigenfunction for the system. We thus invoke two parallel procedures. First, we solve this eigenvalue problem. Second, we use an initial value approach to solve the film's evolution equations directly for a given initial interfacial disturbance. We then compare the results of these two independent methods and analyze their predictions.

4.3.1 Numerical Solution of the Eigenvalue Problem

The basis of our method is a theorem by Floquet which asserts that the solution of a linear differential equation whose (non-constant) coefficients are periodic with a common period is the product of an exponential and a periodic function, the latter having the same period as the coefficients. As such, we write the response (ξ, A) to a monochromatic disturbance of wave number α in terms of a Bloch function as

$$\begin{pmatrix} \xi \\ A \end{pmatrix} = exp(i\alpha z) \sum_{n=-N}^{N} \begin{pmatrix} \hat{\xi}_n \\ \hat{A}_n \end{pmatrix} exp(inkz + \omega t), \tag{4.13}$$

where ω is the complex growth rate from the temporal analysis (i.e., the Laplace transform variable) corresponding to the disturbance wave number α. This primary wave number α acts as a modulating factor in (4.13). Use of (4.13) guarantees a bounded solution in the z domain if (4.13) converges as $N \to \infty$ at any fixed instant t. Let $\eta - \phi = \left(\hat{\eta} - \hat{\phi}\right)e^{i\alpha z} +$

$\left(\hat{\eta}-\hat{\phi}\right)^{*}e^{-ikz}$. Then (4.13) translates (4.7) into an infinite set of algebraic equations for $(\hat{\xi}_n, \hat{A}_n)$.

$$\sigma Q^{-}(n)\left(\hat{\xi}_{n-1}-\hat{A}_{n-1}\right)+(\omega+P(n))\,\hat{\xi}_n+P(n)\hat{A}_n+\sigma Q^{+}(n)\left(\hat{\xi}_{n+1}-\hat{A}_{n+1}\right)=0, \quad (4.14a)$$

$$\sigma Q^{-}(n)\hat{A}_{n-1}+(\omega+P(n))\,\hat{A}_n+\sigma Q^{+}(n)\hat{A}_{n+1}+C(n)\hat{\xi}_n=0, \quad (4.14b)$$

where, by defining $\beta(n)=\alpha+nk$,

$$P(n)=i\beta(n),\ Q^{-}(n)=(\hat{\eta}-\hat{\phi})i\beta(n)\ ,\ Q^{+}(n)=(\hat{\eta}-\hat{\phi})^{*}i\beta(n),$$

$$C(n)=-We_0 i\beta(n)\left(1-\beta(n)^2\right). \quad (4.15)$$

The eigenvalue ω is determined by setting the determinant of (4.14) to zero. ω is a function of We_0, σ, k, and α. By truncating the matrices (4.14) for a given value of N, we can calculate the eigenvalue numerically for a fixed value of σ. We choose the dimension M=2(2N+1) of the matrices (4.14) large enough (typical N=11) and check that converged eigenvalues do not significantly change when we increase N.

4.3.2 Matrix Perturbation Theory of the Eigenvalue Problem

Since (4.14) contains the small parameter σ, we can also employ determinant / matrix perturbation theory in σ to determine the corrugation correction to the eigenvalue ω. In order to facilitate the perturbation technique, we use the following procedure to make (4.14) more tractable. We first add (4.14a) and (4.14b) to get the more symmetric from

$$\sigma Q^{-}(n)\hat{\xi}_{n-1}+(\omega+P(n)+C(n))\,\hat{\xi}_n+(\omega+2P(n))\hat{A}_n+\sigma Q^{+}(n)\hat{\xi}_{n+1}=0. \quad (4.16)$$

We then write (4.16) and (4.14b) in matrix form as:

$$\mathbf{M}\cdot\mathbf{x}+\mathbf{P}\cdot\mathbf{a}=\mathbf{0}, \quad (4.17)$$

$$\mathbf{C}\cdot\mathbf{x}+\mathbf{N}\cdot\mathbf{a}=\mathbf{0}, \quad (4.18)$$

where $\mathbf{x}=\left[\ldots\hat{\xi}_n\ldots\right]^{t}$, $\mathbf{a}=\left[\ldots\hat{A}_n\ldots\right]^{t}$,

$$\mathbf{M}=\begin{bmatrix} \ddots & \ddots & & [0] \\ \ddots & \ddots & \ddots & \\ & \sigma Q^{-}(n) & (\omega+P(n)+C(n)) & \sigma Q^{+}(n) \\ & [0] & \ddots & \ddots \end{bmatrix}, \mathbf{P}=\begin{bmatrix} \ddots & & [0] \\ & (\omega+2P(n)) & \\ [0] & & \ddots \end{bmatrix},$$

$$\mathbf{C}=\begin{bmatrix} \ddots & & [0] \\ & C(n) & \\ [0] & & \ddots \end{bmatrix}, \mathbf{N}=\begin{bmatrix} \ddots & \ddots & & [0] \\ \ddots & \ddots & \ddots & \\ & \sigma Q^{-}(n) & (\omega+P(n)) & \sigma Q^{+}(n) \\ & [0] & \ddots & \ddots \end{bmatrix}. \tag{4.19}$$

We assume that $\mathbf{P}$ is invertible, i.e., that $\omega \neq -2P(n)$ for all n, for the following perturbation formulation and will compare perturbation results with those obtained by solving (4.14) numerically to see if our purposed scheme is reasonable. We can thus eliminate $\mathbf{a}$ and obtain the following matrix equation for $\mathbf{x}$:

$$\left(\mathbf{C}-\mathbf{N}\mathbf{P}^{-1}\mathbf{M}\right)\cdot\mathbf{x}=\mathbf{0}. \tag{4.20}$$

A non-trivial solution to (4.20) requires that the matrix $(\mathbf{C}-\mathbf{N}\mathbf{P}^{-1}\mathbf{M})$ have a zero determinant. This provides us with the following alternative equation for ω. As we shall see below, it is convenient to solve for ω in a perturbative manner.

$$\Delta=\begin{vmatrix} \ddots & \ddots & \ddots & & [0] \\ \ddots & \ddots & \ddots & \ddots & \\ \sigma^2\tilde{Q}_2^{-}(n)+O(\sigma^4) & \sigma\tilde{Q}_1^{-}(n)+O(\sigma^3) & S(n)+\sigma^2F(n)+O(\sigma^4) & \sigma\tilde{Q}_1^{+}(n)+O(\sigma^3) & \sigma^2\tilde{Q}_2^{+}(n)+O(\sigma^4) \\ [0] & & \ddots & \ddots & \ddots \end{vmatrix}=0, \tag{4.21}$$

where

$$S(n)=\frac{(\omega+P(n))^2-P(n)C(n)}{\omega+2P(n)}$$

$$F(n) = \frac{Q^-(n)Q^+(n-1)}{\omega + 2P(n-1)} + \frac{Q^-(n+1)Q^+(n)}{\omega + 2P(n+1)}$$

$$\tilde{Q}_1^{\pm}(n) = Q^{\pm}(n)\left(\frac{\omega + P(n)}{\omega + 2P(n)} + \frac{\omega + P(n \pm 1) + C(n \pm 1)}{\omega + 2P(n \pm 1)}\right),$$

$$\tilde{Q}_2^{\pm}(n) = Q^{\pm}(n)Q^{\pm}(n+1), \qquad \text{(4.22a-d)}$$

Expansion of (4.21) in powers of σ yields

$$\Delta_0 + \sigma^2\Delta_2 + O(\sigma^4) = 0, \qquad \text{(4.23)}$$

$$\text{where } \Delta_0 = \prod_j S(j), \qquad \text{(4.24a)}$$

$$\Delta_2 = \sum_j \prod_{i \neq j} S(i)F(j) - \sum_j \left[\prod_{i \neq j, j-1} S(i)\tilde{Q}_1^-(j)\tilde{Q}_1^+(j-1)\right]. \qquad \text{(4.24b)}$$

The contributions to Δ_2 only include $O(\sigma^2)$ terms of the principal diagonal elements $\sigma^2 F(n)$ and the product of first off-diagonal elements $\sigma\tilde{Q}_1^{\pm}(n)$ appearing in the determinant, but do not include the second off-diagonal elements $\sigma^2\tilde{Q}_2^{\pm}(n)$ which are always multiplied by off-diagonal elements in the determinant. Note that the above is based on the base flows that we have developed up to $O(\sigma)$. The $O(\sigma^2)$ base flows only contribute to the principal diagonal, the first off-diagonal, and the second off-diagonal elements to $O(\sigma^4)$, $O(\sigma^3)$, and $O(\sigma^2)$, respectively; they thus do not contribute to Δ_2 for determining the leading order corrugation correction to the eigenvalue. As we shall see later, the eigenvalue spectrum exhibits a k-periodic structure in α-space. Therefore, we need only calculate the corrugation's correction to the primary eigenvalue ω_0 branch (the branch that reduces to the n=0 branch $-P(0)$ at $\sigma = 0$ and is denoted j=0), and then extend that to the other branches via the k-periodicity in α-space.

For a given α, (4.23) normally gives the $O(\sigma^2)$ correction to the leading eigenvalue ω_0, which we usually assume is a simple root of $\Delta_0 = 0$. However, since

$\omega_0 = -i\alpha \pm \alpha\sqrt{We_0(1-\alpha^2)}$ can lead to double roots at $\alpha = \pm 1$, one may, instead find an $O(\sigma)$ correction around α=1. If we use the Taylor expansion of (4.23) to solve for the correction $\delta\omega$ to ω_0, we find that $\delta\omega = -\sigma^2\Delta_2(\omega_0)\Big/\left(\frac{\partial\Delta_0}{\partial\omega}\right)_{\omega_0}$ to leading order in σ and $\delta\omega$. As $\alpha \to 1$, $\left(\frac{\partial\Delta_0}{\partial\omega}\right)_{\omega_0} \to 0$. Thus $\delta\omega$ is not uniform in α. In order to obtain an analytic and uniform (in α) expression to unify both the $O(\sigma)$ and $O(\sigma^2)$corrections, we adopt an alternative perturbation scheme. As we shall see below, we take advantage of the fact that Δ_0 contains the dispersion relation for determining ω_0 of the primary branch and the contributions from the other branches. If one only retains this dispersion relation at $O(\sigma^0)$, and lumps all corrections from Δ_0 into Δ_2 at the $O(\sigma^2)$ contribution, the $O(\sigma^2)$ part of this modified equation will vanish at ω=ω_0 except for the contribution from the primary α and its first harmonic $\alpha \pm k$ branches. This suggests that, instead of using the Taylor expansion above, one should employ an iteration scheme to solve for ω to greatly simplify the formulation.

Note that $S(0) = \left[(\omega + i\alpha)^2 - We_0\alpha^2(1-\alpha^2)\right]/(\omega + 2i\alpha)$, whose numerator is the $O(\sigma^0)$ dispersion relation for ω_0, and Δ_0= $\left[(\omega + i\alpha)^2 - We_0\alpha^2(1-\alpha^2)\right]\left[\prod_{j\neq 0} S(j)\Big/(\omega + 2i\alpha)\right]$. We isolate $S(0)$ by dividing by $\prod_{j\neq 0} S(0)\Big/(\omega + 2i\alpha)$ and removing terms *not* containing $S(0)$ from the sums in (4.24b). These latter terms are non-zero at ω=ω_0 and we isolate them in a term that we call G below that only involves interactions with the first harmonics. The remaining terms that are zero at ω_0 combine to give Σ as follows:

$$\left[(\omega+i\alpha)^2-We_0\alpha^2(1-\alpha^2)\right]+\sigma^2(\omega+2i\alpha)\left\{i\alpha\left\|\hat{\eta}-\hat{\phi}\right\|^2 G+\Sigma\right\}=0, \qquad (4.25)$$

where

$$\Sigma=\frac{1}{\prod_{j\neq 0}S(j)}\left[\sum_{j\neq 0}\prod_{m\neq j}F(j)S(m)-\sum_{j\neq 0,1}\prod_{m\neq j,j-1}S(m)\tilde{Q}_1^-(j)\tilde{Q}_1^+(j-1)\right],$$

$$G(\omega)=\left(G^+ + G^-\right), \qquad (4.26)$$

$$G^{\pm}=\left[P(\pm1)C(\pm1)-i\sqrt{We_0(1-\alpha^2)}P(\pm1)(2\omega+2P(\pm1)+C(\pm1))-P(\pm1)^2\frac{iWe_0(1-\alpha^2)}{i+\sqrt{We_0(1-\alpha^2)}}\right]\times$$

$$\left[C(\pm1)P(\pm1)-(\omega+P(\pm1))^2\right]^{-1}.$$

Again, the $O(\sigma^0)$ part of (4.25) determines $\omega_0=-i\alpha\pm\alpha\sqrt{We_0\left(1-\alpha^2\right)}$. One can solve for ω to the next order with an iteration scheme based on evaluating the $O(\sigma^2)$ part of (4.25). One evaluates the $O(\sigma^2)$ part of (4.25) at the j^{th} iterated $\omega_0^{(j)}$ of ω_0 and solves for the $(j+1)^{th}$ iterate $\omega_0^{(j+1)}$ from the $O(\sigma^0)$ part, or

$$\omega_0^{(j+1)}+i\alpha=\pm\sqrt{We_0\alpha^2(1-\alpha^2)-\sigma^2(\omega_0^j+2i\alpha)\left(\left\|\hat{\eta}-\hat{\phi}\right\|^2 i\alpha G(\omega_0^j)+\Sigma(\omega_0^j)\right)}. \qquad (4.27)$$

Thus, let $\omega_0^{(1)}=\omega_0$. Since $\Sigma\left(\omega_0^{(1)}\right)=0$, the $O(\sigma^2)$ part of (4.25) reduces to the term containing G, which only includes interactions between the primary wave α and its first harmonics $(\alpha\pm k)$. Therefore, the correction to the eigenvalue ω_0 is

$$\delta\omega^{\pm}\equiv\omega_0^{(2)}-\omega_0=\pm\sqrt{We_0\alpha^2(1-\alpha^2)-\sigma^2\left\|\hat{\eta}-\hat{\phi}\right\|^2(\omega_0+2i\alpha)i\alpha G(\omega_0)}\mp\sqrt{We_0\alpha^2(1-\alpha^2)}$$

$$=\frac{\mp\sigma^2\left\|\hat{\eta}-\hat{\phi}\right\|^2(\omega_0+2i\alpha)i\alpha G(\omega_0)}{\sqrt{We_0\alpha^2(1-\alpha^2)-\sigma^2\left\|\hat{\eta}-\hat{\phi}\right\|^2(\omega_0+2i\alpha)i\alpha G(\omega_0)}+\sqrt{We_0\alpha^2(1-\alpha^2)}}. \qquad (4.28)$$

From (4.28), one can verify that $\delta\omega^+ \sim O(\sigma)$ as $\alpha \sim 1$; otherwise $\delta\omega^+ \sim O(\sigma^2)$. It is also worth expanding (4.28) around both special points $\alpha = 0$ and $\alpha = 1$ to understand the details of the corrugation's interactions.

For $\alpha \to 0$, the growth rate correction $\delta\omega_r$ (the real part of $\delta\omega$) becomes

$$\delta\omega_r^+ = \frac{\left\|\hat{\eta} - \hat{\phi}\right\|^2 \sigma^2}{1 + We_0(1-k^2)}\left(3 + (1 - We_0)(1-k^2)\right) \cdot \alpha\sqrt{We_0} + O(\alpha^2). \qquad (4.29)$$

This gives the $O(\alpha\sigma^2)$ correction to ω_r as $\alpha \to 0$. The factor $\alpha\sqrt{We_0}$ comes from the circumferential curvature part of the capillarity. Recall that, as $\alpha \to 0$, $\omega_{0_r} = \alpha\sqrt{We_0}$ destabilizes for the long waves. However, the corrugation may give rise to a more or less unstable correction for the long waves, depending on the sign of $\left(3 + (1 - We_0)(1-k^2)\right)\left(1 + We_0(1-k^2)\right)^{-1}$. Recall that $1 + We_0(1-k^2) > 0$ (<0) leads to an in-phase (out-of-phase) interface-wall configuration of the base flow.

When α is close to 1, let $\alpha' = 1 - \alpha << 1$. Assuming $\alpha' << \sigma^2$, the expansion of (4.28) about $\alpha = 1$ ($\alpha' = 0$) yields

$$\delta\omega^{\pm} = \pm\sigma\left\|\hat{\eta} - \hat{\phi}\right\| \sqrt{\left(\frac{We_0 C_+}{We_0 C_+ + k^2} + \frac{We_0 C_-}{We_0 C_- + k^2}\right)_{\alpha=1}} - \sqrt{2We_0}\alpha'^{\frac{1}{2}} + O(\sigma\alpha'^{1/2},\ \alpha'), \quad (4.30)$$

where $C_\pm = (\alpha \pm k)^2\left(1 - (\alpha \pm k)^2\right)$ denotes the coupling to the first wall harmonics $(\alpha \pm k)$.

$\sqrt{We_0}\alpha'^{\frac{1}{2}} = \sqrt{We_0(1-\alpha^2)}$, which contains both the longitudinal and the circumferential capillary contributions that balance at $\alpha' = 0$. At α=1, (4.30) gives the coefficient for the $O(\sigma)$ correction. Depending on We_0 and k, when the expression inside the square root in (4.30) becomes positive, as we shall see later, the growth rate correction will show a dramatic change around α=1 since it is $O(\sigma)$. This $O(\sigma)$ instability can dominate for a long time scale that is $O(\sigma^{-1})$.

Due to the corrugation, the neutral state α^* is perturbed from $\alpha=1$ and we now calculate it. Let $\delta\alpha^* = 1-\alpha^*$, $|\delta\alpha^*| << 1$. Set $\omega_r^+ = 0$ (for the upper branch) in (4.27) to solve for $\delta\alpha^*$:

$$\delta\alpha^* = \frac{1}{2}\sigma^2\left\|\hat{\eta}-\hat{\phi}\right\|^2\left(\frac{C_+}{We_0C_+ + k^2}+\frac{C_-}{We_0C_- + k^2}\right)_{\alpha=1}. \tag{4.31}$$

The shift of the neutral state is $O(\sigma^2)$. Interestingly, when $\delta\omega_r^+>0$ for (4.30) is destabilizing, the $O(\sigma)$ instability excited at $\alpha=1$ results in $\delta\alpha^*>0$ and the neutral state is shifted to the right in α-space, thereby increasing the set of unstable waves. However, when $\delta\omega_r^+=0$ but $\delta\omega_i^+ \neq 0$ at $\alpha=1$, the neutral state shifts to the left in α and shrinks the set of unstable waves.

4.3.3 Initial Value Problem

In order to compare the dynamics of the interface's evolutions with the results of the eigenvalue spectrum calculated above, we also solve equation (4.7) directly as an initial value problem. We discretize the space variable by employing a Bloch-like form:

$$\begin{pmatrix}\xi(z,t)\\ A(z,t)\end{pmatrix} = \sum_{n=-N}^{N}\begin{pmatrix}\xi_{cn}(t)\\ A_{cn}(t)\end{pmatrix}cos((\alpha+nk)z)+\begin{pmatrix}\xi_{sn}(t)\\ A_{sn}(t)\end{pmatrix}sin((\alpha+nk)z), \tag{4.32}$$

subject to the initial condition $\xi(z,t=0)=cos(\alpha z)$, $A(z,t=0)=-sin(\alpha z)$. Substituting (4.32) into (4.7) yields a system of ordinary differential equations for the amplitudes $\xi_{cn}(t)$, $\xi_{sn}(t)$, $A_{cn}(t)$, and $A_{sn}(t)$. We implement a 12th order Adam-Moulton algorithm from the IMSL library to solve these ODEs. For a fixed number N of modes the numerical solution is accomplished within a 0.1% absolute error tolerance. The convergence is checked by increasing the number of modes until the spatial evolution at a fixed time does not significantly change.

5. Results and Discussion

5.1 Eigenvalue Spectrum

By using the Floquet-Bloch eigenfunctions above, our calculation finds features of the eigenvalue spectrum that are rather different from those of the straight tube. Figures 4 show typical eigenvalue (real part only) spectra for various wall wave numbers k. Here we only show the part of the eigenvalue spectrum in the upper half plane since the part in the lower half plane corresponds to negative growth and gives stable results. The solid curves represent the usual $\sigma = 0$ straight tube results and the primary branch (dots) only has a small $O(\sigma^2)$ correction to this result. Thus this branch begins at the origin, goes through the maximum and intersects the α-axis close to one. The $\alpha \to 1$ expansion above accounts for this shift from one. The eigenvalue spectra show that corrugations not only lead to a k-periodic structure in α-space, which is obvious from the k -periodicity of the coefficients in (4.7) or from (4.14), but also illustrate the $O(\sigma^2)$ deviation of the growth rate from that of σ=0. Depending on k, adjacent branches may overlap, particularly for $k \lesssim 2 = 2+O(\sigma^2)$, as shown in Figures 4(a) and (b). This leads to more than one positive eigenvalue for a given initial disturbance for some range of α. As a result, because the evolution contains all of its modes, modes with different growth rates can compete until the dominant mode wins and characterizes the instability for long times within the linear regime. We shall demonstrate this effect below in the context of the initial value approach.

5.2 Interfacial Evolution

We begin by solving the initial value problem, for the case of $We_0 = 1.0$, $k = 1.8$, $\sigma = 0.2$ corresponding to Figure 4(b), and impose an initial short wave disturbance with $\alpha = 1.2$. Recall that at $\alpha = 0$, such a disturbance yields non-growing, non-decaying temporal oscillations. Figures 5(a) and (b) show the growth rate and

oscillation frequency respectively of the interfacial evolution at a particular z position. To compare the initial value problem solution with the predictions from the eigenvalue spectrum, we first verify the temporal maximum of interface's amplitude to see if it follows the growth predicted by the eigenvalue spectrum. This amplitude history for long times matches the growth predicted by the real part of the eigenvalue spectrum very well, as shown in Figure 5(a). Here, we have used the (higher) value ω_r from the secondary branch. Notice that even though the calculated amplitude grows over several orders of magnitude, the calculation is only quantitatively relevant in the linear regime; otherwise the non-linear effects must be considered.

We would also like to compare the oscillation frequencies predicted by both approaches. Because the linear growth of the interface is exponential and thus covers many orders of magnitude, directly comparing the oscillation is inconvenient. Figure 5(b) factors out the growth rate that has been tested in Figure 5(a). The resulting scaled oscillation neither grow nor decay, even for long times. This indicates that the evolution follows the correct growth rate. Its regular oscillatory pattern agrees with the oscillation frequency predicted by the imaginary part of the Bloch eigenvalue very well.

With the growth rate and frequency already confirmed, Figures 6(a) and (b) show the corresponding evolutions in time of the entire interface. As shown in Figure 6(a), the initial short wave ($\alpha = 1.2$) interface perturbation grows slightly at earlier times t=2.65. Then the interaction with the wall's corrugation modifies the wave length. As a result, the t =5.61 curve has more than one wave length. Figure 6(b) shows the further development of the interface. Notice that by t=7.74, the dominant wave length is already evident and the interface grows dramatically for longer times. This dominant wavelength is about 10, which is significantly longer than the initial short wave disturbance. Its corresponding wave number, about 0.6, is just the wall's first unstable harmonic $|\alpha - k|$. The other first wall harmonic is $\alpha + k$=3.0, which is expected to have no growth from the primary and secondary branches, but growth at much longer times from the tertiary branch. Thus in

contrast to the $\sigma = 0$ case, whose short waves are standing and purely convective, corrugation can modulate a short wave initial disturbance and excite unstable long waves.

There is a transition between the dominance of the primary, originally stable and the secondary, unstable branches. One can express the response to an arbitrary disturbance in terms of the superposition of eigensolutions in the following form

$$\xi(z,t) = \sum_{\text{branch } j} a_j f_j(z) e^{\omega_{<j>} t}, \tag{5.1}$$

where $\omega_{<j>}$ and $f_j(z)$ are the j-th growth rates and the corresponding eigenfunctions, respectively, and a_j are coefficients determined by the initial condition. We only consider contributions from the primary (p) and the secondary (2) branches :

$$\xi(z,t) = a_p f_p(z) e^{\omega_p t} + a_2 f_2(z) e^{\omega_{<2>} t} + \ldots, \tag{5.2}$$

For the case in Figures 5 and 6, $\text{real}\left(\omega_p - \omega_{<2>}\right) = -\text{real}(\omega_{<2>}) < 0$. One can solve for the eigenvectors when the eigenvalue correction is $O(\sigma^2)$ with an initial condition along the $\sigma = 0$ primary eigenvector. From this, one can show that $a_p \sim O(1)$ and $a_2 \sim O(\sigma)$. Eqn. (5.2) then suggests that the oscillatory primary branch dominates for short times and the secondary unstable branch becomes important for long times. The transition between them implies there exists a critical time t^* at which the instability sets in, when, say, $a_2 e^{\omega_{<2>} t}$ is about 1-10 times $a_p e^{\omega_p t}$, i.e., $\sigma\left|e^{\omega_{<2>} t}\right| \sim \beta\left|e^{\omega_p t}\right|$ for $\beta \sim$ 1-10. One can estimate this critical time as

$$t^* \approx ln\left(\beta\sigma^{-1}\right)/\text{real}(\omega_{<2>} - \omega_p). \tag{5.3}$$

The parameters of Figure 4(b) give $t^* \approx 3.3 - 8.0$ for $\beta \sim$ 1-10, which predicts this moment very well in a comparison with Figure 5(b). We can now explain the evolution shown in Figures 6. The initial short wave disturbance (wave length ~5.3) oscillates but does not grow since the primary eigenvalue is imaginary. By the first non-zero time

shown, the secondary mode, whose wave length is about 10.5 (~ double the initial wave length) is smaller, but is no longer negligible compared with the initial disturbance. This results in every other minimum/maximum being enlarged preferentially. This latter wave length becomes further amplified with time – the two are comparable at around $t \lesssim 7.7$. By 11.20, the initial short wave disturbance is small relative to the growing mode.

As $\sigma \to 0$ (no corrugation), (5.3) leads to $t^* \to \infty$, which means that only the primary branch survives without any other branches contributing to the linear dynamics. Therefore, the smaller the corrugation, the later the transition from the primary to the secondary branch takes place. Thus, for the case of $\sigma = 0$ or $k = 1$, both the eigenvalue method's and initial value problem's solution results reduce to those of the straight with applying Fourier modes. A small deviation from $\sigma = 0$ or $k = 1$ will yield multiple branches as shown in Figures 4 that arise at long times.

In summary, the corrugated wall's wave number k plays a critical role, by coupling to the wave number of the initial disturbance, in determining the system's stability. In particular, even disturbances that would otherwise be stable, by virtue of this coupling, excite unstable harmonics. Thus the corrugated wall system is rarely stable for most disturbances α.

5.3 The Growth Rate Correction

As we have seen in Figures 4, in addition to the appearance of eigenvalue branches besides the primary branch as a result of wall corrugation, the corrugation also induces a growth rate deviation from the $\sigma = 0$ primary branch. This correction can involve a complicated interaction among the disturbed flow, inertia and capillarity, with wave numbers from different eigenvalue branches, e.g., the primary α with its first harmonics $\alpha \pm k$, contributing (see eqn. (4.27)). Figures 7 show this $\sigma \neq 0$ growth rate correction for the primary branch. These figures compare the analytical expression in

(4.28) from matrix perturbation theory with the numerical results, and the agreements are very good. A comparison below with the analytic limiting forms (4.29) and (4.30) confirms that the corrugation correction to the growth rate is generally $O(\sigma^2)$ except near $\alpha \sim 1.0$, where it is $O(\sigma)$. The correction displays local maxima and minima between two asymptotic regions of α=0 and α=1.0. These should involve stronger inertia-capillarity, or capillarity-capillarity interactions between the α and $\alpha \pm k$ waves, particularly capillarity-capillarity interactions. Because different waves lead to different maxima or minima for different capillary strengths, i.e., $We_0(\alpha \pm k)^2\left(1-(\alpha \pm k)^2\right)$, they interact in a manner deriving from $G^{\pm}$ and result in a more complicated maximum/minimum curve for the correction to the growth rate.

(i) *Long wave expansion*

In the long wave regime, the growth rate correction given by (4.29) is $O(\sigma^2\alpha)$. Whether this correction is stabilizing or destabilizing for long waves depends on the sign of $\left[3+(1-We_0)(1-k^2)\right]\left[1+We_0(1-k^2)\right]^{-1}$. For $k<1$, $1+We_0(1-k^2)>0$ and the base flow interface is in-phase with the wall. From (4.29), this correction is stable when

$$We_0 > (4-k^2)/(1-k^2). \tag{5.4}$$

In other words, interestingly, sufficiently *high* tension can contribute a stable correction at long waves.

For $1<k<k^*$, where k^* is the natural frequency of the base flow, the base flow configuration is still in-phase and (5.4) is the condition for the correction being unstable. The in-phase condition $k<k^*$ gives k <2. For $1<k<k^*$, if We_0>1, then k^*<2. Combining with k>1 leads this case to automatically satisfy (5.4) and results in an unstable correction for long waves. In other words, $1<k<k^*$ and We_0>1 can lead to an unstable correction for long waves.

When the base flow interface is out-of-phase with the wall ($1+We_0(1-k^2)<0$ or $k>k^*>1$), (5.4) is again the condition for a stable long wave correction. If $k<2$, the out-of-phase condition $k>k^*$ gives $k^*<2$ or $We_0>1$. Therefore, $2>k>k^*$ automatically satisfies (5.4) and results in a stable correction.

For the special case of $We_0=1$, $\left(3+(1-We_0)(1-k^2)\right)>0$ for all k in (4.29), all out-of-phase base flows ($1+We_0(1-k^2)<0$) contribute to stable corrections while all in-phase situations ($1+We_0(1-k^2)>0$) have unstable corrections for long waves. In Figures 7, both cases (a) k=1.8 and (b) k=2.3 are out-of-phase configurations and thus show negative corrections near α=0. These long wave expansions agree with both the analytic and the numerical corrections very well. They all show stable corrections for long waves. It is interesting to note that this slightly stabilizing long wave correction seems to persist for an even larger α range for k=2.3 than for k=1.8. This is because (4.29) is less sensitive to a small α at large k.

(ii) *The $\alpha=1$ Expansion*

Recall that for $\sigma=0, \alpha=1$ is the neutral state. Two eigenvalues $\omega_0^{\pm}=-i\alpha\pm\sqrt{We_0\left(1-\alpha^2\right)}$ merge at $\alpha=1$ and lead to a linear growth with time, i.e., $|\xi|\sim t\,e^{\omega t}$ at leading order in ε. The corrugation excites an $O(\sigma)$ unstable correction near $\alpha=1$ as shown in Figures 7. Due to the corrugation, $\alpha=1$ is no longer a double root for $\sigma\neq 0$, but it may lead to an $O(\sigma)$ growth at $\alpha=1$. As also shown in Figures 7, the numerical curves around $\alpha\lesssim 1$ show much less unstable corrections than that at $\alpha=1$, and agree well with the asymptotes given by (4.30). This suggests that this effect is due to $-\sqrt{We_0(1-\alpha^2)}\sim-\sqrt{2We_0\alpha'}$ for $\alpha'=1-\alpha<<1$, which arises from a slight imbalance between the circumferential and longitudinal curvatures of the capillarity.

Inspecting (4.30) for $\alpha = 1$, we find that $C_+ < 0$ for all $k > 0$, and $(We_0 C_+ + k^2) < 0$ for $We_0 \geq 1/5$ and all $k > 0$. When $0 < k < 2$, $C_- > 0$, and thus gives $(We_0 C_- + k^2) > 0$ for all We_0. Using (4.30) with the above conditions, we find that $We_0 \geq 1/5$ and $0 < k < 2$ are sufficient conditions for $\delta\omega_r(\alpha = 1) > 0$, i.e., for exciting an unstable $O(\sigma)$ correction. This is also a sufficient condition to shift the neutral state to the right, which we now discuss.

At $\sigma = 0$, the neutral state occurs at $\alpha = 1$. As noted earlier, corrugation can shift the neutral state slightly from its value $\alpha = 1$ at $\sigma = 0$. Eqn. (4.31) suggests that this shift in the neutral state is $O(\sigma^2)$. Figure 8 shows the plot of the neutral state shift vs. k for different We_0. $\delta\alpha^* > 0 (< 0)$ corresponds to a positive (negative) shift from $\alpha = 1$, that is, to a shorter (longer) critical wave length than the mean circumference. Since each We_0 determines a corresponding k^* (the natural frequency of the base flow), each curve separates into two branches near the singular point $k = k^*$. As with the amplitude ratio of the base flow's interface to the wall's in Figure 2, the left and right branch curves correspond to the in-phase and out-of-phase interface-wall configurations of the base flow. Because $k^* = \sqrt{1 + 1/We_0}$, the curves shift to smaller k (>1) as We_0 increases. All left-branch curves again cross at $k = 1$ ($\eta = \phi$) and thus give no corrections to the neutral state. For $0 < k < 1$, the shift is small and positive, and it decreases slightly with k. For $1 < k < k^*$ (in-phase base flow), the shift is positive and increases with k; it also increases with We_0 for a fixed k. On the other hand, for $k > k^*$ (out-of-phase base flow), the shift decreases steeply and monotonoically with k, and appears to be negative for larger k. This case also shows a decreasing shift as We_0 increases for a fixed k. As a result, the smaller We_0, the larger the k needed for a given negative shift. Note that, because of (4.30) and (4.31), an $O(\sigma)$ growth ($\delta\omega_r > 0$) at $\alpha = 1$ also implies a positive shift of the neutral state, or vice versa. The sufficient condition $We_0 \geq 1/5$ and $0 < k < 2$ for exciting an $O(\sigma)$ instability at

$\alpha = 1$ also results in a positive shift of the neutral state. As shown in Figure 8, curves satisfying this sufficient condition contribute to positive shifts in their neutral states.

5.4 The Intersection Points of Different Eigenvalue Branches

As noted in the last section, a double $O(\sigma^0)$ eigenvalue can excite an $O(\sigma)$ stability correction. At $\sigma = 0$, a double root occurs at α=1.0 between the primary branch and its mirror image about the α axis ($\omega = -i\alpha \pm \alpha\sqrt{We_0(1-\alpha^2)}$). However, under certain circumstance, similar $O(\sigma)$ corrections can arise when different eigenvalue branches cross for $\sigma \to 0$. For instance, such a situation can occur between the upper primary and the lower secondary sub-branches. At $O(\sigma^0)$, the eigenvalue of the primary branch is $\omega_p^{\pm} = -i\alpha \pm \alpha\sqrt{We_0(1-\alpha^2)}$, and that of the secondary branch is $\omega_{<2>}^{\pm} = -i(\alpha - k) \pm |\alpha - k|\sqrt{We_0(1-(\alpha-k)^2)}$, where the superscript "+" and " - " denote the upper and the lower sub-branches, respectively. At $\alpha = 1$, the primary branch has $\omega_p^{\pm} = -i$. Similarly, at $\alpha = k-1$, the secondary $\omega_{<2>}^{\pm} = i$. However, when $\alpha = k/2$ $= k^* \equiv \sqrt{1 + 1/We_0}$, a particular relationship between We_0 and k, $\omega_p^+ = \omega_{<2>}^- = 0$, i.e., the upper primary and the lower secondary sub-branches form a double zero eigenvalue at this α. This occurrence at $\alpha = k/2$ produces a resonance condition very similar to those studied by Rines (1970) and Mitra & Greenberg (1984). Here, however, this condition also requires that α be equal to the natural frequency k^* of the base flow. We use (4.14) to directly calculate the maximum growth rate for $We_0 = 1, k$=$2k^*$=$2\sqrt{2}$ and $\sigma = 0.2$ to demonstrate this resonance. Figure 9 shows a plot of the maximum growth rate vs. the wave number α of an initial disturbance. A large jump appears from $1 \le \alpha \le k-1 \approx 1.8$ and seems to form a bridge between the primary and secondary branches. The growth rate for this short wave range is just the correction to that ($\omega_{0_r} = 0$) of $\sigma = 0$ – it has about the

same magnitude as σ, as shown in Figure 9. This effect clearly becomes more pronounced as σ increases. As we shall see below, this should be due to three $O(\sigma)$ instabilities excited at $\alpha \approx 1$ (from both primary sub-branches), $k/2$ (from one primary and one secondary sub-branches), and $k-1$ (from both secondary sub-branches). We analyze the mechanism for these interactions below.

Figure 9 contains three multiple roots at $O(\sigma^0)$ for $\alpha \le k-1$: (i) at $\alpha = 1$, between both the upper and the lower primary sub-branches; (ii) at $\alpha = k/2$, between the upper primary and the lower secondary sub-branches, and (iii) at $\alpha = k-1$, between both the upper and the lower secondary sub-branches. As a result, for $1 \le \alpha \le k-1$, both primary sub-branches interact with each other at $\alpha = 1$, and one of them interacts with the other secondary sub-branch at $\alpha = k/2$. The two secondary sub-branches interact with each other at $\alpha = k-1$. We shall again employ an iteration scheme as we did earlier to solve for ω for different ranges of α.

For $0 \le \alpha \le k/2$ (or close to $k-1$), the interaction branches include both the primary sub-branches and the secondary lower sub-branch. In our analysis of Δ_0 (4.24a), we isolate the part of $S(0)$ that contains the $O(\sigma^0)$ dispersion relation $d(0)=(\omega+i\alpha)^2 - We_0\alpha^2\left(1-\alpha^2\right)$ which determines $\omega_p^{\pm}$ in the first bracket of (4.25). In a similar manner, we isolate $S(-1)$, which includes the $O(\sigma^0)$ dispersion relation $d^-(-1)=\omega+i(\alpha-k)+|\alpha-k|\sqrt{We_0\left(1-(\alpha-k)^2\right)}$ that determines $\omega_{<2>}^-$, as well. We can thus rewrite $\Delta_0 = d(0)d^-(-1)\left[\left(\prod_{j\neq 0} S(j)\right)S(0)\Big/ d(0)d^-(-1)\right]$, and (4.23), by dividing by $\left[\left(\prod_{j\neq 0} S(j)\right)S(0)/d(0)d^-(-1)\right]$, becomes

$$\left[(\omega+i\alpha)^2 - We_0\alpha^2\left(1-\alpha^2\right)\right]\left[\omega+i(\alpha-k)+|\alpha-k|\sqrt{We_0\left(1-(\alpha-k)^2\right)}\right]$$

$$=\sigma^2\frac{-\Delta_2}{\prod_{j\neq 0}S(j)}d^-(-1)(\omega+2P(0))\Big|_{\omega_{p0}} . \qquad (5.5)$$

The $O(\sigma^0)$ part of (5.5), which is the product of the $O(\sigma^0)$ dispersion equations, contains the primary (the first bracket) and the lower secondary sub-branches (the second bracket). To solve for ω by iteration, we begin by evaluating the right hand side at $\omega_{p0}=-i\alpha+|\alpha|\sqrt{We_0(1-\alpha^2)}$ from the upper primary sub-branch and solve for the 1st iterated $\omega_p^{(1)}$ from the left hand side. We then iterate.

At the initial round of the iteration $\omega_p^{(1)}=\omega_{p0}$, and the right hand side of (5.5) reduces to,

$$-\sigma^2\left\{F(0)d^+(-1)-\left[\frac{\tilde{Q}_1^-(0)\tilde{Q}_1^+(-1)}{d^+(-1)}(\omega+2P(-1))+\frac{\tilde{Q}_1^-(1)\tilde{Q}_1^+(0)}{S(1)}d^-(-1)\right]\right\}(\omega+2P(0)),$$

where $d^+(-1)=\omega+i(\alpha-k)-|\alpha-k|\sqrt{We_0\left(1-(\alpha-k)^2\right)}$ is the $O(\sigma^0)$ dispersion relation for determining the upper secondary branch $\omega_{<2>0}^+$. Eqn. (5.5) only involves interactions between α and $\alpha\pm k$ waves. The subsequent iterations contain the non-nearest neighbor interactions (as in Σ of (4.25)) which vanish at ω_{p0}. Also note that when $\alpha=k-1$, the right hand side of (5.5) diverges because of $d^+(-1)=0$ for $\omega=i$. For $\alpha=1$, (5.5) becomes

$$(\omega+i)^2\left[\omega+i(1-k)+|1-k|\sqrt{We_0\left(2k-k^2\right)}\right]=\sigma^2H(\omega_{p0},\ \alpha=1) \text{ with } \omega_{p0}=-i\ ,$$

where H is the coefficient of the $O(\sigma^2)$ part of (5.5). A simple perturbation *Ansatz* of $\omega=\omega_{p0}+\delta\omega$ shows that the correction to $\omega_{p0}=-i$ is again $O(\sigma)$.

For $\alpha=k/2=k^*$, $\left(\omega+2ik^*\right)\omega^2=\sigma^2H(\omega_{p0},\ \alpha=k/2)$ with $\omega_{p0}=0$, and the correction to $\omega_{p0}=0$ is also $O(\sigma)$. Similarly, for $k-1\le\alpha\le k$ (it may also be the case that α somewhat smaller than $k-1$ also leads to a large eigenvalue because of the above

resonances), the interaction branches are both secondary sub-branches, and we have, in analogy with (4.25),

$$\left[(\omega+i(\alpha-k))^2-We_0(\alpha-k)^2\left(1-(\alpha-k)^2\right)\right]=\sigma^2\frac{-\Delta_2}{\prod_{j\neq-1}S(j)}(\omega+2P(-1))\Bigg|_{\omega^+_{<2>0}}. \qquad (5.6)$$

The left hand side of (5.6) has the secondary branches. The iteration for solving ω is done similarly by evaluating the right hand side at $\omega^+_{<2>0}=-i(\alpha-k)+|\alpha-k|\sqrt{We_0(1-(\alpha-k)^2)}$ from the upper secondary sub-branch. Similarly, the right hand side of (5.6) at the 1st iterated $\omega=\omega^+_{<2>0}$ becomes

$$-\sigma^2\left\{F(-1)-\left[\frac{\tilde{Q}_1^-(-1)\tilde{Q}_1^+(-2)}{S(-2)}+\frac{\tilde{Q}_1^-(0)\tilde{Q}_1^+(-1)}{S(0)}\right]\right\}(\omega+2P(-1)),$$

which involves interactions between the α, $\alpha-k$, and $\alpha-2k$ waves. For $\alpha=k-1$, (5.6) gives an $O(\sigma)$ correction to $\omega_{<2>0}=i$ due to the merging of two secondary sub-branches.

For $k=2\sqrt{2}$, $\sigma=0.2$ and We_0=1.0, and $0\le\alpha\le k\approx 2.83$, we use (5.5) and (5.6) to calculate the growth rate for k =[0,1.9] and k =[1.2,3.0], respectively. The reason we choose a wider range of k for each calculation is to see how far each interaction goes. Each calculation is first done with one iteration. The result is shown in Figure 10. We also compare them with those found by directly solving (4.14) numerically. The agreement is very good for most α from 0 to 3.0, except for α near 1.0 and 2.8. For $0\le\alpha\le 1$, the equation (5.5) curve shows a typical capillary growth rate curve. It should follow the upper primary branch suggested from the $O(\sigma^0)$ part of (5.5). At $\alpha=1$, it has a positive growth rate (0.2288). This is due to an $O(\sigma)$ correction from the interaction between both primary sub-branches. Upon increasing α to a value slightly greater than one, as we check, the eqn. (5.5) curve does not go to zero. Instead, it has a small, sharp rise with respect to the

growth at $\alpha = 1$ and seems to deviate from (4.14). However, when we iterate twice for ω from (5.5) for the same range of α, the results (including those near $\alpha = 1$) agree very well with the numerical solutions to (4.14). Since (5.5) includes two primary and one secondary sub-branches, the result suggests that even though near $\alpha = 1$ a major interaction comes from both primary sub-branches, the coupling of the (lower) secondary branch to the primary branch probably dominates. This $O(\sigma)$ instability at $\alpha = 1$ seems strong enough to persist for even larger α as Figure 10 suggests. It then meets another $O(\sigma)$ growth excited near $\alpha = k/2 \approx 1.4$, where there is a strong interaction between the upper primary and the lower secondary sub-branches as well. Thus, the growth rate remains about the same magnitude between $\alpha = 1$ and $\alpha = k/2$. This strong interaction near $\alpha = k/2$ continues further for $k/2 < \alpha < k-1$. In this regime, the secondary branch's influence appears to become more important since it dominates at $\alpha \approx k-1$=1.8. When near $\alpha \approx 1.8$, the (5.5) curve appears to become singular. Because the left hand side of (5.5) contains the upper secondary sub-branch's contribution $d^{+}(-1)$ in the denominator, the resulting growth rate behaves more singularly near $\alpha = k-1$. But the tendency of the (5.4) growth rate seems to match that of (5.6). This is because (5.4) includes the lower secondary branch; (5.6) contains both secondary sub-branches at $O(\sigma^0)$ and the secondary branch should contribute most strongly to the growth rate near $\alpha = k-1 \approx 1.8$. The growth rate of (5.6) decays to zero for α far smaller than $k-1$. This is because the upper secondary sub-branch does not interact them with the primary branch at $O(\sigma^0)$ in (5.6).

We have thus explained the interaction between the different eigenvalue branches. For $k = 2k^{*}$, the primary branch interacts with the secondary branch near $\alpha = k/2$. Due to the periodicity of the eigenvalue spectrum, we expect that this particular interaction should also occur at $\alpha = nk/2$ (n = 1, 3, ...), as found by Rhines (1970) and Mitra & Greenberg (1984) in the wavy river bed problem.

The interesting bridge between the branches in Figure 10 begs the question of what the dynamic response of the interface would be for an initial disturbance in this bridge regime. We now perform an initial value simulation to examine the interfacial dynamics of this interaction for $1 \le \alpha \le k-1$ in Figure 10. We choose $\xi(z, t=0) = cos(\alpha z)$ and $w(z, t=0) = 0$ as initial conditions. In order to more conveniently display and discuss the results, we let $a_0(t)$ and $a_{-1}(t)$ represent the temporal amplitudes of the primary mode $cos(\alpha z)$ and its first harmonics $cos((\alpha - k)z)$ for $\xi(z, t)$ in (4.32).

We begin at the center of the bridge where $\alpha = k/2 = \sqrt{2}$, corresponding to the merging of the upper primary and lower secondary sub-branches at $O(\sigma^0)$. Figure 11 shows the temporal evolutions for the interface in terms of $a_0(t)$, and $a_{-1}(t)$ at a particular position. For short times, the interface oscillates and slowly grows. This is because the initial disturbance is short wave $\alpha = \sqrt{2}$ (>1) and early times are dominated by the primary oscillatory branch. This oscillation gradually diminishes and the interface then shows purely exponential growth for longer times. We again compare this growth with that from the Bloch eigenvalue (the real part) spectrum and they also agree very well. The disappearance of the oscillation for long times and the later purely exponential growth suggest that the dominant eigenvalue(s) is (are) real.

Since by choice of parameters, $a_0(t)$ and $a_{-1}(t)$ correspond to the same wave number, both have almost identical oscillating-growing patterns, except that they are out-of-phase for the earliest times. However, $a_0(t)$ seems to dominate and remains about a factor of 20 times $a_{-1}(t)$. It is interesting to note that the interfacial evolution (Figure 12) $a_0(t)$ and its primary (short) wave $\alpha = \sqrt{2}$ dominate throughout the evolution that we have followed, since, by choice of parameters, the higher harmonics will not lead to any longer waves. Therefore, as shown in Figure 12, the spatial evolution shows that the interface monotonoically grows with time with the single wave number $\sqrt{2}$ with the shape of the

initial disturbance. The figure displays neither oscillation nor traveling because the eigenvalue (suggested by Figure 11) has zero imaginary part.

Figures 13 show the temporal histories of $|a_j(t)|$ $(j = 0, -1)$ for different choices of α, slightly away from the above special point $\alpha = \sqrt{2}$, in the bridge region. At first glance, the resulting behaviors seem rather different from Figure 11. They show that $a_0(t)$ and $a_{-1}(t)$ alternatively dominate after the initial transient. The periodic rise and fall of $a_0(t)$ and $a_{-1}(t)$ seems to indicate non-zero imaginary parts of eigenvalues. The further away α is from $\sqrt{2}$, the faster this oscillation, i.e., the larger the imaginary part of the eigenvalue. Note that $a_{-1}(t)$ is comparable in magnitude to $a_0(t)$ for long times. They oscillate out-of-phase and this suggests that they compete with each other even during the long-term evolution that is in the linear regime. One should thus expect that there may not be one dominant wave for such long times because neither α nor $(\alpha - k)$ can dominate.

Figure 13(c) examines the details of the interfacial growth for α=1.20. For short times ($t \lesssim 10$), $a_0(t)$ is non-growing and irregularly oscillating because of a strong interaction between the primary α and the first harmonic $(\alpha - k)$ waves. Soon, $a_{-1}(t)$ starts to develop and has a magnitude similar to $a_0(t)$. For long times ($t \gtrsim 10$), both amplitudes grow exponentially and show a constant oscillatory period. This again implies that there is a dominant eigenvalue controlling the dynamics for long times. Both amplitude curves (i.e., their maxima) agree very well for long times with the growth from the real part of the Bloch eigenvalue. One half of the period of oscillation is 7.31 (t=10~60), corresponding to the width of one hump in Figure 13(c), since we plot $|a_j(t)|$. It also agrees very well with the value (7.322) deduced from the imaginary part of the Bloch eigenvalue. Note that for long times, both waves not only grow, but they also have similar magnitudes so as to compete with each other as they oscillate out-of-phase. This is different from the usual cases in which, as previously shown in Figure 6(b), only one (the first harmonic) wave

dominates for long times. As we shall see below, the corresponding spatial evolutions also differ from those of the earlier normal cases, particularly for long (linear) times.

Figures 14(a) and (b) show the corresponding spatial evolutions for α=1.2 for short and long times, respectively. As shown in Figure 14(a), for short times ($t \lesssim 5.0$), the interface slightly modulates and amplifies due to an interaction with the wall's first harmonics. When $t = 10.0$, the interfacial growth is evident, but the interface grows non-uniformly in space. For even longer times as in Figure 14(b), the interface further amplifies. The non-uniform growth in space still continues, and no clear dominant wave length appears. This implies that a competition between the primary (with wave number 1.2) and the first harmonic (with wave number ~1.62) waves is so strong that neither dominates for the long times. They simply jockey for dominance. This competition is indeed suggested by Figure 13(c) and the resulting evolution pattern can be seen by the following observation. We observe that the interface at $t = 5.0$ and that at $t = 20.0$ show fairly similarly shaped wave patterns (of different amplitudes), and so do those at $t = 10.0$ and $t = 25.0$. In addition, the interfaces at $t = 5.0$ and $t = 10.0$ are roughly out of phase, and so are those at $t = 20.0$ and $t = 25.0$. Recall that, the oscillation period is about 14.6, as suggested by Figure 13(c). These thus demonstrates oscillatory growing patterns resulting from a strong competition between the primary and its first harmonic waves in the bridge region.

6. Summary and Conclusion

We have examined the base flows and the corresponding linear stability of the core-annular flow of two inviscid fluids in a slightly corrugated tube in the asymptotic limits of a thin annular thickness ε and a small corrugation amplitude σ. For sufficiently strong capillarity relative to inertia ($We \sim 1/\varepsilon$), both the leading order base state and its corresponding linear stability are determined completely by the film's flow. The core's dynamics slave those of the film. When the wave number of the wall k is equal to the natural frequency k^* of the base flow, the base flow's interface grows in the z-direction because of resonance. If the linear theory remains valid for large deviations as well, this suggests that the base flow solution may break up downstream. The base flow's interface can have a phase shift relative to the wall. This phase shift depends on the difference between k^2 and k^{*2}. Unlike the viscous system whose the interface-wall phase shift is a continuous function of the surface tension and k, the interface-wall phase shift in the inviscid case is either 0^0 (in-phase) for $k<k^*$, or 180^0(out-of-phase) for $k>k^*$. For the special case of $k=1$, where the wall's wave length matches the undisturbed interfacial circumference, the capillary effect vanishes to the leading order. The base flow's interface follows the shape of the wall exactly and the resulting flow field is locally parallel to leading order in σ. For this special case, the corresponding linear stability reduces to the straight-tube result to leading order in ε. The effect of corrugation first enters at the next order in σ.

This theory can be extended to an even stronger capillarity $We >> 1/\varepsilon$ and to a less strong capillarity $1 << We << 1/\varepsilon$ without a change of formulation. For $We >> 1/\varepsilon$, capillarity dominates inertia. The base flow's interface becomes less deformable and thus remains cylindrical to leading order. For $1 << We << 1/\varepsilon$, inertia is dominant. As in the $k=1$ case, this leads to a locally parallel base flow and to the linear stability of the straight pore to the leading order.

With the leading order base flow for asymptotically small corrugations, we asymptotically derive two coupled evolution equations that govern the linear stability of the base flow to this order. We apply Floquet-Bloch theory to derive the eigenvalue spectra and, in parallel, perform numerical simulations for the initial value problem defined by the coupled amplitude equations for various initial conditions. From the eigenvalue spectra, we find that the growth rate of the inviscid system is $O(1)$ for t non-dimensionalized by R_0/W_0. Not surprisingly, this growth is faster than that of the viscous system whose growth rate is $O(\varepsilon)$, as determined in our earlier work (Wei & Rumschitzki, 2000-Chapter II). This is because in the inviscid system the inertia responds immediately to the capillary pressure to accelerate or decelerate the flow. In contrast, in the viscous system, the viscosity balances the capillary pressure and retards the response. As in the viscous system, the corrugation leads to periodic eigenvalue spectra because of the periodic coefficients in the evolution equations. The eigenvalue spectra exhibit more than one growth rate for some ranges of monochromatic initial disturbance wave lengths. Depending on the wave number of the wall k, adjacent eigenvalue branches may or may not overlap. If they do, then there is no stable disturbance regime for α. But, for $k>2$, the eigenvalue spectrum generally has a gap of stable disturbance between adjacent eigenvalue branches in the short wave regime. The eigenvalue branches' overlapping also leads to a competition between the primary and other branches at different time scales. For an initial monochromatic disturbance, the dynamics follows the primary branch for short times. Depending on the wave number α of the initial disturbance, the maximum growth rate may belong to the secondary branch. In such cases the secondary branch can dominate at longer times of $O(ln(\sigma^{-1}))$. In contrast to the straight tube case, where a disturbance with wave length ($\alpha>1$) shorter than the undisturbed circumference only leads to steady convective waves, the wall's corrugation couples short wave disturbances to the wall's harmonics

which can include unstable longer waves. These excited long waves (due to the secondary branch) can dominate for long times.

We have also developed a matrix perturbation theory to analytically calculate the corrugation's correction to the eigenvalue spectrum. Also similar to viscous results, the corrections are normally $O(\sigma^2)$. The difference is that $O(\sigma)$ corrections can also occur for the inviscid system. This $O(\sigma)$ correction is the result of the merging of different eigenvalue branches at $O(\sigma^0)$ and it can excite an instability for some ranges of parameters. Such a merging generally occurs at $\alpha \approx 1.0$ for the primary branch whose upper and lower eigenvalue sub-branches at $O(\sigma^0)$ merge at $\alpha = 1$. However, another type of the $O(\sigma)$ instability can arise from the merging between the (upper) primary and (lower) secondary branches for the $O(\sigma^0)$ eigenvalues. Such a merger is possible for short waves $\alpha > 1$ and $k > 2$, particularly in the singular case when $\alpha = k/2 = k^*$, the natural frequency of the base flow. The resulting eigenvalue spectrum is rather different from the usual one. This $O(\sigma)$ type of instability couples with the normal type around $\alpha = 1.0$ (from the primary branch alone) and $k - 1$ (from the secondary branch alone), and seems to form a bridge connecting the primary and secondary branches. As a result, a generally stable regime in short waves for $k > 2$ no longer exists in this case. Due to the periodicity of the eigenvalue spectra, this instability also occurs at $\alpha = nk/2$ ($n = 1,3, \ldots$), a situation similar to one found by Rhines (1970) and Mitra and Greenberg (1984) for the case of a river flowing over a corrugated bed. In comparison with our earlier work for the viscous system, $k > 2$ always leads the viscous system's eigenvalue spectra to have a stable gap between the primary and the secondary branches for short waves $\alpha \geq 1$. For similar ranges of k and α, the inviscid system's eigenvalue spectra normally also have such gaps of stability. But, for the singular case of $k = 2k^*$, i.e., for a particular combination of

parameters, such a stable region for short waves may no longer exist. Instead, it may induce an $O(\sigma)$ instability that becomes dominant for time scales of $O(\sigma^{-1})$.

Our viscous study was motivated by applications such as secondary oil recovery. Even though in most applications viscosity plays an important role, when the inertia is not negligible or when one is interested in short-time dynamics, we hope that the viscous and inviscid theories can bracket the expected stability features (e.g., the growth rate). For a typical example, consider a liquid-liquid displacement. Consider an oil film (10 cp viscosity) surrounding a water slug (1 cp viscosity) with an interfacial tension of 10 dyne/cm in a 200 μm-diameter pore. For a film thickness of $10\,\mu m$, $\varepsilon \sim 0.1$. If the velocity of slug is about 10 cm/s for an initial stage of the displacement, the resulting Reynolds number based on core quantities is about 10. The Weber number is about 100. With these parameters, the inviscid straight pore theory gives a maximum linear growth rate about 1.58 s^{-1}, i.e., about a 0.4 s doubling time. In contrast, the viscous straight pore theory gives a corresponding maximum growth rate of about 0.5 min^{-1}, i.e., a doubling times of about 80 s. The inviscid theory predicts a growth about 200 times faster than the viscous one. Let us consider, for a moment, how pore corrugation can affect the inviscid system's stability. Consider a monochromatic, sinusoidal corrugation of small amplitude, say 1.0 μm (still detectable), giving $\sigma = 0.1$ and a wall wave length of $350\,\mu m$ ($k = 1.8$), shorter than the mean pore circumference of $628\,\mu m$. Imposition of a short wave disturbance of $500\,\mu m$ or $\alpha = 1.26 > 1$ would not lead to growth in a straight tube. However, with the given corrugation, this perturbation excites an unstable wave of $\alpha' = |1.26 - 1.8| = 0.54$ or $L = 1164\,\mu m$ with the growth rate 1.43 s^{-1} after a time of order $ln(1/\sigma)$ 16 s. This is the major effect of corrugation.

The linear theory for which we have presented calculated figures is based on a wall whose corrugation is of a single wave length. Real geometries may contain more than one wave length. By decomposing them into a Fourier series, the present theory can deal with a

wall whose corrugation has multiple wave lengths. We can employ similar techniques to solve for the corresponding leading order base flow and the linear stability due to the periodicity of the eigenvalue spectra. In fact, equation (3.9) is still valid for an arbitrary order one wall shape function and, likewise, (4.7) gives its linear stability. A more complicated wall shape will however, yield a matrix (4.14) which is no longer sparse. In such a case, the wall's multiple wave lengths may lead to a serious overlapping between different eigenvalue branches. The upshot is that a corrugated wall rarely yields a stable inviscid system. This agrees with our earlier work for a viscous core-annular flow with a two-wavelength wall.

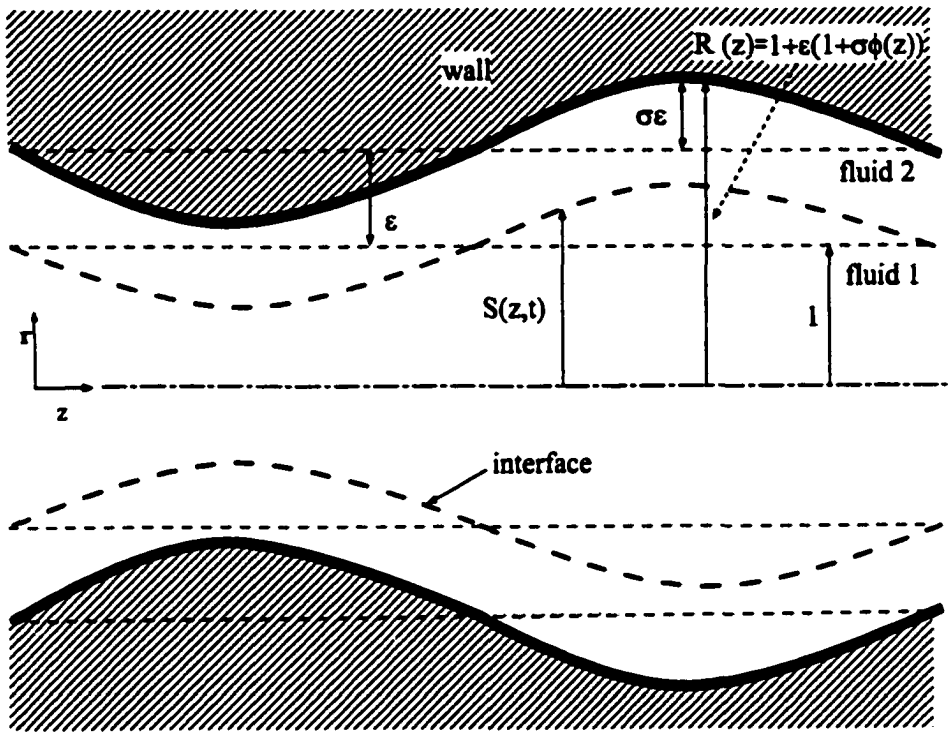

Figure 1

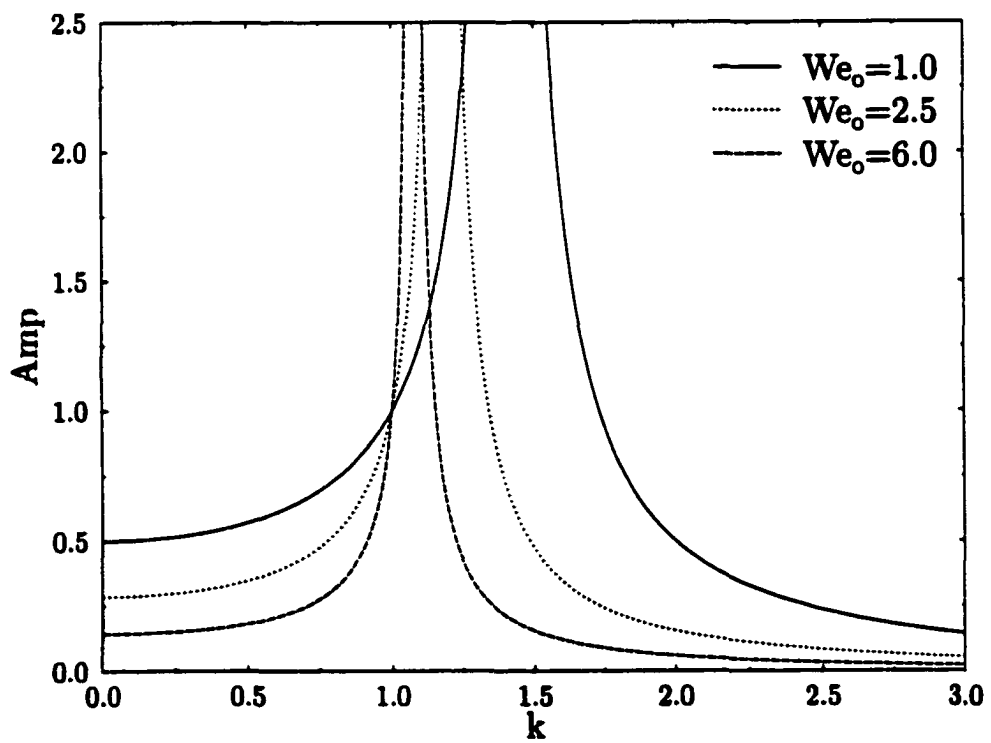

Figure 2

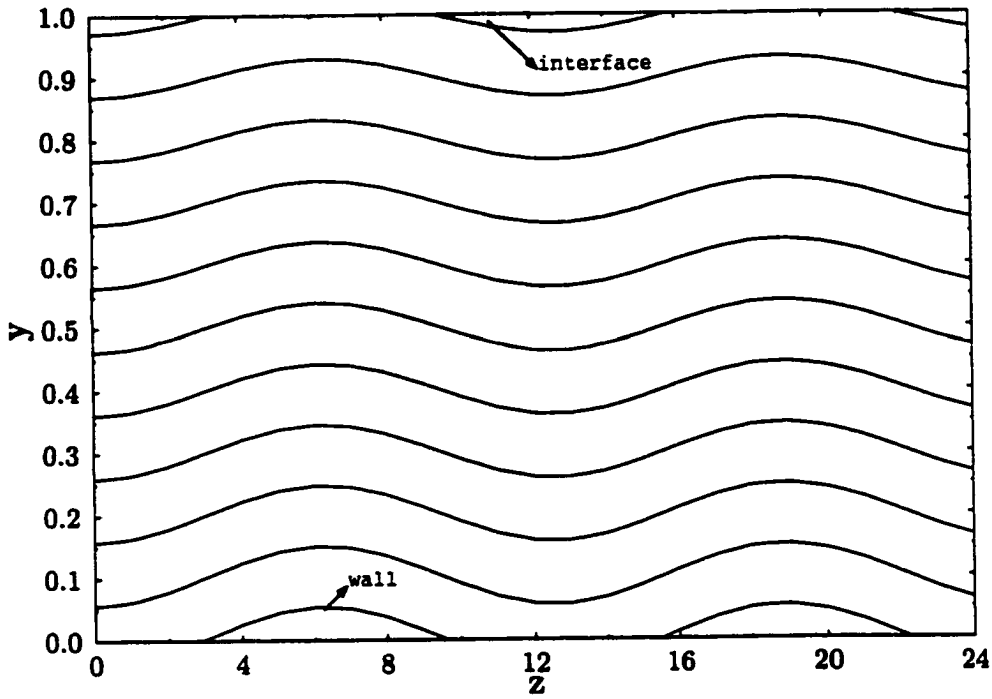

We_0=1.0, k=0.5, σ=0.05

Figure 3 (a) (The flow is from the left to the right)

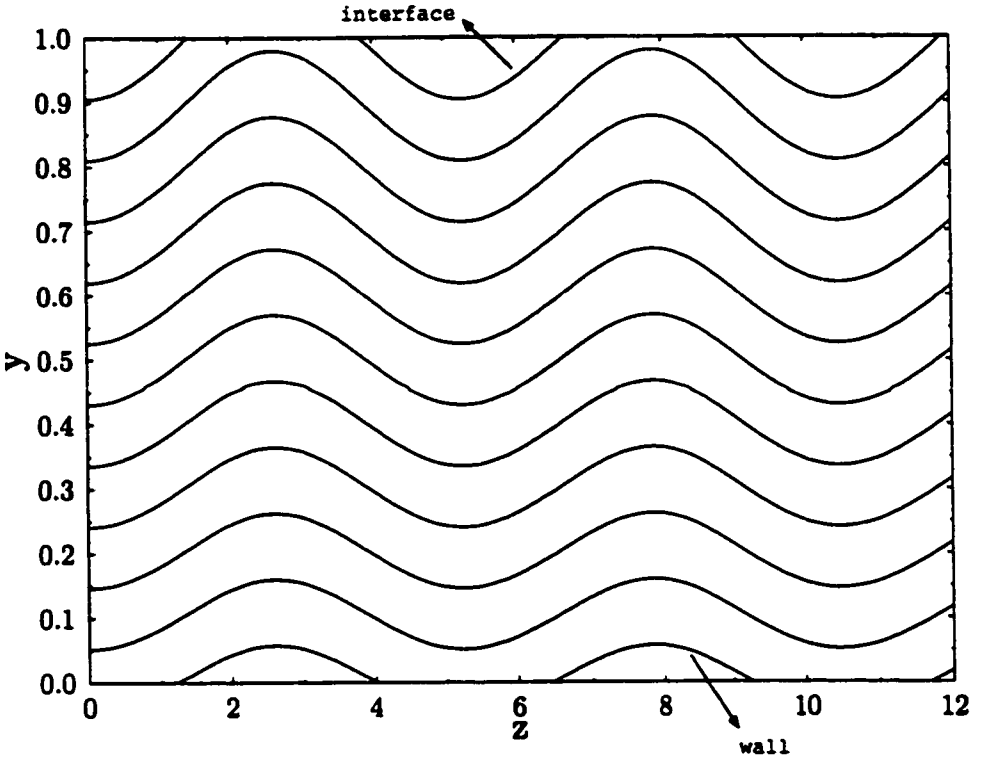

Figure 3 (b)

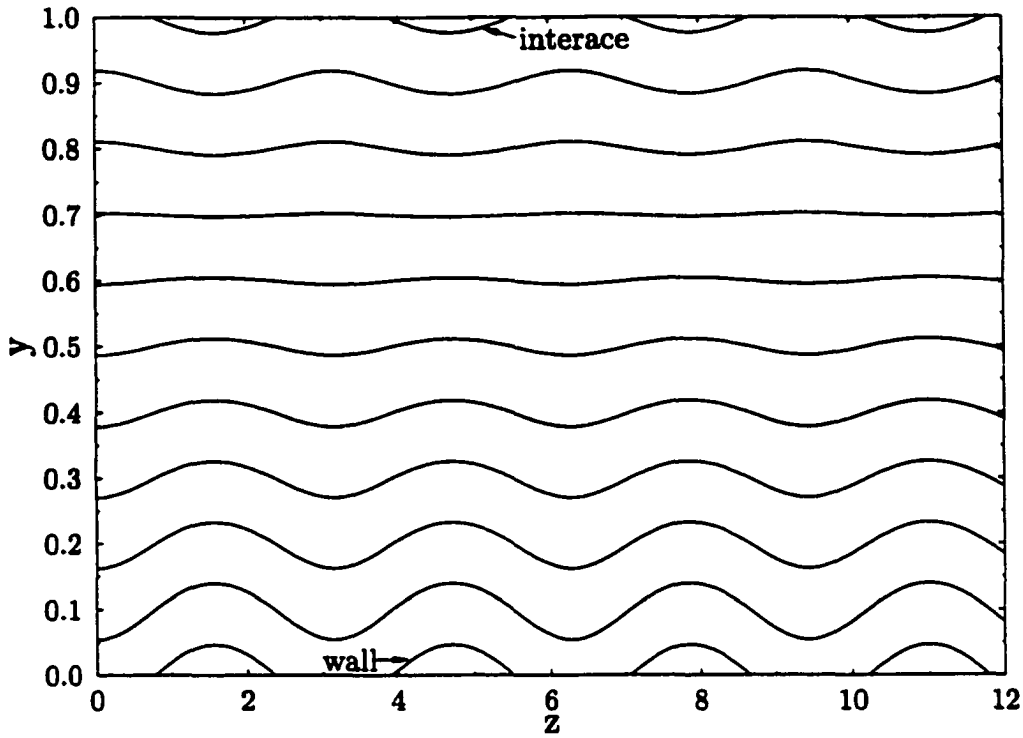

We_o=1.0, k=2.0, σ=0.05

Figure 3(c)

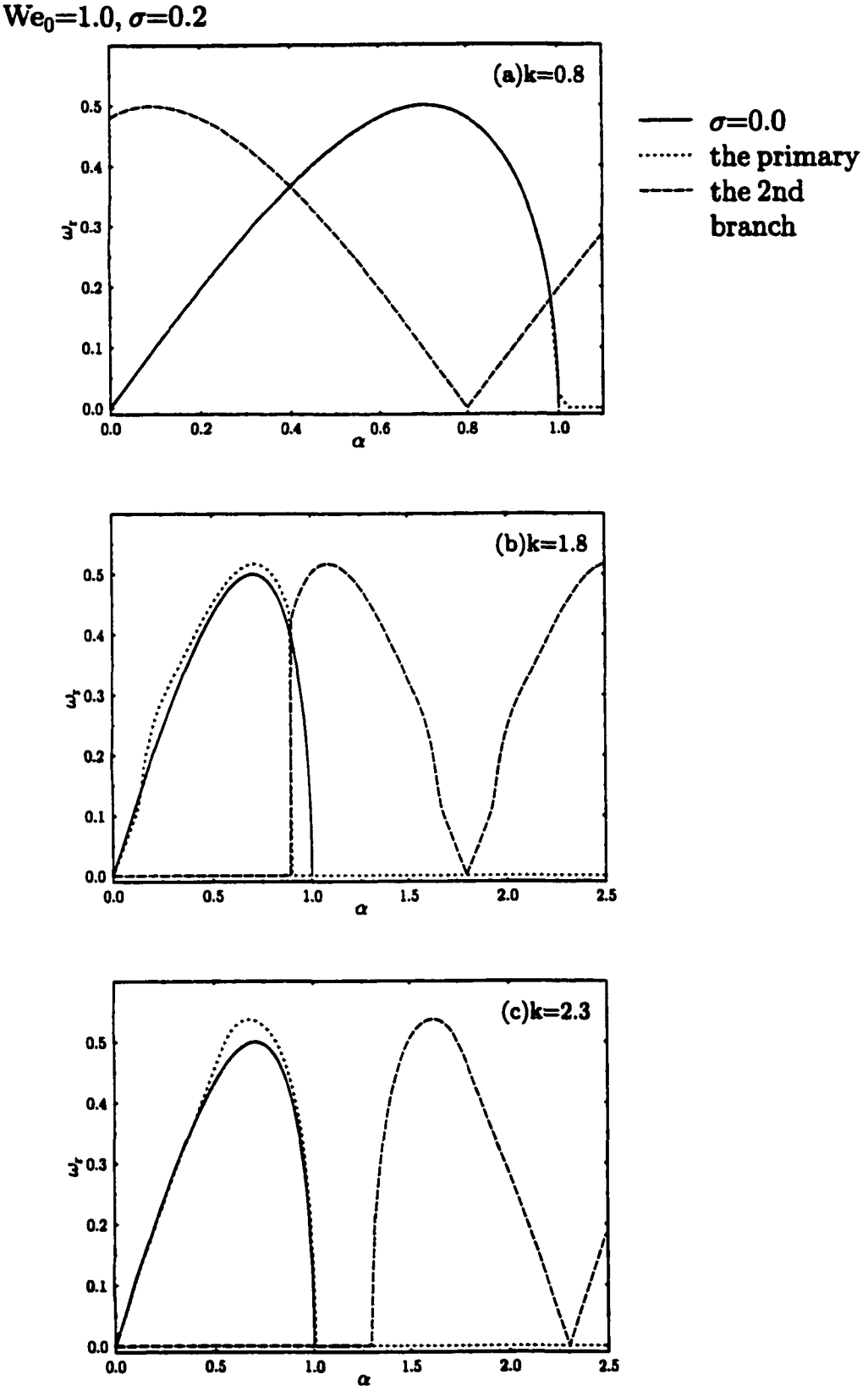

Figure 4

α=1.2,k=1.8,σ=0.2

$\xi(z,t=0) = \cos(\alpha z)$, $w(z,t=0) = -\sin(\alpha z)$

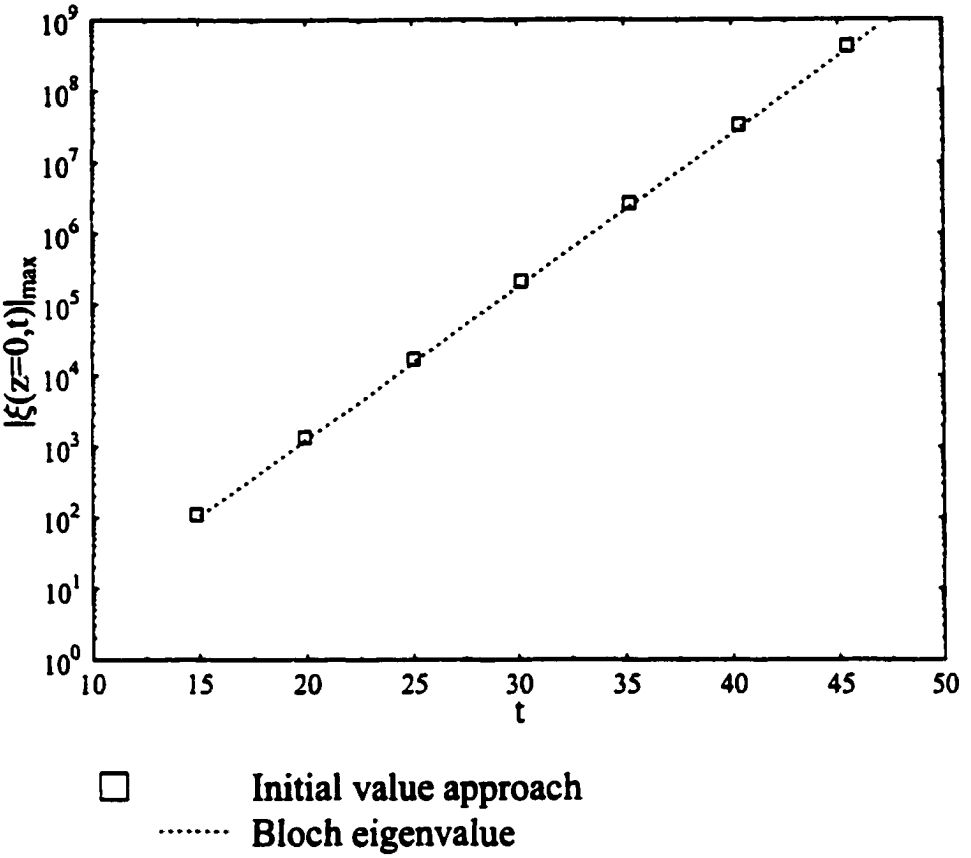

Figure 5(a)

α=1.2,k=1.8,σ=0.2

$\xi(z,t=0)=\cos(\alpha z)$, $w(z,t=0)=-\sin(\alpha z)$

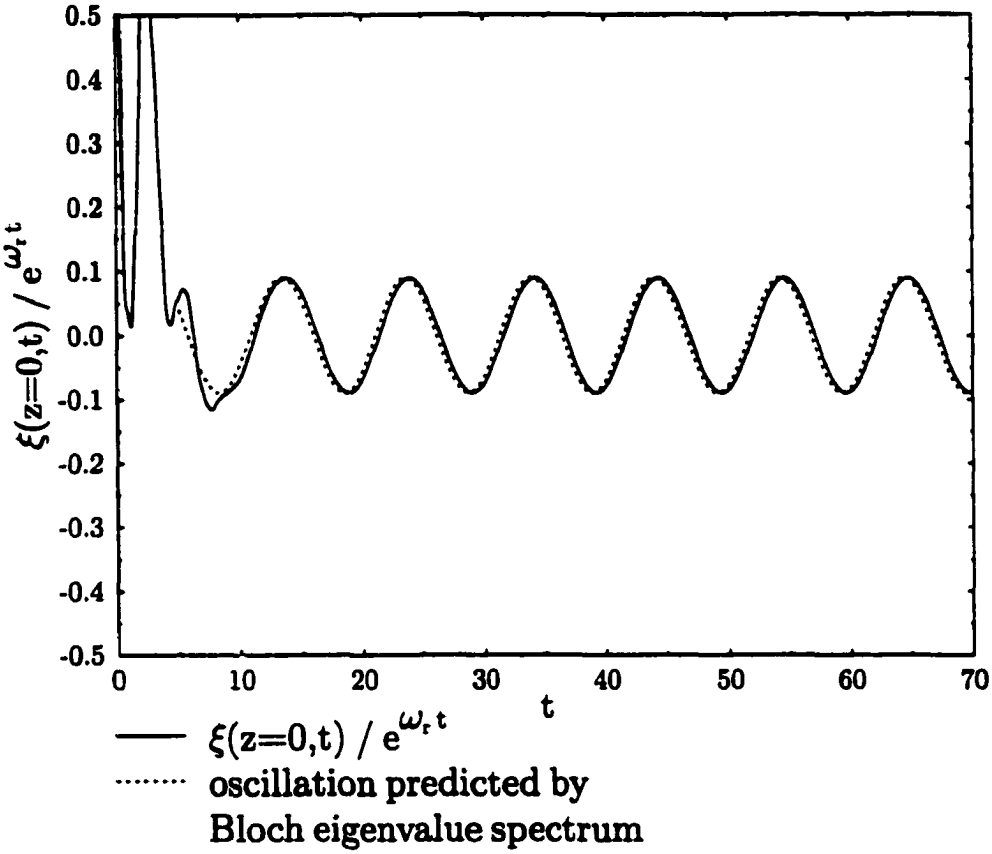

Figure 5 (b)

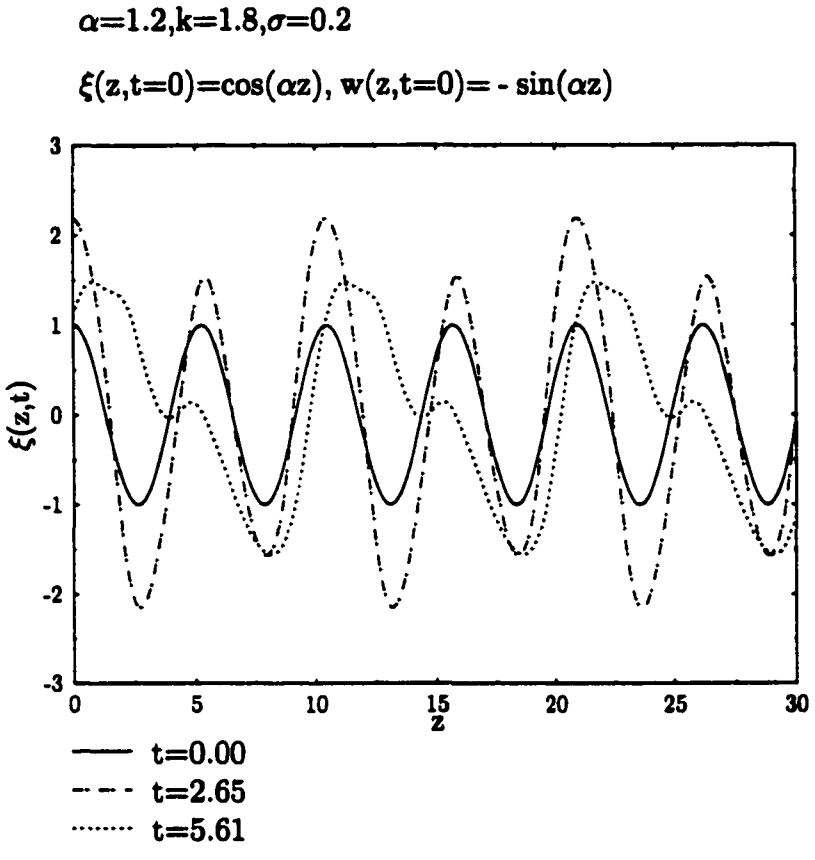

Figure 6(a)

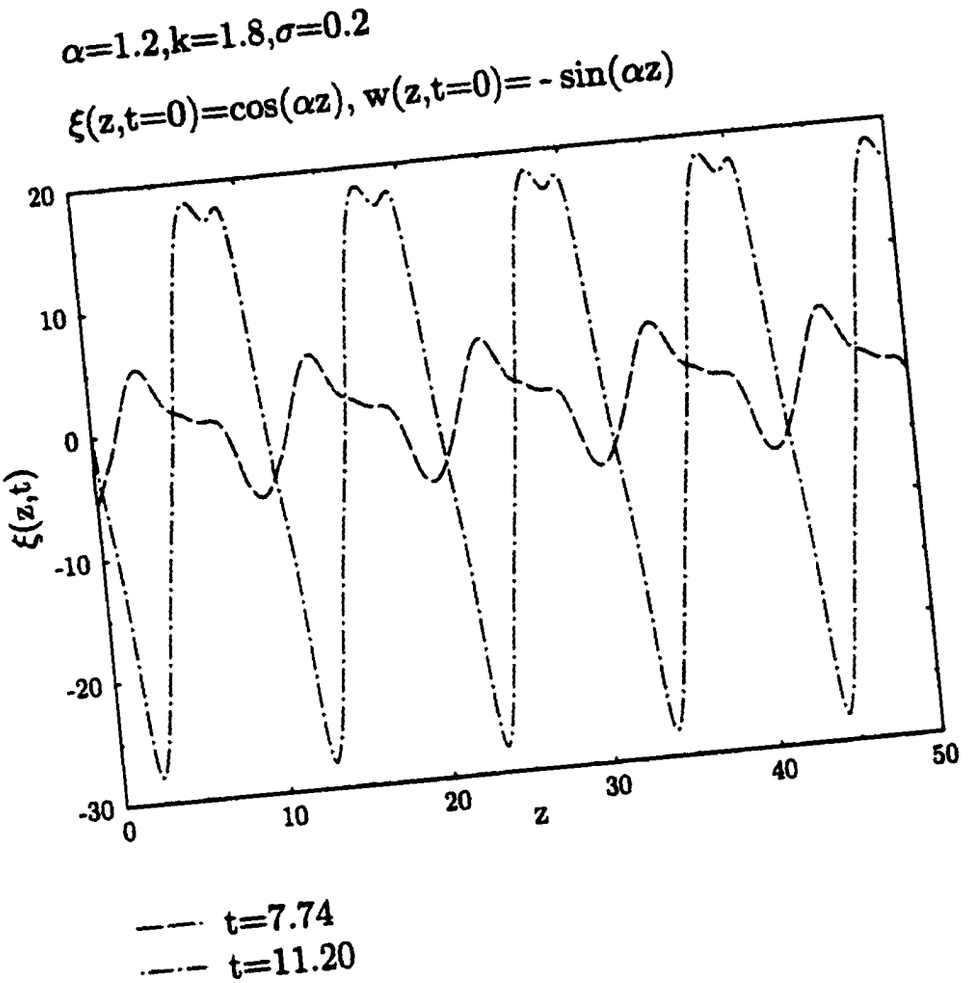

Figure 6(b)

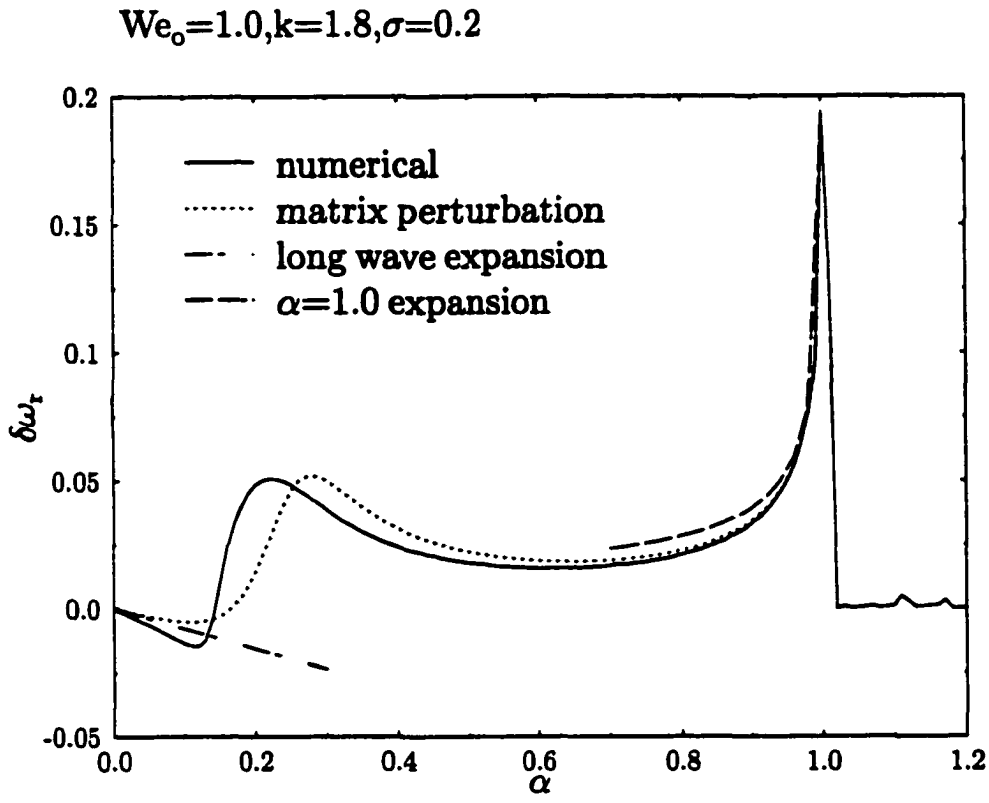

Figure 7 (a)

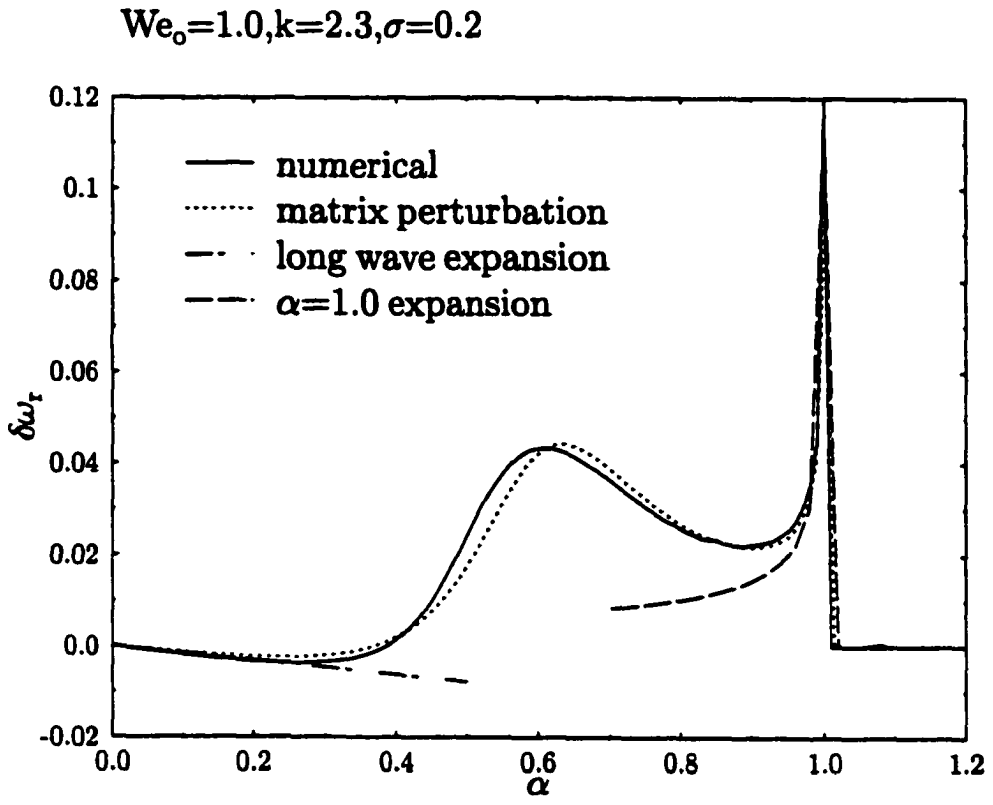

Figure 7(b)

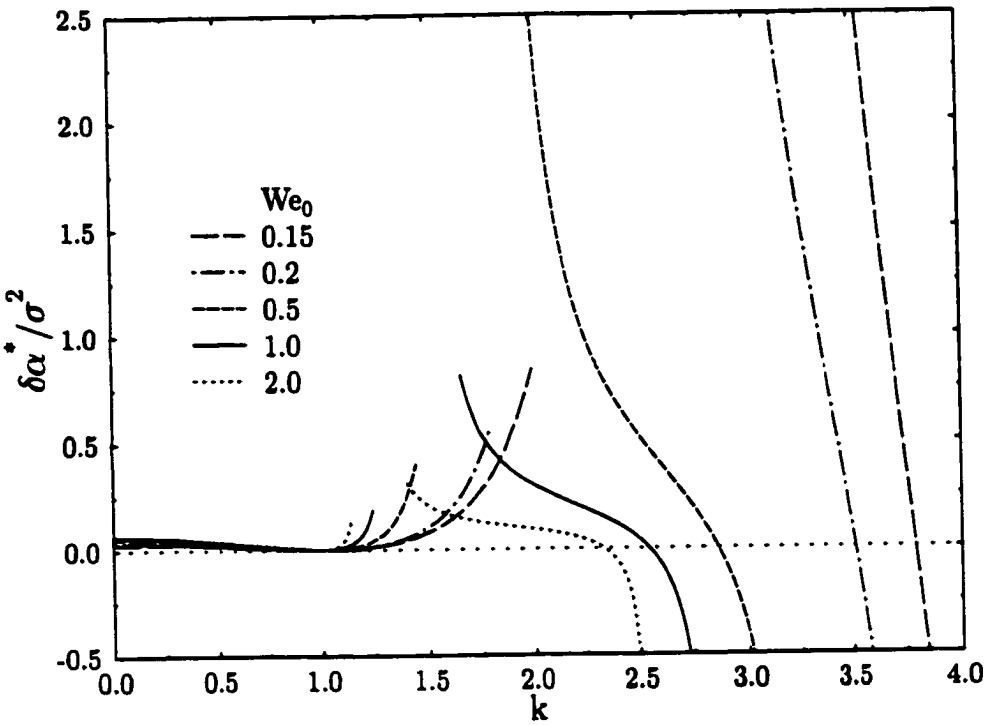

Figure 8

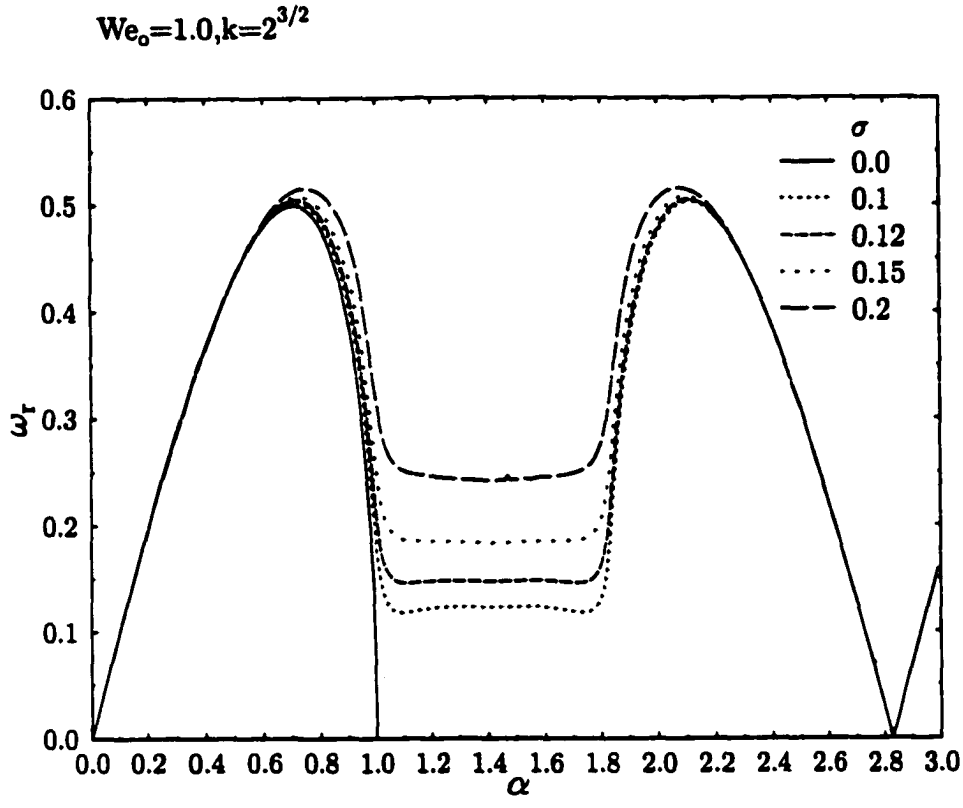

Figure 9

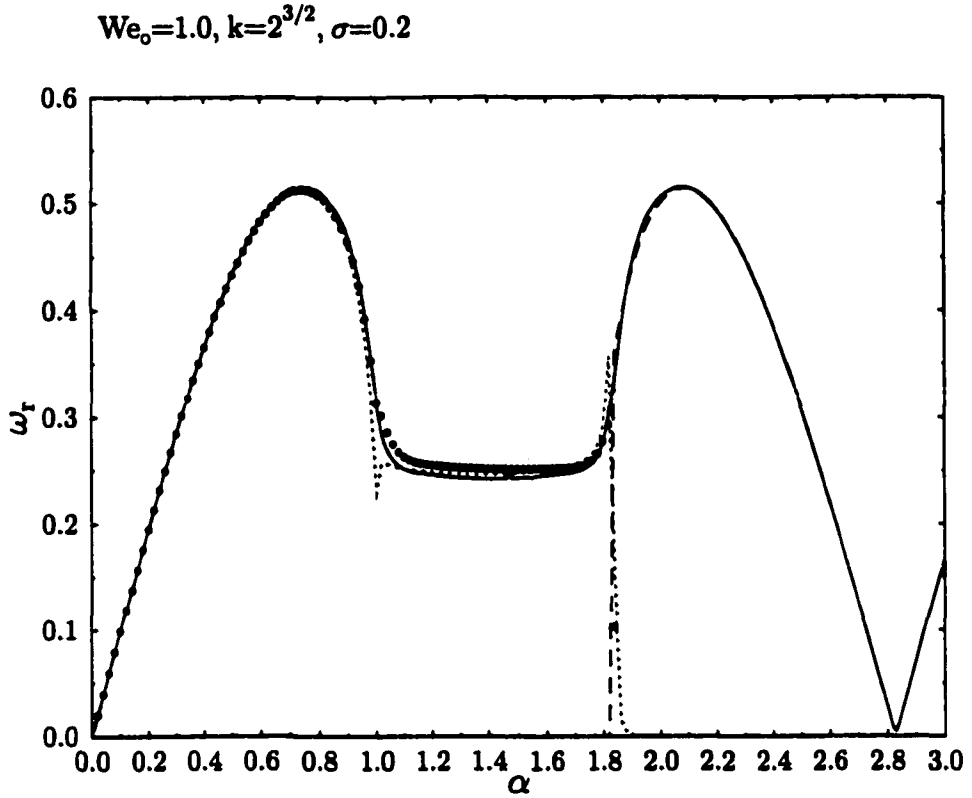

Figure 10

$\alpha=2^{1/2}$, $k=2^{3/2}$, $\sigma=0.2$

$\xi(z,t=0) = \cos(\alpha z)$, $w(z,t=0)=0$

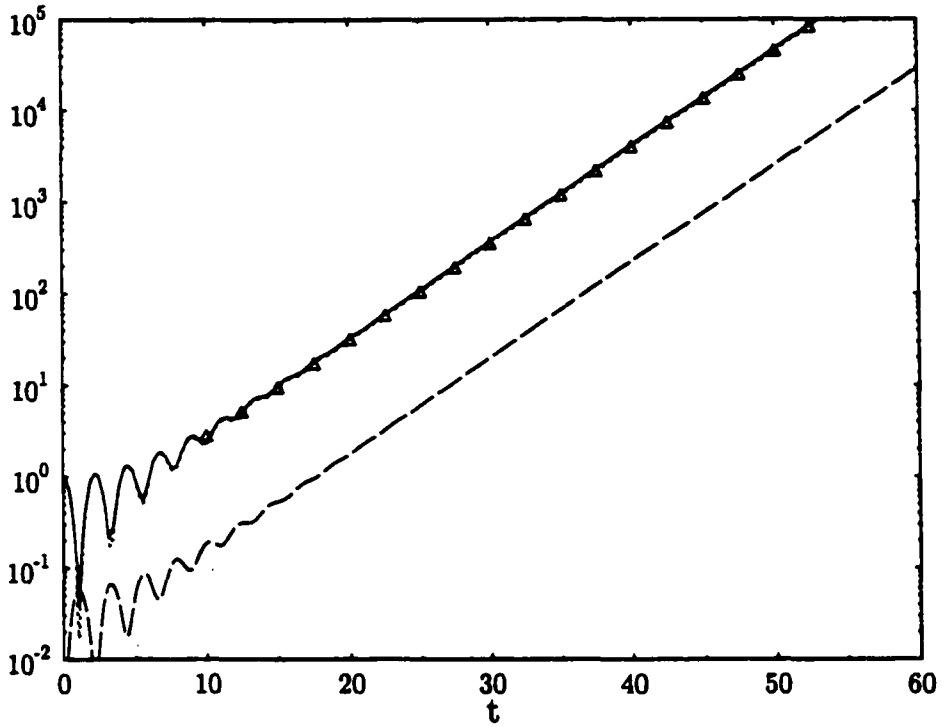

—— $\xi(z=0,t)$

····· $a_0(t)$

— — · $a_{-1}(t)$

△ Bloch eigenvalue

Figure 11

$\alpha=2^{1/2}$, $k=2^{3/2}$, $\sigma=0.2$

$\xi(z,t=0)=\cos(\alpha z)$, $w(z,t=0)=0$

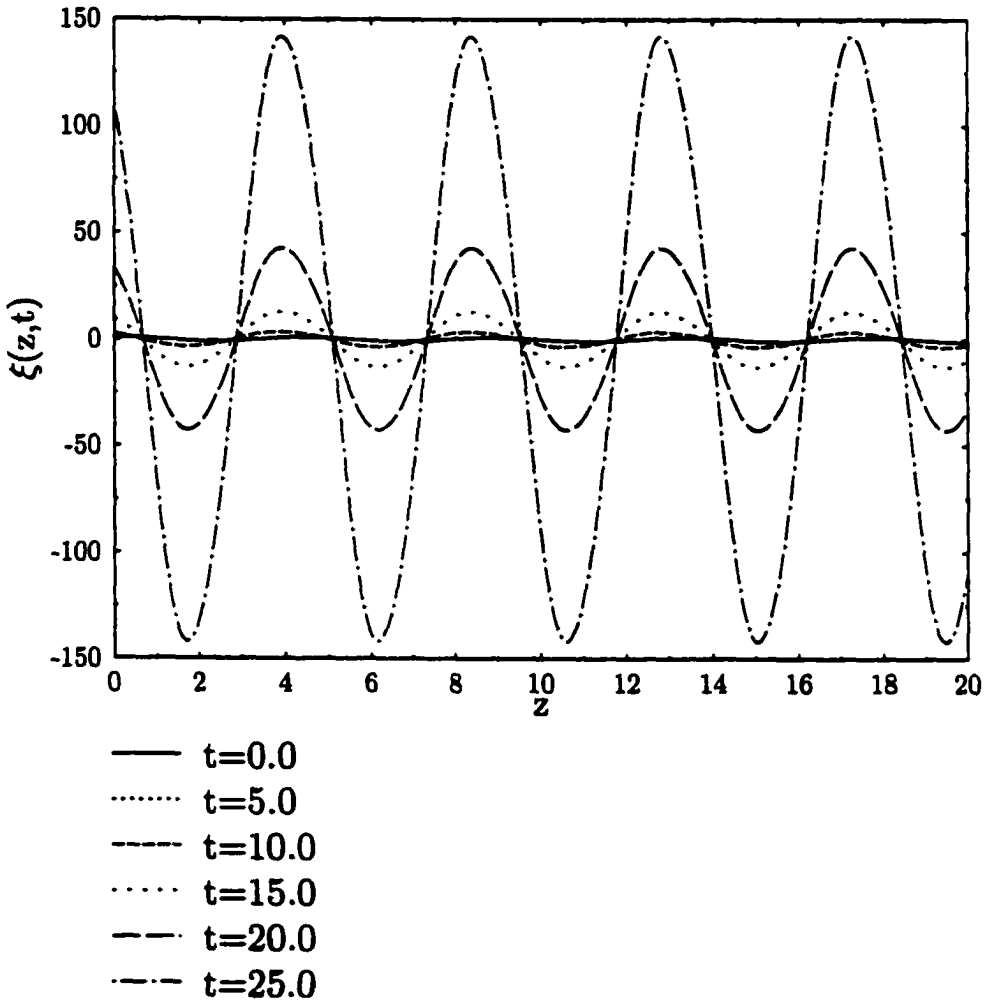

Figure 12

α=1.40, k=$2^{3/2}$, σ=0.2

$\xi(z,t=0) = \cos(\alpha z)$, $w(z,t=0)=0$

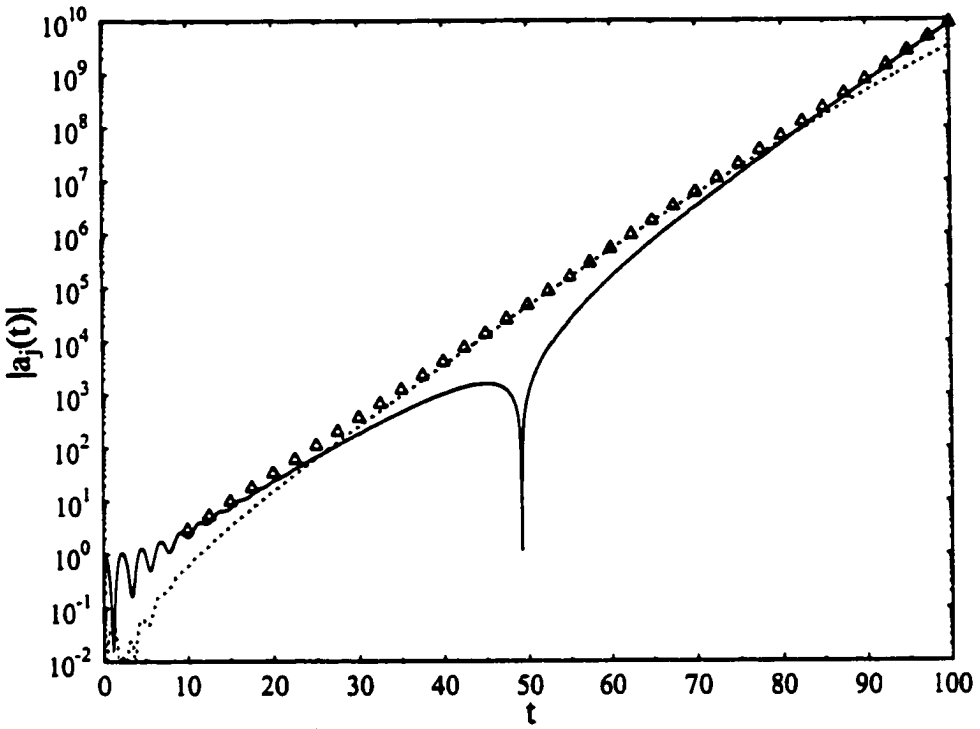

Figure 13(a)

α=1.35, k=$2^{3/2}$, σ=0.2

$\xi(z,t=0) = \cos(\alpha z)$, w(z,t=0)=0

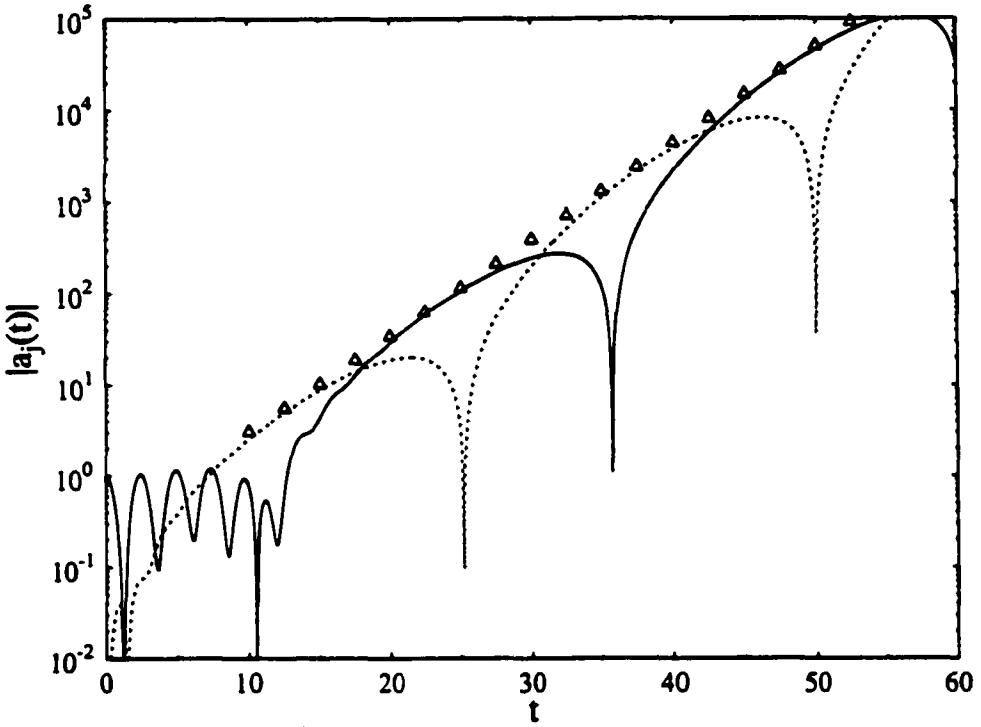

Figure 13 (b)

α=1.2, k=$2^{3/2}$, σ=0.2

$\xi(z,t=0) = \cos(\alpha z)$, w(z,t=0)=0

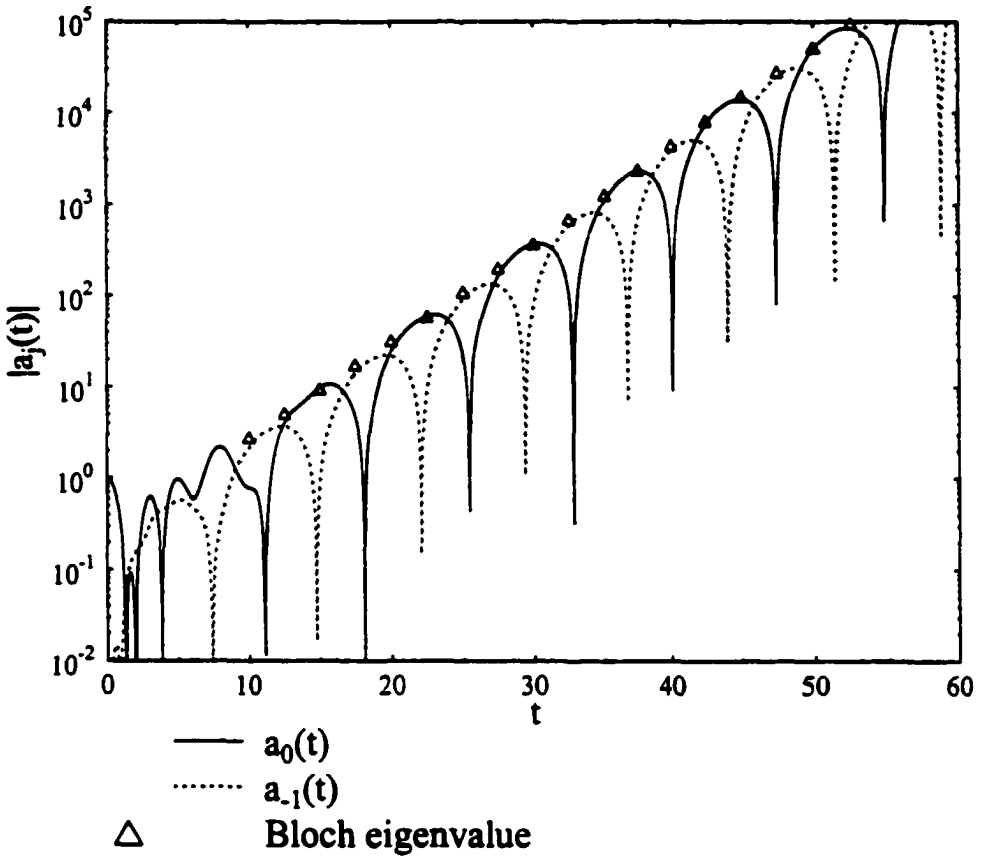

Figure 13(c)

α=1.2, k=$2^{3/2}$, σ=0.2

$\xi(z,t=0)=\cos(\alpha z)$, $w(z,t=0)=0$

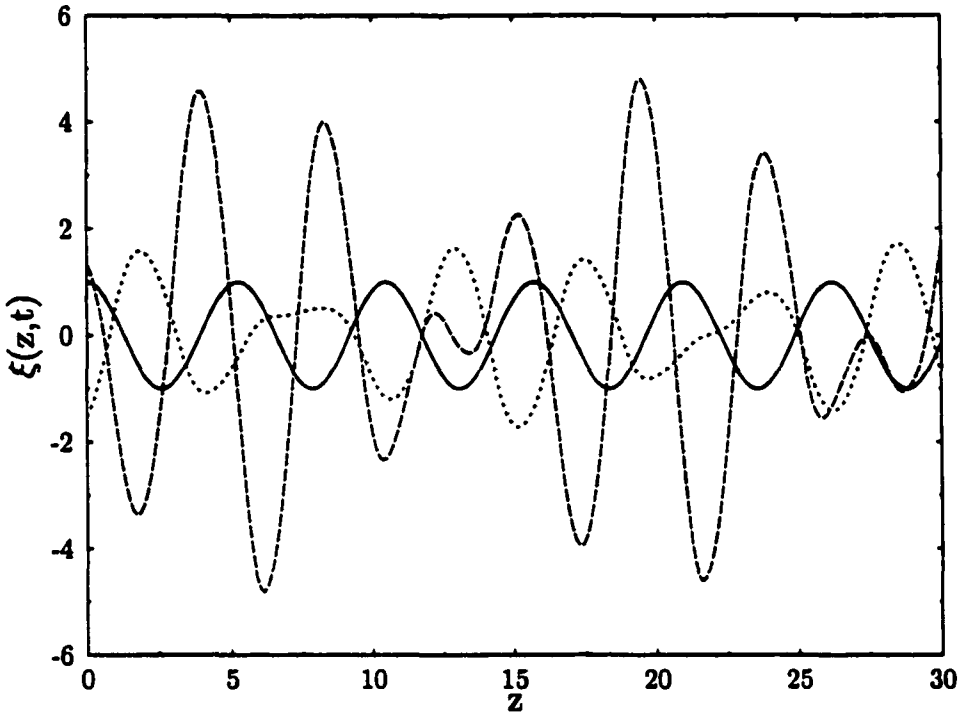

Figure 14(a)

α=1.2, k=$2^{3/2}$, σ=0.2

ξ(z,t=0)=cos(αz), w(z,t=0)=0

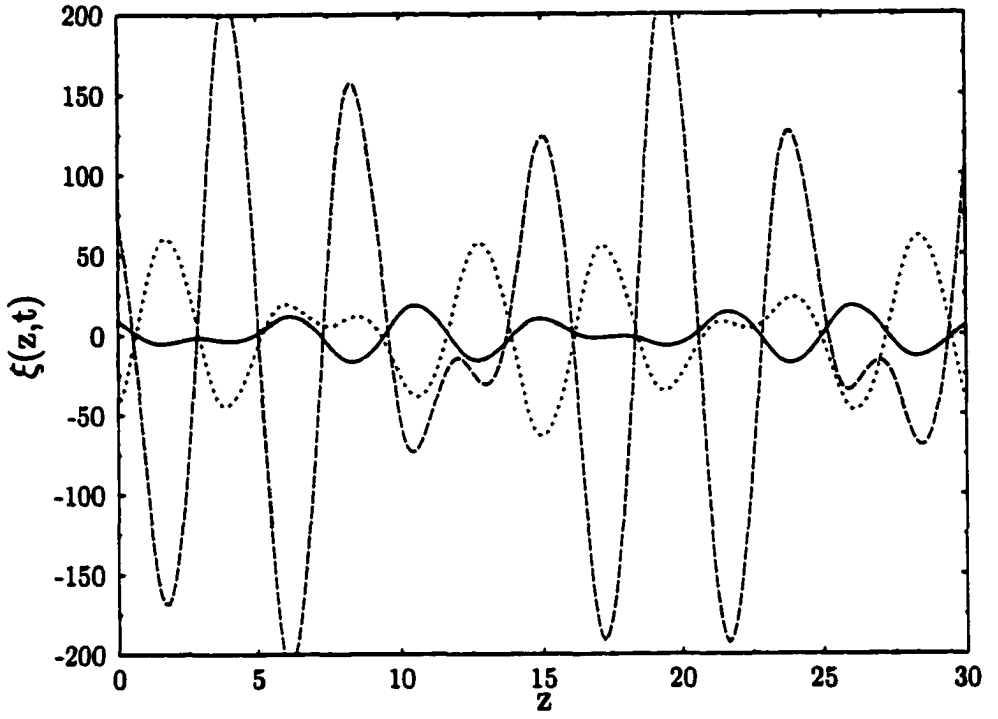

Figure 14(b)

V Concluding Remarks

In this thesis, we systematically examine the effects of pore corrugation on the stability of a core-annular flow in a pore in the limit of a thin annular film ($\varepsilon \to 0$) and a small corrugation ($\sigma \to 0$). Both viscous and inviscid systems are investigated. The former includes linear and weakly non-linear stability analyses, and the latter examines only the linear stability, including its fascinating resonant cases.

Chapter II examines the linear stability problem of a viscous CAF. The leading order base flow and the corresponding linear stability are asymptotically developed for the case of a sufficiently strong interfacial tension. The linear stability is controlled by the film's interfacial evolution, and the core just slaves the film. It yields a partial differential equation whose coefficients are periodic in space, because they derive from the leading order periodic base flow. We employ Floquet-Bloch analysis to obtain the eigenvalue spectra for this linear stability equation and compare the results with the numerical solution of the initial value problem for the interfacial dynamics for a given single initial condition and a range of parameters. In addition to a corrugation-derived $O(\sigma^2)$ correction to the growth rate, the most striking results are that the eigenvalue spectra show k-periodic and multiple-branch structures that are unstable to short waves of the initial disturbances. In contrast to the straight cylinder theory where an initial disturbance with wave length shorter than the circumference of the undisturbed fluid-fluid interface is stable, with corrugation it can be modified by interaction with the wall's corrugation (via the leading order base flow) to become longer. It then leads to an instability. That is, an unstable higher wall corrugation harmonic is excited by the initial disturbance. As a result, the key to determining the features of the linear stability is the wave number k of the wall. The system is unstable for all wave number disturbances unless $k>2$. The spectrum for $k>2$ has stable gaps in the short wave ranges, and thus may be stable to certain specific monochromatic disturbances.

Since real pores have more than one wall wave length, we have extended this study to the case with multiple wall wave lengths. As such, such flows are rarely linear stable.

In Chapter III, we extend the linear analysis into the weakly non-linear regime. In the weakly nonlinear regime, earlier studies of straight tubes yielded Kuromoto-Sivashinsky type amplitude equations governing the interface's evolution, or related equations depending on the exact scalings of the system's parameters. Linearly unstable long waves saturate in the weakly nonlinear regime because the KS non-linearity steepened, and effectively shortened the wavelengths of the growing linearly unstable long waves. The longitudinal tension then stabilized these shortened waves. The weakly non-linear analysis in a corrugated tube leads to the competition between unstable long waves being shortened and stabilized on the one hand, and these shorter waves exciting new unstable longer waves on the other. We derive and numerically solve the weakly non-linear amplitude equations for this situation and explore the results of this competition for various parameter regimes. For moderate or less strong interfacial tensions, the long wave linear instability excited by the corrugation as in Chapter II still can be suppressed by the stabilization from the nonlinear steepening.

As shown in Chapter II and III, we have preliminarily understood the role corrugation plays in determining a viscous CAF's stability. In Chapter IV, we again study the effect of corrugation on the linear stability of an *inviscid* CAF. This serves as a complementary problem to the viscous CAF to see how inertia interacts with the corrugation. By using similar techniques to those used in Chapter II, we again develop the leading order base flow and its linear stability. The linear stability is governed by a coupled set of film evolution equations for the case of strong interfacial tensions. Floquet-Bloch analysis is again used for the linear stability analysis. Eigenvalue spectra sharing similar features with the viscous case are found. They exhibit multiple-branch and k-periodic structures, but shortwave disturbances do not decay. The initial value approach shows an analogous instability due to the excitation of higher wall harmonics. We develop a matrix perturbation

theory along with an iterative perturbation techniques to calculate the correction to the growth rate. We find that the correction to the growth rate is $O(\sigma^2)$ unless a double root of the growth rate occurs in the $O(\sigma^0)$ eigenvalues arising from different branches. Such a case can lead to a large $O(\sigma)$ correction to the growth rate. This occurs near the disturbance wave number $\alpha = 1$ as a result of the interaction between two eigenvalue branches that at $\sigma = 0$ differ only by their sign, and thus coincide when they pass through zero (for $\sigma = 0$) at $\alpha = 1$. For a particular combination of parameters, another similar type of interaction can arise as two different eigenvalue branches coincide, which can similarly lead to an $O(\sigma)$ correction. In particular, for a certain value of the Weber number, when the wave number k of the wall equals twice that of the natural frequency k^* (>1) of the base flow, an $O(\sigma)$ correction appears at $\alpha = k^* > 1$ in the short wave regime. The most striking result of this interaction is that the eigenvalue spectrum forms a bridge connecting between the primary and secondary branches. For $1 < \alpha < k$, the corresponding dynamics show that the primary α wave competes with its first harmonic $(\alpha - k)$ wave and neither dominates even for long times in the linear regime. The long-term interfacial evolution grows in an oscillatory manner where these two modes alternatively predominate.

The research presented in this dissertation has led to a better understanding of how corrugation affects the stability of a core annular flow. This study brings to light the key role played by the wall corrugation and has hopefully provided new insights into the potential instability mechanisms that may be at work in secondary oil recovery and in respiratory bronchioles due to cross-sectional non-uniformity.

References

ABRAMOWITZ, M. & STEGUN, I. A. 1972 *Handbook of Mathematical Functions*. Dover.

AUL, R. W. 1989 The motion of drops and long bubbles through small capillaries: coalescence of drops and annular film stability. Ph.D. thesis, Cornell University. Itchaca, NY.

AUL, R. W. & OLBRICHT, W. L. 1990 Stability of a thin annular film in a pressure-driven, low Reynolds number flow through a capillary. *J. Fluid Mech.* **215**, 585-599.

BONTOZOGLOU, V., KALLIADASIS, S. & KARABELAS, A. J. 1991 Inviscid free-surface flow over a periodic wall. *J. Fluid* Mech. **226**, 189-203.

CHANDRASEKHAR, S. 1968 *Hydrodynamic and Hydromagnetic Stability*. Oxford,U.K

CHANG, H.-C. 1987 Evolution of nonlinear waves on vertically falling films - a normal form analysis. *Chem . Engrg . Sci .* **42**, 515-533.

CHAUHAN, A., MALDARELLI, C., RUMSCHITZKI, D. S. & PAPAGEORGIOU, D. T. 1996 The temporal and spatial instability of an inviscid compound jet, *Rheologica Acta*, 35, 567.

CHAUHAN, A., MALDARELLI, C., RUMSCHITZKI, D. S. 2000 The temporal instability of a compound thread, *J. Fluid Mech.*, in press.

CHEN, K., BAI, R. & JOSEPH, D. D. 1990 Lubricated pipeling. Part 3. Stability of core-annular flow in vertical pipes. *J. Fluid Mech.* **214**, 251-286.

CHEN, K. & JOSEPH, D. D. 1991 Long waves and lubrication theories for core annular flow. *Phys. Fluids*, **A 3**, 2672-2679.

CHOW, J. C. F. & SODA, K. 1972 Laminar flow in tubes with constriction. *Phys. Fluids*, **15**, 1700-1706.

DASSORI, C. G., DEIBER, J. A. & CASSANO, A. E. 1984 Slow two-phase flow through a sinusoidal channel. *Int. J. Multiphase Flow.* **10**, 181-193.

DAVIES, A. G., GUAZZELLI, E. & BELZONS, M. 1989 The propagation of long waves over an undulated bed. *Phys Fluids* **A 1**, 1331-1340.

ENGELUND, F. & FREDSOE, J. 1982 Sediment ripples and dunes. *Ann. Rev. Fluid Mech.* **14**, 13-37

FRENKEL, A. L., BABCHIN, A. J., LEVICH, B. G., SHLANG,T. & SIVASHINSKY, G. I. 1987 Annular flows can keep unstable films fro breakup: nonlinear saturation of capillary instability. *J. Colloid Interf. Sci.* **115**, 225-233.

FRISCH, U., SHE, S. & THUAL, O. 1986 Viscoelastic behavior of cellular solutions to the Kuramoto-Sivashinsky model. *J. Fluid Mech.* **168**, 221-240.

GAUGLITZ, P. A. & RADKE, C. J. 1988 An extended evolution equation for liquid film break up in cylindrical capillaries. *Chem. Eng. Sci.*, **43**, 1457-1465.

GAUGLITZ, P. A. & RADKE, C. J. 1990 The dynamics of liquid film break up in constricted cylindrical capillaries. *J. Colloid Interf. Sci.* **134**, 14-40.

GEORGIOU, E. C., PAPAGEORGIOU, D. T., MALDARELLI, C. & RUMSCHITZKI, D. S. 1992 An asymptotic theory for the linear stability of a core-annular flow in the thin annular limit. *J. Fluid Mech.* **243**, 653-677.

GOREN, S. L. 1962 The instability of an annular thread of fluid. *J. Fluid Mech.* **27**, 309-319.

HALPERN, D. & GROTBERG, J. B. 1993 Surfactant effects on fluid-elastic instabilities of liquid-lined flexible tubes: a model of airway closure. *J. Biomech. Eng.* **115**, 271-277.

HAMMACK, J. L. & SEGUR, H. The Korteweg-de Vries equations and water waves Part 2: Comparison with experiments. *J. Fluid Mech.* **65**, 289-314.

HAMMOND, P. S. 1983 Nonlinear adjustment of a thin annular film of viscous fluid surrounding a thread of another within a circular cylindrical pipe. *J. Fluid Mech.* **137**, 363-384.

HICKOX, C. E. 1971 Instability due to viscosity and density stratification in axisymmetric pipe flow. *Phys. Fluids,* **14**, 251-262.

HOOPER, A. P. & GRIMSHAW, R. 1985 Nonlinear instability at the interface between two viscous fluids. *Phys. Fluids* **28**, 37-45.

HU, H. H. & JOSEPH, D. D. 1989 Lubricated pipelines : stability of core-annular flow. Part 2*J. Fluid Mech.* **205**, 359-396.

HU, H. H., LUNDGREN, T. & JOSEPH, D. D. 1990 Stability of core-annular flow with a small viscosity ratio. *Phys. Fluids*, **A 2**, 1945-1954.

HYMAN, J. & NICOLAENKO, B. 1986 The Kuramoto-Sivashinsky equation: a bridge between PDE's and dynamical systems. *Physica D*, **18**, 113-126.

HYMAN, J., NICOLAENKO, B. & ZALESKI, S. 1986 Order and complexity in Kuramoto-Sivashinsky model of weakly turbulent interfaces. *Physica D*, **23**, 265-292.

JOHNSON, R. S. 1973 On the development of a solitary wave moving over an even bottom. *Proc. Camb. Phil. Soc.*, **73**, 183-203.

JOHNSON, R. S. 1994 Solitary wave, soliton and shelf evolution over variable depth. *J. Fluid Mech.* **276**, 125-138.

JOSEPH, D. D., RENARDY, Y. & RENARDY, M. 1984 Instability of the flow of immiscible liquids with different viscosites in pipe. *J. Fluid Mech.* **141**, 309-317.

KALLIADASIS, S. & CHANG, H-C. 1994 Drop formation during coating of vertical fibres. *J. Fluid Mech.* **261**, 135-168.

KANG, F. & CHEN, K. 1995 Gravity-driven two-layer flow down a slightly wavy periodic inclined at low Reynolds number. *Int. J. Multiphase Flow.* **21**, 501-513.

KAWAHARA, T. 1983 Formation of saturated solitons in a nonlinear dispersive system with instability and dissipation. *Phys. Rev. Lett.* **51**, 381-383

KAWAHARA, T. & TOH, S. 1988 Nonlinear dispersive periodic waves in the presence of instability and damping. *Phys. Fluids* **28**, 1636-1638.

KELLY, E. 1967 On the stability of an inviscid shear layer which is periodic in space and time. *J. Fluid Mech.* **27**, 657-689.

KENNEDY, J. 1963 The mechanics of dunes and antidunes in erodible-bed channels. *J. Fluid Mech.* **27**, 521-545.

KERCHMAN, V. & FRENKEL, A. L 1994 Interactions of coherent structures in a film flow: simulations of a highly nonlinear evolution equation. *Theor. Comput. Fluid Dyn.* **6**, 235-254 .

KERCHMAN, V. 1995 Strong nonlinear interfacial dynamics in core-annular flows. *J. Fluid Mech.* **290**, 131-166.

KORTEWEG, D. J. & de VRIES, G. 1895 On the change of form of long waves advancing in a rectangular canal, and on a new type of long stationary waves. *Phil. Mag.* (5), **39**, 422-433.

LIU, Y. & YUE, K. P. 1998 On generalized Bragg scattering of surface waves by bottom ripples. *J. Fluid Mech.*. **356**, 297-326.

MIKAMI, T & MASON, G 1975 The capillary break-up of a binary liquid column inside a tube. *Can . J . Chem . Eng* . **53**, 372-377.

MITRA, A. & GREENBERG, M. D. 1984 Slow interactions of gravity waves and a corrugated seabed*J. Appl. Mech.* **51**, 251-255.

NACHBIN, A. & PAPANICOLAOU, G. C. 1992 Water waves in shallow channels of rapidly varying depth. *J. Fluid Mech.* **241**, 311-332.

OTIS, D. R., JOHNSON, M., PEDLEY, T. J. & KAMM, R. D. 1993 The role of pulmonary surfactant in airway closure. *J. Appl. Physiol.* **75**, 1323-1333.

PAPAGEORGIOU, D. T., MALDARELLI, C. & RUMSCHITZKI, D. S. 1990 Nonlinear interfacial stability of core-annular film flows. *Phys. Fluids,* **A 2**, 340-352.

PAPAGEORGIOU, D. T. SMYRLIS, Y. 1991 The Route to Chaos for the Kuramoto-Sivashinsky Equation. *Theor. Comput. Fluid Dyn.* **3**, 15-42.

PARK, C. W. & HOMSY, G. M. 1984 Two-phase displacement in Hele-Shaw cells: theory. *J. Fluid Mech.* **139**, 291-308.

PLATEAU, J. 1873 *Statique Experimentale et Theorique des Liquides Soumis aux Seules forces Moleculaires*, Gauthier-Villars.

POZRIKIDS, C. 1988 The flow of a liquid film along a periodic wall. *J. Fluid Mech.* **188**, 275-300.

PREZIOSI, K., CHEN, K. & JOSEPH, D. D. 1989 Lubricated pipelines: stability of flow. *J. Fluid Mech.* **201**, 323-356.

RADEV, S & TCHAVDAROV, B 1988 Linear capillary instability of compound jets. *Int. J. Multiphase Flow* **14**, 67-79.

RANSOHOFF, T. C., GAUGLITZ, P. A. & RADKE, C. J. 1987 Snap-off of gas bubbles in smoothly constricted noncircular capillaries. *AIChE. J.* **33**, 753-765.

RATULOWSKI, J. & CHANG, H. C. 1989 In Snap-off at strong constrictions : effect of pore geometry. In *Surface-Based Mobility Control*: : *Progress in Miscible Flood Enhanced Oil Recovery* (ed. D. Smith). ACS Symposium Series, vol. 33, pp. 282-314. Hemisphere.

RAYLEIGH, LORD 1879 On the capillary phenomena of jets. Appendix I. *Proc. Roy. Soc.* **A, 29**,71.

RHINES, P. B. 1970 Wave propagation in a periodic medium with application to the ocean. *Rev. Geophys. Space Phys.* **8**, 2, 303-319.

RUSSELL, J. S. 1844 Report on waves. *Rep. 14th Meet. Brit. Assoc. Adv. Sci.*, York, 311-390. John Murray, London.

SAFFMAN, P. G. & TAYLOR, G. I. 1958 The penetration of a fluid into a porous medium or Hele-Shaw cell containing a more viscous liquid. *Proc. R. Soc. London Ser.* **A 245**, 312-329.

SAMMARCO, P., MEI, C. C. & TRULSEN, K. 1994 Nonlinear resonance of free surface waves in a current over a sinusoidal bottom: a numerical study. *J. Fluid Mech.* **279**, 377-405.

SIVASHINSKY, G. I. & MICHELSON, D. M. 1980 On irregular wavy flow of a liquid film down a vertical plane. *Prog. Theor. Phys.* **63**, 2112-2114.

SLATTERY, J. C. 1974 Interfacial Effects in the Entrapment and Displacement of Residual Oil. *AIChE. J.* **20**, 1145-1154.

SMYRLIS, Y. & PAPAGEORGIOU, D. T. 1990 Computational study of chaotic and ordered solutions of the Kuramoto-Sivashinsky equation. ICASE Report.

TOMOTIKA, S. 1935 On the instability of a cylindrical thread of a viscous liquid surrounded by another viscous liquid. *Proc. Roy. Soc.* **A, 150**, 322-337.

TOUGOU, H. 1978 Long waves on a film flow of a viscous fluid down an inclined uneven wall. *J. Phys. Soc. Japan.* **44**, 1014-1019

WANG, Y. C. 1981 Liquid film flowing slowly down a wavy incline. *AIChE. J.* **27**, 207-212.

WEI, H. H. & RUMSCHITZKI, D. S. 2000 The linear stability of a core-annular flow in a corrugated tube. *IUTAM Symposium on Non-Linear Sigularities in Deformation and Flow*, in press.

YIH, C. S. 1967 Instability due to viscosity stratification. *J. Fluid Mech.* **27**, 337-352.

ZABUSKY, N. J. & KRUSKAL, M. D. 1965 Interactions of 'solitons' in a collisionless plasma and the recurrence of initial states. *Phys. Rev. Lett.*, **15**, 240-243.

ZHU, Y. 1995 Resonant generation of non-linear capillary-gravity waves. *Phys . Fluids* **7**, 2294-2296.